2016-03-09

Synapse Development: Ribonucleoprotein Transport from the Nucleus to the Synapse: A Dissertation

Vahbiz Jokhi
University of Massachusetts Medical School

SYNAPSE DEVELOPMENT: RIBONUCLEOPROTEIN TRANSPORT FROM THE NUCLEUS TO THE SYNAPSE

A Dissertation Presented

By

VAHBIZ JOKHI

Submitted to the Faculty of the

University of Massachusetts Graduate School of Biomedical Sciences, Worcester

in partial fulfillment of the requirements for the degree of

DOCTOR OF PHILOSOPHY

03/09/2016

Program in Neuroscience

SYNAPSE DEVELOPMENT: RIBONUCLEOPROTEIN TRANSPORT FROM THR NUCLEUS TO THE SYNAPSE

A Dissertation Presented By

VAHBIZ JOKHI

This work was undertaken in the Graduate School of Biomedical Sciences
Program in Neuroscience

The signatures of the Thesis Advisor signifies
validation of Dissertation content

Vivian Budnik, PhD., Thesis Advisor

The signatures of the Dissertation Defense Committee signifies completion and approval as to style and content of the Dissertation

Eric Baehrecke, PhD., Member of Committee

Melissa Moore, PhD., Member of Committee

Mary Munson, PhD., Member of Committee

Thoru Pederson, PhD., Member of Committee

Leslie Griffith, M.D., PhD., External Member of Committee

The signature of the Chair of the Committee signifies that the written dissertation meets the requirements of the Dissertation Committee

Marc Freeman, Ph.D., Chair of Committee

The signature of the Dean of the Graduate School of Biomedical Sciences signifies that the student has met all graduation requirements of the School

Anthony Carruthers, Ph.D,
Dean of the Graduate School of Biomedical Sciences
03/09/2016

With the blessings of Bapu and Ma, I dedicate this thesis to
Dad, Mom & Binaaz
for their love and support

Acknowledgements

The last five years have been an incredible learning process and it is an immense pleasure to thank all the people without whom this body of work would not have been possible. First of all, I wish to express my sincere gratitude to my thesis advisor and mentor, Vivian Budnik for her continuous guidance and support. She gave me the freedom and resources to explore new horizons and at the same time always made herself available for insightful discussions and kept me focused. Over the years, she improved my writing and presentation skills and helped me become a better scientist and stronger person.

I have been very fortunate to have the guidance of a supportive committee: Marc Freeman, Melissa Moore, Mary Munson, Thoru Pederson and Eric Baehrecke. Apart from their scientific brilliance, insights and valuable advice, they have been very approachable, given me their time and have always been there to encourage and motivate me. I would like to take this opportunity to specially thank Melissa Moore, who has also been a great collaborator, for her advice, kindness and faith in me in times when I questioned my own capabilities. I sincerely thank Marc for all his unwavering support and advice for my career goals. I admire Melissa and Marc for their commitment to mentorship. I would like to thank David Weaver for being an extremely kind and helpful program director and other faculty of the Neuroscience department: Claire Benard, Patrick Emery and Mike Francis for their words of encouragement and support. I would also like to thank Dr. Leslie Griffith for agreeing to be the external examiner for my defense. A special thank you for the late Dr. Suresh Mahajan for inspiring me to pursue research.

I owe a special thanks to Kate Koles, James Ashley, Cassandra Brewer, Alex Koon, Ceren Korkut, Romina Barria, Daniel Ge and Yuly Fuentes for creating a wonderful learning environment in my early years in the lab. I sincerely thank them all for training me, teaching me how to design experiments, troubleshoot and providing me with critical input about my projects. I have learnt a lot from them. I thank Yihang, my lab sister, for all her support over the years. She has been a great colleague and close friend. Graduate school would not have been the same without her. I would like to convey my thanks to all the members of the past and present members of the Budnik lab: Rachel, Gloria, Travis, Caty and Lee for a wonderful work environment; and especially Franz, Baojin for teaching me how to relax, have fun and enjoy the science. A sincere thanks to my collaborators, Emilliano Ricci and Akiko Noma; I learnt new perspectives and techniques from them.

I would like to thank my wonderful friends in the US and back at home for their encouragement and support. A special thank you to Rupal, my closest friend, Rodabeh, Rupa and Firdaus for always being there for me despite the distance. My wonderful friends in USA have enriched my experience in graduate school. I want to take this opportunity to thank Ankit-Pallavi-Soham-Tanishi, Sneha-Varun, Sandhya-Karthik-Haasini, Swapnil, Satyajeet-Harshada Pallo, Ankita, Mayuri, Meetu and Ami-Hemal for being like family away from home. Life in UMass has been enjoyable thanks to all the adventures, camping trips, hikes, birthdays and festivals celebrated together. I especially am grateful for the wonderful memories, love and support through the years.

A heartfelt gratitude to Mihir, for being my most thoughtful friend and my support system (punching bag). I cannot thank him enough for handling my hyperness and for

always being there through the highs and lows, and for being proud of all my achievements.

Finally, I owe my deepest gratitude to my family. Meher Maasi, Adil Maasa, Adil kaka, Bacha mumma and Bomy- thank you all for your unconditional love, support and good wishes. My loving parents, Jasmine and Aspi, and my sister Binaaz, thank you for being my pillars of support and strength, motivating me to study further, inspiring me to dream big and helping me pursue my all goals and ambitions in life. Words aren't enough to express my gratitude to mom-dad for all your hard work and efforts in making me who I am. I am extremely lucky and blessed to have you all in my life and wouldn't be able to achieve any of this without your belief, love and support.

Abstract

A key process underlying synapse development and plasticity is stimulus-dependent translation of localized mRNAs. This process entails RNA packaging into translationally silent granules and exporting them over long distances from the nucleus to the synapse. Little is know about (a) where ribonucleoprotein (RNP) complexes are assembled, and if in the nucleus, how do they exit the nucleus; (b) how RNPs are transported to specific synaptic sites.

At the *Drosophila* neuromuscular junction (NMJ), we uncovered a novel RNA export pathway for large RNP (megaRNP) granules assembled in the nucleus, which exit the nucleus by budding through the nuclear envelope. In this process, megaRNPs are enveloped by the inner nuclear membrane (INM), travel through the perinuclear space as membrane-bound granules, and are de-enveloped at the outer nuclear membrane. We identified Torsin (an AAA-ATPase that in humans is linked to dystonia), as mediator of INM scission. In torsin mutants, megaRNPs accumulate within the perinuclear space, and the mRNAs fail to localize to postsynaptic sites leading to abnormal NMJ development. We also found that nuclear envelope budding is additionally used for RNP export during *Drosophila* oogenesis.

Our studies also suggested that the nuclear envelope-associated protein, Nesprin1, forms striated F-actin-based filaments or ‘‘railroad tracks,’’ that span from muscle nuclei to postsynaptic sites at the NMJ. Nesprin1 railroad tracks wrap aoround the postsynaptic regions of immature synaptic boutons, and serve

to direct RNPs to sites of new synaptic bouton formation. These studies elucidate novel cell biological mechanisms for nuclear RNP export and trafficking during synapse development.

Table of Contents

List of Tables

List of Figures

List of Abbreviations

NMJ	Neuromuscular junction
mEJPs	miniature excitatory junctional potentials
GluRIIA	Glutamate receptor II-A
DFz2	*Drosophila* Frizzled receptor-2
DFz2C	C terminal fragment of *Drosophila* Frizzled receptor
LamC	Lamin-C
aPKC	atypical protein kinase C
DLG	Discs large
LAP1	Lamin associated polypeptide 1
LULL1	Luminal domain Like LAP1
PABP2	Poly(A) Binding Protein 2
HRP	Horse radish peroxidase
Wg	Wingless
NPC	Nuclear pore complex
NR	nucleoplasmic reticulum
INM	inner nuclear membrane
NE	nuclear envelope
ONM	outer nuclear membrane
HSV	herpes simplex virus
RNP	ribonucleoprotein
RBP	RNA binding proteins
FNI	Frizzled Nuclear Import
NPC	nuclear pore complex
NUP	nucleoporin
FG	Phenylalanine Glycine
AAA+	ATPases associated with various activities
Nesprins	Nuclear Envelope SPectRIN repeat proteins
KASH	Klarsicht/ANC-1/Syne homology
LINC	LInkers of Nucleoskeleton to Cytoskeleton
NEB	nuclear envelope budding
CS	Canton S

Copyright Information

Parts of this dissertation have been published or submitted for publication as:

Speese SD*, Ashley J*, **Jokhi V**, Nunnari J, Barria R, Li Y, Ataman B, Koon A, Chang YT, Li Q, Moore MJ, Budnik V. *Nuclear envelope budding enables large ribonucleoprotein particle export during synaptic Wnt signaling.* **Cell. 2012** May 11; 149(4):832-46.

Jokhi V, Ashley J, Nunnari J, Noma A, Ito N, Wakabayashi-Ito N, Moore MJ, Budnik V. *Torsin mediates primary envelopment of large ribonucleoprotein granules at the nuclear envelope.* **Cell Rep. 2013** Apr 25; 3(4):988-95.

Packard M*, **Jokhi V***, Ding B, Ruiz-Canada C, Ashley J, Budnik V. *Nucleus to synapse Nesprin1 railroad tracks direct synapse maturation through RNA localization*. **Neuron**. **2015** May 20; 86(4):1015-28 (*Equal contribution)

Jokhi V, Hassinger L, Thomson T, Budnik V. *Role of the nuclear envelope pathway in the exit of mRNAs during oogenesis in Drosophila.* (Manuscript in preparation)

Chapter I

Introduction

Long-term changes in synapses are the underlying basis of our ability to learn and remember. This requires modifications in synaptic structure and strength, termed as "*plasticity*" in response to environmental cues (Wiersma-Meems et al., 2005; Mayford et al., 2010). Localized translation of mRNAs at synaptic sites is a key process underlying synaptic plasticity. This requires mRNAs to be packaged and transported over long distances from the cell body (Richter 2001; Barco et al., 2008; Wang et al., 2010). Little is known about where these mRNAs are packaged, how they exit the nucleus and how they are targeted to specific synaptic sites. The goal of the studies in this thesis was to understand the mechanisms underlying these processes.

Synaptic plasticity

The circuitry of the human brain contains about a 100 billion neurons and each individual nerve cell can make up to 10,000 different synaptic connections. It is these synaptic connections that allow communication between neurons, which orchestrates various sensory, motor and cognitive behaviors. While overall the structure/position of each neuron is genetically hard-wired, individual synapses are dynamically changing throughout an individual's lifetime. Synapses have the ability to modulate their strength and structure based on environmental cues- a process termed "synaptic plasticity" (Griffith and Budnik, 2006). This circuitry sculpting and rewiring underlies the basis of perception, emotion, learning and memory (Kandel, 2001).

The concept of “plasticity” dates back to the early 1900s, when Santiago Ramon y Cajal, the father of modern neuroscience, while studying regenerative “plasticity” upon spinal cord injury, discovered that there are dynamic structural changes in neuronal connections in the central nervous system (CNS) (DeFelipe, 2002) (Cajal, 1904). His findings led to a new era in neuroscience and encouraged neuroscientists to explore different aspects of synaptic plasticity. In 1906, Ernesto Lugaro and Eugenio Tanzi, proposed that neurons could change in an adaptive fashion to enable learning (Berlucchi and Buchtel, 2009) . Years later, in 1949, this concept was further elaborated upon by Donald Hebb in *The Organization of Behavior; a Neurophysiological Theory*. Hebb postulated that “when an axon of cell A is near enough to excite a cell B and repeatedly and persistently takes part in firing it, some growth process or metabolic change takes place in one or both cells such that A’s efficiency, as one of the cells firing B, is increased (Hebb, 1949). Hebb’s rule that “neurons that fire together wire together” (Brown and Milner, 2003; Hebb, 1949) has been the foundation of neural network theory. T. Bliss and T. Lomo described experimental evidence supporting the Hebbien theory, when upon high frequency stimulation of the presynaptic neuron, they observed long-lasting increased excitatory post-synaptic potential accompanied by a decrease in the threshold required to fire an action potential in the postsynaptic neuron (Bliss and Lomo, 1973). They termed this increase *long-lasting potentiation,* now referred to as *long-term potentiation* (LTP). Such changes in synaptic strength are bidirectional, wherein a failure to

consistently activate a target neuron to induce potentiation leads to long-term depression (LTD) (Dudek and Bear, 1992).

The significance of LTP in learning and memory came from studies wherein pharmacological blockade of LTP resulted in spatial memory impairments in rats that were previously trained in a Morris water maze (Morris et al., 1986). LTP can be divided into two stages e-LTP (early) and l-LTP (late). While molecular mechanisms underlying e-LTP involve post-translational modifications of proteins, l-LTP involves localized synthesis of new proteins (Klann and Dever, 2004).

Neuronal RNA granules and localized RNA

Previously, it was postulated that new protein synthesis takes place in the cell body and proteins are subsequently transported to distal compartments of the neuronal cell. When polyribosomes were first observed at the base of synaptic spines, (Steward and Levy, 1982), it raised the possibility that RNAs could be locally translated upon receiving a synaptic signal. This was supported by the experiments in rat hippocampal slices, where the cell body is spatially separated from the synaptic neuropil. The neuropil treated with protein synthesis inhibitors like anisomycin and cycloheximide showed a reduction in neurotrophin-mediated synaptic plasticity (Kang and Schuman, 1996). Thus this would require that mRNAs, which are localized at synaptic sites, to be packaged and transported over long distances away from the cell body. Researchers injected

fluorescently-tagged transcripts of myelin basic protein (MBP) into oligodendrocytes and observed that the mRNA assembled into granules and was rapidly transported along microtubules (Ainger et al., 1993). In another study, using a membrane permeable nuclei acid stain, SYTO14, it was observed that RNA granules are rapidly transported in neurons (Knowles et al., 1996).

These latter results raised the question of the composition of RNA granules. Subsequently, it was demonstrated that these RNA granules contain transcripts that were packaged with proteins and transported as translationally silent granules. It has been suggested that these localized mRNAs are associated with “stalled” ribosomes, which upon membrane depolarization led to local translation (Krichevsky and Kosik, 2001). A number of RNA binding proteins (RBPs), such as eukaryotic initiation factor 4E (eIF4E) binding proteins, fragile X mental retardation protein (FMRP), cytoplasmic polyadenylation element-binding protein (CPEB), Staufen, zipcode binding protein (ZBP), play roles in packing and trafficking of RNAs in translationally silent granules (Kiebler and Bassell, 2006).

The mRNAs encoding microtubule associated protein2 (MAP2) (Kindler et al., 1996), activity-regulated cytoskeleton associated protein (Arc) (Lyford et al., 1995), β-actin (Tiruchinapalli et al., 2003), CaMKIIα (Mayford et al., 1996) and NMDA receptors are some of the transcripts synaptically localized and increased neuronal activity leads to rapid trafficking of these RNAs into dendrites (Martin and Zukin, 2006). Furthermore, these studies revealed that the absence of these

transcripts, (e.g. CaMKII) lead to defects in l-LTP and long-term memory (Miller et al., 2002). With improved technologies like compartmentalized cultures wherein neuronal cell bodies can be separated from their projections, and high-throughput sequencing, 2000-4500 localized transcripts have been identified in both dendrites and axons, respectively (Holt and Schuman, 2013).

Localized RNAs play a role in synapse formation and refinement, axon growth guidance, dendritic spine morphology and synaptic plasticity (Holt and Schuman, 2013; Swanger and Bassell, 2011). The study of these RNA granules is of significant importance because a large number of neurological disorders are linked to RNA binding proteins (RBP) which play roles in RNA granule translation, (e.g. Fragile X syndrome FMR1) (Mazroui et al., 2002), or granule assembly, (e.g. FUS whose mutation underlies Amyotrophic lateral sclerosis) (Bosco et al., 2010).

In this thesis, I present our findings on Wnt signaling-mediated assembly of localized RNAs, their export from the nucleus and trafficking to the synapse at the *Drosophila* larval neuromuscular junction.

The Drosophila Larval Neuromuscular Junction: A model to study synapse development and plasticity

Discoveries in *Drosophila* have greatly contributed to our understanding of a number of neurobiological processes such as neurotransmitter release, ion channel function, synapse physiology, axon path finding, synapse development

and plasticity. The *Drosophila* larval neuromuscular junction (NMJ) is a simple yet powerful model system for studying synapse development and plasticity (Ruiz‐Cañada and Budnik, 2006). The larval NMJ consists of a single synapse between a presynaptic motor neuron, and the post-synaptic muscle cell, which is organized in a stereotypic fashion. This provides researches the ability to study synapses with single cell resolution as well as allowing comparison of the same synapse across multiple animals. During larval development from first instar to third instar, there is a 100-fold increase in the body wall muscle size (Figure1.1). In order to maintain synaptic efficacy, the motor neuron terminals grow in a contiguous fashion, by the addition of new synaptic varicosities or “boutons”, which are the sites of neurotransmitter release (Gorczyca et al., 1993; Keshishian and Chiba, 1993; Zito et al., 1999) (Figure1.2). Alongside developmental plasticity, the NMJ can be used to study activity and experience-dependent synaptic plasticity (Ataman et al., 2008; Koon et al., 2011).

The NMJ is highly accessible for both, electrophysiology and imaging. The larval cuticle is transparent, allowing for live imaging of the synapse at different stages of development (Koon et al., 2011; Zito et al., 1999). Furthermore, the Drosophila NMJ is glutamatergic (Jan and Jan, 1976), similar to vertebrate central synapses, and the molecular players and mechanisms underlying NMJ development are highly conserved across species. Together, these make findings in this model system highly relevant for all organisms. The larval NMJ has provided seminal contributions to our understanding of synapse

development, plasticity and has become a popular model to study the etiology of neurodegenerative and neuromuscular diseases such as muscular atrophy, myotonic dystrophy and Amyotrophic lateral sclerosis (ALS) (Lloyd and Taylor, 2010).

The success of this system can be attributed to the availability of genetic tools such as bipartite Gal4/UAS expression system (Brand and Perrimon, 1993) (that allows for temporal and spatial control of knockdown or expression of transgenes), the availability of mutants from decades of forward genetic screens and collections of transgenic RNAi lines targeting essentially all fly genes. The short life cycle of *Drosophila*, and a myriad of genetic tools allow for easy genetic manipulation in a relatively short time. Thus, taken together the tractability and accessibility of the system makes the NMJ a convenient and powerful model system.

Figure1.1- *Drosophila* larval body wall muscle and development of the NMJ

A. (Adapted from Budnik and Ruiz-Canada, 2006) Wandering third star stage (left) and first instar stage (right) larval body wall muscle preparations. Muscles are labeled with FITC-conjugated phalloidin. During larval development, the number of muscles does remains unchanged, however each muscle can increase up to100-fold in size. Abdominal segments 1-7 are labeled as A1 to A7.

B. A schematic illustrating NMJ expansion. The presynaptic terminals of the motor neuron grow by addition of new synaptic boutons as the body wall muscle grows in size. (Image courtesy: Vivian Budnik)

Figure1.1- *Drosophila* larval body wall muscle and development of the NMJ

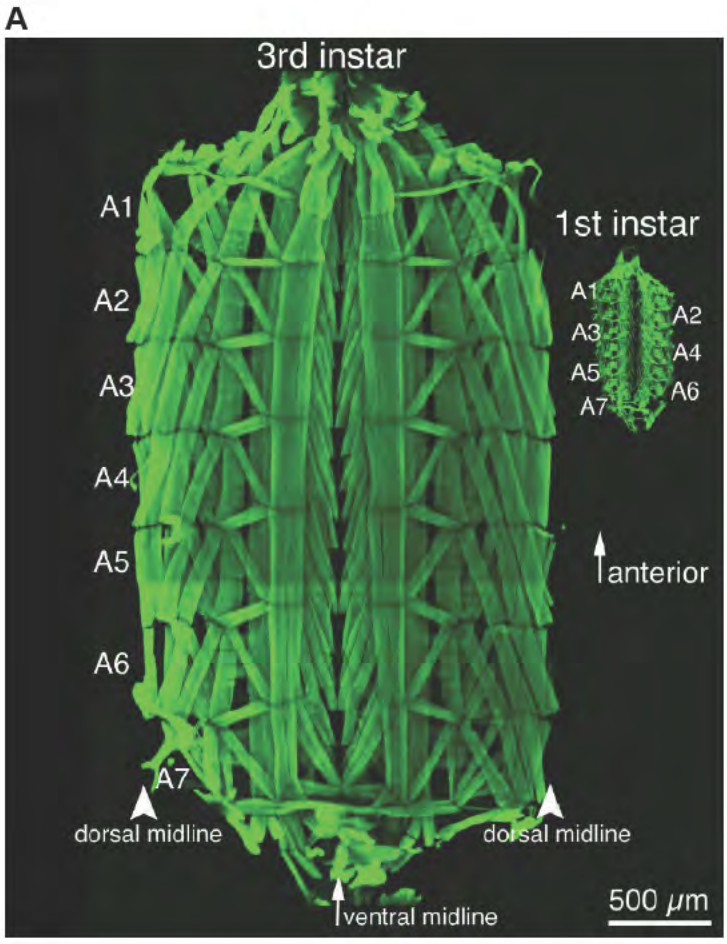

General anatomy of the *Drosophila* larval NMJ

The *Drosophila* larva consists of seven segments, A1 to A7. Each hemisegment consists of 30 skeletal, body wall muscles aligned in a stereotypic fashion (Figure 1.1A). Each muscle cell consists of a single multinucleated myofiber. The cell bodies of the motor neurons are present in the ventral ganglion and they project their axons onto the muscle (Figure 1.2A). (Landgraf and Thor, 2006). The terminals of the motor neurons consist of round varicosities, which are termed “synaptic boutons”, and they are the sites of neurotransmitter release. Similar to vertebrate NMJ, the *Drosophila* NMJ is glutamatergic (Petersen et al., 1997). Ultrastructural analysis of boutons reveals that they contain synaptic vesicles, active zones and mitochondria. Active zones appear as electron dense T-shaped structures probably due to highly enriched protein content (Jia et al., 1993).

Development of mature synapses (during larval growth or activity-dependent new bouton formation) begins with the addition of new synaptic boutons. Initially, these naïve or “ghost” boutons contain synaptic vesicles but lack any post-synaptic specializations. Subsequently, recruitment of post-synaptic components such as scaffolding proteins and glutamate receptors results in synapse maturation (Ataman et al., 2008).

Figure 1.2- Larval neuromuscular junction

(A) An illustration of larval anatomy: brain, ventral ganglion (red) and muscles (green). (Top right) A schematic of motor neuron terminals or “boutons” at muscles 6 and 7.

(B) Synaptic boutons from a 3rd instar larval preparation, double-stained with presynaptic membrane marker anti-HRP (green) and postsynaptic protein anti-DLG (red). (B’) An illustration of the presynaptic (green) and postsynaptic (red) compartments.

Throughout this dissertation, muscles 6 and 7 at segments A2-A4 were examined.

Figure 1.2- Larval neuromuscular junction

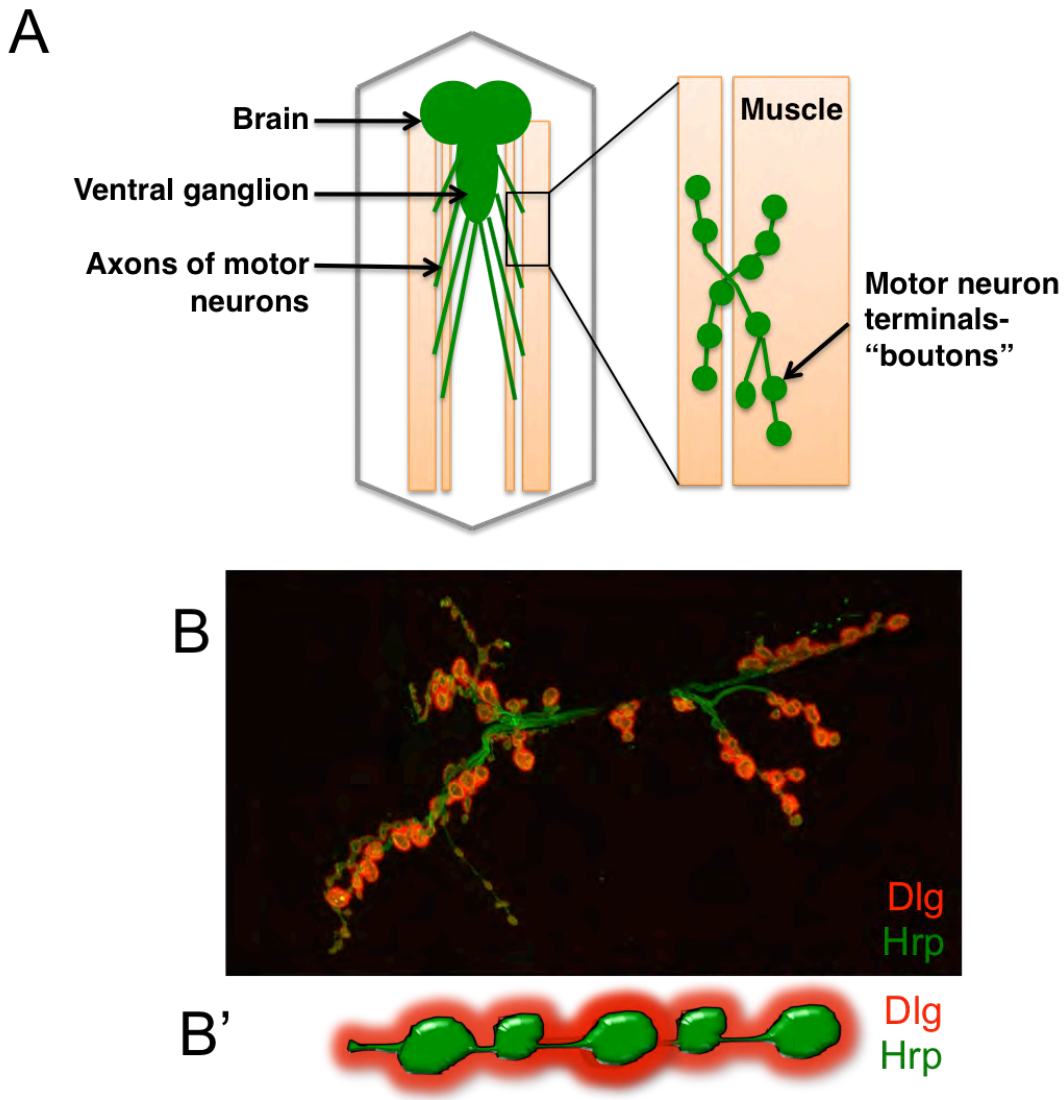

Wnt Signaling Pathway

Since the identification of RNP assembly and export from the nucleus in Chapter II is linked to Wnt signaling, this pathway is described here in more detail.

Wnts are secretory proteins that are known to play a role in patterning, axon guidance, dendritic morphogenesis, synapse development and plasticity (Budnik and Salinas, 2011; Ciani et al., 2004). The Wnt family has multiple members, 5 in worms, 7 in flies, 15 in zebrafish and 19 in mice and a myriad of Frizzled receptors which include 3 in worms, 5 in flies, 12 in zebrafish and 11 in mammals, along with non-conventional receptors such as Derailed (DRL), which belongs to the receptor tyrosine kinase (RYK) family. The combinatorial use of different Wnts and its multiple receptors can mediate diverse cellular functions (Speese and Budnik, 2007). Wnt pathway mutants in humans have been linked to Alzheimer's disease, Huntingtin's disease and schizophrenia (Caricasole et al., 2005; De Ferrari and Moon, 2006).

Wnt signaling has different down-stream modulators. In the canonical pathway, Wnt binding to Frizzled receptors activates Dishevelled (DLV) that stabilizes cytoplasmic β-catenin, which can enter the nucleus and regulate gene expression (Clevers and Nusse, 2012; Wodarz et al., 1999). In the divergent canonical pathway, DVL binds to microtubules and inhibits GSK3β-mediated phosphorylation of microtubule-associated proteins, thereby increasing microtubule stability (Ciani et al., 2004). This pathway plays a role in presynaptic

differentiation, receptor clustering and axon growth cone remodeling (Korkut, 2009). Other pathways include the planar polarity pathway, Wnt/Calcium pathway and the Frizzled Nuclear Import (FNI) pathway (FNI- described in detail below).

Wnt Signaling Pathway at the Drosophila NMJ

The role of Wnts specifically at the NMJ is conserved across species, from worms to mammals (Korkut, 2009; Speese and Budnik, 2007). At the fly NMJ, Wnt1/Wingless (Wg) released by presynaptic boutons activates bidirectional transduction pathways in the pre- and post-synaptic compartments. *Packard et al*. used a temperature sensitive Wg mutant to block Wg signaling at the NMJ and observed both, a decrease in synaptic outgrowth and altered bouton morphology (Packard et al., 2002). A subset of these boutons lacked proper assembly of the postsynaptic specializations, like Discs large (DLG), a scaffolding protein and GluR assembly and were termed “ghost boutons” (Ataman et al., 2006). The ultrastructural analysis of these boutons revealed that they lacked active zones, mitochondria and had a poorly developed subsynaptic reticulum. These defects could be rescued by expressing Wg in the motor neuron. Consistent with this result, overexpression of Wg in the motor neuron led to increased synaptic outgrowth, thus establishing a role of Wg signaling in NMJ development. Wnt signaling (a divergent canonical Wnt pathway described above) in the motor neuron regulates the cytoskeletal dynamics required for NMJ

growth and postsynaptically it activates the Frizzled Nuclear Import (FNI) pathway (Mathew et al., 2005).

In this pathway, Wg binds to the Drosophila Frizzled-2 (DFz2) receptor on the muscle surface and triggers internalization of the receptor, which is then trafficked to the nucleus via interaction between the carboxy-terminal PDZ-binding sequence of DFz2 and dGRIP (Drosophila homologue of GRIP, a 7-PDZ-domain glutamate-receptor binding protein) (Ataman et al., 2006b). An 8 kDa C-terminal fragment of the receptor (DFz2C) is cleaved (by an as yet unknown protease) and is imported into the nucleus (Mathew et al., 2005). Activity-dependent remodeling of synapses is also linked to Wnt signaling (Ataman et al., 2008). Spaced stimulation by either high potassium-induced stimulation or optogenetic stimulation enhances Wg secretion leading to bouton outgrowth and formation of ghost boutons- which here represent a transient state of new bouton formation that initially lack any postsynaptic specializations but over time acquire active zones and GluRs. Concurrently, nuclear import of DFz2C is also increased. Since FNI pathway mutations have increased “ghost” or immature boutons, the nuclear role of DFz2C was linked to synapse maturation, however the underlying mechanisms were unknown.

In Chapter II of this dissertation, in collaboration with Sean Speese and James Ashley, we found that nuclear DFz2C associates with large ribonucleoprotein granules that localize in the perinuclear (between inner and outer nuclear membrane) space and exit the nucleus by budding through the

nuclear envelope (NE) instead by canonical export through the Nuclear Pore Complex (NPC). This mechanism resembles the nuclear egress of Herpes viruses (discussed below).

RNA granule assembly and export from the Nucleus

The nuclear pore complex (NPC), composed of multiple copies of ~30 nucleoporins (NUPs) is a barrier that selectively gates cargos entering or exiting the nucleus (Grunwald et al., 2011). mRNAs once transcribed are coated with the 5' cap-binding, poly-(A) binding protein, exon junction complex (EJC) and other such proteins and thus exist in the cell as ribonucleoprotein (mRNP) particles (Moore, 2005). mRNAs exit the nucleus by forming a complex with NXF1/Tap1 or Crm1, both of which are export factors. They bind mRNPs and interact with FG (Phenylalanine Glycine) repeats of the NUPs, which form a molecular sieve-like permeability barrier (Kohler and Hurt, 2007) and facilitate the exit of the transcripts.

Transcripts that have common function or that are localized to specific subcellular sites can be co-packaged into a single RNP granule, which includes the mRNAs, and RBPs that regulate the fate of the transcripts (Gerber et al., 2004; Keene and Tenenbaum, 2002). An intriguing question has been where these supramolecular assemblies of RNP granules are assembled (Moore, 2005), in the nucleus or the cytoplasm?

The nuclear pore also serves as a size-exclusion barrier, allowing

macromolecular assemblies of <39nm diameter to exit the nucleus (Grunwald et al., 2011). However, the Balbiani ring mRNA (40kb) of *Chironomous tetanus* is packaged in a 50nm particle, which undergoes structural rearrangement of RNP packaging and threads or squeezes out of the NPC (Zhao et al., 2002). Furthermore, not all pores are identical and some NPCs may be specialized to handle export of specific mRNPs (Grunwald et al., 2011). While in some cases there is possibly bulk RNA export, in other instances RNA export can be selective process since not all mRNAs are exported immediately after transcription and maybe retained in the nucleus until signals to export the RNP are received (Wickramasinghe and Laskey, 2015).

Export of β-actin mRNA has been studied extensively and it has been found that β-actin mRNAs exit the nucleus one molecule at a time (Grunwald and Singer, 2010). Given the size barrier of the NPC and the studies revealing that RNAs can exit the nucleus as singletons, it was thought that supramolecular assemblies of RNP granules takes place solely in the cytoplasm. A large number of RNP granules are assembled in the cytoplasm. For example, processing bodies (PBs) and stress granules (SGs) that serve to silence mRNA translation are found in a large number of cell types and are assembled in the cytoplasm (Thomas et al., 2011).

However, in our study at the Drosophila NMJ, we found large RNP granules (~200nm) that assembled in the nucleus/perinuclear region, raising the question of how they can be exported via the nuclear pore complex.

Nuclear egress of Herpes Viruses- another mode of nucleocytoplasmic communication

A unique mode of nucleocytoplasmic communication is the nuclear egress of herpes viruses. The process of viral maturation involves two steps: a) the double-stranded viral DNA genome is first encased in an icosahedral proteinaceous capsid in the nucleus, b) the capsid is then surrounded by proteinaceous material (tegument), followed by envelopment by an outer lipid envelope derived from cellular membranes in the cytoplasm. However, the transition of the virion from the nucleus to the cytoplasm involves a unique mechanism. Electron microscopy studies of herpes virus infected cells reveal that herpes virus capsids exit the nucleus by budding through the nuclear envelope (Mettenleiter et al., 2009; Mettenleiter et al., 2013a).

The viral capsid assembled in nucleus is too large (~125nm) to exit via the NPC. Instead they exit the nucleus by remodeling the nuclear lamin network and nuclear envelope. Nuclear Lamins are Type V intermediate filament proteins that form a structural meshwork just beneath the inner nuclear membrane (INM). This framework forms a barrier that must be broken down in order for the virion to gain access to the INM (Johnson and Baines, 2011). Two Herpes virus proteins, pUL34 and pUL31 interact with each other and associate with the INM where they recruit protein kinase C (Park and Baines, 2006), which can phosphorylate and induce the local thinning of the Lamin framework. Other viral proteins pUL17, pUL25 and glycoproteins then dock at the INM, select mature capsids and begin

the primary envelopment process by budding into the inner nuclear membrane. This leads to the formation of an INM bound virion in the perinuclear space. (Figure 1.3A) The viral glycoproteins then mediate fusion between the virion vesicle and outer nuclear membrane (ONM), and the virion is released naked into the cytoplasm (Figure 1.3B). This budding pathway was thought to be exclusive to herpes family of viruses.

We now know that akin to HSV budding, there is an endogenous pathway for budding large RNA granules out of the nucleus and that Herpes viruses likely high jacked this pathway for their own export (Chapter II). Thus to elucidate the mechanism of the pathway, we screened for host candidates that facilitate egress.

Figure 1.3- Herpes Virus egress

Illustration of Herpes virus egress pathway. This includes local breakdown of Lamins to primary envelopment at the INM. This results in the formation of a membrane-bound virion residing in the perinuclear space, which then fuses with the outer nuclear envelope to complete the de-envelopment process.

Figure 1.3- Herpes Virus egress

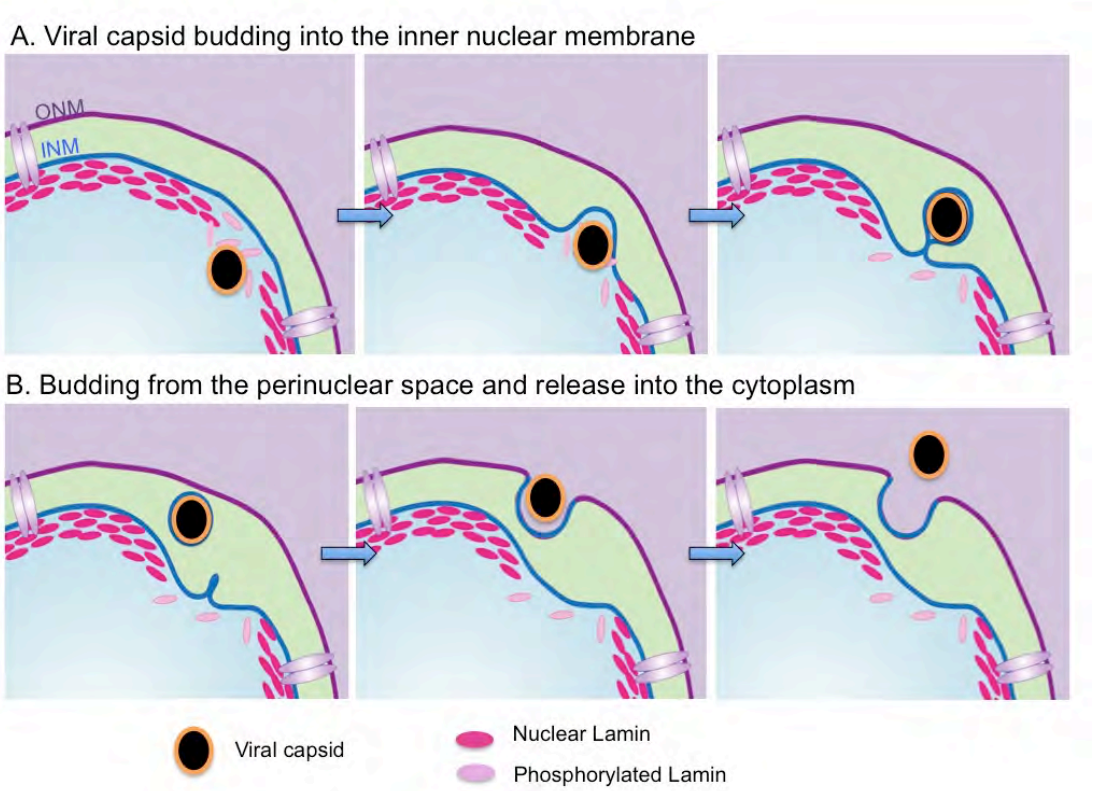

Torsin- AAA ATPase and its role in nuclear membrane remodeling

With the aim of understanding the mechanism underlying nuclear envelope budding for RNP export we decided to exploit what was known about herpes virus egress. Torsin, a host protein, plays a role in Herpes Virus egress (Maric et al., 2011b), where expression of dominant-negative Torsin leads to an accumulation of virus-like vesicles in the perinuclear space and ER.

Torsin-1A belongs to the AAA+ family of ATPases (ATPases associated with various activities) that resides in the lumen of the endoplasmic reticulum (Kustedjo K, 2000). Mammals have four torsin isoforms; Torsin-1A, Torsin-1B, Torsin-2A and Torsin-3A. A hallmark of members of this family is a 200-250 amino acid ATPase domain. This ATPase domain encompasses several motifs, such as the ATP-binding motif, Walker A and the ATP-hydrolysis motifs Walker B, Sensor 1 and Sensor 2 (Hanson and Whiteheart, 2005; Laudermilch and Schlieker, 2016). AAA-ATPases generally assemble into homohexameric rings and interact with their substrates via a central pore (Iyer et al., 2004; Neuwald AF, 1999). They play a role in a variety of cell biological processes like cytoskeletal dynamics (dynein), protein folding and degradation (Clp/Hsp100 family), membrane trafficking and organelle biogenesis (Vps4) (Breakefield et al., 2001). Interestingly, AAA-ATPases can remodel membranes by disassembling supramolecular complexes: a) N-ethylmaleamide sensitivity factor (NSF) plays a role in vesicle fusion by recycling of v-SNARE and t-SNARE and b) Vps4

provides the motive force to disassemble the ESCRT III complex during mutli-vesicular body biogenesis (Iyer et al., 2004).

A three base pair deletion, (ΔGAG, ΔE- 30% penetrant) in Torsin-1A has been implicated in early-onset dystonia (Ozelius et al., 1997), a movement disorder characterized by involuntary muscle contractions. Onset of symptoms occurs between ages 5-28, a time window critical for learning and plasticity in the brain (Granata et al., 2008). Early research, given the ER localization and AAA-ATPase function of Torsin, suggested that it plays a role in protein quality control (Hewett et al., 2003). In recent years, Torsin has been shown to have a role at the NE (Goodchild et al., 2005; Naismith et al., 2004) via its interaction with Lamin associated polypeptide 1 (LAP1), a transmembrane INM protein (Goodchild and Dauer, 2005). This is consistent with the observations that the Dystonia modeled TorsinΔE mutant (Cao et al., 2005) and the torsin substrate-trap mutant Torsin^{E-Q} (that binds to ATP but does not hydrolyze it, forming a "locked" complex) both abnormally accumulate at the NE (Naismith et al., 2009). Torsin interacts with LULL1 (Luminal domain Like LAP1) in the ER, where LULL1 functions to recycle Torsin back to the nuclear envelope (Vander Heyden et al., 2009). Interestingly, Torsin knockout (Torsin$^{-/-}$) and dystonia knock-in mouse models (Torsin$^{\Delta E/\Delta E}$) both display abnormal blebbing of INM in neurons in the spinal cord and cortex (Goodchild et al., 2005). This apparent neuronal specificity is due to presence of Torsin-1B in non-neuronal tissue, since double knockdown of Torsin-1A and 1B results in similar defects in the nuclear envelope in non-

neuronal cells (Kim CE, 2010). Intriguingly, knockdown of LAP1 alone results in defects at the nuclear envelope in neuronal as well as non-neuronal cells. Recent studies demonstrate that LAP1 is essential for not just recruiting Torsin to the NE but also for stimulating ATPase activity of Torsin (Zhao et al., 2013).

Interestingly, the blebbing phenotypes in the mouse models bear some resemblance to perinuclear RNP granules (Chapter II and Speese et al., 2012). Given the roles of Torsin in Herpes virus egress, Torsin was a prime candidate for playing a role in the budding of cellular RNPs. Furthermore, being an ATPase; Torsin could potentially mediate membrane remodeling.

In *Drosophila*, there is only one Torsin isoform. Knockdown of Torsin results in locomotion defects in the larvae and is lethal by the pupal stage of the life cycle (Wakabayashi-Ito et al., 2011). We investigated the role of Torsin in RNP budding in Chapter III.

Figure1.4- Domains and localization of Torsin

(A) Representation of the conserved domains across AAA-ATPases. Like other AAA-ATPases, Torsin has the ATP-binding domain (Walker A) and the ATP hydrolysis domains (Walker B, Sensor 1 and Sensor 2).

(B) Torsin (purple) resides in the perinuclear space and ER. It is recruited to the NE via interaction with LAP1 and it interacts with LULL1 in the ER.

Figure1.4- Domains and localization of Torsin

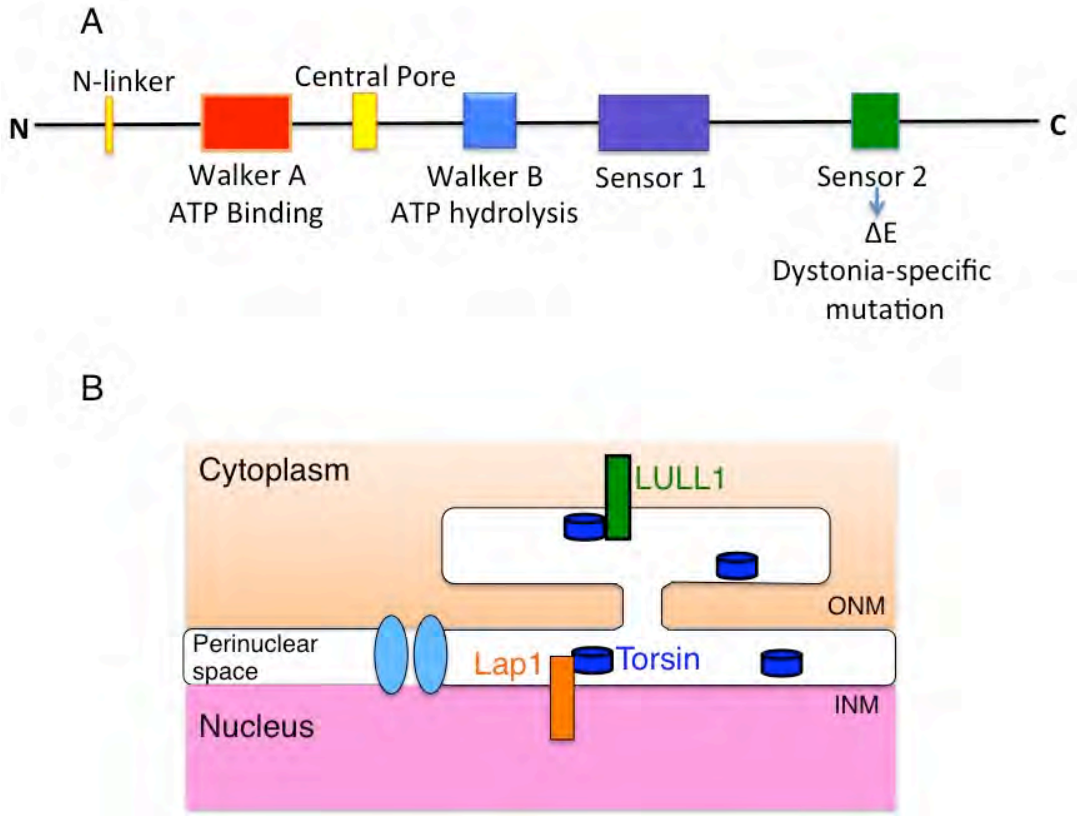

Targeted localization of released RNA granules in the cytoplasm

Once RNAs exit the nucleus, the next question is how are they targeted to specific synaptic sites. In the case of a neuron with a 100 different synapses, how would an RNP know its correct destination? Little is known about targeted RNP localization.

As mentioned in Neuronal RNA granules section, work by Ainger et al., 1993 and Knowles et al., 1996 demonstrated that RNA granules are rapidly transported along microtubules. In these studies RNA granule trafficking was disrupted upon colchicine treatment (a microtubule-depolymerizing agent) but not upon Cytochalasin-D (an actin-depolymerizing agent) treatment. This was some of the early work that suggested that long-range transport of RNA granules was mediated by microtubules (MTs).

In order to transport RNAs to specific sites, they are bound by RNA binding proteins (RBPs), adaptor proteins and motor proteins (Buxbaum et al., 2015). RBPs like hnRNP A2 (myelin basic protein mRNA), ZBP (β-actin mRNA), CPEB (CaMKIIα mRNA), all play a role in neurons or oligodendrocytes to traffic specific transcripts (Sinnamon and Czaplinski, 2011). In order to translocate the RNPs, the kinesin and dynein families of processive motor proteins are required traffic cargo along microtubules in the anterograde and retrograde directions respectively (Gagnon and Mowry, 2011).

In neuronal RNA trafficking the role of kinesin has been best characterized. Kinesins are composed of two heavy chains (KHC or KIF5) and

two light chains (KLC). In Kanai et al., 2004, researchers purified neuronal RNA granules that were enriched for CaMKIIα and Arc mRNA and associated 42 RBPs (Kanai et al., 2004). Their study revealed that kinesin traffics RNPs distally to dendrites. This transport was enhanced upon overexpression of KIF5, while blocking kinesin reduced dendritic trafficking of select transcripts. Studies also indicate that actin filaments and their motors, such as MyosinV, play a role in the translocation of RNPs to dendritic spines (Fujii et al., 2005).

During *Drosophila* oogenesis, *oskar* mRNA is localized to the posterior of the developing oocyte. This localization of oskar is essential to establish the anterior-posterior axis, and requires an interplay of both microtubules and actin-based motors (Krauss et al., 2009). While microtubules mediate long-range movements of RNPs from the nucleus to the posterior of the oocyte, precise short-range localization and entrapment of *oskar* RNPs at the posterior is mediated by actin (Krauss et al., 2009). However, these long versus short-range interactions are still ill defined. Recent studies have demonstrated that actin can serve as tracts for long-range transport of vesicles (Schuh, 2011). However, very little is known about the long-range transport of mRNP cargo along actin tracks.

Nesprin: A "railroad track" in the cytoplasm

Nesprins (Nuclear Envelope SPectRIN repeat proteins) are a conserved family of proteins localized to the ONM (Starr DA, 2002). The characteristic structural features of Nesprins include an N-terminal motif that allows interaction

with the cytoskeleton, a central rod region which is composed of multiple spectrin repeats, transmembrane domain and a C-terminal KASH (Klarsicht/ANC-1/Syne homology). Some Nesprin isoforms can span both ONM and INM and interact with nuclear Lamins (Razafsky and Hodzic, 2009). KASH domain proteins interact with SUN (Sad1, UNC-84) domain proteins, which reside in the INM (Hodzic et al., 2004). The C-terminal SUN domain resides in the perinuclear space, whereas the N-terminal region interacts with the nucleoskeleton, which is LaminA/C or LaminB. SUN domain proteins recruit KASH proteins to the nuclear envelope (Razafsky and Hodzic, 2009). Together they form the LINC complex (LInkers of Nucleoskeleton to Cytoskeleton) and function as a molecular scale, defining the distance between the nuclear envelopes.

Drosophila has two SUN domain proteins (Klaroid and Giacomo) and two KASH domain proteins (Klarsicht and msp-300/Nsp1). While Nsp1 interacts with actin, Klarsicht interacts with microtubules. Nsp1 is a giant protein and has several isoforms, some in excess of 1.4 megaDaltons. At the *Drosophila* NMJ, Nsp1 plays roles in positioning the muscle nuclei (Elhanany-Tamir et al., 2012b) and GluRIIA assembly at the postsynapse (Morel et al., 2014b). While studying the localization of Nsp1, we found Nsp1 formed long filaments, extending from the nucleus to the synapse, which served as tracks for RNP transport (described in Chapter V).

Figure 1.5- A schematic representation of Nsp1

Nsp1 is a giant transmembrane protein that is inserted in the outer nuclear membrane. At the cytoplasmic end it interacts with Actin, and via its KASH domain it can interact with SUN domain proteins in the perinuclear space. SUN domain proteins interact with Lamins, which represent the nucleoskeleton.

Figure 1.5- A schematic representation of Nsp1

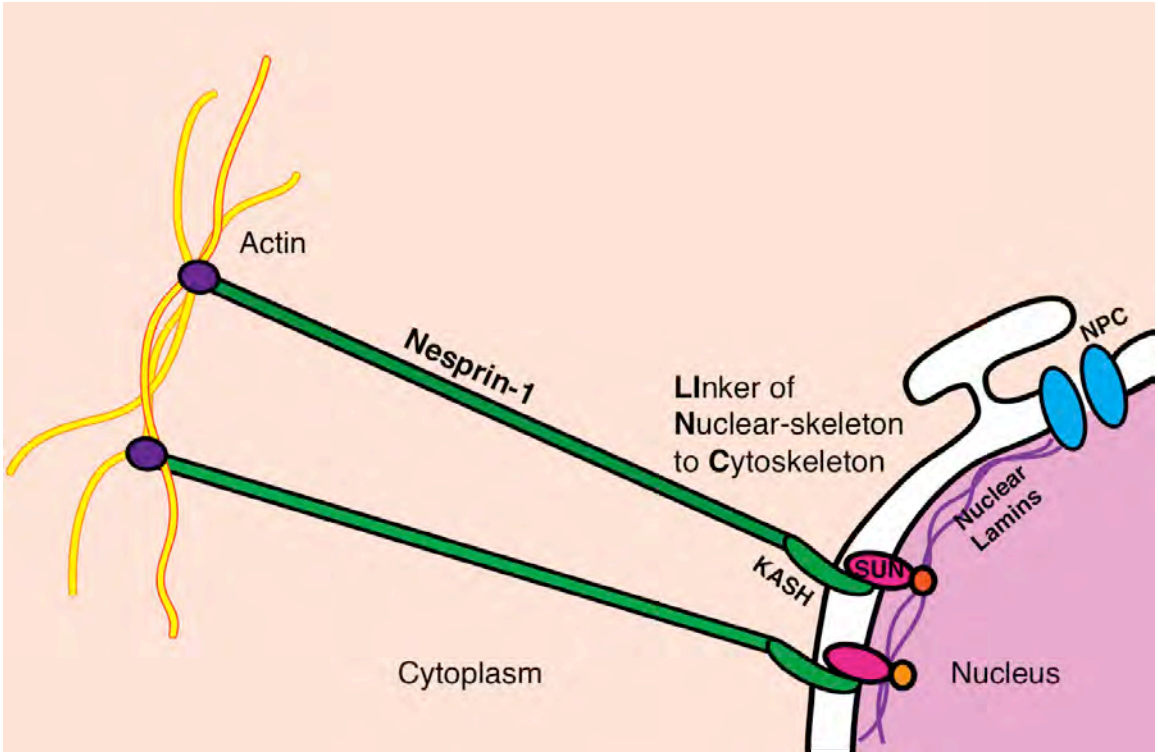

In summary, in Chapter II of my thesis, I will present findings from a project led primarily by Sean Speese, a former postdoc in the lab, which resulted in the discovery of a novel pathway for large RNP export. Our investigations into the FNI pathway and the nuclear role of DFz2C lead to the seminal discovery that, as a consequence of Wg signaling, large RNP granules containing synaptically localized transcripts are assembled in the nucleus in association with Dz2C and exit the nucleus by budding through the nuclear envelope.

In Chapter III, I present the studies that provide further mechanistic insights in the nuclear envelope budding pathway (NEB) pathway. We found that Torsin, a AAA-ATPAse, whose mutation in humans is linked to dystonia, mediates remodeling of the INM. Torsin likely mediates scission of the INM during primary envelopment of mega-RNPs. Thus in the absence of Torsin, these RNPs fail to exit the nucleus and are trapped, maintaining connection to the INM, in the lumen of the nuclear envelope. This study provides significant insight into the role of Torsin in synaptic development. In Chapter IV, I describe how the Drosophila ovary can be used as a model system to further elucidate mechanisms underlying megaRNP budding.

In Chapter V, I describe how long-range transport of synapse-specific RNPs from the nucleus to the synapse is mediated. We show that Nsp1-F-actin filaments serve as “railroad” tracks to transport synaptic RNAs from the nucleus to specific synaptic sites.

Preface to Chapter II

This chapter describes the discovery of nuclear envelope budding as a novel RNA export pathway within the context of Wnt signaling and synaptic development at the *Drosophila* NMJ.

My contributions to this chapter are: Figures 2.1P-S, 2.5 A2-A4 C-D, 2.7B-E G-K, 2.8E-L
Sean Speese contributed: Figures 2.1A-L, 2.2, 2.3A C-H, 2.4A-D F, 2.5A-B E-G,
James Ashley contributed: Figures 2.1M-O, 2.3B, 2.6A-B, 2.7 A-B, 2.8A-D, M
Romina Barria contributed: Figures 2.1D-L, 2.7A F J-K L
John Nunnari contributed: Figures 2.3A C-H, 2.4A-D, 2.5 E-G
Yihang Li contributed: Figure 2.7M
Alex Koon contributed: Figures 2.6A-B
Vivian Budnik contributed Figure 2.4E

The following chapter has been published as:

Speese SD*, Ashley J*, **Jokhi V**, Nunnari J, Barria R, Li Y, Ataman B, Koon A, Chang YT, Li Q, Moore MJ, Budnik V. *Nuclear envelope budding enables large ribonucleoprotein particle export during synaptic Wnt signaling.* **Cell. 2012** May 11; 149(4):832-46.

Chapter II

Nuclear Envelope Budding Enables Large Ribonucleoprotein Particle Export during Synaptic Wnt Signaling

Introduction

Wnts are secreted signaling proteins that are important for embryonic pattern formation and cellular differentiation (Siegfried E, 1994) and also play pivotal roles during activity-dependent synaptic development (Budnik and Salinas, 2011). In mammals, Wnts promote synapse differentiation and plasticity and contribute to neuronal excitability (Budnik and Salinas, 2011; Cerpa et al., 2011; Varela-Nallar L1, 2010). At the *Drosophila* larval neuromuscular junction (NMJ) the Wnt-1, Wingless (Wg), is released by presynaptic boutons in a manner regulated by neuronal activity and is critical for proper synaptic bouton differentiation (Ataman et al., 2008; Packard et al., 2002). In the absence of Wg signaling, NMJs fail to expand properly during larval development (Miech et al., 2008). Further, a subset of synaptic boutons (ghost boutons) is devoid of active zones and postsynaptic structures and fails to recruit postsynaptic proteins (Ataman et al., 2006b; Packard et al., 2002). Wg release by motorneurons activates alternate transduction pathways in motorneurons and muscles (Mathew et al., 2005; Packard et al., 2002). In postsynaptic muscles, Wg turns on the Frizzled Nuclear Import (FNI) pathway in which the Wg receptor, DFrizzled-2 (DFz2), is internalized and transported to muscle nuclei (Ataman et al., 2006; Mathew et al., 2005). Subsequently, a C terminal cleavage product, DFz2C, is imported into the nucleus (Mathew et al., 2005) via canonical nuclear import machinery (Mosca and Schwarz, 2010) where it localizes to discrete foci (Ataman et al., 2008; Mathew et al., 2005). A similar transduction pathway has

been reported for the Wnt receptor Ryk during mammalian cortical neuron development (Lyu et al., 2008). However, the nuclear function of these DFz2C/Ryk C-terminal fragments remains unexplored. We report that FNI signaling leads to nuclear DFz2C fragments being organized into ribonucleoprotein particles containing mRNAs encoding postsynaptic proteins. These particles exit the nucleus via a mechanism akin to the nuclear egress of herpes virus capsids. During viral capsid egress, the nuclear lamina is disrupted through phosphorylation by protein kinase C (PKC), which is required for the budding of an inner nuclear membrane (INM) bound viral particle into the perinuclear space (between the INM and the outer nuclear membrane [ONM]). Subsequent fusion of the INM surrounding the virus with the ONM releases the naked viral capsid into the cytoplasm. We find that localization of DFz2C granules to the perinuclear space requires the A-type lamin, LamC. Further, formation of INM invaginations, through which the DFz2C granules exit, requires atypical PKC (aPKC), which likely phosphorylates LamC. Significantly, disruption of this process leads to phenotypes paralleling those observed in laminopathy models. Our studies thus provide evidence for an unanticipated mechanism by which cellular mRNAs can exit the nucleus, insight into the mechanisms of postsynaptic apparatus assembly in response to Wnt signaling, and a potential explanation for how certain human lamin mutations result in muscular dystrophy.

RESULTS

DFz2C and Lamin C form specializations at the nuclear lamin

To elucidate the nuclear function of DFz2C, we sought to determine the subnuclear localization of DFz2C foci in muscle cells using confocal microscopy (Figure 2.1). DFz2C foci localized to the nuclear periphery (Figure 2.1A) and consisted of accumulations of discrete DFz2C puncta (Figure 2.1A; arrows). Co-labeling with antibodies to the *Drosophila* A-type lamin, LamC, a component of the nuclear lamina that forms a lattice beneath the inner nuclear membrane (INM), revealed that LamC forms "framework-like" structures surrounding the DFz2C puncta (Figure 2.1A). Thus, DFz2C fragments are associated with a specialization of the nuclear lamina.

Formation of DFz2C foci was dependent on the presence of LamC, as null mutants in *lamC* virtually eliminated DFz2C foci (Figure 2.1B). Likewise, LamC framework-like structures depended on DFz2, as mutations in *dfz2*, downregulation of *dfz2,* or DFz2 overexpression [which behaves as a dominant negative (Mathew et al., 2005; Packard et al., 2002)] significantly decreased the number of LamC foci (Figure 2.1B). Further, both DFz2C foci and LamC framework-like structures were significantly upregulated in the hyperexcitable K^+ channel double mutant *eag Sh*, which exhibits increased synaptic activity (Wu et al., 1983) (Figure 2.1B). This parallels previous data showing that the number of nuclear DFz2C foci correlates with synaptic activity (Ataman et al., 2008). Thus,

DFz2C foci and LamC framework-like structures are mutually dependent for their formation, and synaptic activity leads to analogous changes in their numbers.

Mutations in the human *LMNA* gene lead to a diverse set of disorders (Burke and Stewart, 2002), including muscular dystrophies (Burke and Stewart, 2002; Mejat et al., 2009) such as autosomal dominant Emery-Dreifuss muscular dystrophy (AD-EDMD) (Mejat et al., 2009; Ostlund et al., 2001). Expression of the AD-EDMD mutant protein results in formation of LMNA-positive "O-ring" structures in the nucleus (Ostlund et al., 2001; Schulze et al., 2005). The same structures are also observed when expressing a mutant *lamC* transgene modeled after the human mutant gene (Schulze et al., 2005) Notably, we also observed nuclear O-ring structures in the muscles of *Drosophila* larva heterozygous for a LamC-GFP-trap (*lamC*$^{GFP\text{-}trap}$/+), in which GFP is inserted in frame within the region encoding the LamC rod domain (Morin et al., 2001) (Figure 2. 1C). In this strain, we found that both DFz2C and LamC-GFP acquired the form of an O-ring, and both the appearance of DFz2C as individual granules and LamC as a framework surrounding the granules was lost (Figure 2.1C). This suggests that insertion of GFP within the rod domain in *lamC*$^{GFP\text{-}trap}$ alters the normal behavior of the protein, and underscores the dependence of DFz2C foci on wild type LamC.

The strong dependence of DFz2C foci on normal LamC predicts that mutations in *lamC* should elicit phenotypes resembling those of mutations disrupting the FNI Wnt signaling pathway. Consistent with this, *lamC* null

mutants, larvae expressing LamC-RNAi in muscle and *lamC*$^{GFP\text{-}trap}$/+ larvae all exhibited a significant increase in the number of “ghost boutons” (Figure 2.1D-J), undifferentiated synaptic boutons that are a hallmark of FNI pathway disruption (Ataman et al., 2006a; Packard et al., 2002). These undifferentiated ghost boutons lack the entire complement of postsynaptic proteins, including the PSD-95 homolog, Discs-Large (DLG) (Figure 2.1F-I), and glutamate receptors (Ataman et al., 2006a). In both *lamC* null animals and those expressing LamC-RNAi in muscles, synaptic arbors were morphologically disrupted, being composed of enlarged tubular boutons instead of the normal small “beads on a string”(Figure 2.1L). This phenotype is also observed in *wg* mutants (Packard et al., 2002). Like other mutations affecting the FNI pathway, *lamC* null mutants also exhibited a decrease in the number of mature boutons (Figure 2.1K). Recent evidence in mice indicates that NMJ defects precede muscle degeneration during laminopathies (Mejat et al., 2009).

Synaptic transmission was also altered in a similar manner in *lamC* and *dfz2* mutants, as well as upon overexpressing DFz2 in muscles, conditions that severely reduce the number of DFz2C/LamC foci. In the above genotypes, the frequency of spontaneous miniature excitatory junctional potentials (mEJPs) was significantly increased (Figure 2.1M). The amplitude of mEJPs was also increased in these strains (Figure 2.1N), suggesting a defect in postsynaptic receptors. This suggestion was supported by morphological analysis of GluRIIA clusters, which showed an increase in volume normalized to bouton volume and

an increase in total signal intensity (Figure 2.1P-S). Nevertheless, the amplitude of EJPs was normal (Figure 2.1O). This is not surprising, as larval NMJs are capable of homeostatic compensation as a result of changes in postsynaptic activity (Petersen et al., 1997). A slightly different profile was observed in *lamC*$^{GFP\text{-}trap}$/+ larvae, in which DFz2C/LamC foci are still present, albeit with abnormal morphology. Although mEJP amplitude was increased (Figure 2.1N), mEJP frequency was unaltered (Figure 2.1M) and EJP amplitude showed a small but significant decrease compared to wild type controls (Figure 2.1O). Taken together, our results indicate that the nuclear lamina plays a specific role in synapse development and function by participating in the FNI signaling pathway in postsynaptic muscles.

Figure 2.1- Subnuclear localization of DFz2C and LamC at larval muscle nuclei, their interdependence, and defective NMJs in *lamC* mutants.

(A) LamC (green) and DFz2C (red) immunolabeling (deconvolved) of a muscle nucleus containing a DFz2C/LamC foci (box; enlarged in right panels) localized to the periphery of the nucleus (arrowhead in XZ plane panel). Arrows point to a DFz2C granule within the framework-like structure formed by LamC.

(B) Number of DFz2C and LamC foci per nucleus normalized to wild type controls in the indicated genotypes. ***= p< 0.0002; *= p<0.05. Number of foci analyzed is wild type=450, *LamC*=413, *dfz2*/Df=302, *eag Sh*=530, Gal4 driver control (C57-Gal4/+)= 328, muscle expression of DFz2 =617, muscle expression of DFz2-RNAi =593.

(C) Localization of LamC-GFP (green) and wild type LamC (blue) in a muscle nucleus from the $lamC^{GFP\text{-}trap}$/+ strain in relationship to DFz2C (red), the DFz2C/LamC foci appear as “O-rings” (box; enlarged in right panels). Inset in upper left panel is the same nucleus but overexposed to show low levels of LamC-GFP at the nuclear lamina. Calibration bar is 5 μm for A (left column), 2 μm for A and C (right columns), 7μm for C (left column). All images are single confocal slices.

(D-I) Third instar larval NMJs at muscles 6 and 7 double labeled with antibodies to HRP (red) and DLG (green) in (D,E) a wild type NMJ at (D) low and (E) high magnification, (F, G) a *lamC* null mutant NMJ at (F) low and (G) high magnification, and (H, I) an NMJ from a larva expressing LamC-RNAi in muscles

using the C57-Gal4 driver (LamC-RNAi-muscle). Arrowheads point to “ghost boutons”, which are devoid of DLG immunoreactivity. Calibration bar is 30 μm for D, F, H, and 12 μm for E, G, I.

(J, K) Morphometric analysis of NMJs showing (J) the number of ghost boutons, and (K) the number of boutons.

***= p<0.0001; **= p<0.001; number of NMJs analyzed are 10 for wild type; 19 for *lamC;* 16 for LamC-RNAi-muscle and $LamC^{trap\text{-}GFP}$/+.

(L) Morphology of synaptic boutons in (top) wild type and (bottom) *lamC* mutant, showing the “beads on a string” and “tubular” morphology of NMJ branches in wild type and *lamC* mutant respectively. Calibration bar is 12μm.

(M-O) Electrophysiological analysis of larval NMJs showing (M) frequency of spontaneous mEJPs, (N) amplitude of spontaneous mEJPs, and (O) amplitude of evoked EJPs

***= p<0.0001; **= p<0.001; *=p<0.05; number of NMJs analyzed are 8 for wild type; 8 for *lamC*; 5 for $LamC^{trap\text{-}GFP}$/+; 5 for *dfz2*/Df; and 7 for DFz2 overexpression in muscle.

(P,Q) Third instar larval NMJs double labeled with antibodies to HRP (red) and DGluRIIA (green) in (P) wild type and (Q) a larva expressing LamC-RNAi in muscles. Calibration bar is 5 μm.

(R,S) Morphometric analysis of GluRIIA clusters at the larval NMJ showing (R) Normalized volume of GluRIIA immunoreactivity in relation to bouton volume and (S) Normalized total intensity of GluRIIA immunoreactivity.

Figure 2.1- Subnuclear localization of DFz2C and LamC at larval muscle nuclei, their interdependence, and defective NMJs in *lamC* mutants.

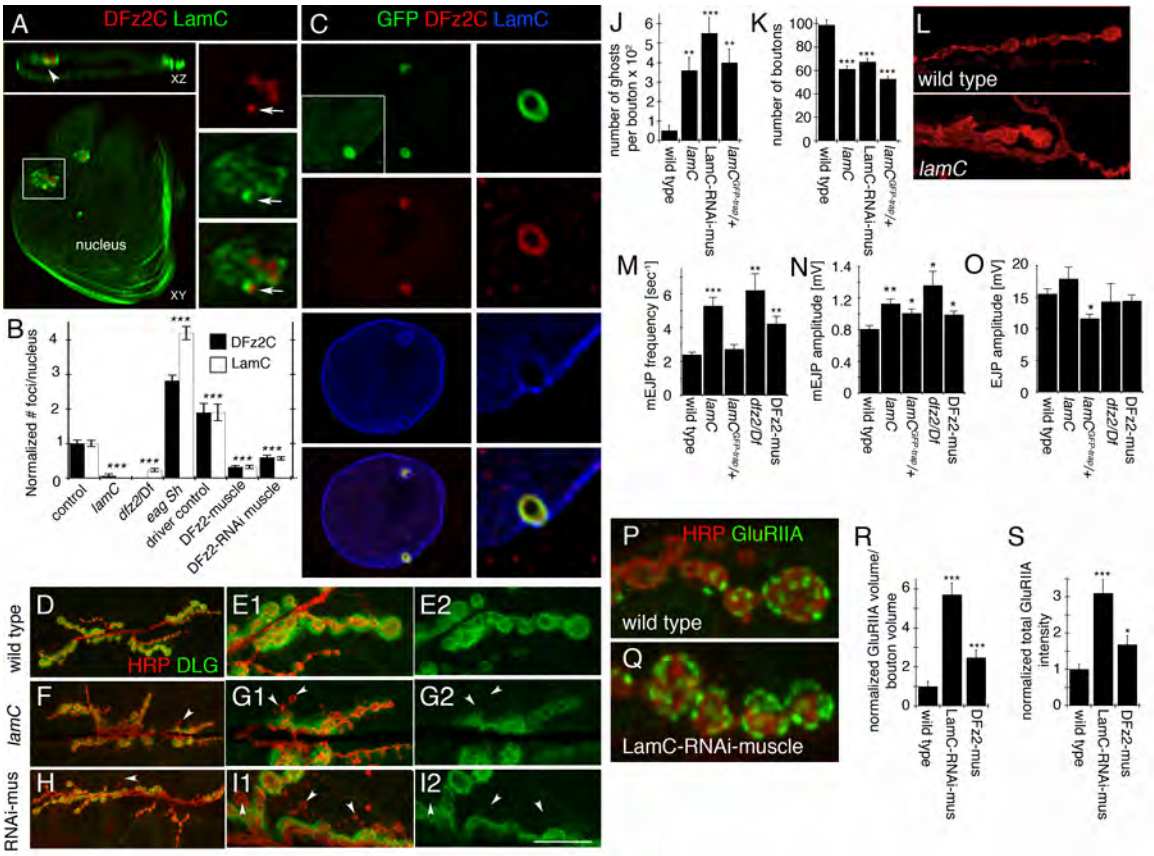

DFz2C granules are localized at invaginations of the inner nuclear membrane

The association of DFz2C foci with the nuclear periphery and their dependence on LamC is suggestive of a specialized function of the nuclear lamina. Vertebrate A-type lamins are known to form foci at sites of DNA replication (Kennedy et al., 2000). However, DNA was undetectable at the DFz2C/LamC foci as determined by co-labeling with DNA markers (Figure 2.2A, B; N=30 foci). LamA/C also localizes to and is required for expansion of the nucleoplasmic reticulum (NR), double-walled invaginations of the nuclear envelope involved in signaling and transport (Gehrig et al., 2008; Lagace and Ridgway, 2005). NR contain both the inner (INM) and outer (ONM) nuclear membranes and are labeled by markers of the nuclear pore complex (Lagace and Ridgway, 2005). Using membrane markers, we found that 92% of the DFz2C foci were wrapped by nuclear membrane (Figure 2.2C; N= 60 DFz2C foci), but unlike the NR, DFz2C foci were not coincident with nuclear pore complexes (Figure 2.2E; N= 35 DFz2C foci).

The NR define lumens projecting into the nucleus but continuous with the cytoplasm, as revealed by cytoplasmic injection of fluorescent dextrans with molecular masses above the cutoff for passive diffusion through nuclear pores (~40 kDa) (Keminer and Peters, 1999; Lagace and Ridgway, 2005). However, we observed no association between DFz2C/LamC foci and a Texas Red-conjugated 70 kDa dextran injected into muscle cells (Figure 2.2D; N= 40 DFz2C

foci). Thus DFz2C/LamC foci are not within reticuli continuous with the cytoplasm. Instead they are either surrounded by the INM at the nuclear periphery or are located within the perinuclear space (between the INM and ONM).

Yet another type of nuclear membrane invagination is INM infolding. Such INM infoldings occur during nuclear egress of herpes viruses (e.g. HSV and CMV) in mammalian cells (Buser et al., 2007; Darlington and Moss, 1968). Herpes viral particles are assembled in the nucleus and are far too large to be exported through nuclear pores. Instead, they become enveloped by the INM as they bud into the perinuclear space. This is followed by a de-envelopment process, in which the INM-derived envelope fuses with the ONM, releasing the naked nucleocapsids into the cytoplasm (Lee and Chen, 2010).

Figure 2.2- Localization of DFz2C/LamC foci at larval muscle nuclei in relationship to DNA, nuclear membrane, and nuclear pore complexes, and permeability of foci to cytoplasmic 70 KDa-dextran

(A-E) Larval muscle nuclei containing DFz2C/LamC foci (arrows) showing the relationship of the foci with (A, B) the DNA markers propidium iodide and Hoechst respectively, showing the absence of DNA labeling at the foci, (C) the membrane marker Concanavalin-A (ConA; deconvolved), showing that foci are wrapped by membrane, (D) 70 KDa dextran injected into the cytoplasm (deconvolved), showing that the dextran does not penetrate the foci, (E) mAb414 antibody which labels the nuclear pore complex (NPC;(Davis and Blobel, 1986)), showing that DFz2C granules do not colocalize with areas of the nuclear envelope containing nuclear pore complexes. E1 shows a raw image of the nucleus, which has been deconvolved in E2. E3 is a high magnification view of the focus shown in E2.

All images are single confocal slices; c= cytoplasm; n=nucleoplasm; calibration bar is 14 μm for A, 8 μm for B, E1-2, and 4 μm for C, D, E3.

Figure 2.2- Localization of DFz2C/LamC foci at larval muscle nuclei in relationship to DNA, nuclear membrane, and nuclear pore complexes, and permeability of foci to cytoplasmic 70 KDa-dextran

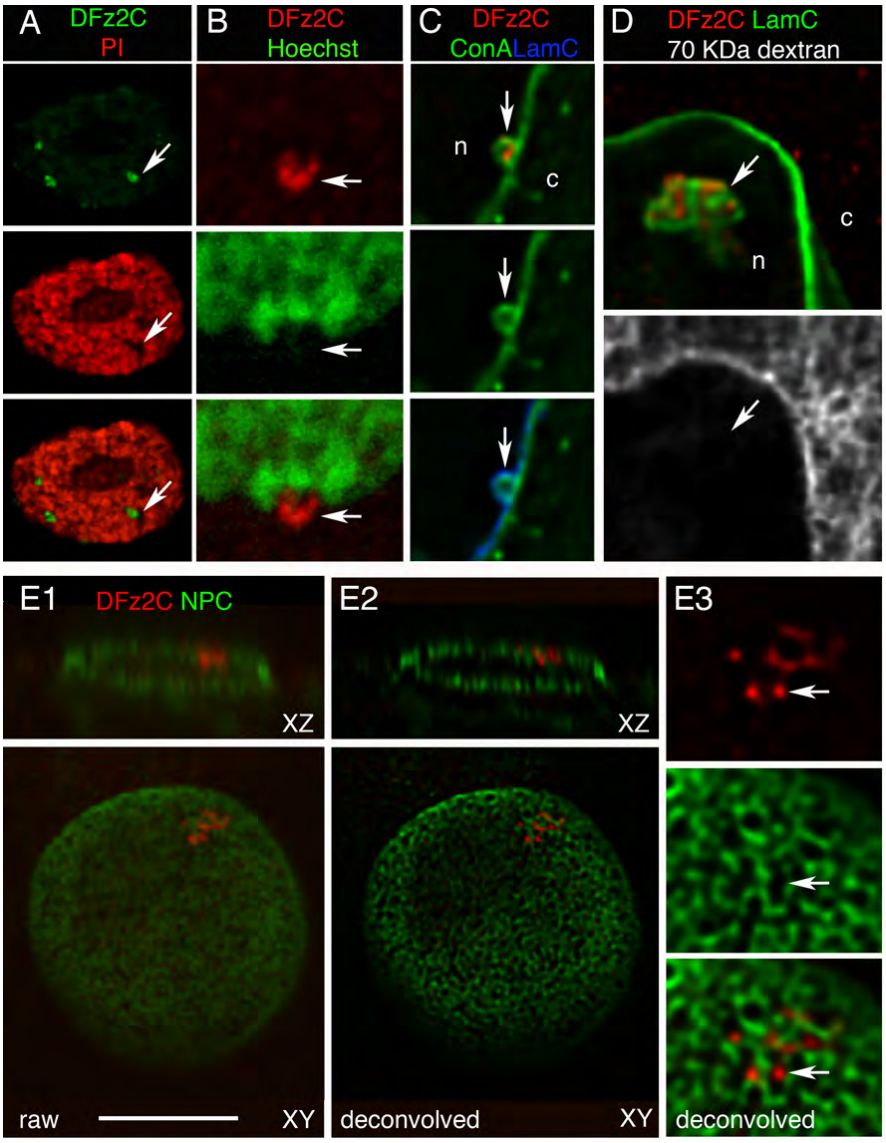

Ultrastructural analysis of DFz2C/LamC foci and resemblance to Herpes Virus egress

To determine if the DFz2C/LamC foci correspond to INM infoldings, we carried out an ultrastructural analysis of muscle nuclei (Figure 2.3). In electron micrographs (EMs) we could routinely observe nuclear membrane invaginations bounded by a single membrane, likely the INM (Figure 2.3A, B; N= 7 preparations; 9 foci). We also observed large electron-dense granules (average diameter = 192±0.01 nm: min/max 143/286; N=31 granules from 7 foci) (Figure 2.3A, B), located within the enlarged perinuclear space bounded by these INM invaginations (Figure 2.3A, B). Similar INM invaginations were also observed in a Schneider-2 (S2) cell line endogenously expressing DFz2 and Wg, which also display nuclear DFz2C foci (Figure 2.3C, D). Similar to muscle, S2 cells can also import DFz2C into the nucleus in the presence of Wg (Mathew et al., 2005). DFz2C antibody labeling of these electron dense granules in larval muscle cells, confirmed that they correspond to the DFz2C foci observed at the light microscopy level (Figure 2.3F, H; see Figure 2.3H' for no antibody control; N=29 animals; 93 foci).

The DFz2C granules within the INM invaginations appeared to be bounded by membrane (Figure 2.3D; arrow). If these granules are enveloped by the INM, then Lamin immunoreactivity could surround the dense granules. Indeed, LamC immunoreactivity lined the outer edge of the DFz2C granules (Figure 2.3E, G; see Figure 2.3G' for no antibody control; N= 29 animals; 93

foci), which correlates well with our observations of DFz2C/LamC foci at the light level.

Some DFz2C foci were also associated with ONM evaginations highly reminiscent of herpes nucleocapsids emerging from the nuclear envelope (Buser et al., 2007) (Figure 2.4A-D; arrows; see cartoon in Figure 2.4E for models of how viral capsids are thought to be released). Such evaginations often contained the DFz2C electron dense granules (Figure 2.4A; asterisks), but some were devoid of granules (Figure 2.4B, F), as has been observed after HSV egress from the perinuclear space (Buser et al., 2007; Granzow et al., 2001). Consistent with this idea, we also observed electron dense granules in the cytoplasm, close to the evaginations (Figure 2.4E; arrowhead). At the light level, evaginations of the lamina containing DFz2C labeling were also observed (Figure 2.4F). Thus, DFz2C foci are composed of electron dense, DFz2C- and LamC-associated granules that localize within the perinuclear space and are bounded by the INM. Further, these granules appear to be released into the cytoplasm either by evagination of the ONM or fusion of an INM bound granule localized to the perinuclear space, with the ONM (Figure 2.4E). Interestingly, in *lamC*$^{GFP\text{-}trap}$/+, in which DFz2C/LamC foci are morphologically disrupted, the foci appeared as large electron dense and amorphous structures associated with the nuclear envelope, in which no individual DFz2C granules could be distinguished (Figure 2.4D; arrows), also correlating with our light level analysis (Figure 2.1C).

Figure 2.3- Ultrastructural organization of DFz2C/LamC foci

Transmission electron micrographs of larval muscle or S2 cell nuclei containing DFz2C/LamC foci.

(A) Low magnification view of a focus (box) within a muscle nucleus. Inset: enlargement of the region enclosed by the box.

(B-D) High magnification views of INM invaginations containing electron dense granules (g) from (B) larval muscle (C, D) S2 cells. Note that the dense granules appear to be bounded by membrane (arrow in D).

(E-H) Immunoelectron micrographs of larval muscle nuclei labeled with (E, G) antibodies to LamC and 18 nm gold conjugated second antibody shown at (E) low and (G) high magnification. Note that the LamC label surrounds both the nuclear granules and the nuclear lamina; (F, H) antibodies to DFz2C and LamC with 12 nm and 18 nm gold conjugated second antibody, respectively, shown at (F) low and (G) high magnification. (G', H') Micrographs of foci in larval body wall muscle preparations processed for immunoelectron microscopy, in which the primary antibody was omitted, using (G') 18 nm gold-conjugated second antibody and (H') 12 nm gold-conjugated second antibody. Note DFz2 signal associated with the granules within the nuclear invaginations.

N= nucleus; C= cytoplasm; nu= nucleolus; h=heterochromatin; inm= inner nuclear membrane; onm= outer nuclear membrane; m= myofibrils; z= perforated z band. Calibration bar is 0.5 μm for A, 0.3 μm for B, D, 0.4 μm for E, F, 0.1 μm for C, G, H.

Figure 2.3- Ultrastructural organization of DFz2C/LamC foci

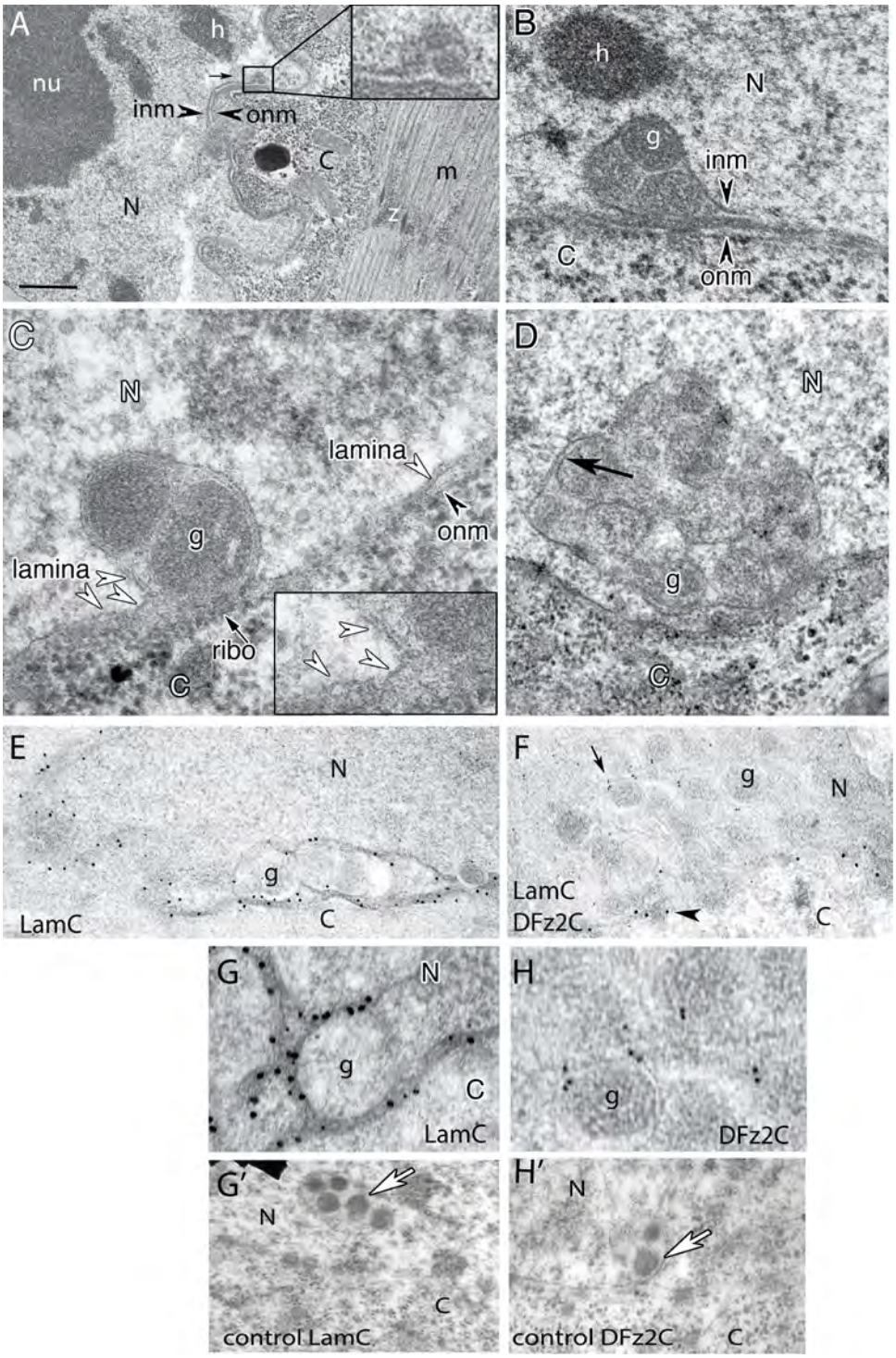

Figure 2.4- Evagination of the Nuclear Envelope Resembling HSV Egress

(A) Electron micrograph of a larval muscle nucleus region exhibiting a double-walled evagination (arrow) containing two RNA granules (asterisks). The evagination displays a “neck” possibly for pinching off or driving scission of the INM (see model in (E): steps 2 and 3 in blue pathway).

(B) Another double-walled evagination (arrow) appearing to have undergone INM scission (see model in F: step 2 in blue pathway). A RNA granule can be seen nearby in the cytoplasm (arrowhead).

(C) A double-walled evagination near a granule (g)-containing INM invagination.

(D) View of an abnormal focus shown at (D1) low and (D2) high magnification in a *lamC*$^{GFP\text{-}trap}$/+ preparation. Note the presence of electron dense amorphous material associated with the nuclear lamina (arrow).

(E) Cartoon depicting a model for two potential pathways for the release of granules from the nucleus, based on mechanisms of HSV egress and our observations in this article. The two nuclear egress pathways (red and blue annotations) are not mutually exclusive, and while the end result of either pathway is the release of membrane-free granules to the cytoplasm, they are morphologically different.

(F) A single slice through a SIM reconstruction of a muscle nucleus showing a possible egression event.

C = cytoplasm, N = nucleus, h = heterochromatin, NP = nuclear pore complex.

Scale bars: (A), (B), and (C) 0.3 µm; and (D2) 0.5 µm; (D1) and (F4) 1 µm; (F1–F3) 5 µm

Figure 2.4- Evagination of the Nuclear Envelope Resembling HSV Egress

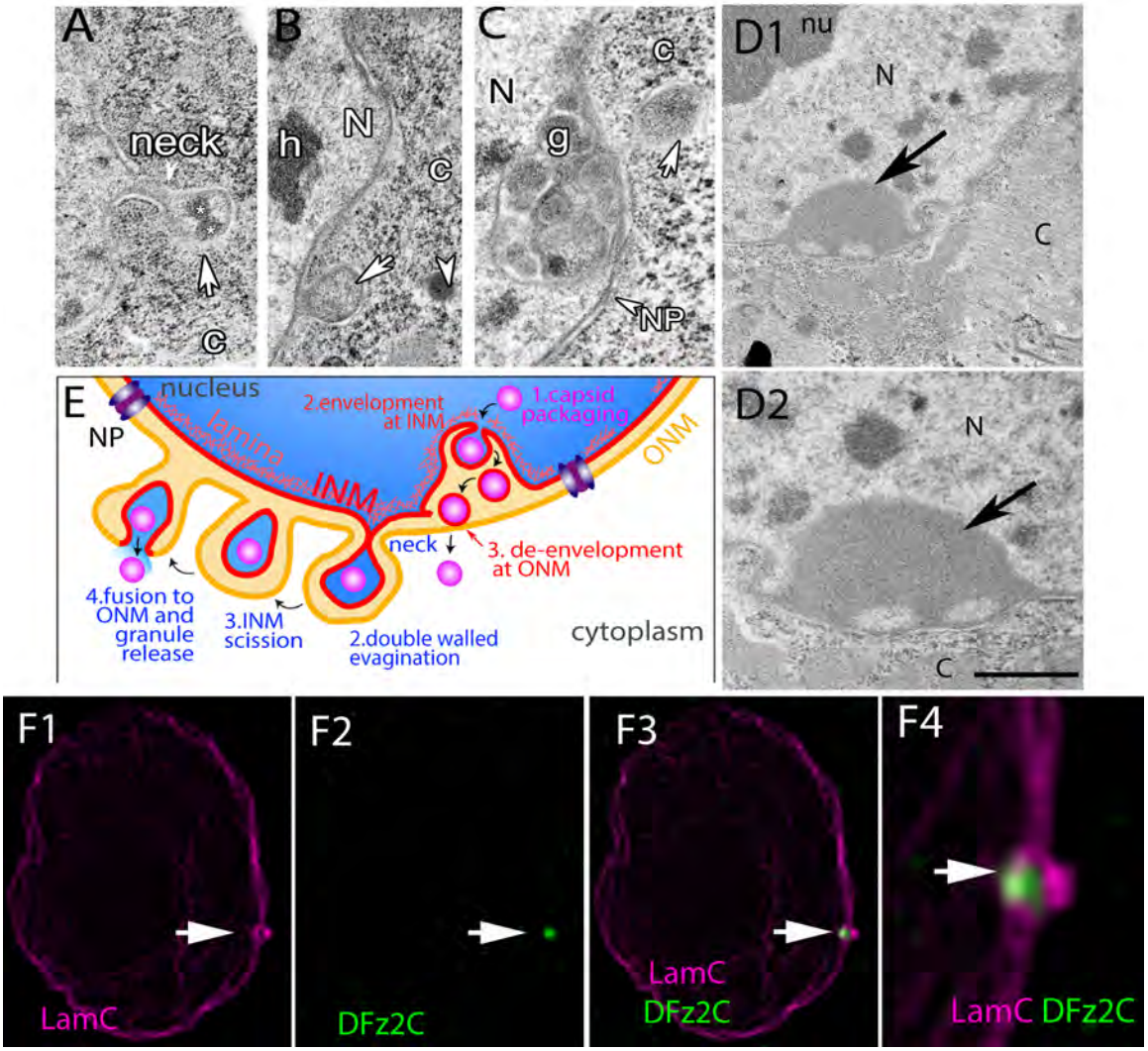

DFz2C/LamC foci contain RNAs that exit the nucleus

Whereas HSV nucleocapsids contain dsDNA, DFz2C/LamC foci occur in DNA-free regions (Figure 2.2A, B). To determine if the DFz2C-immunoreactive granules contained RNA instead, we screened the *Drosophila* flytrap database for fly stains expressing GFP fused in-frame with endogenous proteins involved in RNA binding, maturation or localization (34 strains; Table 2.1), and determined if any such GFP fusion proteins localized at or near the DFz2C/LamC foci. One such strain contained GFP fused in-frame with endogenous Poly(A) Binding Protein 2 (PABP2/PABPN1). In PABP2-GFP muscle nuclei GFP signal was observed both as diffuse nucleoplasmic fluorescence expected for PABP2 and bright GFP foci at the nuclear periphery (Figure 2.5A). This was distinct from the localization of NLS-GFP when expressed with a muscle Gal4 driver, which yielded diffuse staining throughout the nucleoplasm (Figure 2.5A2,A3; of 498 LamC foci examined in 6 animals, 0% showed discrete NLS-GFP enrichment at the foci). The GFP distribution in PABP2-GFP larval nuclei was similar to the endogenous PABP2 distribution revealed by labeling wild-type larvae with an antibody against *Drosophila* PABP2 (Benoit et al., 1999) (Figure 2.5A1). About 40% of the bright PABP2-GFP foci were juxtaposed with DFz2C/LamC foci and 32% of the DFz2C foci were juxtaposed with a bright PABP2 focus (N=118 foci). Further, there was a significant positive correlation between the number of PABP2 and DFz2C foci per nucleus (Figure 2.5B2; $R= 0.52$; $p<0.0001$). Further, the presence of bright PABP2 foci was dependent both on LamC and DFz2C, as

both the *lamC* null mutation and a strong *dfz2* loss of function mutation drastically decreased the number of PABP2 foci (Figure 2.5B). This suggests that the PABP2 foci are formed in conjunction with DFz2C/LamC foci.

PABP2 binds to the short poly(A) tail of immature transcripts in the nucleus, promoting poly(A) tail elongation by poly(A) polymerase (Kuhn et al., 2009). To determine if the DFz2C granules contained polyadenylated RNA we conducted fluorescent in-situ hybridization (FISH) with Digoxigenin-conjugated oligo-dT. Sixty four percent of the LamC foci contained high oligo-dT fluorescence (Figure 2.5C; N= 25 foci in 6 preparations) and the signal was completely eliminated by RNase treatment (Figure 2.4D; 0% of LamC foci contained oligo-dT fluorescence; N= 26 foci in 6 preparations).

The presence of RNA at the foci was additionally supported by performing Bernhard's regressive EDTA stain on thin sections. This procedure chelates the electron dense uranyl acetate label from DNA, but not from RNA (Bernhard, 1969), as evidenced by the preferential retention of electron dense staining in the ribosomes dotting the nuclear envelope (Figure 2.5 E1, arrowhead) and in the cytoplasm (Figure 2.5 E1, E3, F1, F3), and its near elimination from DNA (Figure 2.5 E2, F2). Notably, the large electron dense granules at the nuclear periphery were resistant to EDTA treatment (Figure 2.5 E1, F1, G). Taken together, these data indicate that DFz2C granules contain RNA, and at least some of these RNAs are polyadenylated.

In the Bernhard's regressive EDTA EM mages, we also observed electron dense granules similar to DFz2C granules in the cytoplasm close to the nuclear envelope (Figure 2.5G; arrows), supporting the idea that DFz2C granules are released from the perinuclear space into the cytoplasm. To directly monitor whether RNA granules found at the DFz2C/LamC foci were released into the cytoplasm, we conducted live imaging of the foci from larval body wall muscle preparations, using the RNA-specific dye E36 (Li et al., 2006). In these experiments, fluorescent granules emerging from nuclei in E36-labeled preparations were imaged blind by time-lapse microscopy at focal planes spanning the entire nuclear volume. Then, preparations were fixed and labeled with antibodies to LamC and DFz2C. Images from the fixed preparations were then sized and superimposed to the live images using a number of fiduciary markers, including the nucleolus, trachea, and the distance between two imaged nuclei (Figure 2.6A, B; Movie 1, 2; please click at links at the end of Supplemental Material to download the movies). As expected, E36-positive aggregates and granules were observed in both nucleus and cytoplasm. Close examination revealed E36-positive puncta emerging from the LamC foci and exiting the nucleus. Thus, at least some of the foci-associated RNA granules translocate to the cytoplasm.

Figure 2.5- PABP2 and poly(A) RNA are associated with DFz2C/LamC foci.

(A) Confocal slice of a larval muscle nucleus showing the relationship between a DFz2C/LamC focus and PABP2-GFP foci (arrows), displayed at (top) low and (bottom) high (deconvolved) magnification. (A1) Deconvolved confocal image of a muscle nucleus labeled with LamC and PABP2 antibodies showing intense PABP2 foci, above nucleoplasmic levels of PABP2, localized adjacent to LamC foci.(A2 and A3) Single confocal slice through the nucleus of larva expressing nls-GFP in muscle cells, at (A2) low magnification and (A3) high magnification.

n = nucleus; c = cytoplasm. Scale bars: (A1) and (A2) 2 µm, (A3) 7 µm.

(B) Number of PABP2 foci per larval muscle nuclei, normalized to control, showing that PABP2 foci depend on normal *lamC* and *dfz2* function. ***=p<0.0001; number of foci analyzed is control=229, *LamC*=175, *dfz2*/Df= 301. (B2) Number of DFz2C foci versus number of PABP2-GFP foci in muscle nuclei. Numbers below each data point represent the number of nuclei found at each value.

(C, D) Confocal slice of a larval muscle nucleus labeled with poly (dT) FISH and anti-LamC, either (C) under normal conditions, or (D) treated with RNase.

(E-G) View of DFz2/LamC foci at a larval muscle nucleus in sections (E) treated with the Bernhard's regressive EDTA (rEDTA) technique and (F) not treated with EDTA (same preparation as in (E)). N= nucleus; C= cytoplasm. (E2, F2) High magnification views at the nuclear area of E1 and F1 around a DFz2C granule showing the presence of a dark meshwork surrounding the granule. While this

meshwork is bleached after EDTA treatment (E2), DFz2C granules retain electron density (F2). (E3, F3) High magnification of E1 and F1, showing ribosomes in the cytoplasm, which retain electron density after EDTA treatment.

(G) Low magnification view of a larval muscle focus showing retention of electron density by DFz2C granules after rEDTA treatment (g; arrow). Arrowheads point to ribosomes at the ONM. Arrow points to a cytoplasmic granule of the same size and morphology as DFz2C granules at INM invaginations.

Calibration bar is 8μm for A (top row), 3μm for A (bottom row), 8μm for C, D, 0.6μm for E1, F1, 0.2μm for E2-3, F2-3, and 1μm for G.

Figure 2.5- PABP2 and poly(A) RNA are associated with DFz2C/LamC foci.

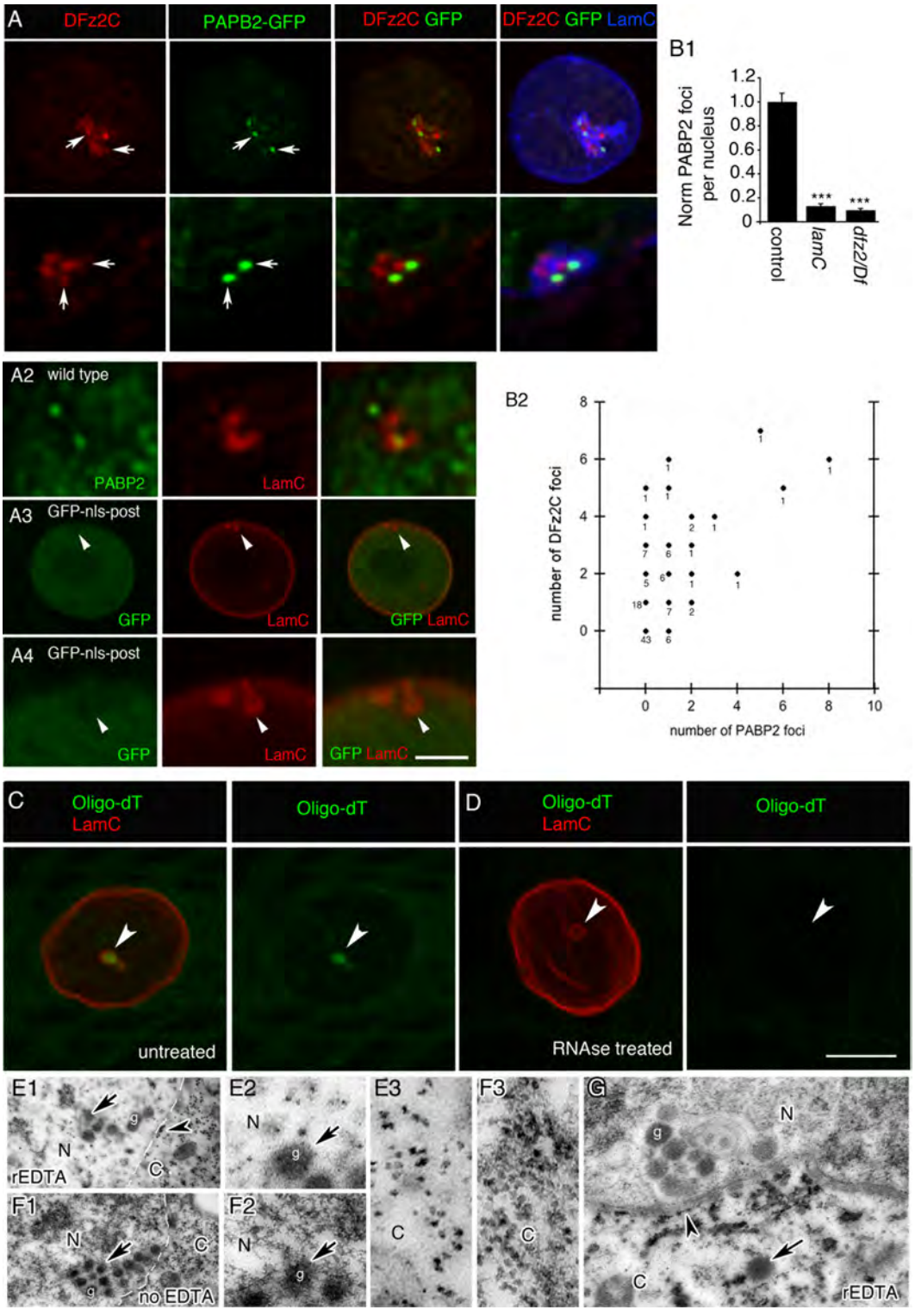

Figure 2.6- RNA granules from DFz2C/LamC foci exit larval muscle nuclei.

(A, B) Spinning disk confocal images of nuclei imaged live from larval body wall muscle preparations after incubation with E36 RNA dye (green). After time-lapse imaging, samples were fixed and labeled with antibodies to DFz2C and/or LamC. N=nucleus; nu=nucleolus. Complete movies are shown in Supplementary Movie 1 and 2. Calibration bar is 10μm for A(top row), B(top row), and 4μm for A(bottom row), B(bottom row).

Top rows in A, B show (top panel) a single image of a larval body wall muscle nucleus labeled with E36, (middle panel) the same nucleus after fixation and immunolabeling with DFz2C and/or LamC antibodies, and (right panel) their superposition obtained after resizing using fiduciary markers. Arrowheads mark the position of the E36 and DFz2C/LamC foci.

Bottom rows in A, B display time-lapse imaging series, showing an E36 labeled granule exiting the nucleus of a larval body wall muscle. Arrows mark the initial position of the granule, while arrowheads point to the granules while moving away from the nucleus. Time marks correspond to hr:min:sec.

Figure 2.6- RNA granules from DFz2C/LamC foci exit larval muscle nuclei.

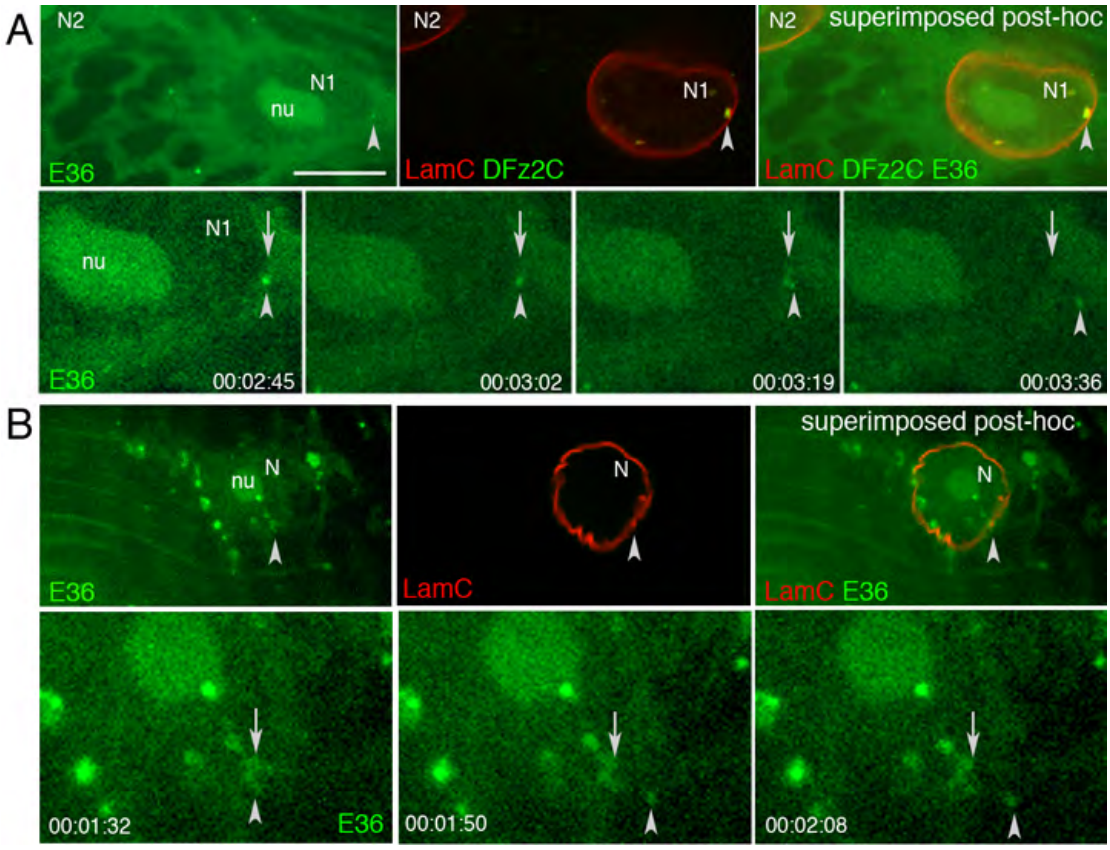

Atypical Protein Kinase C is required for DFz2C/LamC foci formation

HSV nucleocapsids recruit a host protein kinase C (PKC), which phosphorylates A and B-type Lamin, disrupting the nuclear lamina at the INM and allowing the capsid to bud into the perinuclear space (Park and Baines, 2006). The PKC involved in this process is likely not a conventional PKC (Leach and Roller, 2010). Notably, we observed that a binding partner of *Drosophila* atypical PKC (aPKC), Bazooka (Baz)/Par3, colocalized with LamC, both in the nuclear lamina and at foci (Figure 2.7A). Low levels of aPKC immunoreactivity were also detected inside the nucleus (Figure 2.7B). These observations raised the possibility that aPKC might be involved in remodeling the lamina around INM invaginations defining DFz2C/LamC foci. To test this, we modified aPKC activity in muscles. In particular, we downregulated aPKC by expressing an aPKC-RNAi transgene in muscles, or increased aPKC activity by expressing a constitutively active form of aPKC (PKM) using the muscle-specific Gal4 driver, C57-Gal4. Expressing aPKC-RNAi in muscles nearly eliminated DFz2C/LamC foci (Figure 2.7C, D, J), suggesting that aPKC is required for foci formation. This conclusion was supported by pharmacological experiments showing that feeding larvae for 21 hours with 100 μM chelerythrine, a PKC inhibitor (Herbert et al., 1990), significantly reduced the number of DFz2C/LamC foci (Figure 2.7E, J). Conversely, increasing aPKC activity by expressing PKM in muscles dramatically increased both the size and number of LamC foci (Figure 2.7F, J), suggesting that increasing aPKC activity promotes LamC foci formation. However, these foci

were completely devoid of DFz2C signal (Figure 2.7F). Thus, although constitutively activating aPKC throughout larval development promotes reorganization of the lamina, it prevents normal loading of LamC foci with DFz2C granules. To both limit PKM expression and allow for temporal control of its delivery, we expressed PKM under control of the heat-shock promoter (hs-PKM). At permissive temperature hs-PKM larvae displayed an increase in the number of DFz2C/LamC foci compared to wild type animals, likely due to the known leakiness of the hs promoter (Figure 2.7J; (Hans et al., 2011)). A much larger increase in DFz2C/LamC foci was produced by a 30 min heat shock at 30˚C followed by 2 hr at permissive temperature prior to dissection (Figure 2.7G, J), while no significant change in the number of DFz2C/LamC foci was elicited in wild type controls subjected to the same temperature shift paradigm (Figure 2.7J). In these larvae, LamC foci also contained DFz2C immunoreactivity (Figure 2.7G), consistent with the idea that while chronic PKM expression interferes with DFz2C foci formation, acute PKM activation allows for normal formation of DFz2C granules within the LamC foci.

Interestingly, labeling body wall muscles with an antibody specific for phosphorylated PKC substrates (Zhang et al., 2002a) resulted in intense immunoreactivity at the foci (Figure 2.7H), and treatment of the samples with lambda-phosphatase eliminated this signal (Figure 2.7I). Western blotting of body wall muscle extracts with the phosphorylated PKC substrate antibody revealed a band at the same molecular weight as LamC (Figure 2.7L). The intensity of this

band increased in larvae expressing PKM in muscles and, conversely, it decreased when aPKC-RNAi was expressed in muscles (Figure 2.7L). Consistent with the idea that this band corresponded to LamC, immunoprecipitation of body wall muscle extract with LamC antibodies revealed that LamC is recognized by the phosphorylated PKC substrate antibody (Figure 2.7M). Further, the intensity of this band, when the blots were probed with the antibody against phosphorylated PKC substrate, was increased in LamC immunoprecipitates from larvae expressing PKM in muscles (Figure 2.7M). Taken together, the above results suggest that PKC-dependent phosphorylation is necessary and sufficient to locally remodel the lamina in order to form DFz2C/LamC foci. Downregulating the aPKC-binding partner, Baz/Par3, by expressing Baz-RNAi in muscles, virtually eliminated the foci (Figure 2.7J), suggesting that Baz might function in conjunction with aPKC.

We next assessed whether altering aPKC activity or Baz levels elicits ghost bouton formation. Previous studies demonstrated that both downregulation and constitutive activation of aPKC, as well as downregulation of Baz, leads to a reduction in the number of synaptic boutons at the NMJ, partly due to a local function of these proteins in cytoskeletal regulation at the NMJ (Ramachandran et al., 2009; Ruiz-Canada et al., 2004). However, whether ghost boutons were formed in the above genotypes was not tested. To determine if ghost boutons were present, we downregulated aPKC or Baz or expressed PKM, all specifically in muscles. NMJs in all of the above genotypes displayed a significant increase

in the number of ghost boutons (Figure 2.7K). Thus, like mutations that interfere with DFz2C foci formation, manipulations in aPKC and Baz lead to the formation of undifferentiated boutons.

Figure 2.7- aPKC is required for foci formation, possibly by phosphorylating LamC.

(A-I) Single confocal slices of larval body wall muscle nuclei labeled with antibodies to either Baz, aPKC, PKC-phosphorylated substrate (aPKC subs), or DFz2C (green), double labeled with antibodies to LamC (red) in wild type and genetic variants altering aPKC activity showing (A) that Baz is localized at the nuclear lamina and LamC foci, in exact colocalization with lamC, (B) that aPKC is diffusely localized within the muscle nuclei, (C) a representative image of a DFz2C/LamC foci in wild type body wall muscle nucleus, (D) that expressing aPKC-RNAi in muscles, using the C57-Gal4 driver, virtually eliminates DFz2C/LamC foci, (E) that feeding larvae with the aPKC inhibitor, chelerythrine, drastically decreases the number of DFz2C/LamC foci, (F) that expressing PKM in muscles leads to an enlargement and increase in the number of LamC foci, which are devoid of DFz2C, (G) that expressing PKM for just 30 min in hs-PKM larvae leads to a substantial increase in the number of DFz2C/lamC foci, (H)- that labeling body wall muscles with an antibody against PKC phosphorylated substrates shows an enrichment of immunoreactivity at the LamC foci, and (I) that this label is eliminated after treatment of the samples with lambda phosphatase. Calibration bar is 15μm.

(J) Normalized number of foci per nuclei upon altering aPKC activity. Number of nuclei analyzed is 2146 for wild type, 532 for aPKC-RNAi-muscle, 726 for wild type with chelerythrine treatment, 677 for PKM-muscle, 713 for wild type with

heat shock, 601 for hs-PKM without heat shock, 595 for hs-PKM with heat shock, and 652 for Baz-RNAi-muscle.

(K) Normalized number of ghost boutons from the indicated genotypes. Number of animals analyzed is 6 for wild type, muscle expression of aPKC-RNAi, Baz-RNAi, and PKM.

(L) Western blot of body wall muscle extracts probed with antibody against phosphorylated PKC substrates, showing a band of the same molecular weight as LamC (arrow) which increases in intensity in extracts derived from larvae expressing PKM in muscles, and which decreases in intensity in extracts from larvae expressing aPKC-RNAi in muscles. N=3 independent blots.

(M) Immunoprecipitation of body wall muscle extracts with LamC antibody, showing that LamC is labeled by the PKC substrate antibody, and that the intensity of the label increased when using extracts from larvae expressing PKM in muscles. N = 3 independent immunoprecipitations.

Figure 2.7- aPKC is required for foci formation, possibly by phosphorylating LamC.

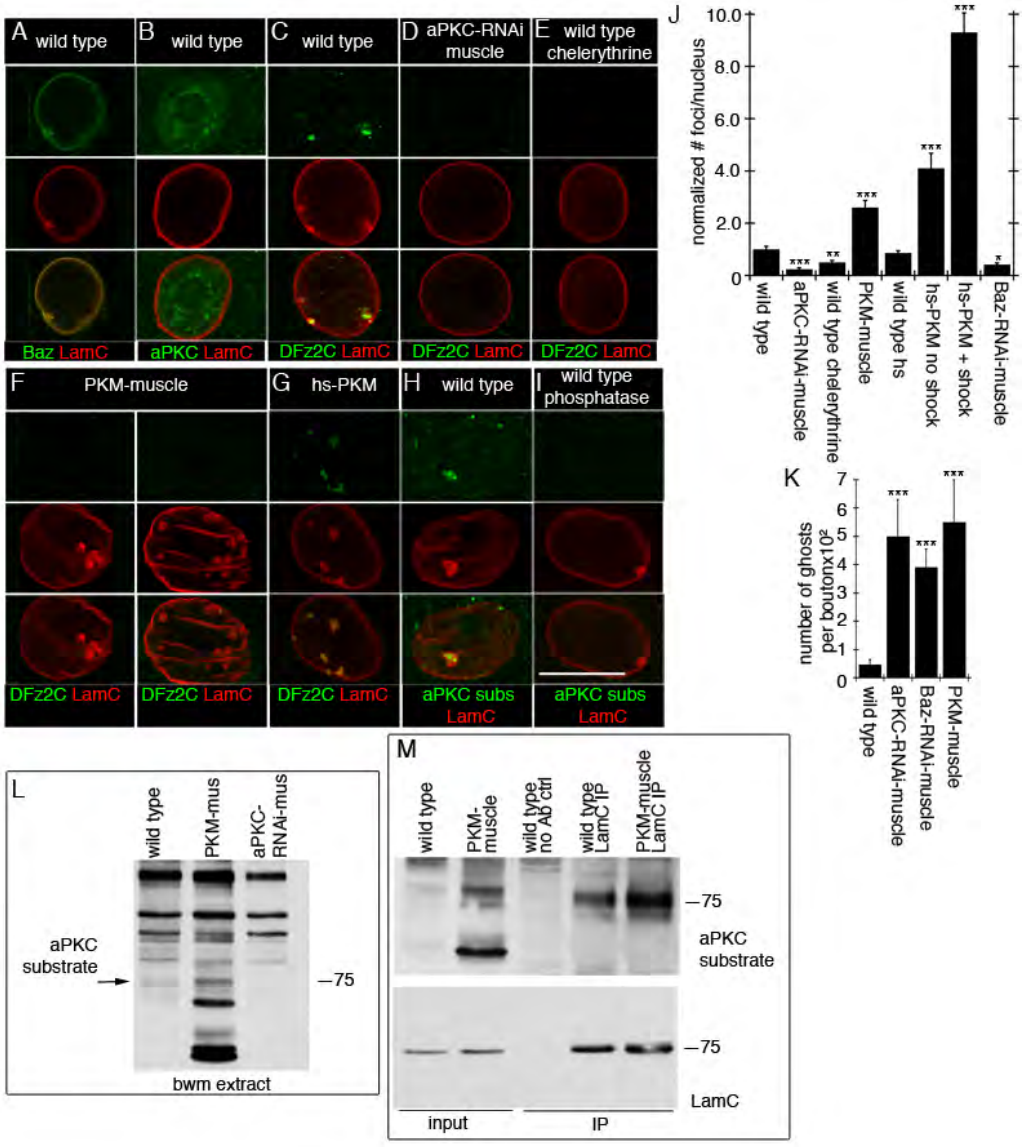

DFz2C/LamC foci contain synaptic protein transcripts

We next sought to identify specific mRNAs trafficked through the foci, possibly for local translation at postsynaptic sites. Using a candidate approach for mRNAs encoding known postsynaptic proteins and others involved in nervous system development, we identified 6 transcripts localizing to the foci among 19 mRNAs tested (Table 2.2). Of these, the PDZ protein Par6 was selected for further study (Figure 2.8). Par6 is part of a tripartite protein complex, consisting of Baz, Par6, and aPKC (Betschinger et al., 2003). At the *Drosophila* NMJ all three proteins localize both pre- and postsynaptically (Ruiz-Canada et al., 2004), and both Baz and aPKC have been implicated in cytoskeleton remodeling during synaptic growth (Ramachandran et al., 2009; Ruiz-Canada et al., 2004). In addition to colocalizing with nuclear LamC foci (Figure 2.8A), Par6 mRNA was observed in puncta near folds of the lamina, where LamC foci were not yet apparent (Figure 2.8B). These could represent granules in the process of formation prior to their translocation into the perinuclear space. Notably, we also observed Par6 mRNA granules within evaginations of the nuclear lamina (Figure 2.87C,D), likely representing the nuclear envelope evaginations observed at the ultrastructural and light microscopy levels.

In S2 cell extracts, an antibody against the C-terminus of DFz2 immunoprecipitated Par6 mRNA but not an mRNA (Mad) absent from DFz2C foci (Figure 2. 8M; Table 2.2). The Par6 primers used were in adjacent exons and the RT-PCR product was of the size expected from spliced mRNA. The identity of

the RT-PCR product was confirmed by sequencing. Thus the Par6 RNA associated with DFz2C is spliced, suggesting that it is mature.

The presence within DFz2C granules of mRNAs encoding postsynaptic apparatus components raises the possibility that these granules are trafficked to the NMJ where the mRNAs within are locally translated, as has been demonstrated for RNA granules in neurons (Wang et al., 2010). Indeed, local translation of GluRs has been reported at the NMJ (Sigrist et al., 2000) and the SSR contains polyribosomes (Sigrist et al., 2000). Using two different Par6 probes we found that Par6 mRNA was associated with the NMJ (Figure 2.8H-J) and no signal was observed with a *wg* probe (Figure 2.8K). The NMJ Par6 signal was virtually eliminated upon expressing LamC-RNAi in muscles (Figure 2.8L) confirming the specificity of the signal. Further, ghost boutons present in *lamC* mutants were devoid of postsynaptic Par6 protein, and showed a marked decrease in overall postsynaptic Par6 levels (Figure 2.8E, F). Taken together these data suggest that proper localization and local translation of at least one postsynaptic transcript, Par6, requires the FNI pathway.

Figure 2.8- *par6* transcript is localized to nuclear body wall muscle LamC foci and the NMJ, and forms a complex with DFz2C.

(A-D, G-L) *In situ* hybridization to larval body wall muscles using *par6* or *wg* probes showing (A) association of *par6* mRNA with a LamC focus (arrow); (B) localization of *par6* transcript near a nuclear membrane fold; (C, D) localization of *par6* transcript to cytoplasmically directed projections of the nuclear boundary. A2-D2 are high magnification views of the nuclei shown in A1-D1. (G) Absence of FISH signal when using a *wg* probe; (H) a low magnification view of *par6* mRNA at the postsynaptic larval NMJ; (I-J) synaptic *par6* mRNA localization using 2 different *par6* probes; (K) absence of synaptic *wg* mRNA localization; (L) synaptic *par6* mRNA localization in a larva expressing LamC-RNAi in muscle, showing virtual elimination of postsynaptic *par6* mRNA.

(E-F) Larval NMJs labeled with antibodies against HRP and Par6 in (E) wild type and (F) *lamC* mutant showing a ghost bouton (arrow) devoid of Par6 immunoreactivity and an overall decrease in Par6 levels throughout the NMJ.

Calibration bar is 15μm for A1, B1, G, 7μm for A2, B2, 5μm for C1, D1, J, 2.5μm for C2, D2, 20μm for H, and 10μm for E, F, I, K, L.

(M) Immunoprecipitation of *par6* RNA using DFz2C antibodies. Left: immunoprecipitation of DFz2C fragment using anti-DFz2C antibody. Middle: RT-PCR from S2 cell RNA showing the presence of *par6* and *mad* transcripts in S2 cells. Right: RT-PCR of the DFz2C immunoprecipitate showing the presence of *par6* but not *mad* transcripts.

Figure 2.8- *par6* transcript is localized to nuclear body wall muscle LamC foci and the NMJ, and forms a complex with DFz2C.

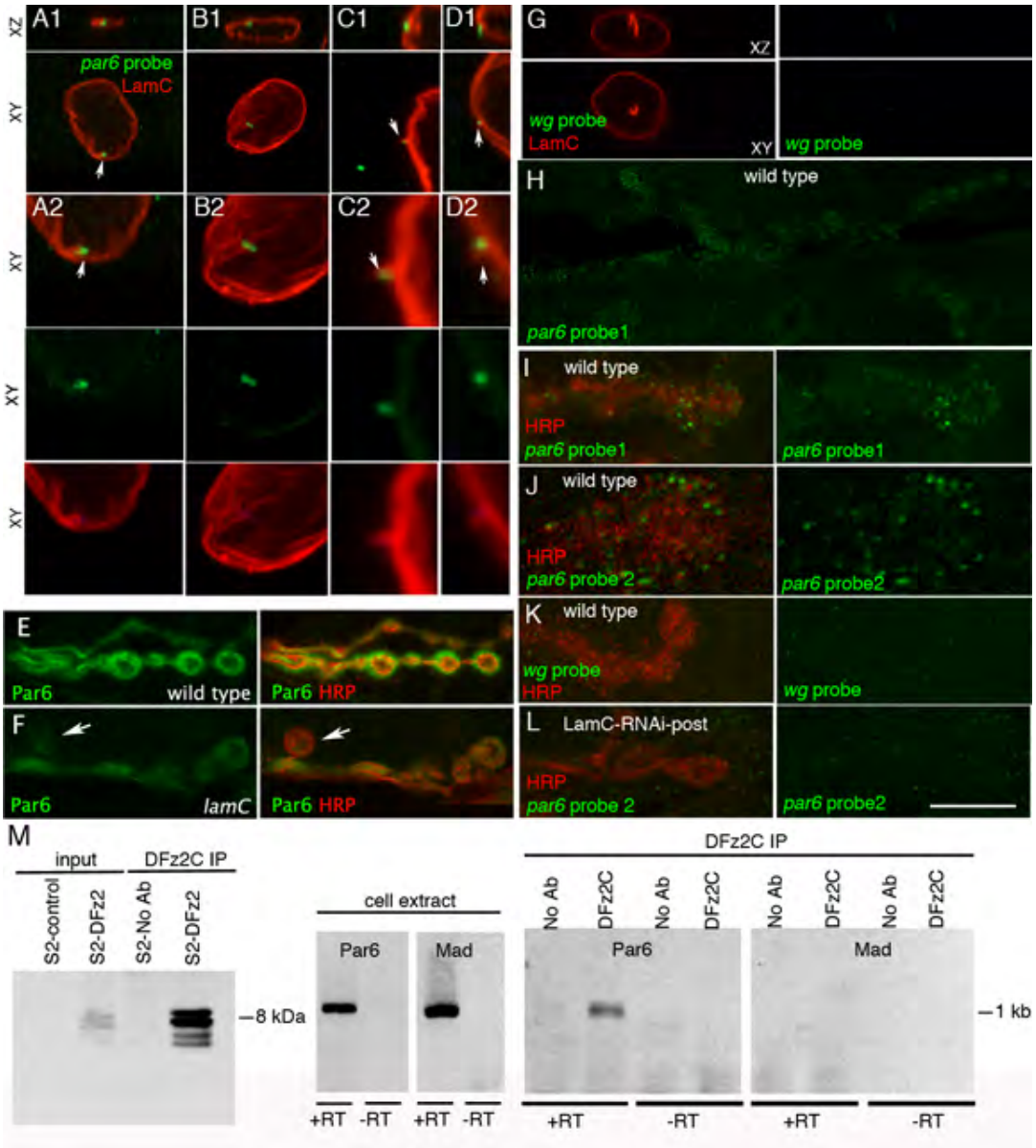

DISCUSSION

The canonical view of nucleocytoplasmic transport posits that the sole gateway into and out of the nucleus is the nuclear pore complex (NPC). Thus all RNAs and RNPs synthesized and assembled in the nucleus are thought to access the cytoplasm by transiting the NPC. Our study now provides evidence for an alternative RNP export pathway: nuclear envelope budding. We uncovered this pathway while investigating Wnt-dependent NMJ synapse development in *Drosophila* larval body wall muscles. We find that C-terminal fragments of the Wg receptor DFz2 accumulate in nuclear foci in association with large RNA granules localizing to the space between the INM and ONM. These granules are found at sites of INM invaginations, are bounded by LamC, and can be seen leaving the nucleus. Further, the granules contain transcripts encoding postsynaptic proteins, and mutations interfering with foci formation prevent proper differentiation of synaptic boutons. Thus we suspect that, after exiting the nucleus by budding, the DFz2C RNP granules translocate to sites of synapse formation where local translation of the encoded proteins contributes to synapse assembly.

In addition to describing a novel pathway for nuclear export of endogenous RNPs, our work sheds light on the previously mysterious mechanisms by which mutations in nuclear lamins and INM proteins lead to muscular dystrophies and related movement disorders (Burke and Stewart, 2002; Mejat et al., 2009). Further, by showing that nuclear import of a membrane

receptor fragment serves to promote export of mRNA transcripts, this work adds a novel twist to the molecular mechanisms governing membrane to nucleus communication in Wnt signaling pathways.

Nuclear envelope budding and herpes viral egress

The nuclear budding pathway described here bears remarkable resemblance to the nuclear egress mechanism employed by herpes viruses. Herpes capsids containing dsDNA are assembled in the nucleus, where they form multimegadalton complexes much too large to pass through NPCs. Instead, they exit via INM envelopment and ONM de-envelopment (Figure S2.3H) (Lee and Chen, 2010; Roller, 2008). Until now this highly unusual nuclear export pathway had been thought unique to this family of viruses, and not representative of any endogenous nuclear export pathway (Roller, 2008). Rather it was supposed that herpes viruses had hijacked the lamina disassembly pathway operational during nuclear replication (Haas and Jost, 1993).

Both herpes virus egress and replication-dependent nuclear envelope disassembly involve multiple phosphorylation events (Roller, 2008). In capsid egress, viral proteins pUL34 and pUL31 are targeted to the INM where they recruit viral pUS3 kinase and host PKCs (Park and Baines, 2006; Reynolds et al., 2004; Ryckman and Roller, 2004). Both pUS3 and the host PKCs disrupt the nuclear lamina by phosphorylating lamins, including LMNA, and other lamina-associated proteins (Bjerke and Roller, 2006; Leach and Roller, 2010; Milbradt et

al., 2010). Both pUL34 and pUL31 have also been suggested to induce INM curvature around the capsid, facilitating budding into the perinuclear space (Klupp et al., 2007).

We present multiple lines of evidence supporting the idea that local lamina remodeling at sites of DFz2C granule formation is driven by the same mechanisms at work in viral capsid egress and that these mechanisms have profound implications for synapse development. First, atypical PKC is required for both lamina remodeling and formation of INM invaginations containing DFz2C granules (Figure 2.6D-F, J). Second, the apparent phosphorylation level of a species with identical electrophoretic mobility to LamC paralleled changes in aPKC activity (Figure 2.6L), and this same band was immunoprecipitated with antibodies to LamC (Figure 2.6M). Third, the aPKC recruitment factor Baz also localized to DFz2C/LamC foci (Figure 2.6A), and Baz downregulation in muscles prevented DFz2C/LamC foci formation (Figure 2.6J). Fourth, altered aPKC activity through RNAi or expression of a constitutively active enzyme, as well as decreasing Baz levels, resulted in an increase in ghost bouton number (Figure 2. 6K), similar to other disruptions of the FNI pathway (Figure 2. 1J). Fifth, downregulation of the FNI pathway through LamC-RNAi, or DFz2 overexpression in muscles, led to an increase in GluRIIA clustering similar to that observed in mutations in *dapkc* and *baz* (Figure 2. 1P-S and Ramachandran et al 2009; Ruiz-Canada et al 2004). This increase in GluR clustering was reflected by an elevation of mEJP amplitude (Figure 2. 1N), as also observed in *dapkc* and *baz*

mutants. Finally, immunofluorescence from an antibody recognizing phosphorylated PKC substrates was greatly enhanced at DFz2C/LamC foci (Figure 2.6H, I). Thus we propose that herpes viruses have in fact hijacked a nuclear export pathway employed by endogenous RNPs.

Other reports of perinuclear granules

That nuclear envelope budding has not been previously investigated as a means for endogenous RNP egress raises the question of whether this is a highly specialized mechanism utilized only by *Drosophila* larval muscle cells, or is a more widespread phenomenon. Our results and reports in the literature strongly support the latter view. Notably, we observed DFz2C/LamC foci in both *Drosophila* salivary gland (Figure S2.1C) and in S2 cell nuclei (Figure 2.3C, D), both of which appear to utilize the FNI signaling pathway. Others have also reported INM infoldings containing electron dense granules (suggested to be aggregates of RNPs) in *Drosophila* salivary glands and midgut cells at specific developmental stages (Gay, 1956; Hochstrasser and Sedat, 1987). Similar perinuclear granules have likewise been observed in diverse contexts, from plants (Dickinson, 1971) to mammals, where they are particularly prevalent in early embryonic stages (Hadek and Swift, 1962; Szollosi, 1965). Indeed, that such granules might reflect an alternate mode of nucleocytoplasmic export has been previously proposed (Gay, 1956; Szollosi and Szollosi, 1988), but it had not been experimentally validated until now. The combination of our data with the

numerous cytological reports of perinuclear granules strongly supports the notion that nuclear envelope budding is a general mechanism for nuclear export of large RNP granules in many cell types.

Congenital neuromuscular diseases and nuclear budding

Mutations across the human *LMNA* gene lead to a diverse set of disorders (Burke and Stewart, 2002) termed laminopathies, with extreme variability in their tissue specificity and pathogenesis. Some manifest as muscular dystrophies affecting specific skeletal muscles (Burke and Stewart, 2002; Mejat et al., 2009). While laminopathies affecting muscles have been historically classified as myopathies, recent evidence in mice indicates that gross NMJ defects are detectable well before any signs of muscle degeneration (Mejat et al., 2009). Similarly, we observed no alterations in *Drosophila* larval muscle morphology or organization in the same *lamC* mutants wherein defects at the NMJ were clearly evident (Figure 2.1F-L, S2.1L). Thus, the underlying basis of many muscle-specific laminopathies could be disruption of nuclear budding leading to improper NMJ development. Consistent with this are observations that insertion of GFP sequences in the highly conserved rod domain of fly LamC (this report and (Schulze et al., 2009)) results in formation of LMNA-positive "O-ring" structures in the nucleus, as well as disruption of both DFz2C granule organization and NMJ development. Similar O-rings have been observed in humans with autosomal

dominant Emery-Dreifuss muscular dystrophy (AD-EDMD) (Ostlund et al., 2001; Schulze et al., 2009), which is caused by mutations in this same rod domain.

An additional link between congenital neuromuscular disease and nuclear budding is provided by studies of Dystonia, a sustained muscle contraction disorder (Robottom et al., 2011). Dystonia symptoms are ameliorated by botulinum toxin treatment (Lim and Seet, 2010), suggesting defects in neurotransmission. The AAA+ ATPase TorsinA is responsible for most cases of early-onset autosomal-dominant primary dystonia (Breakefield et al., 2001). Besides its role in synaptic vesicle recycling (Granata et al., 2008), a recent study indicates that TorsinA is required for HSV nuclear egress (Maric et al., 2011b). Moreover, ultrastructure analysis of developing motorneurons in *torsinA* mutant mice revealed accumulations of vesicular structures in the perinuclear space (Goodchild et al., 2005). Taken together, these results raise the intriguing possibility that TorsinA functions to promote nuclear envelope scission during nuclear budding, and that alterations in RNP granule export might contribute to the phenotypic characteristics of Dystonia.

Role of DFz2C granules in synapse development

Using a candidate approach, we identified several transcripts colocalizing with DFz2C/LamC foci encoding postsynaptically localized proteins required for synapse development and plasticity. Packaging of these RNAs into DFz2C granules appeared quite specific, as numerous transcripts encoding other

synaptic proteins were absent from the foci. The observation that RNAs in DFz2C foci exit the nucleus and that at least one of the transcripts, Par6, is localized to synaptic boutons, suggests that mRNAs exported by nuclear envelope budding translocate to postsynaptic sites for local translation, as has been well documented for large RNA granules in neurons (Wang et al., 2010). However, where such RNA granules are initially formed has not been eese et

An important future direction will be to determine whether each granule contains a single mRNA, or is a combination of transcripts. Further, the exact role of DFz2C in assembly and/or transport of granules is at present unclear. Neither is it known whether DFz2C remains associated with the granules after nuclear egress. Intriguingly, DFz2C contains a C-terminal PDZ binding motif, raising the possibility that it may provide a zip code for targeting the granules to postsynaptic sites.

Combined, our results provide novel insight into how synapses communicate with the nucleus to regulate both gene expression and nuclear envelope architecture. In the future it will be of great interest to determine the extent to which the nuclear budding pathway extends to other Wnt receptors and whether it contributes to localized protein expression in response to other signal transduction pathways.

Table 2.1- GFP-Trap Lines Screened

Trap ID	symbol	Name; function	Gene ID
CA06921	Hrb98DE	Heterogeneous nuclear ribonucleoprotein at 98DE	CG9983
CA06961	pUf68	poly(U) binding factor 68kD	CG12085
CA07692	Spt6	chromatin binding	CG12225
CB02119	Rm62	RNA interference	CG10279
CB02655	sqd	Squid; mRNA binding	CG16901
CB03028	SF2	nuclear mRNA splicing	CG6987
CB03248	xl6	nuclear mRNA splicing	CG10203
CB04769	eIF3-S9	translation initiation factor	CG4878
CC00233	sm	Smooth; mRNA binding	CG9218
CC00236	shep	Alan Shepard; mRNA binding	CG32423
CC00479	pum	Pumilio	CG9755
CC00511	CG32062	Ataxin-2 binding protein 1; transcription factor binding	CG32062
CC00645	CG7185	alternative nuclear mRNA splicing,	CG7185
CC00737	Tudor-SN	transcription coactivator activity	CG7008
CC01220	CG33123	leucine-tRNA ligase activity	CG33123
CC01391	CG11266	CAPER; alternative nuclear mRNA splicing	CG11266
CC01563	Hrb98DE	Heterogeneous nuclear ribonucleoprotein at 98DE	CG9983
CC01925	tra2	transformer 2; regulation of nuclear mRNA splicing	CG10128
CC02043	Aats-glupro	Glutamyl-prolyl-tRNA synthetase	CG5394
CC06033	Hrb87F	Heterogeneous nuclear ribonucleoprotein at 87F	CG12749
CC06119	CG9809	Spargel; mRNA binding	CG9809
G00108	CG32423	Alan Shepard; mRNA binding	CG32423
G00261	shep	Alan Shepard; mRNA binding	CG32423
P00002	sqd	Squid; mRNA binding	CG16901
YB0052LE	Rm62	RNA interference	CG10279
YB0060	sqd	Squid; mRNA binding	CG16901
YB0077	Rm62	RNA interference	CG10279
YB0256	Rm62	RNA interference	CG10279
YC0015	Hrb98DE	Heterogeneous nuclear ribonucleoprotein at 98DE	CG9983
YC0023	sm	Smooth; mRNA binding	CG9218
YD0623	Rm62	RNA interference	CG10279
ZCL0588	Hrb98DE	Heterogeneous nuclear ribonucleoprotein at 98DE	CG9983
ZCL0734	sqd	Squid; mRNA binding	CG16901
ZCL2020	Pabp2	poly(A) RNA binding.	CG2163

Table 2.2- Transcripts Tested for Their Localization at LamC Foci

Gene	Probe ID	Forward Primer	Reverse Primer	Signal at foci
Evenness Interrupted/Wntless	Evi/Wls	AAGGTCACACTGCTTTGTTG	ACAGAAAGAGGAAATAAATGGCTG C	no
Atypical Protein Kinase C	aPKC	TTTAAGACAGAGGCCGCACG	ACACATCTTCCAGGCCAAGC	no
dCASK/Caki	dCASK	AGTTTCAGAAGAACACGGAC	AAGAAGTGACCGTATAGCTG	yes
Saxophone	Sax	GGCCCAGTAAACGCAATACG	CTATCACGCAGGAGCCGTTC	no
Mothers against Dpp	Mad	ATGGATTTCAATCCAACAGG	GTCTCCCATCGCAAGGGTCT	no
Wishful thinking	Wit	GCTTTGTAGGGAGGTGTTGC	ACACTTTCTGTTTCACCATC	no
Thick vein	Tkv	CACACCCAAGCTGACCACAC	TACATCATCCTCCTGCCAGC	yes
Shibire	Shi	TTGGCGTGGTGAATAGATCC	CCATCGGGACTAAATAAAGC	no
Par6	Par6 probe 1	GTCGAAGAACAAGATAAACACAACG	GCAGCACTCCATCCTTGACATC	yes
Par6	Par6 probe 2	GGATTAACCCGGCGATACAG	GACGAGTATTGGACACAATGAC	yes
Bazooka/Par3	Baz	CCAGCGCCTCCCATTCCGGT	GATAAGCAGCGCCGTGTTGC	no
Discs-Large	DLG	ATGGCGATGATAGCTGGTTATACG	CTCTTGGTCGCTGCCATCTTC	no
Actin 5C	Act5C	AAATGTGTGACGAAGAAGTTGCTG	TTAATACGCTGGAACCACACAAC	no
Fasciclin 2	FasII	GCTCGAAATGATCGGAATAG	CACAGCAAGAGGCAAACCAG	no
dPak	dPak	TCCAAGAAGCCAGTGGAGAAG	TATTCTTGTCCAGCGTCGTCG	yes
Beta Spectrin	ßspec	TATGTGGATATGCGGGATGG	ATAACGCTCCGATTCCAGTTC	no
Ca^{2+}/ Calmodulin-dependent protein kinase II	CamKII	TGTACGCGTTTTTCGGACAATTACG	CGACTGTAGTACTGCGATCAACGG	yes
Membrane associated guanylate kinase Inverted	Magi	GCCAATAATCACGGCCACGAC	TCCCGTCACTTCCCACAATC	yes
Glutamate Receptor IIC	GluRIIC	AGTTCGACGAGGATGGACAG	GGTCAACACCTTCCAGATTGTC	no
Wingless	Wg	CATTGCCAAGGTCGGCG	GCCGGTATCGACGAATTCC	no

Movie 2.1- RNA Granule Leaving the Foci

This movie represents a single confocal slice through a body wall muscle nucleus stained with E36 dye. The entire movie represents 3 min, 36 s in real time (18 s per time point), or 12 frames, played back at 3 frames per second. Arrowhead points to exiting granule. N = nucleus, nu = nucleolus

http://www.cell.com/cell/fulltext/S0092-8674(12)00420-5#

Movie 2.2- RNA Granule Leaving the Foci

This movie represents a projection of three confocal slices (~1.5 µm) through a body wall muscle nucleus stained with E36. The movie represents 2 min, 8 s in real time (17 s per timepoint), or 8 frames, played back at 3 frames per second. Arrowhead points to exiting granule. N = Nucleus, nu = nucleolus.

http://www.cell.com/cell/fulltext/S0092-8674(12)00420-5#

EXPERIMENTAL PROCEDURES

Fly Strains. All flies were reared on standard *Drosophila* medium at temperatures between 18-29 ˚C, depending on the nature of the experiment. The following strains were used: Canton S (CS) (*wild type*); *w;LamC*^{EX296} / *w;LamC*^{EX265}, *P*-element excisions predicted to be protein nulls (Schulze et al., 2005); *w;;dfz2*^{C1} *FRT2A /Df(3L)dfz2* (Mathew et al., 2005). For muscle rescue of *lamC* nulls we used *w;LamC*^{EX265} */ BG487, LamC*^{EX296}*; UAS-LamC-3 /* +, with BG487-Gal4 driving expression in muscle 6/7 in an antero-posterior gradient (Gorczyca et al., 2007). The following RNAi lines were utilized: UAS-DFz2-RNAi (ID – 44391; Vienna Drosophila RNAi Center [VDRC]) (Dietzl et al., 2007), UAS-LamC-RNAi built in the pWiz vector (see below) and UAS-aPKC-RNAi (Ramachandran et al., 2009). UAS-Par6-RNAi (ID-19371, VDRC), and UAS-Baz-RNAi (Ramachandran et al., 2009). For DFz2 overexpression, we used UAS-DFz2 (Mathew et al., 2005). For PKM expression we used UAS-PKM (Ruiz-Canada et al., 2004) and hs-PKM (Drier et al., 2002). RNAi knockdown, DFz2 overexpression and UAS-PKM expression was carried out using the muscle-specific Gal4 strain C57-Gal4 (Budnik et al., 1996). We also used the GFP traps: PABP2-GFP (ZCL2020) and *lamC*$^{GFP\text{-}trap}$/+ (G00158) (Yale FlyTrap collection); Morin et al., 2001), containing GFP fused in frame to the endogenous loci (Buszczak et al., 2007; Kelso et al., 2004; Morin et al., 2001).

Immunocytochemistry and Fluorescent Dye Labeling. The following antibodies and fluorescent labels were used: mouse anti-LamC, 1:30 (LC28.26;

Developmental Studies Hybridoma Bank (DSHB))(Riemer et al., 1995), rabbit anti-DFz2-C, 1:500(Mathew et al., 2005), mouse anti-nuclear pore complex mAb414, 1:300 (ab24609- Covance)(Aris and Blobel, 1989), rabbit anti-PABP2, 1:1500 (Benoit et al., 1999), rabbit anti-Baz, 1:600 (Wodarz et al., 1999), rabbit anti-aPKC, 1:2000 (Sigma) rabbit anti-PKC substrate, 1:2000 (Cell Signaling Technology), goat anti-Horseradish Peroxidase (HRP) 1:200 comjugated to Dylight 488, 594, or 649 (Jackson Immunoresearch), Alexa Fluor 488 conjugated-Conconavalin-A (ConA) 50 µg/ml (Molecular Probes), Propidium Iodide (PI) 10 µg/ml (Sigma), Hoechst 3342, 100 µg/ml, texas red (TxR)-conjugatged dextran, 50 µg/ml (70kD; Molecular Probes), and E36 RNA dye(Li et al., 2006), 10µM in HL3 saline and 0.2% DMSO. For PI staining, fixed body wall muscle preparations were first treated with 500 µg/ml RNAse A for 20 minutes and then incubated with PI for 20 minutes. Hoechst 3342 staining was applied to preparations for 1.5 hours. Fixable texas red (TxR)-conjugatged dextran was pressure injected into the muscle using a PV380 Pneumatic PicoPump and beveled sharp electrodes. Briefly, sharp electrodes (~4-5 megaohm) were pulled on a Flaming/Brown micropipette puller and then beveled at a15˚ angle to a final resistance of ~2 megaohm. Dextran dye was resuspended in an internal patch clamp solution(Yoshihara et al., 2000) and passed through a 0.2 µm filter via centrifugation. Muscles 6 or 7 from dissected larval body wall muscle preparations bathed in 0.1 mM Ca^{2+} HL3 saline were pressure injected using 4 ms pulses of ~ 8-10 lbs until sufficient dye was injected as determined under

epifluorescence. After injection, the dye was typically given ~ 40 minutes to diffuse before fixation. All fixations were performed at room temperature with ice-cold, freshly made, 4% paraformaldehyde for 15 minutes.

Image acquisition and analysis. Confocal images were acquired using a Zeiss LSM5 Pascal confocal microscope equipped with a Zeiss 63x Plan-Apochromat 1.4 NA DIC oil immersion objective at a digital zoom of 3x which met the Nyquist sampling requirements (pixel size equals 51 nm in XY) and Z step of 170 nm, unless otherwise indicated. Hoechst 3342 images were captured with a spinning disk confocal microscope equipped with a CoolSNAP^{TM} HQ camera (1392x1040) and a Nikon 60x Plan-apochromatic, NA 1.4 objective. FISH images were captured on a spinning disk confocal microscope equipped with a Zeiss 63x Plan-Apochromat 1.4 NA DIC oil immersion objective and a Hamamatsu C9100-13 EM-CCD camera (512x512), with a total magnification of 150X to the CCD (pixel size = 100 nm in XY) and a 200 nm step. For deconvolution, as noted in figure legends, images were deconvolved using measured point spread functions (PSF) and the iterative deconvolution algorithm in the image analysis software package Volocity (Perkin Elmer). Briefly, a PSF was obtained for each acquisition channel (laser lines 488, 543 and 6330 to avoid chromatic aberration issues and reregistering images if necessary) by drying the appropriate wavelength Molecular Probes PS-Speck beads (505/515, 540/560 and 633/660) onto the back of a coverslip and imaging the beads under the same conditions as for the experimental images, with the exception of the laser power and PMT/CCD

gain. To check for changes in the PSF at depth in the muscle, beads were injected into the muscle and imaged as they lay on top of the actin contractile apparatus, roughly the same plane at which nuclei lie. No obvious differences were seen with the PSF from these beads and those at the back of the coverslip, and deconvolution using the two PSFs gave similar results. Thus, PSF measurements from the back of the coverslip were utilized for the remainder of the studies. In Volocity, an iteration limit of 13 was set on the deconvolution process. Deconvolved images were exported as TIFFs from Volocity and opened in Photoshop for image construction.

Quantification of foci, ghost boutons, and bouton volume. Nuclear foci were counted at muscles 6 & 7 from abdominal segments A2 and A3 of wandering third instar larvae. All nuclei in each of these muscles were quantified. The average number of foci per nucleus was calculated by dividing the total number of foci by the total number of nuclei quantified. The number of foci/nucleus was normalized to simultaneously processed wild type controls. Number of nuclei analyzed is: wild type=2596, *eag Sh*=530, DFz2-RNAi-muscle=593, UAS-DFz2-muscle=617, $dfz2^{C1}$/Def=302, $LamC^{EX265}$/ $LamC^{EX296}$=413, C57/+= 328, aPKC-RNAi-muscle=532, wild type with chelerythrine=726, PKM-muscle=677, wild type heat shock=713, hs-PKM no heat shock=601, hs-PKM with heat shock=595, Baz-RNAi-muscle=652. Total number of boutons was quantified in 3rd instar larval preparations double labeled with antibodies to HRP and GluRIII, at segments A3 muscles 6-7. The number of ghost boutons was assessed by

counting HRP immunoreactive boutons that were devoid of GluRIII immunoreactivity. Number of NMJs analyzed: wild type=12, *LamC*^{EX265}/ *LamC*^{EX296} =12, *LamC*^{EX265}/ *LamC*^{EX296} muscle rescue=18).. Number of NMJs analyzed is: wild type=17, *LamC*^{EX265}/ *LamC*^{EX296} =25, LamC-RNAi-muscle=16, *lamC*$^{GFP\text{-}trap}$/+=16. Muscle surface was measured by multiplying the width by the length of muscle 6 in segment A3, determined using a scale within the ocular of the epifluorecence microscope. Number muscles measured is: wild type=18, *LamC*^{EX265}/ *LamC*^{EX296} =31, UAS-LamC-RNAi-muscle=15, *lamC*$^{GFP\text{-}trap}$/+=15. Bouton volume was quantified using Volocity by cropping the image to individual boutons based on HRP staining, and then using the software to measure volume. Number of boutons analyzed is: wild type= 263, *LamC*^{EX265}/ *LamC*^{EX296}=108, *LamC*^{EX265}/ *LamC*^{EX296} muscle rescue=64. For the analysis of PABP2-GFP foci vs. F2zC foci, the number of PABP2-GFP and dFz2C foci in a given nuclei was counted and then plotted against each other (N=113 nuclei) (Fig. SF4B). As not all nuclei have a PABP2-GFP or Fz2C foci a Spearman correlation analysis in Prism5 was run on the data, which suggested there is a significant positive correlation between PABP2 and DFz2C foci (Spearman R=0.52). Analysis of the data with a Generalized Extreme Studentized Deviate (ESD) test suggested there were multiple outliers in the data set (these outliers were not excluded from the graph in Fig. SF4B). To ensure that these were not eliciting an erroneous correlation, the outliers were removed and the analysis performed again. This analysis also suggested a significant positive correlation ($p<0.0001$) between the

two foci (Spearman R= 0.44). The number of PABP2-GFP foci was quantified by placing the PABP2-GFP strain into the two experimental genetic backgrounds. Number of nuclei is: control=229, $LamC^{EX265}$/ $LamC^{EX296}$ =175, $dfz2^{C1}$/Def= 301.

Chelerythrine feeding. Wild type larvae were raised under ideal density (50 just hatched larvae per 5 ml medium) in a 25-degree humidity controlled incubator. When larvae were mid-third instar (selected based on size) they were placed on food plates containing, freshly mixed, either 15µL 26mM Chelerythrine (in water) or 15µL water (control) per 4 ml media and incubated at 25 ˚C for 21 hours prior to fixing. Plates were wraped with aluminum foil as Chelerythrine is light sensitive.

Lambda Phosphatase treatment. Wild type larvae were dissected and fixed and then divided between two 0.5mL tubes, both containing 400 µL of 1X NEBuffer for PMP with 1mM $MnCl_2$. One tube contained 10,000 Units of Lambda protein phosphatase (New England Biolabs) and the other an equal volume of water. Both tubes were incubated on a rotating shaker at 37°C for 1 hour. Samples were then washed in 0.2% Phosphate buffered triton and processed for immunocytochemistry.

Heat shock protocol. Food plates were made as above, but with no drug added. Mid-late third instar larvae were collected from wild type and hs-PKM vials and either left at room temperature (control) or shifted to 30°C for 30 minutes. Then, they were returned to room temperature for a two-hour recovery period prior to dissection.

Statistical Analysis. Statistical analysis was performed on raw data (i.e.- not normalized or transformed). Unpaired two-tailed Student's t-tests were run for comparisons of experiments where a single experimental sample was processed in parallel with a wild type control. If the variance between the samples was significant, an unpaired t-test with Welch's correction was performed. In cases where multiple experimental groups were compared to a single control, a one-way ANOVA was performed, with either a Tukey (if variance was not statistically significant) or Dunnet (if variance was not homogeneous) post-hoc tests. All statistical analysis was carried out in Prism 5 (Graphpad Software, Inc.). Error bars in all graphs represent ±SEM.

E36 RNA dye staining and live imaging. Larvae were grown at 25˚C at low to mid density. One hour prior to dissection and imaging, larvae were placed for 1 hour at 29˚C to increase activity. Single larvae were dissected in 0.1 mM Ca^{++}-containing HL3 saline, leaving body wall muscles and CNS intact. Then, the preparation was incubated in 100 μM E36 for approximately 20 minutes at room temperature, washed, and the nuclei imaged by time-lapse microscopy for approximately 20 min at 150X magnification using a 40X 1.2NA water immersion objective, using an Improvision spinning disk confocal microscope. Image acquisition was carried out through a Z-stack spanning the entire volume of the nuclei, including fiduciary markers, such as trachea, neighboring nuclei and nucleoli. After imaging, samples were fixed and immunostained with antibodies to LamC and/or DFz2C. Samples were imaged again to identify the foci and images

scaled to time-lapse images using the fiduciary markers. For analysis of movies, individual granules were tracked across Z-sections by hand. The movie shown Suppl. Movie 1 is a single confocal slice and represents 3 minutes, 36 seconds (18 seconds per frame), while Suppl. Movie 2 is a Z-stack of 3 slices, as the granule moved across these focal planes and represents 2 minutes, 8 seconds (17 seconds per frame).

Fluorescence In-situ Hybridization (FISH). The FISH protocol is an adaptation of (Tam et al., 2002). Briefly, larvae were dissected, pre-extracted for 5 min in RNAse-free 0.1M Phosphate buffer containing 0.5% Triton-X100 (0.5% PBT) and 10mM Ribonucleoside-vanadyl complex (RVC, New England Biolabs), and then fixed in ice-cold 4% Paraformaldehyde (Sigma) in 0.1M phosphate buffer for 30 minutes. Preparations for synaptic FISH were then transferred directly to 0.2% PBT with 10mM RVC, while preparations for nuclear in situ were fixed for an additional 10 min in ice cold 100% Methanol, and then transferred to 0.2% PBT with 10mM RVC. Preparations were dissected quickly to minimize RNA degradation, with less than 30 min between the first and last preparation. Samples were incubated for a minimum of 20 min in 0.2% PBT, with one exchange of fresh 0.2% PBT with 10mM RVC after 10 min. Samples were then gradually exchanged into hybridization buffer (2X SSC, 10% Dextran Sulfate, 20mM RVC, 50% Formamide), by first mixing with 50% hybridization buffer for 5 min, and then with 100% hybridization buffer for 10 min. Probes (see below) were mixed (equal parts digoxigenin-tagged probe and blocking probe) and

heated to 80℃ for 10 min, then combined with concentrated hybridization buffer (4X SSC, 20% Dextran Sulfate, 40mM RVC) to a final concentration of 2.5ng/μL probe and blocking probe, applied to samples, and incubated at 37℃ for 3 hr (for synaptic FISH) or up to 18 hr (for nuclear FISH). Samples were then washed sequentially in 2X SSC with 50% formamide, 2X SSC, and 1X SSC for 15 min each. Samples were then exchanged back to 4X SSC, and then incubated in 1:100 Sheep anti-Digoxigenin (Sigma) with 20mM RVC for 1 hr at 37℃. Preparations were then washed in 4X SSC, 4X SSC with 0.1% Triton-X100, and 4X SSC for 10 min each, then fixed in 4% paraformaldehyde for 10 min, and washed 3 times in 0.2% PBT for 10 min each. Preparations were subsequently treated for 2 hours with 1:200 Donkey anti Sheep-FITC, washed 3 times in 0.2% PBT, and then overnight in 1:700 Rabbit anti-FITC (Invitrogen) and either 1:30 Mouse anti-LamC (DSHB) (for nuclear FISH) or anti-FITC alone (for synaptic FISH). Finally, preparations were incubated with fluorescently labeled quaternary antibodies labeled with Dylight 488, Dylight 594, or Dylight 649, and Goat anti HRP-Dylight 594 or Dylight 649 (Jackson Immunoresearch).

Probe preparation for FISH. Probes were designed against 0.8-1.4 Kb regions of genes of interest (Suppl. Table 2) that showed minimal (less than 18 bp similarity) to no homology to other genes in the *Drosophila* genome. Probes were PCR amplified from cDNA, purified, and then applied to a Bionick (Invitrogen) nick translation kit, along with digoxigenin-11-dUTP (Roche), incubated for 2.5 hr at 18℃, treated with 5% SDS plus 0.25M EDTA and heated to 65℃ for 10 min.

Probes were then mixed with 10µg salmon sperm DNA for every 1µg probe, and precipitated with ethanol and sodium acetate. Probes were resuspended in 100% formamide to a concentration of 10ng/µL, and stored at -20℃ until needed. Blocking probe was prepared the same way as above, but with dTTP in place of dig-dUTP. PolyT and PolyA probes were 24 nucleotide oligos with digoxigenin tags on both the 3' and 5' ends (Integrated DNA Technologies).

Electron Microscopy. Transmission electron microscopy was carried out as in (Korkut et al., 2009). Immuno-gold labeling was accomplished by a modification of the protocol by (Yamashita et al., 2009). Briefly, larvae were dissected and fixed with 4% formaldehyde containing 2.5 mM $CaCl_2$, 1.25 mM $MgCl_2$ in a 0.1 M HEPES buffer (pH 7.4) for 2 hrs and then with the same fixative in 0.1 M HEPES (pH 8.5) overnight at room temperature. Osmolarity of the fix solution was adjusted to ~ 330 mOsm by the addition of glucose. After fixation, specimens were rinsed in fresh HEPES buffer and dehydrated in a graded series (50%, 70%, 90%, and 100%) of dimethylformamide (DMF) on ice. Samples were infiltrated with DMF and LR White at ratios of 2:1 and 1:2 respectively for 30 min each and finally with pure LR White overnight at 40℃. Polymerization of the resin was carried out overnight at 55℃. Ultrathin sections were collected on Nickel grids and incubated with 20 mM Tris buffer (pH 9.0) for 2 hr at 95℃ in a PCR cycler. After cooling, the grids were washed in 0.1M TBS (pH 7.2) for 30 min at room temperature. Subsequently the grids were incubated with LamC (1:50 to 1:5) and/or DFz2C (1:500 to 1:250) antibodies overnight at 4℃. Grids

were then washed in 0.1 M TBS (pH 7.2) for 30 min at room temperature. Immuno-gold labeling was accomplished with 12 nm or 18 nm colloidal gold particles conjugated to secondary antibodies for 1-3 hrs. After washing in TBS for 30 min the grids were fixed with 2% glutaraldehyde containing 0.05% tannic acid in 0.1 M phosphate buffer (pH 5.5) for 5 min. Some grids were exposed to osmium vapor for 5- 10 min and then all grids were stained with uranyl acetate and lead citrate and viewed with a FEI EM 10 electron microscope at 80 kv.

Regressive EDTA. Regressive EDTA was conducted as in(Monneron and Bernhard, 1969) Briefly, grids were stained with freshly prepared 5% uranyl acetate for 3 min, then rinsed in water for 3 min. Grids were then immersed in 0.2M EDTA pH-7 for 3 -4 hr, washed in water, stained with lead acetate and viewed with a Philips EM10 electron microscope.

Molecular Biology. The UAS-LamC-RNAi construct was subcloned in the *Drosophila* pWiz transformation vector(Lee and Carthew, 2003). Briefly, a 547 base pair fragment

(1:ATCGATCTCAAGCTTGGCCTTCTCTTTGGCGGTCTCATCGAGCAGCTTGC
GAGCGGCGGCCAGCTCCTTCTCATAGACCGCCTTCAGATTAGAGGTCTCCC
TGTTGACGGTATCCTGGGCGAGATTCAGTTCCTGGGTGAGCCGGCTGTTCT
CGTTCTCCAGGTTGCGCATGCGATCGATGTAGCAGGCCAGGCGATCGTTCA
AATGCTGCAGTTCCTCCTTCTCCTGCTGCCGGCTGGTGCGCGTGGGCGAG
GTGGGTGAGGTGGCGCCCACCCTTGACGAGGTGGATGCCCCGCCCACCG
GCGTGGAGGTGGAGGCGCGCGAAACGCGTGTGTTCAATGTGACGCGGCGT

GCTGACATTTTTGCAATGTGTTTTCTTTTCTTTTTGCGAGGTGCGAGTTGCTA
AGTTAAGTACGTAATCCTCTCAAGTCACTGTCAATATTTTTCCAGACGTTTGA
TTCTGAATTTTTTTTTGCTTGTACGTCCGCCTGCTTTGACGACTAAAAATTGAC
TGAAACTTTGACTCGAAACGAACGGCTATCATCGAC:547) was cloned from a cDNA library and ligated in opposing orientations into the EcoR1/AvrII and NheI/XbaI sites of pWiz, which flank a consensus *Drosophila* intron from the *white* gene, thus creating a double stranded snapback RNA when expressed.

Western Blot. Body wall muscles were dissected and homogenized in lysis buffer with phosphatase inhibitors (Ramachandran et al., 2009) and 2-3 larval equivalents were loaded in each lane of a 10% acrylamide gel and transferred to a nitrocellulose membrane. The membrane was then blocked with 3% BSA, and probed with either Rabbit anti-PKC phosho-serine substrate (Cell signaling) or Mouse anti-LamC (DSHB). After second antibody incubation, using either Donkey anti-rabbit or anti-mouse secondary antibodies conjugated to peroxidase, a Chemiluminescent detection kit (GE life sciences) was used to detect the signal.

Preface to Chapter III

In this chapter we begin to elucidate the molecular mechanisms underlying mega-RNP budding. We identify Torsin, a AAA-ATPase, implicated in early onset dystonia, as a mediator of the inner nuclear membrane scission during nuclear envelope budding of large RNA granules.

My contribution to this Chapter are: Figures 3.1, 3.2A-G, 3.3A-L, 3.4A-G, 3.6, 3.7A-B
John Nunnari contributed: 3.2A-G, 3.3A-D, 3.4C-G
James Ashley contributed: Figure 3.5, 3.7C-D
Vivian Budnik contributed: Figure 3.2H-I

The following chapter has been published as:

Jokhi V, Ashley J, Nunnari J, Noma A, Ito N, Wakabayashi-Ito N, Moore MJ, Budnik V. *Torsin mediates primary envelopment of large ribonucleoprotein granules at the nuclear envelope.* **Cell Rep. 2013** Apr 25; 3(4):988-95.

Chapter III

Torsin mediates primary envelopment of large ribonucleoprotein granules at the nuclear envelope

INTRODUCTION

Polarized assembly of cellular complexes often depends on formation of translationally silent RNA transport granules containing mRNAs and associated structural and regulatory components (e.g., proteins and miRNAs). These RNA-protein complexes (RNPs) are shuttled to distinct cellular locales where, upon specific stimuli, the mRNAs are translated into protein building blocks for local cellular architectures and macromolecular complexes (Richter, 2001). Particularly notable is RNP transport in the nervous system, where long-term changes in synaptic structure and function frame key events enabling organisms to respond to their changing environment. A special case of this adaptation is the ability of organisms to learn and remember (Wiersma-Meems et al., 2005). In these processes, localized translation of mRNAs links synaptic plasticity-inducing stimuli to the synthesis of effector proteins underlying enduring changes in synaptic structure and function (Barco et al., 2008).

Until recently, it was thought that all mRNA export occurred one molecule at a time through the nuclear pore complex (NPC) suggests that mRNAs are exported one molecule at a time (Grunwald et al., 2011; Kohler and Hurt, 2007). However, we recently uncovered a previously unrecognized mechanism by which large ribonucleoprotein (megaRNP) granules exit the nucleus via nuclear envelope-(NE) budding (Speese et al., 2012), a mechanism previously shown to be utilized for the nuclear export of large Herpes-type viral capsids (Maric et al., 2011a; Mettenleiter et al., 2006). This budding process and the signaling pathway that it

initiates are essential for normal synaptic bouton development at the *Drosophila* larval NMJ (Ataman et al., 2006a; Mathew et al., 2005; Speese et al., 2012). NE-budding entails primary envelopment of viral capsids (Mettenleiter et al., 2006) or megaRNPs (Speese et al., 2012) by the inner nuclear membrane (INM); scission of this envelope from the INM creates a membrane bound particle within the perinuclear space, which subsequently fuses with the outer nuclear membrane (ONM) to allow nuclear escape of the enclosed material. However, the molecular mechanisms required for primary envelopment, INM scission and fusion were previously unknown. Here we identify Torsin, a AAA-ATPase that in humans is linked to both dystonia (Breakefield et al., 2008) and Herpes virus nuclear egress (Maric et al., 2011a), as a major mediator of primary megaRNP envelopment during NE-budding, likely functioning to promote INM scission. In *torsin* mutants, including those mimicking genetic abnormalities in dystonia patients, megaRNPs accumulate within the perinuclear space and the mRNAs contained within fail to reach synaptic sites, preventing normal synaptic protein synthesis, and thus proper synaptic bouton development.

RESULTS

Torsin mutants result in nuclear DFz2C/LamC foci morphology

In humans, the dystonia-specific Torsin1A (TOR1A) mutation TOR1A$^{\Delta E302/303}$ (also known as TOR1A$^{\Delta GAG}$; referred to as Torsin$^{\Delta E}$ in this paper) at the DYT1 gene locus is linked to early onset primary dystonia (Tanabe et al., 2009). Mouse models expressing *TOR1A*$^{\Delta E302/303}$ accumulate abnormal vesicular structures at the NE (Goodchild et al., 2005; Naismith et al., 2004). These NE structures show a striking resemblance to the perinuclear megaRNPs we recently reported in *Drosophila* (Speese et al., 2012), raising the intriguing possibility that these structures could be related. In cultured Schneider-2 (S2) cells and *Drosophila* larval muscles, megaRNP clusters at the NE can be marked at the light microscopy level by antibodies to the C-terminus of the Wnt receptor, DFrizzled2 (DFz2C) and the INM-associated protein, Lamin C (LamC). DFz2C and LamC partially colocalize at NE-associated foci (DFz2C/LamC foci) (Mathew et al., 2005; Speese et al., 2012). To determine if NE defects observed in *TOR1A* mutant animal models reflect defects in NE-budding, S2 cells were treated with Torsin-dsRNA, targeting the sole *Drosophila* homolog of mammalian *TOR1A* (Wakabayashi-Ito et al., 2011). This resulted in significant abnormalities in DFz2C/LamC foci at the NE. In untreated S2 cells, NE-DFz2C foci appear as bright immunoreactive spots embedded in a thickening of the lamina, marked by LamC (Speese et al., 2012) or the B-type lamin LamDm0 (Figure 3.1A). In contrast, Torsin-dsRNA-treated cells displayed small DFz2C-immunoreactive

puncta dotting the NE, and thickenings of the lamina were barely visible or absent (Figure 3.1B; see below for quantification of this phenotype in vivo). In mammals, Torsin isoforms are derived from four genes: Tor1A, Tor1B, Tor2A, and Tor3A. The DYT1 mutation in Tor1A specifically affects the neuronal NE (Goodchild et al., 2005), consistent with the belief that dystonia is a disease of the nervous system. This neuronal specificity is likely due to compensation by expression of torsinB in nonneuronal tissues, as knockdown of TOR1B in a DYT mutant background caused NE defects in nonneuronal cells (Kim et al., 2010). In Drosophila, there is a single torsin gene, thus overcoming difficulties associated with redundancy. Moreover, we previously showed that NE budding occurs in several cell types, including larval body wall muscle cells wherein the large nuclei are particularly suitable for high-resolution studies (Speese et al., 2012). In addition, the glutamatergic larval NMJ is a powerful model system in which to understand mechanisms of synapse development and function.

To determine the significance of the S2 cell NE phenotype upon Torsin downregulation, DFz2C/LamC foci were examined in torsinKO78-null mutants (Wakabayashi-Ito et al., 2011) and in larvae in which Torsin was specifically downregulated in muscles by expressing Torsin RNAi using the muscle-specific Gal4 driver C57-Gal4 (Budnik et al., 1996). As in untreated S2 cells, NE DFz2C/LamC foci were observed in wild-type larvae as DFz2C immunoreactive spots surrounded by a thickening of LamC immunoreactivity (Speese et al., 2012) (Figure 3.1C). In contrast, in larvae expressing Torsin-RNAi in muscles

(Figure 3.1D) or in torsin-null mutants, DFz2C foci were observed as small puncta decorating the NE but lacking any detectable thickening of the lamina. These phenotypes were quantified by determining the percentage of nuclei containing DFz2C spots surrounded by a thickening of the lamina (normal foci; Figure 3.1G) and the percentage of nuclei containing small NE-associated DFz2C puncta lacking LamC thickening (Figure 3.1H). There were highly significant differences between wild-type controls and both torsin null mutants as well as larvae expressing Torsin-RNAi in muscles (Figures 3.1G and 3.1H).

Typical of AAA-ATPases, Torsin contains Walker A and Walker B domains involved in ATP binding and ATP hydrolysis, respectively (Neuwald et al., 1999; Wakabayashi-Ito et al., 2011; Walker et al., 1982), as well as Sensor1 and Sensor2 domains also involved in ATP hydrolysis (Iyer et al., 2004). A conserved amino acid deletion in the Sensor2 domain (Torsin$^{\mathbf{\Delta}E}$; Torsin$^{\mathbf{\Delta}E306}$ in Drosophila) is dominantly linked to dystonia (Ozelius et al., 1997). In addition, an amino acid substitution in the Walker B domain (Torsin$^{E\rightarrow Q}$; Torsin^{E177Q} in Drosophila) leads to a Torsin protein that can dominantly bind to its substrate but is unable to hydrolyze ATP and therefore remains bound to this substrate, thus constituting a substrate trap (Goodchild et al., 2005; Wakabayashi- Ito et al., 2011). To determine if Torsin$^{\mathbf{\Delta}E}$ or Torsin$^{E\rightarrow Q}$ transgene expression would also disrupt DFz2C/LamC foci morphology, we expressed these proteins in larval muscles. Expressing Torsin$^{\mathbf{\Delta}E}$ mimicked the torsin-null and Torsin-RNAi phenotypes (Figures 3.1E, 3.1G, and 3.1H). In contrast, Torsin$^{E\rightarrow Q}$ expression resulted in the

formation of numerous NE LamC foci, most of which were devoid of DFz2C immunoreactivity (Figures 3.1F1 and 3.1G–1I). Careful examination of these depleted LamC foci by confocal microscopy demonstrated that many contained a small DFz2C puncta, but this signal was barely visible (Figure 3.1F2, arrows). The above phenotypes observed upon expressing Torsin**D**E and TorsinE***I***Q were the specific results of the mutations in the Torsin transgenes, as larvae expressing a wild-type Torsin transgene were indistinguishable from wild-type not expressing this transgene (Figures 3.1G–3.1I).

Figure 3.1- Morphology of Nuclear DFz2C/Lam Foci Is Disrupted in Torsin Mutations

(A and B) Localization and morphology of DFz2C/Lam foci at the nuclei of S2 cells in (A) untreated cells and (B) cells treated with Torsin-dsRNA.

(C–F) Localization and morphology of nuclear DFz2C/LamC foci in larval muscles of (C) wild-type and (D–F) larvae expressing (D) Torsin RNAi, (E) TorsinDE, and (F) TorsinE/Q in muscles. F1 is a low-magnification view. F2 shows a high-magnification view of DFz2 puncta in the YZ and XY planes. (A)–(F) correspond to singe confocal slices.

(G–I) Percentage of nuclear foci showing (G) normal organization of DFz2C/LamC, (H) the presence of small DFz2C puncta associated with the lamina (see text), and (I) the presence of thickenings of the lamina devoid of DFz2C signal. Mus, muscle; N ([number of nuclei;number of larvae]), [908;6],[731;6],[639;6],[802;6],[846;6],[733;6],[693;6]. Error bars represent ±SEM;***$p < 0.0001$.

Calibration scales are 14 mm (4 mm for insets) in (A) and (B) and 10 mm (6 mm for insets) in (C)–(F).

Figure 3.1- Morphology of Nuclear DFz2C/Lam Foci Is Disrupted in Torsin Mutations

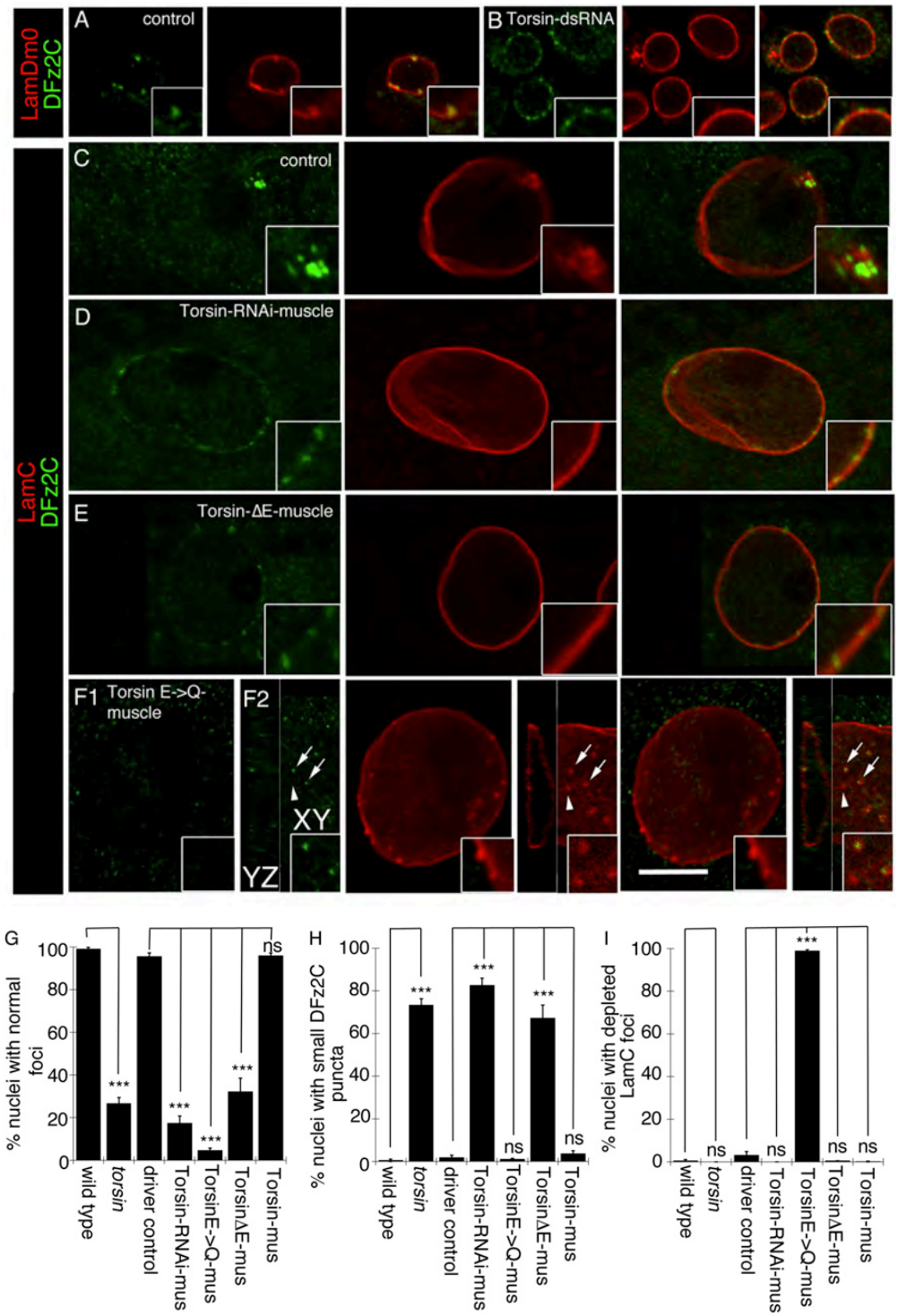

Ultrastructural Organization of NE-Associated megaRNPs Is Disrupted in Torsin Mutations

To determine the ultrastructural correlates of the above phenotypes, untreated and Torsin-dsRNA-treated S2 cells were examined by transmission electron microscopy (TEM). As previously described (Speese et al., 2012), untreated S2 cells displayed local singlets or clusters of megaRNPs within INM invaginations at discrete regions of the NE (Figures 3.2A, 3.2H, and 3.2I), paralleling light microscopy observations (Figure 3.1A). In contrast, in Torsin-dsRNA-treated cells, these local megaRNPs at the NE were reduced by ~75% (Figures 3.2H and 3.2I), and instead many mega-RNP granules were often observed in rows of singlets lining the perinuclear space (Figures 3.2B and 3.2C). In these regions, the perinuclear space appeared distended (green in Figures 3.2B and 3.2C) and the ribosome-decorated ONM appeared to evaginate. About half of megaRNPs appeared attached to the INM through a collared neck (arrows in Figures 2B, 2C, 2H, and 2I; see Experimental Procedures for definition). However, NPCs and the rest of the NE appeared normal (Figures 3.3A–D). In addition, the distribution of a number of nuclear proteins, such as the fly Emerin homolog Bocksbeutel (Figures 3.3E and 3.3I); dMan1 (Figures 3.3F and 3.3J); Otefin, a protein required for NE assembly (Figures 3.3G and 3.3K); and the Drosophila homolog of Hsap, Squid, a ribonuclear protein (Figures 3.3H and 3.3L), were normally distributed in the mutants. Thus, downregulating Torsin results in abnormal attachment of

megaRNPs to the INM, raising the possibility that Torsin could be involved in INM scission after primary megaRNP envelopment. Corroboration of the above results in vivo was obtained by examining larval body wall muscles of torsin-null mutants. As in S2 cells, megaRNPs tethered to the INM by a collared neck were observed in torsin-null mutant muscles and epithelial cells (Figures 3.2D, 3.2E, 3.2H, and 3.2I), suggesting this pathway functions in even more tissues than previously characterized. Similarly, muscles expressing Torsin$^{E\rightarrow Q}$ displayed INM-tethered megaRNPs (Figures 3.2F, 3.2H, and 3.2I). In ~30% of cases, megaRNPs in muscles expressing Torsin$^{E\rightarrow Q}$ appeared as large (>250 nm), amorphous, dense structures directly apposed to the INM (Figures 3.2G–3.2I). Thus, disruption of Torsin function in vivo leads to abnormal megaRNP tethering to the INM.

Figure 3.2- Ultrastructural Organization of NE-Associated megaRNPs Is Disrupted in Torsin Mutations

(A–G) Electron micrographs of nuclear regions in (A–C) S2 cells, (D, F, and G) larval body wall muscles, and (E) larval epithelial cells showing NE-associated megaRNPs. Red, nucleus; blue, cytoplasm; green, perinuclear space. N, nucleus; C, cytoplasm. (A) Untreated S2 cell showing a normal nuclear focus (arrow) containing electron-dense megaRNP granules. (B and C) NE of Torsin-dsRNA-treated S2 cells displaying megaRNPs tethered to the INM by collared necks (arrows), shown at (B) low and (C) high magnification. ribo, ribosome. (D and E) NE in torsin-null mutants also showing megaRNPs tethered to the INM (arrows). (F and G) NE in muscle cells expressing TorsinE/Q showing the presence of (F) a megaRNP (arrow) tethered to the INM and (G) a large, amorphous megaRNP (arrow) tightly apposed to the INM. mi, mitochondria.

(H) Percentage of megaRNP granules present in INM invaginations (black), with collared necks (blue) and being large and amorphous (red).

(I) Average number of megaRNP granules in INM invaginations (black), with collared necks (blue), being large and amorphous (red), or per focus (gray). N [number of granules;foci]), [159;36],[366;122],[207;33],[166;68],[181;88]. Error bars represent ±SEM; *$p < 0.05$; **$p < 0.001$; ***$p < 0.0001$).

Figure 3.2- Ultrastructural Organization of NE-Associated megaRNPs Is Disrupted in Torsin Mutations

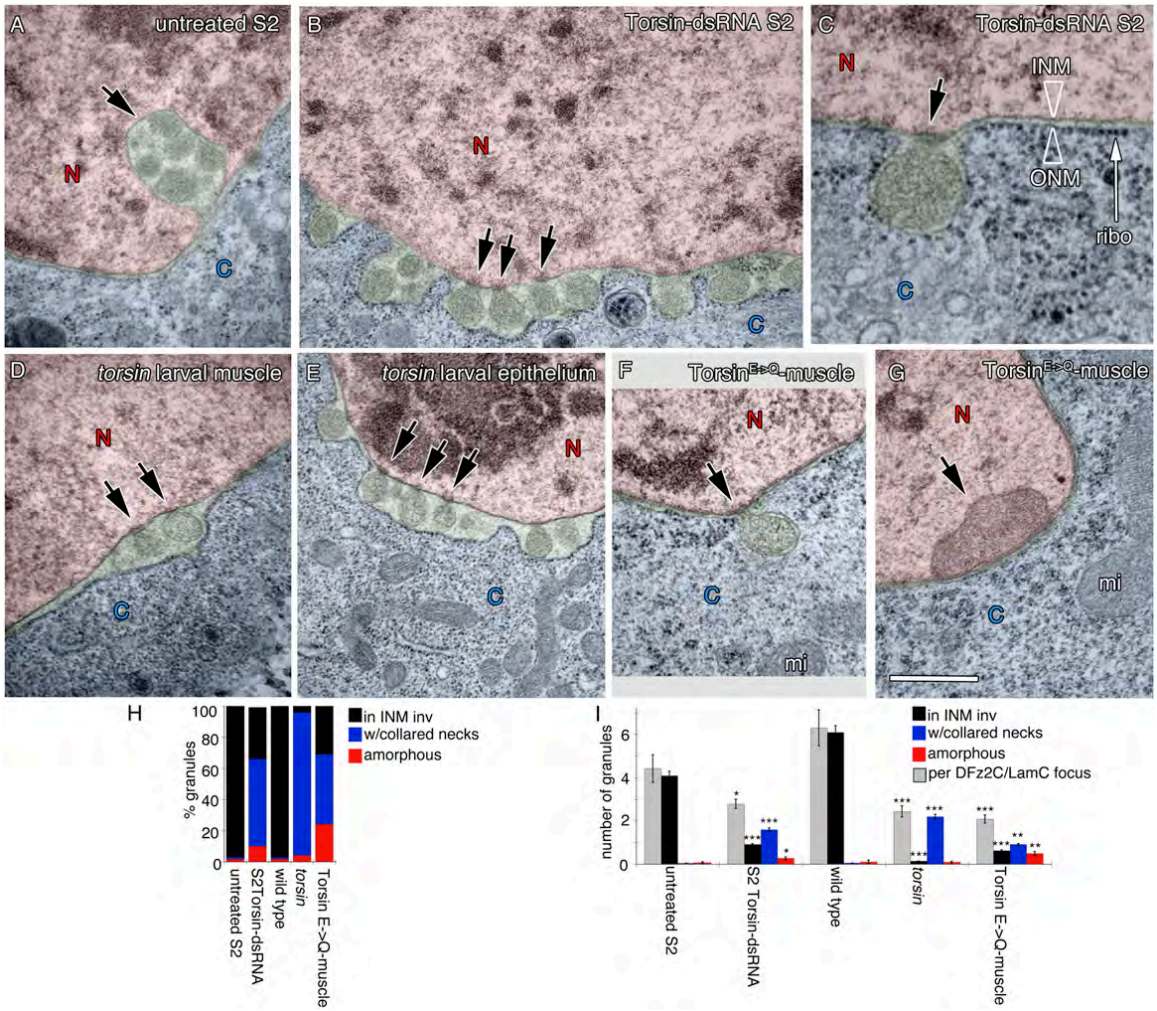

Figure 3.3- Ultrastructure of the NE and localization of NE proteins in wild type and *torsin* mutants

(A-D) Electron micrographs of the NE at larval body wall muscles from (A, B) untreated and (C, D) Torsin-dsRNA-treated S2 cells, shown at (A, C) low magnification and (B, D) high magnification. Arrows point to NPCs. N=nucleus, C=cytoplasm, g=megaRNP. (E-L) Confocal images of muscle nuclei labeled with antibodies to (E, I) Bocksbeutel, (F, J) dMan1, (G, K) Otefin, (H, L) Squid, in (E-H) wild type, and (I-L) *torsin* null mutant muscles 6 or 7. Calibration scale is 300 nm for A, C, 90 nm for B, D and 30 μm for E-L.

Figure 3.3- Ultrastructure of the NE and localization of NE proteins in wild type and *torsin* mutants

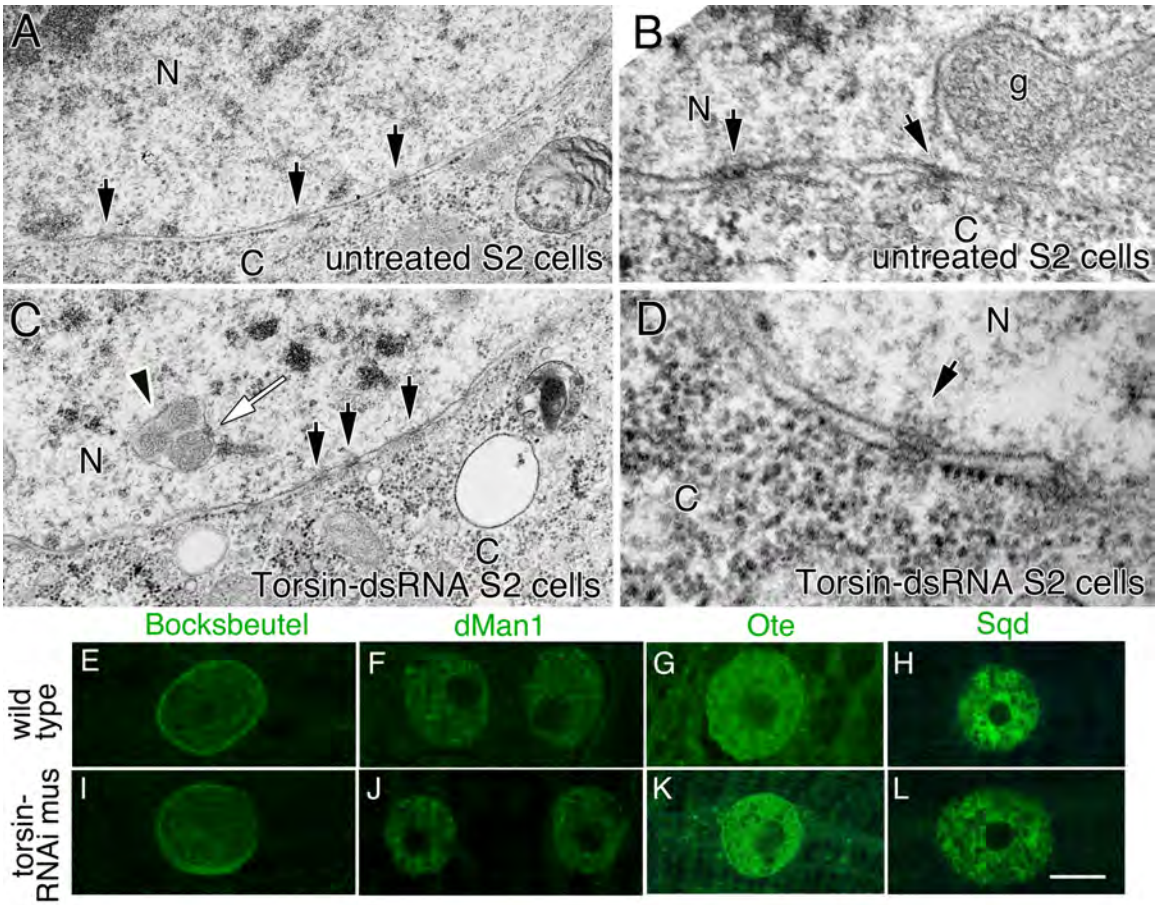

The Torsin$^{E\rightarrow Q}$ Protein Accumulates at megaRNP Collared Necks

If Torsin is involved in INM scission during megaRNP primary envelopment, then the substrate trap Torsin$^{E\rightarrow Q}$ should accumulate at the electron-dense collared necks. This prediction was tested by generating wild-type and Torsin$^{E\rightarrow Q}$ variants fused to a mini-SOG tag (Shu et al., 2011) at their C termini. Mini-SOG is a flavoprotein derived from Arabidopsis Phototropin 2 that when illuminated by blue light produces oxygen species that can convert diaminobenzidine into an electron-dense precipitate (Shu et al., 2011). We first determined if C-terminally tagged Torsin was localized to the NE. Although mini-SOG excitation results in fluorescence emission, its rapid bleaching upon illumination prevented highresolution acquisition of images. Therefore, we generated Flag-tagged Torsin constructs and expressed them in S2 cells. The wild-type Torsin-Flag signal localized to bright spots coinciding with Lamin foci at the NE; low levels were also observed at the NE and in the cytoplasm (Figure 3.4A). In contrast, Torsin$^{E\rightarrow Q}$-Flag was observed in a punctate pattern lining the NE (Figure 3.4B). Consistent with the above observations, S2 cells expressing Torsin-SOG displayed an electron-dense signal at sites of megaRNP occurrence in the NE (Figures 3.4C and 3.4E; see Figures 3.5A and 3.5B for specificity control). An electron-dense SOG induced signal surrounded each megaRNP (Figures 3.4C and 3.4E) in a relatively homogenous fashion, but local accumulations of the signal were also apparent (arrows in Figure 3.4E). A SOG specific signal was also observed at the INM and ONM in proximity to

megaRNPs (Figure 3.4E). In contrast, in cells expressing the substrate trap Torsin$^{E\rightarrow Q}$-SOG, a SOG-induced signal was concentrated at collared necks of INM-associated megaRNPs and little SOG signal surrounded the megaRNPs (Figures 3.4D and 3.4F). In cases where large amorphous megaRNPs were tightly apposed to the INM in Torsin$^{E\rightarrow Q}$, the SOG signal was considerably denser at the sites of contact between the megaRNP and the INM (Figure 3.4G). These observations suggest that Torsin is present at sites of NE budding. Further, accumulation of the Torsin$^{E\rightarrow Q}$ substrate trap protein at collared necks of megaRNPs suggests that these necks represent the normal site of Torsin action and provide evidence that Torsin is involved in scission of the INM during primary envelopment.

Figure 3.4- The Torsin$^{E\rightarrow Q}$ Protein Accumulates at megaRNP Collared Necks

(A and B) S2 cells expressing (A) wild-type Torsin-Flag and (B) the TorsinE/Q-Flag showing that Torsin-Flag accumulates at foci and TorsinE/Q is punctate at the NE.

(C–G) Electron micrographs of nuclear regions of S2 cells expressing (C and E) Torsin-SOG showing an electron-dense signal surrounding megaRNPs (arrows point to areas of increased signal density). (D, F, and G) TorsinE/Q-SOG showing that signal accumulates (D and F) at megaRNP collared necks or (G) at appositions of amorphous megaRNPs with the INM.

Calibration scales are 7 mm (A and B), 0.7 mm (C and D), and 0.3 mm (E–G).

Figure 3.4- The Torsin$^{E\rightarrow Q}$ Protein Accumulates at megaRNP Collared Necks

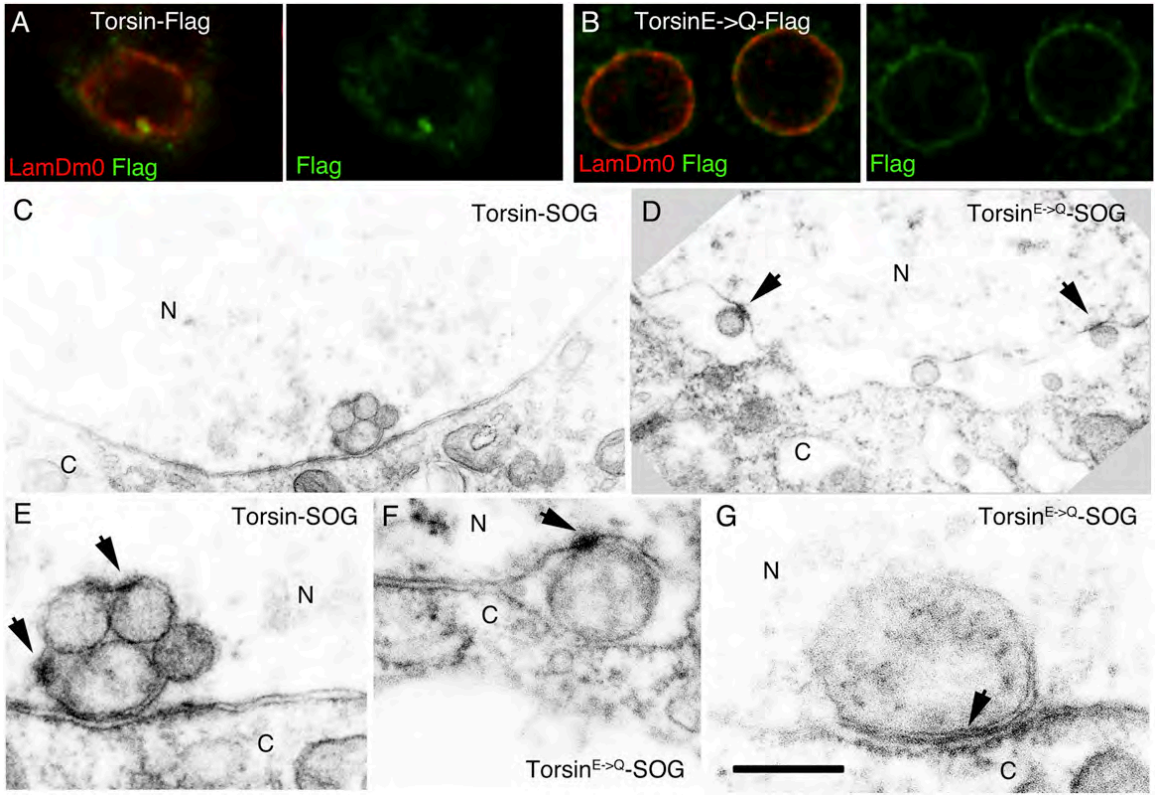

Figure 3.5- Torsin-SOG controls

(A, B) Electron micrographs of nuclear regions of S2 cells expressing Torsin-SOG without photoconversion, showing no increase in electron dense signal surrounding megaRNPs. (A1, B1) Are imaged under the same conditions as the micrographs in (Figure 3.4), while (A2, B2) have been taken at longer exposures to show structures more clearly. Calibration scale= 0.5μm

Figure 3.5- Torsin-SOG controls

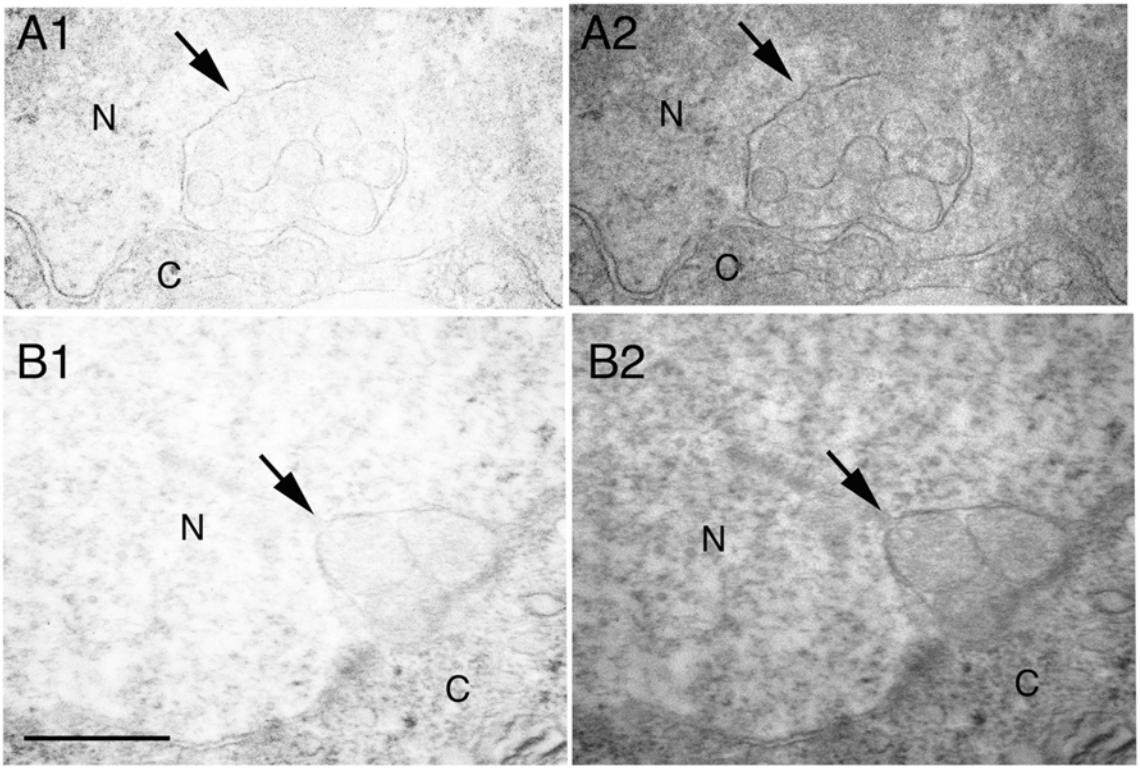

The Distribution of mRNAs at the NE and Synaptic Sites Is Disrupted in torsin Mutants

Our previous study revealed that in Drosophila larval muscles, megaRNPs contain transcripts encoding postsynaptic proteins, including the PDZ scaffolding proteins Par6 and MAGI (Speese et al., 2012). In the case of Par6, interfering with megaRNP formation by inhibiting the Frizzled nuclear import (FNI) pathway or LamC expression results in decreased NMJ localization of par6 mRNA (Speese et al., 2012), decreased postsynaptic Par6 protein levels (Speese et al., 2012), and marked defects in NMJ structure (Ataman et al., 2006, 2008; Packard et al., 2002; Speese et al., 2012). In particular, under these conditions, NMJs fail to expand normally as muscles grow in size during larval development, and a subset of synaptic boutons (called ghost boutons) remain in an immature state. These ghost boutons fail to recruit postsynaptic proteins and to organize postsynaptic specializations, such as the postsynaptic density and subsynaptic reticulum (Ataman et al., 2006, 2008; Packard et al., 2002; Speese et al., 2012).

The above observations support a model in which alterations in Torsin function inhibit nuclear megaRNP exit by slowing or blocking INM scission during primary envelopment. As a consequence, such alterations should result in abnormal transcript localization both in the nucleus and at synaptic sites as well as decreased synaptic protein synthesis, abnormal NMJ expansion, and an accumulation of ghost boutons. To ascertain the localization of megaRNP transcripts known to be present in megaRNPs at the NE, we carried out

fluorescence in situ hybridization (FISH) using par6 and magi RNA probes. As previously described (Speese et al., 2012), in wild-type muscles, par6 and magi mRNAs are enriched at NE foci associated with LamC foci or nuclear folds marked by antibodies to LamC (Figures 3.6A and 3.6B, top row). In contrast, in torsin-null mutants, par6 and magi FISH signals appeared as foci that, while associated with the NE, were on the cytoplasmic side of the LamC signal (Figures 3.6A and 3.6B, bottom row panels; Figure 3.6C). This is in agreement with the light and electron microscopy studies, showing that altering Torsin function prevents megaRNP nuclear egress and results in megaRNPs remaining attached to the INM within the perinuclear space.

When we examined FISH signals at the NMJ in wild-type controls, par6 mRNA was concentrated at subsynaptic sites as previously reported (Figure 3.6D, top panels) (Speese et al., 2012). However, this synaptic par6 FISH signal was virtually eliminated in torsin-null mutants (Figure 3.6D, bottom panels). Similarly, the synaptic localization of magi mRNA was significantly decreased in the torsin mutants (Figure 3.6E). The marked decrease in par6 and magi mRNA levels at the NMJ appeared specific for the NE-budding pathway, as no significant differences around the NMJ in torsin mutants were observed upon FISH of discs-large (dlg) RNA, which is not associated with nuclear DFz2C/LamC foci (Figures 3.7A-C) (Speese et al., 2012). Thus, in the absence of Torsin function, synaptic mRNAs known to be present in megaRNPs exhibit reduced localization at the NMJ, but a non-megaRNP mRNA does not. We also examined

Par6 and MAGI protein levels using antibodies specific to Drosophila Par6 (Ruiz-Canada et al., 2004) and MAGI (this report). In wild-type larvae, Par6 and MAGI immunoreactivity localized primarily to the postsynaptic muscle region of the NMJ (Figures 3.6F and 3.6G, top panels). In addition, Par6 immunoreactivity was observed in a diffuse manner at presynaptic boutons (marked by the anti-HRP signal), being particularly prominent at presynaptic microtubule bundles (Ruiz-Canada et al., 2004) (Figure 3.6F, top panels) and at low levels at the muscle cell cortex (Figure 3.6F, top panels). MAGI immunoreactivity was also observed at presynaptic compartments, but without noticeable concentration at microtubule bundles (Figure 3.6G, top panels). In torsin-null mutants, postsynaptic localization of Par6 immunoreactivity as well as muscle cell cortex signal was severely reduced (Figure 3.6F, bottom panels; Figure 3.6H), while presynaptic localization of Par6 at microtubule bundles appeared normal (Figure 3.6F, arrows). Similarly, postsynaptic MAGI protein localization was severely reduced in these mutants (Figure 3.6G, bottom panels; Figure 3.6I). Unlike Par6 and MAGI, DLG immunoreactivity was not changed in torsin mutants (Figure 3.6J; Figure 3.7D), suggesting that the defect is not general but affects only a subset of postsynaptic proteins. Thus, disrupting Torsin function prevents normal localization of some synaptic mRNAs and, as a consequence, normal postsynaptic levels of their encoded proteins. The functional consequence on NMJ structure of reduced Par6 and MAGI mRNA and protein levels at the postsynaptic compartment in torsin mutants was assessed by counting the

number of normal and undifferentiated ghost boutons observable in the last (third-instar) larval stage. Interfering with Torsin function resulted in a significantly reduced number of synaptic boutons (Figures 3.6J and 3.6K) and a significantly increased number of undifferentiated ghost boutons (Figure 3.6J, arrowheads; Figure 3.6L).

Figure 3.6- The Distribution of mRNAs at the NE and Synaptic Sites Is Disrupted in torsin Mutants

(A and B) FISH to body wall muscles showing the nuclear distribution of (A) par6 and (B) magi transcripts in wild-type and torsin mutants.

(C) Quantification of FISH signal outside the nucleus. N [nuclei;larvae], [18;6],[18;6],[18;6],[14;6].

(D and E) FISH to body wall muscles showing the distribution of (D) par6 and (E) magi transcript at the NMJ in wild-type and torsin-null mutants.

(F and G) Distribution of (F) Par6 and (G) Magi immunoreactivity at the NMJ in wild-type and torsin mutants.

(H and I) Quantification of postsynaptic (H) Par6 and (I) Magi immunoreactive signal, normalized to wild-type control. N([NMJs;larvae]) is [16;6],[18;6] (H) and [17;6],[15;6] (I).

(J) NMJs in wild-type and torsin mutants labeled with anti-HRP and anti-DLG showing reduced size and increased ghost boutons (arrowheads) in torsin mutants.

(K and L) Quantification of the number of (K) synaptic boutons and (L) ghost boutons. N([NMJs;larvae]), [19;10],[18;10],[19;10],[19;10],[20;10],[19;10],[19;10] for (K)

and (L). Error bars represent ±SEM; **p < 0.001; ***p < 0.0001.

Calibration scale are 3 mm (A and B), 10 mm (D–G), and 20 mm (J).

Figure 3.6- The Distribution of mRNAs at the NE and Synaptic Sites Is Disrupted in torsin Mutants

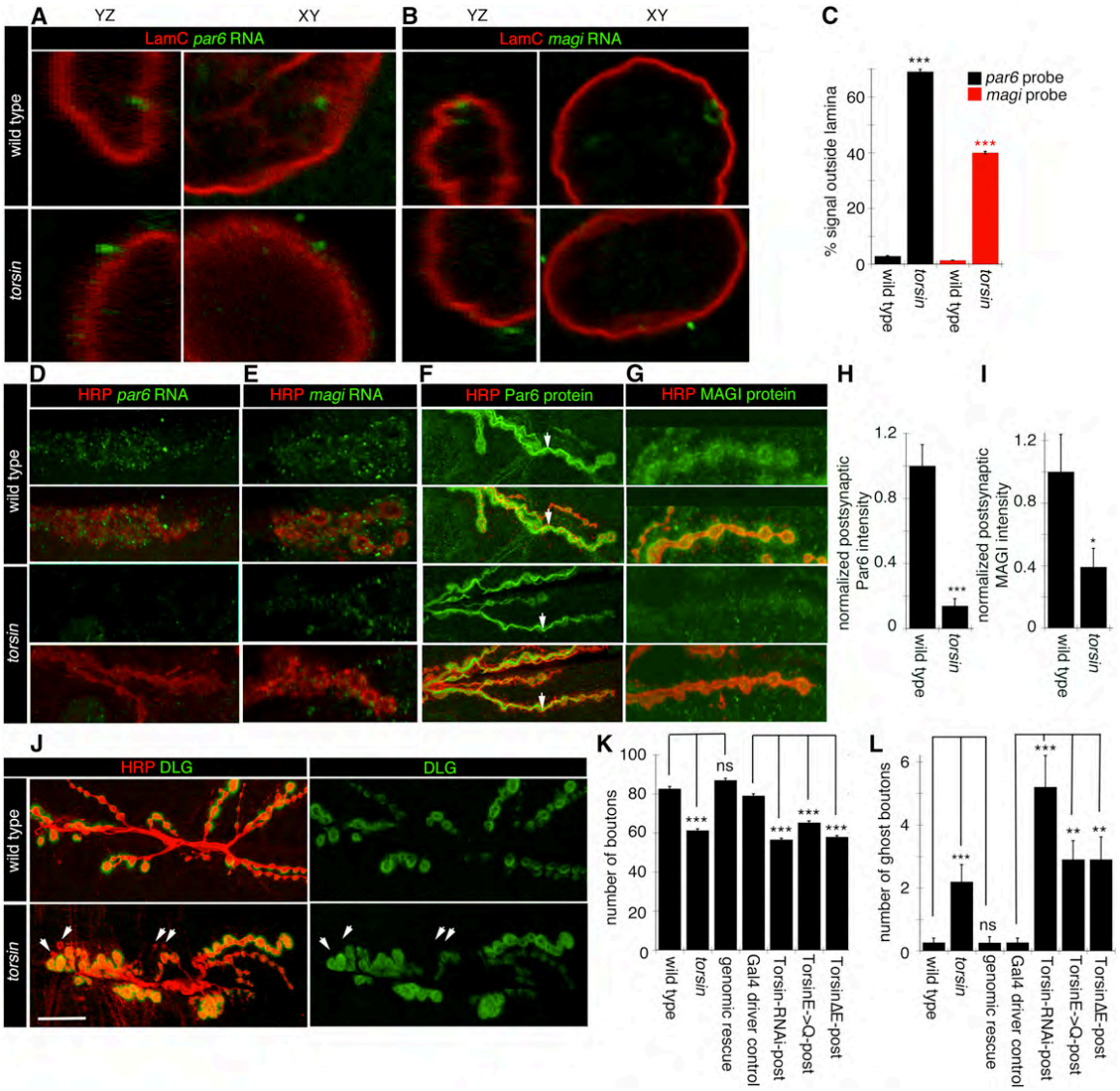

Figure 3.7- Postsynaptic DLG signal

FISH to body wall muscles of (A) wild type and (B) *torsin* mutants in preparations labeled with antibody to HRP and a RNA probe to *dlg*. (C,D) Quantification of postsynaptic levels of (C) *dlg* RNA and (D) DLG protein levels normalized to wild type controls. N in C is (NMJ;larvae; left to right)=[10;5] N in D is ([NMJs;larvae; left to right])= [9;5]. Calibration scale is 10 μm. Error bars represent ±SEM.

Figure 3.7- Postsynaptic DLG signal

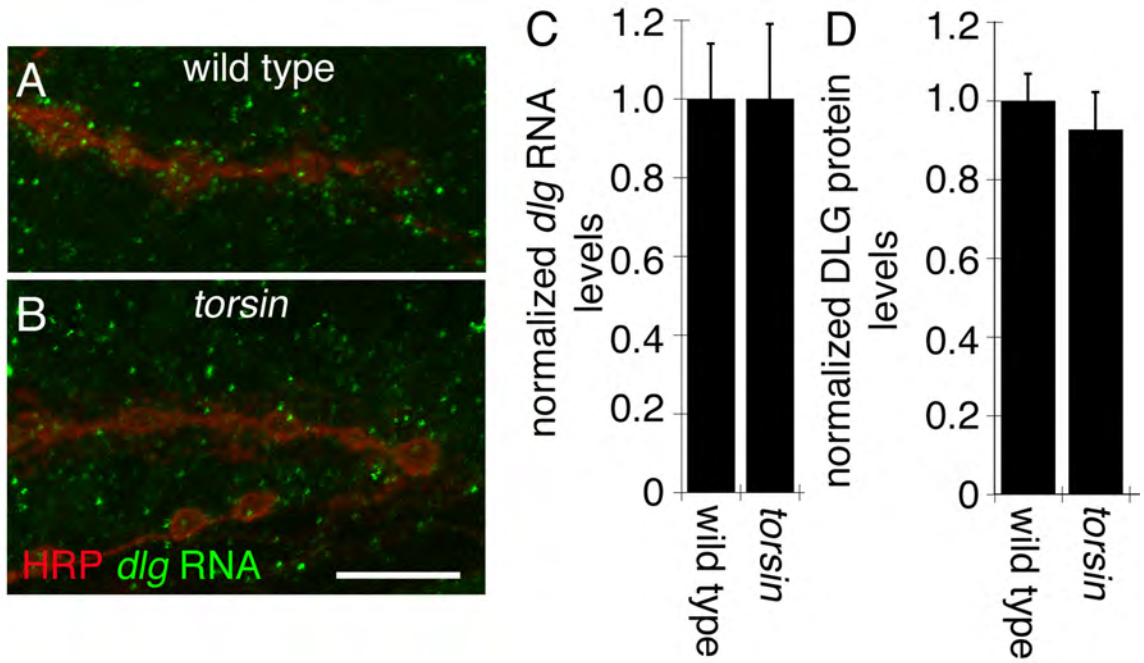

DISCUSSION

Together, these results demonstrate that inhibiting Torsin function results in megaRNP accumulation at the NE, likely due to a defect in INM scission during primary envelopment. As a consequence, synaptic transcript-containing megaRNPs fail to efficiently exit the nucleus, limiting trafficking of the mRNAs contained within to postsynaptic sites where they are normally enriched. This reduced synaptic mRNA localization results in reduced levels of specific postsynaptic proteins during NMJ expansion and thus in poorly developed NMJs containing fewer synaptic boutons and increased numbers of undifferentiated ghost boutons lacking postsynaptic proteins. These results provide mechanistic insight into the molecular machinery underlying nuclear egress of megaRNPs by NE budding. They also provide a mechanism by which Torsin influences synaptic development as well as important clues as to how torsinA dysfunction might lead to the alterations in synaptic plasticity observed in DYT1 mouse models and human patients.

EXPERIMENTAL PROCEDURES

Fly Strains. We used wild type (CantonS; CS); *torsin*^{KO78} (Wakabayashi-Ito et al., 2011), UAS-Torsin (Wakabayashi-Ito et al., 2011), UAS-Torsin$^{\Delta E}$, UAS-Torsin$^{E\rightarrow Q}$, Torsin-genomic rescue (Wakabayashi-Ito et al., 2011) and UAS-Torsin-RNAi (ID –110073; Vienna Drosophila RNAi Center (Dietzl et al., 2007), C57-Gal4 (Budnik et al., 1996). Flies were reared on standard *Drosophila* medium at 25˚C. RNAi crosses and controls were performed at 29˚C.

Molecular Biology. Torsin dsRNA was prepared by amplifying exon1 by PCR using the primers TAATACGACTCACTATAGGGATGATGAGCTTTCCACGCATG and TAATACGACTCACTATAGGGCATCTATTCTCGCCGGAATGTTTC and *in-vitro* transcribed using Ambion MEGAscript T7 kit. Torsin dsRNA (DRSC36478) was also obtained from the *Drosophila* RNAi Screening Center (DRSC). To generate Torsin$^{\Delta E}$ and Torsin$^{E\rightarrow Q}$, a 1.2kb Torsin cDNA was amplified using the primers ATAATAGCGGCCGCATGATGAGCTTTCC and ATAATATCTAGATCAGTAAATGGCCATGG. The product was digested with NotI and XbaI and cloned into pBSK-II vector. Site directed mutagenesis was performed using the primers for UAS-Torsin$^{\Delta E}$ CTAATGGAGGAGTTTATTATGTCAATGATTTTTTGGTTGTTCGC and GCGAACAACCAAAAAATCATTGACATAATAAACTCCTCCATTAG and the primers for Torsin$^{E\rightarrow Q}$

GTTCATCTTCGAC**CAG**GTGGATAAAATGCCCAGCGG and CCGCTGGGCATTTTATCCAC**CTG**GTCGAAGATGAAC.

Mutagenized constructs were then subcloned into the pUAST-attB vector(Bischof et al., 2007). To generate stably transfected Torsin-SOG S2 cell lines, Torsin and Torsin^{E177Q} cDNAs were amplified using primers ATAATAGGTACCATGATGAGCTTTCC(KpnI) and ATAATAACTAGTGTAAATGGCCATGG(SpeI). Mini-SOG(Shu et al., 2011) was amplified using ACTAGTATGGAGAAAAGTTTCGTG(SpeI) and GCGGCCGCTCATCCATCCAGCTGC(NotI). PCR products were ligated into the pMT-Puro plasmid (Addgene, ID: 17923) and SL2-NP2 cells transfected with 0.5µg DNA using Effectene (Qiagen). Stable cell lines were maintained under 10µg/ml puromycin (Invitrogen) selection. To generate Torsin-Flag constructs, Torsin and Torsin$^{E\rightarrow Q}$ cDNAs were amplified using primers ATAATAGGTACCATGATGAGCTTTCC(KpnI) and ataatatctaga**cta cttgtcatcgtcatccttgtaatc**GTAAATGGCCATGGCCACC (XbaI) (Flag encoded by primer- in bold). The PCR product was ligated into the pMT-Puro plasmid (Addgene, ID: 17923).

S2 cell culture and dsRNA treatment *Drosophila* SL2-NP2 cells were cultured and treated as in (Koles et al., 2012).

Immunocytochemistry. Third instar larval body wall muscles were dissected and fixed as in (Budnik et al., 1996). We used anti-LamC, 1:30 (LC28.26; Developmental Studies Hybridoma Bank (DSHB)); anti-LamDm0, 1:30 (ADL101;

DSHB); anti-DFz2-C(Mathew et al., 2005), 1:500; anti-DLGPDZ2(Koh et al., 1999), 1:40,000; anti-Par6(Ruiz-Canada et al., 2004), 1:50; anti-MAGI, 1:200 (see below); anti-Flag, 1:100 (Sigma), anti-FITC, 1:800 (Thermo Scientific); anti-Bocksbeutel 1:50 (Wagner et al., 2004); anti-dMan1, 1:50 (Pinto et al., 2008), anti-Otefin, 1:100 (Padan et al., 1990) and anti-squid, 1:10 (Goodrich et al., 2004). Secondary antibodies (Jackson ImmunoResearch and Fisher) were anti-rabbit-DyLight488 (1:200), anti-rabbit- FITC (1:200); anti-mouse-DyLight594 (1:200), anti-rat-Dylight488 (1:200), anti-HRP-Dylight594.

Antibody Generation. The MAGI antibody was generated by immunizing rats with a bacterially generated peptide (aa337-558) produced using pET30 (EMD Millipore).

Fluorescence In-situ Hybridization. Procedures for FISH were as in (Speese et al., 2012)

Transmission Electron Microscopy (TEM). TEM was performed as in(Ashley et al., 2005), but muscles 6 and 7 were sectioned sagittally. Cells were fixed in the culture dish, scraped and pelleted at 700xg before TEM processing. For cells expressing miniSOG-tagged Torsin constructs, uranyl acetate or lead citrate was omitted, such that all electron density was due to DAB precipitates. Chapter II

Diaminobenzidine conversion of Mini-SOG. Diaminobenzidine photoconversion was adapted from(Grabham and Goldberg, 1997). Briefly, SL2-NP2 cells stably transfected with Torsin$^{wild\text{-}type}$-miniSOG and Torsin^{E177Q}-miniSOG were fixed with 0.5% glutaraldehyde and 4% paraformaldehyde in 0.1M sodium

cacodylate buffer (pH 7.4) for 1-2 hrs. Cells were rinsed with 3X10 min washes in cacodylate buffer, and treated for 1-1.5 hr in blocking buffer (50mM glycine, 10mM KCN, and 100mM ammonium chloride), followed by a wash with cacodylate buffer. For photooxidation, diaminobenzidine (DAB) (Rockland Biosciences) was freshly diluted to 1mg/ml in 0.1M sodium cacodylate buffer, pH 7.4, and filtered through a 0.22μm filter (Millipore). The solution was then placed on ice, and oxygen was gently bubbled through it for 5 min. Cells were illuminated with a 100W mercury lamp and a BP 470/40 excitation filter, under a 40X objective for about 3-8 min, until visible darkening was observed. Multiple areas on the dish were photoconverted with oxygenated DAB solution replaced every few minutes. Following photoconversion, cells were fixed overnight with 1% glutaraldehyde and 4% paraformaldehyde in 0.1 M sodium cacodylate buffer (pH 7.4). Cells were then postfixed with 1% osmium tetroxide in 0.1M sodium cacodylate buffer for 30 min and processed for TEM as above.

Image Acquisition. Confocal images were acquired using a Zeiss LSM700 confocal microscope equipped with a Zeiss 63x Plan-Apochromat 1.4 NA DIC oil immersion objective at a digital zoom of 3X for high magnification images, and 0.7X for low magnification images. Identical settings were used for control and experimental samples processed on the same day.

Quantification. The number of samples employed for each experiment is specified in the figure legends.

Categorization of DFz2C/LamC foci at the light microscopy level. To morphologically categorize nuclear DFz2C/LamC foci at the light microscopy level, larval body wall muscle preparations labeled with antibodies to DFz2C and LamC, were visually inspected under epifluorescence at 630X magnification. The percentage of nuclei with normal DFz2C foci was determined at muscle 6 (abdominal segments A2-4) by counting the number of nuclei containing DFz2C-immunoreactive spots (about 2μm(Speese et al., 2012)) contained within a thickening of the lamina (Figure 3.1A). Nuclei were cataloged as containing small DFz2C puncta if numerous (5 or more) DFz2 immunoreactive puncta doted the lamina, were below 0.5μm and were not associated with a thickening of the lamina (Figure 3.1B). Nuclei were considered as containing depleted foci if they were devoid of any observable DFz2C immunoreactivity when visually examined under epifluorescence under 630X magnification (Figure 3.1C). Note that a nucleus could be cataloged in more than one category.

Ultrastructural categorization of megaRNPs. Micrographs of foci at 78,000-110,000X total magnification were visually inspected. MegaRNPs were categorized as within INM invaginations if they appeared as a single granule or cluster surrounded by an INM invagination. They were categorized as containing a collared neck if the megaRNP was present within the perinuclear space in association with the INM through an electron dense tether. MegaRNPs were cataloged as amorphous, if they were larger than 250nm and individual megaRNP granules could not be distinguished.

Categorization of NE associated FISH signal. To determine the % of signal outside the lamina, the number of lamina-associated FISH puncta was subdivided into those that were present either in the nucleoplasmic or cytoplasmic side of the LamC-immunoreactive lamina.

Measurements of postsynaptic protein and mRNA levels. Normalized postynaptic protein levels were determined as in(Ramachandran et al., 2009). Briefly, Confocal images of NMJs at muscles 6 and 7 (segment A3) labeled with antibodies to HRP to mark the presynaptic arbor and par6, *magi*, or *dlg* probes were obtained using identical acquisition parameters and analyzed using Volocity software (PerkinElmer). The presynaptic HRP signal was subtracted, and the remaining signal (postsynaptic signal) was normalized to bouton volume. Values were normalized to wild type controls.

Quantification of bouton and ghost bouton number. Bouton number and ghost bouton number was assessed as in(Speese et al., 2012). Briefly, bouton numbers were counted at muscles 6 and 7 (segment A3) in 3rd instar larval preparations labeled with antibodies to HRP and DLG with an epifluorescence microscope under 630X magnification. Total bouton number was counted in the HRP channel. The number of ghost boutons was determined by counting HRP positive boutons that were devoid of DLG immunoreactivity.

Statistical Analysis. Statistical analysis was performed on raw data, or data normalized to wild type controls that were processed simultaneously (number of samples is stated in figure legends). Unpaired two-tailed Student's t-tests were

run for comparisons of experiments where a single experimental sample was processed in parallel with a wild type control. An F-test was applied to the data to compare variance, and if the variances were significantly different, an unpaired t-test with Welch's correction was performed. In cases where multiple experimental groups were compared to a single control, a one-way ANOVA was performed, with either a Tukey (for pairwise comparison) or Dunnet (for comparison to a control) post-hoc tests. All statistical analysis was carried out in Kaleidagraph (Synergy Software) and Prism 5 (Graphpad Software, Inc.). Alpha levels were 0.05 for all tests. For all quantifications, wandering third instar larvae were chosen at random, and as cells were pelleted prior to embedding for TEM analysis, there could be no positional bias within the dish of cells. Error bars in all graphs represent ±SEM.

Preface to Chapter IV

In this chapter we show that nuclear envelope budding is likely to be a generalized mechanism for large RNP export. We show that DFz2C/LamC-associated megaRNP granules are present in the nurse cell nuclei in *Drosophila* ovary and blocking megaRNP budding leads to severe germline defects.

My contribution to this Chapter: Figures 4.1, 4.2, 4.3, 4.4, 4.5
Linda Hassinger contributed: Figure 4.2
Travis Thomson contributed: Figure 4.4 E-H

The following chapter is a manuscript in preparation:

Jokhi V*, Hassinger L, Thomson T and Budnik V. *Nuclear envelope budding regulates RNA localization during Drosophila oogenesis*.

Chapter IV

Nuclear envelope budding regulates RNA localization during *Drosophila* oogenesis

INTRODUCTION

RNA localization is a major mechanism involved in embryonic pattern formation during *Drosophila* oogenesis and embryogenesis (Lasko, 2012). These mechanisms are not exclusive to the above processes but are used throughout the organism during asymmetric RNA translation. Thus, *Drosophila* oogenesis has served as a powerful and pioneering model to uncover the molecular components underlying the transport and localization of mRNAs to their site of translation, the mechanisms that maintain the RNAs translationally silent until they reach their destination, and the stimuli that de-repress translation at target sites. Notably, these mechanisms and components are highly conserved, and are used from worms to humans for localized translation (Meignin and Davis, 2010). A prominent example is the local translation of RNAs at postsynaptic sites during synaptic plasticity, a process central to our ability to learn and remember (Meignin and Davis, 2010).

The mechanisms of trafficking and localization of maternal RNAs during *Drosophila* oogenesis, which are essential to proper establishment of embryonic body axis, have been the focus of intense investigation (Lasko, 2012). The *Drosophila* ovary is composed of 14-16 ovarioles. Each ovariole has a germarium at their most anterior pole, and followed by a string of developing egg chambers. Within each ovariole the entire developmental sequence, from stem-cell cytoblast to mature oocyte can be observed in a linear fashion, from anterior

to posterior. During early stages, stem-cells give rise to stem-cell cystoblasts through asymmetric cell division, and each committed cystoblast undergoes four cell divisions with incomplete cytokinesis to form the egg chambers, which are surrounded by an epithelium of somatic cells known as follicle cells. The resulting 16 germline derived cells remain connected through actin-based canals, the ring canals. One of the 16 cells differentiates into the oocyte and the remainders become nurse cells.

During oogenesis, nurse cells produce maternal RNAs, which are dispensed to the oocyte. Some of these mRNAs become localized at the anterior or posterior oocyte pole, and this localization is a major determinant of the body anterior-posterior (AP) axis plan (Becalska and Gavis, 2009). In initial stages, *oskar (osk)* mRNA becomes localized at the anterior pole of the oocyte and its translation is critical for the posterior localization of *nanos* mRNA. In contrast, *bicoid (bcd)* mRNA localize at the anterior oocyte pole. Another RNA, *gurken* (*grk)*, localizes initially along the posterior cortex of the oocyte, but by mid stage egg chamber development, it becomes tightly localized to the future dorsal anterior corner of the oocyte. This *grk* RNA localization restricts the distribution of Gurken protein and is critical to defining both the AP and dorsal–ventral (DV) axes of the embryo.

Compared to our knowledge of mechanisms of RNA transport and localization in the oocyte, comparatively little is known about the mechanism of export of the above RNAs from the nucleus. A central principle in the cellular biology of

eukaryotic cells, both in unicellular organisms and metazoans is that all RNAs must exit the nucleus through the nuclear pore complex (Grunwald et al., 2011). However, studies from Herpes-type virus nuclear egress (Mettenleiter et al., 2013b) and *Drosophila* muscles and epithelial cells (Speese et al., 2012) have unraveled an alternative mechanism for the nuclear export of RNAs, the process of nuclear envelope (NE) budding. According to this mechanism, nucleocapsids or very large RNPs (megaRNPs) undergo a process of envelopment and de-envelopment at the NE. During envelopment, the nucleocapsids or RNPs disrupt the nuclear lamina, a thick filamentous network underneath the inner nuclear membrane (INM) and remodel the INM, budding into the perinuclear space (between the outer nuclear membrane (ONM) and the INM). This results in the presence of membrane bound RNPs or viral capsids at this site. Subsequent fusion of the membrane rimming the particles with the ONM results in the de-envelopment of the particle, thus releasing a naked viral capsid or RNP to the cytoplasm. This process is blocked by the AAA-ATPase Torsin, which is required in the process of scission of the INM during envelopment (Jokhi et al., 2013a; Maric et al., 2011a). As a consequence, capsids accumulate at the perinuclear space (Maric et al., 2011a), and in the case of RNPs they fail to reach their destination at the postsynaptic region of *Drosophila* larval neuromuscular junction, where they are required for the synthesis of postsynaptic proteins (Jokhi et al., 2013a). In *Drosophila*, the NE-budding mechanism was discovered while studying a Wnt signaling pathway essential for postsynaptic development at the

NMJ, mediated by the Wnt1 Wingless (Wg), the Frizzled Nuclear Import (FNI) pathway (Mathew et al., 2005). In this pathway, the Wg receptor DFz2 is internalized in postsynaptic muscles, and a cytoplasmic C-terminal fragment of the receptor (DFz2C) is cleaved and imported into the muscle nuclei. Within the nucleus, DFz2C associates with megaRNP granules that exit the nucleus through NE-budding, and that are destined to become localized at the postsynaptic region of the NMJ, during NMJ expansion at larval stages (Speese et al., 2012).

Structures similar to megaRNPs have been identified in mammalian fertilized oocytes and early embryos at the perinuclear space (Szollosi and Szollosi, 1988). In addition, Wnt signaling is essential for the development of germline stem-cells, and is localized at the germarium in cap cells (Song and Xie, 2003), as well as in somatically-derived follicular cells that surround the developing oocyte (Song and Xie, 2003). Thus, we sought to determine if NE-budding, particularly through the FNI Wg signaling pathway operates during *Drosophila* oogenesis.

We found that LaminC (LamC) foci containing the Wingless (Wg) receptor, DFrizzled-2 (DFz2), Nuclear poly(A)-binding protein (PABP2), and poly(A) RNA, typical features of megaRNPs at the perinuclear space (Speese et al., 2012), were present in nurse cells from the earliest stages of oogenesis. Downregulation of *torsin*, which inhibits nuclear RNA export through NE-budding resulted in egg chamber development arrest at stage 6. Escapers had abnormal

egg appendages, a hallmark of DV, but also AP polarity defects (Berg, 2005), and delayed or absent *oskar* posterior localization. These results reveal that nuclear export through NE-budding plays a central role in the development of the oocyte.

RESULTS

RNA containing DFz2C /LamC foci are present in nuclei of nurse cells

To determine if NE-budding was observed during *Drosophila* oogenesis, we labeled ovaries with antibodies to LamC and DFz2 and examined nurse cell nuclei at different stages of egg chamber development. We observed the presence of nuclear DFz2C/LamC foci in many of the nurse cell nuclei (Figure 4.1A-C). These foci were particularly abundant at earlier stages of egg chamber maturation (Figure 4.1A, G). These DFz2C/LamC foci resembled the foci visualized in larval body wall muscle and salivary gland epithelial cell nuclei (Speese et al., 2012). A feature of nuclear DFz2/LamC foci in the larva is the presence of nuclear Poly(A)-binding protein-2 (PABP2) within the foci, which has been viewed using antibodies against *Drosophila* PABP2, or via GFP in a PABP2-GFP trap line, in which GFP has been inserted in frame within the *pabp2* gene (Speese et al., 2012). Similarly, we found that DFz2C/LamC foci contained PABP2 (Figure 4.1D). In addition, our studies at the larval NMJ demonstrate that nuclear DFz2C/LamC foci are enriched in poly-adenylated RNA, representing the presence of postsynaptic-specific transcripts (Speese et al., 2012). To establish if nuclear DFz2C/LamC foci in nurse cells were similarly enriched in poly(A)-RNA, we carried out fluorescent *in situ* hybridization (FISH) using a poly(dT) probe. We found that the nuclear foci were clearly enriched in poly(dT) signal (Figure 4.1E). In contrast, FISH using a poly(dA) probe did not result in positive signal within the nucleus and cytoplasm (Figure 4.1F). Thus, the presence of nuclear

DFz2C/LamC foci containing PABP2 and enriched in poly(A)-RNA, suggest that the nuclear foci observed in nurse cells represent mega-RNPs, similar to larval muscles and salivary gland cells.

Figure 4.1- RNA containing DFz2C/LamC foci are present in nuclei of nurse cells of wild type ovaries

(A-C) Ovaries were labeled with antibodies to LamC (red) and DFz2 (green) and nurse cell nuclei were examined at different stages of egg chamber development. (A) Shows labeling in multiple stages of egg chambers (B) Arrows mark nurse cell nuclei with DFz2C/LamC foci (C) High Magnification of a nucleus with multiple DFz2C/LamC foci

(D) Ovaries stained with LamC (red), DFz2 (blue) and PABP2 (green)

(E-F) Immunofluorescence for LamC (red) and fluorescent *in situ* hybridization (FISH) using a (E) poly (dT), (F) poly(dA) probe (green) in ovaries.

(G) Percentage showing DFz2C/LamC foci at different stages of nurse cell nuclei.

Figures represent single slice confocal.

Figure 4.1- RNA containing DFz2C/LamC foci are present in nuclei of nurse cells of wild type ovaries

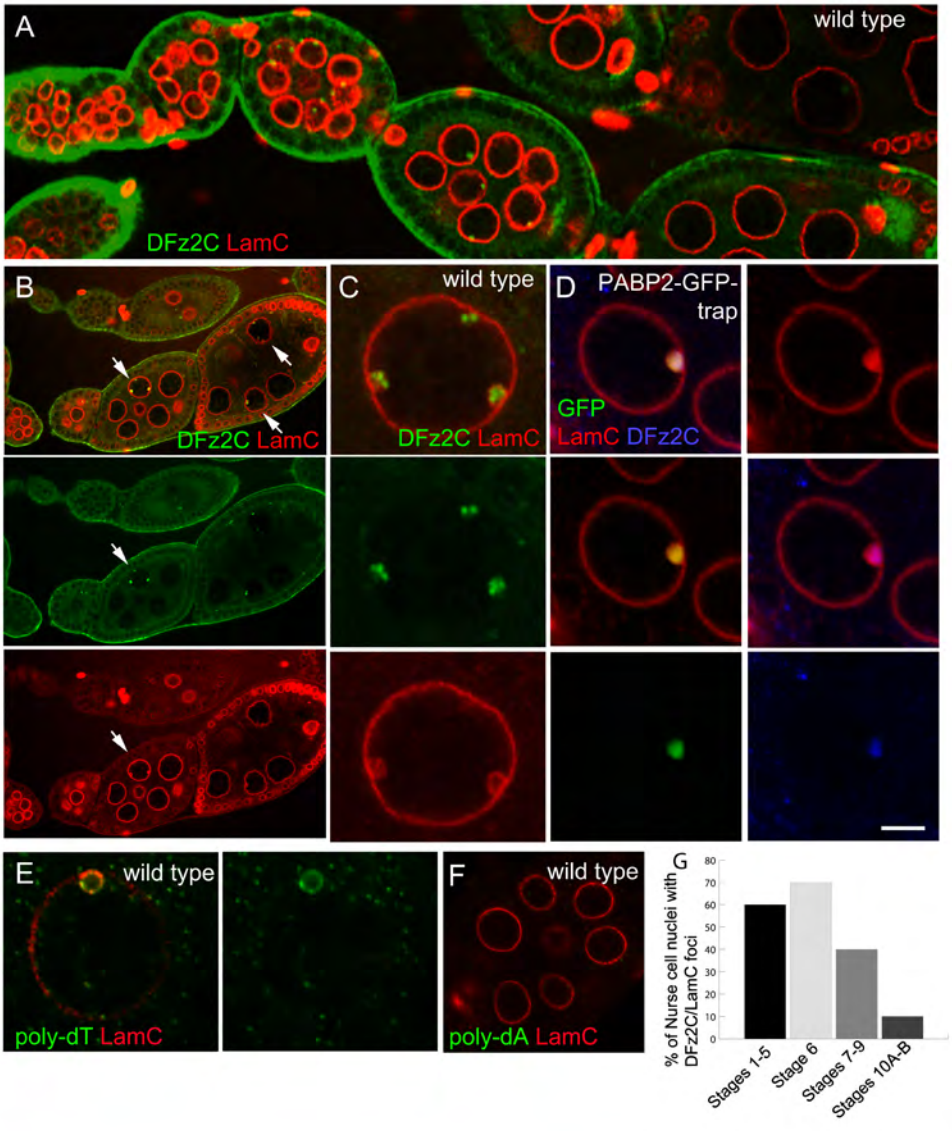

Nurse cells contain nuclear mega-RNPs

To confirm that DFz2C/LamC foci corresponded to the ~200 nm megaRNPs that accumulate at the perinuclear space in the larva, we examined developing egg chambers at ultrastructural level with electron microscopy (EM). We found that nurse cell nuclei contained dense granules at the perinuclear space, similar to the megaRNPs observed in larval tissues (Figure 4.2A). The megaRNPs appeared either as single granules (Figure 4.2B) or in clusters (Figure 4.2C), and, as expected from the process of NE-budding, they were bounded by membrane (Figure 4.2B; inset). As previously shown in the larva, NE membranes surrounding megaRNPs did not contain nuclear pore complexes (NPCs), but NPCs were visualized elsewhere at the NE (Figure 4.2B, C; arrowheads).

Previously, we had shown that NE-budding of mega-RNPs is inhibited by null mutations or downregulation of *torsin*, a gene encoding an AAA-ATPase involved in the scission of the INM during primary envelopment of megaRNPs (Jokhi et al., 2013a). If the granules observed at the EM level in the perinuclear space of nurse cells correspond to megaRNPs, then, similar to the larva, downregulating Torsin should result in the accumulation of megaRNPs at the perinuclear space, attached to the INM. We downregulated Torsin using two different UAS-Torsin-RNAi transgenes targeted to different regions of the *torsin* transcript. Transgene expression was driven by Nanos-Gal4, which expresses Gal4 in most nurse cells, but not in follicle cells. Expression of Torsin-RNAi

resulted in the presence of rows of megaRNPs attached to the INM, which decorated the NE (Fig. A.2D-F). *torsin* null mutant flies are semi-lethal with only a few males, which are sterile that survive to adulthood (Wakayabashi-Ito). To bypass this we generated germline clones for Torsin using FRT and dominant female sterile technique (Chou TB, 1993, 1996) (Figure 4.3A- outline for generating germline clones). The ultrastructural analysis of the *torsin* germline clone was consistent with the RNAi, were megaRNPs were found apposed to the inner nuclear membrane.

Figure 4.2- Nurse cells contain nuclear mega-RNPs

(A-G) Electron micrographs of nurse cell nuclei showing NE-associated megaRNPs. Red=nucleus; blue=cytoplasm; green=perinuclear space. N=nucleus; C=cytoplasm RC=ring canals.

(A) Wild type nurse cell show nuclei have foci (asterisk) containing electron dense megaRNP granules either as (B) a single granule or (C) clusters. Inset in (B) shows magnified image of a part of a megaRNP. ONM=outer nuclear membrane, INM=inner nuclear membrane, ribo=ribosome, NPC= nuclear pore complex, ER= endoplasmic reticulum, g= granules

(D-F) Electron micrographs of Torsin-RNAi nurse cells displaying megaRNPs (arrows) attached to the inner nuclear membrane. Shown at higher magnification levels (E-F).

Figure 4.2- Nurse cells contain nuclear mega-RNPs

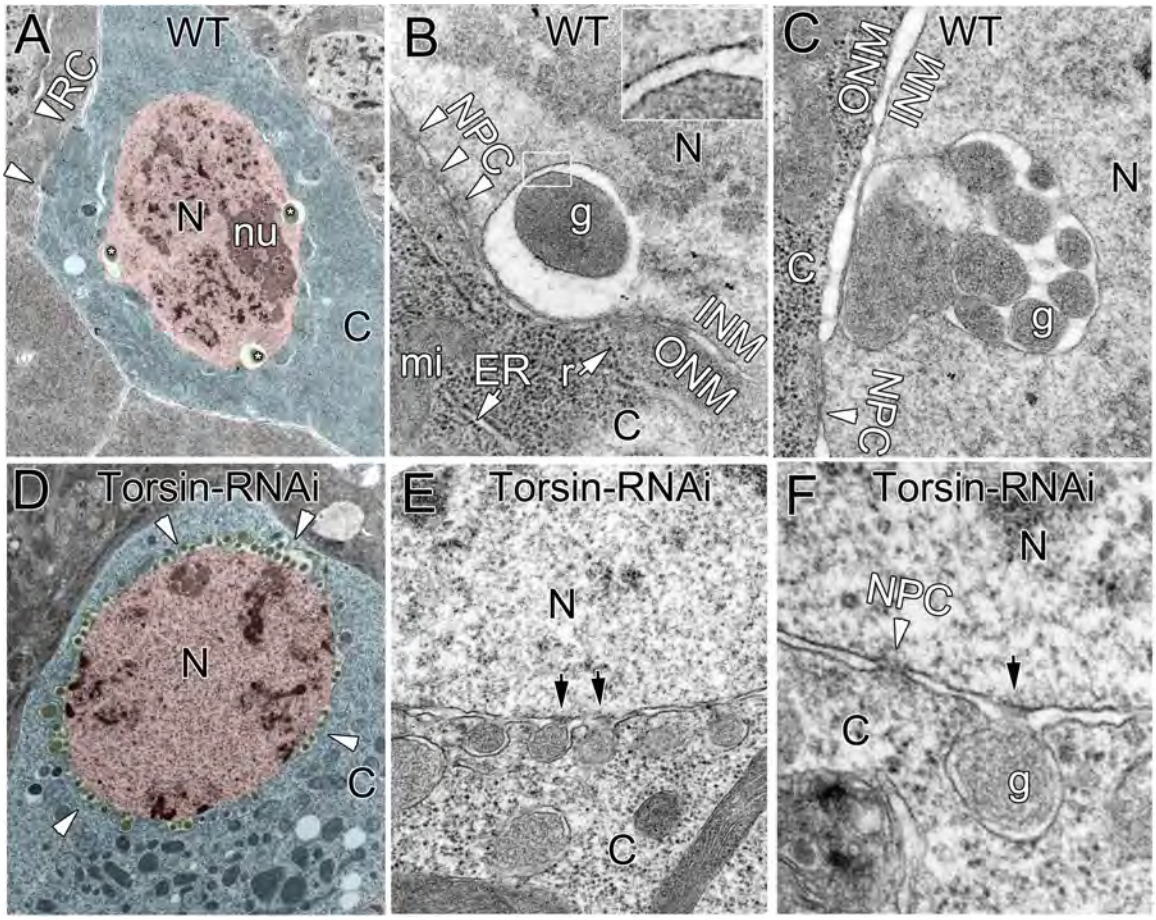

Figure 4.3- Torsin germline clone

(A) A schematic representation of generation of Torsin germline clone using the dominant female sterile (DFS) *ovo*^{D} mutants. The advantage of these mutants is that the *ovo*^{D} transgene kills all of the germ cells, so the only egg chambers that survive are those that have lost *ovo*^{D} and are homozygous for the *torsin* null (Figure adapted from (St Johnston, 2002)).

(B) Ultrastructure *torsin* germline clones where megaRNPs are attached to the inner nuclear membrane

Figure 4.3- Torsin germline clone

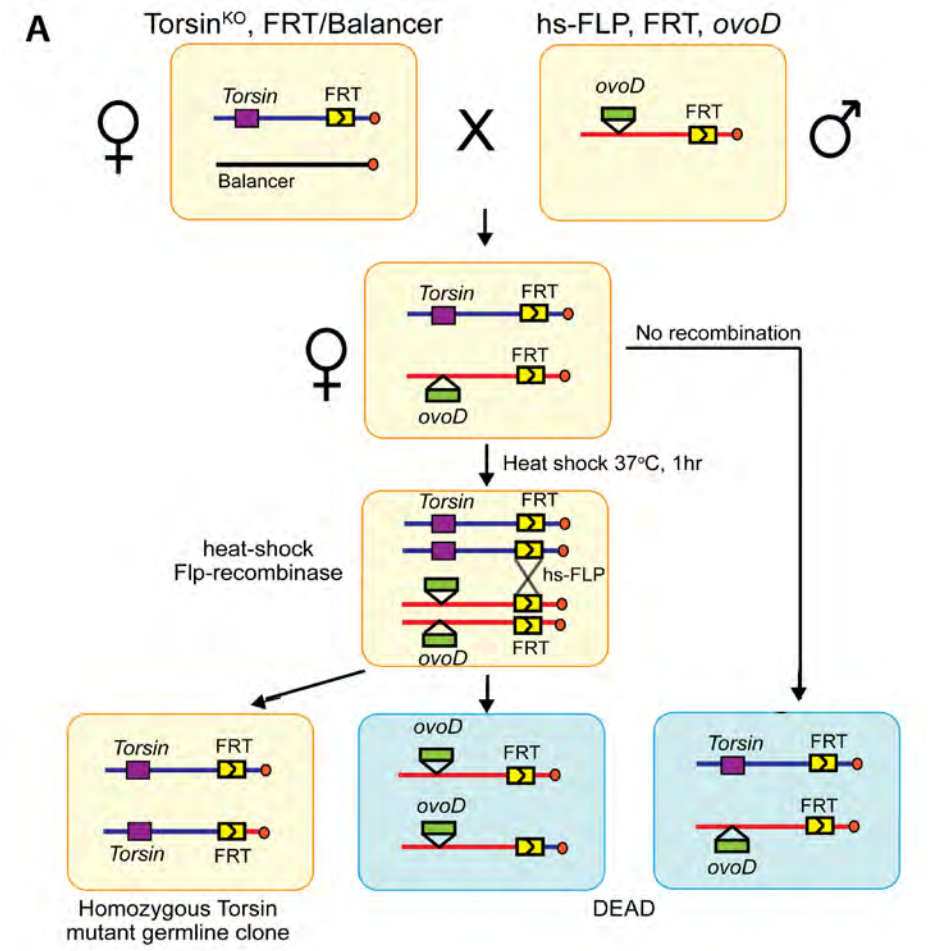

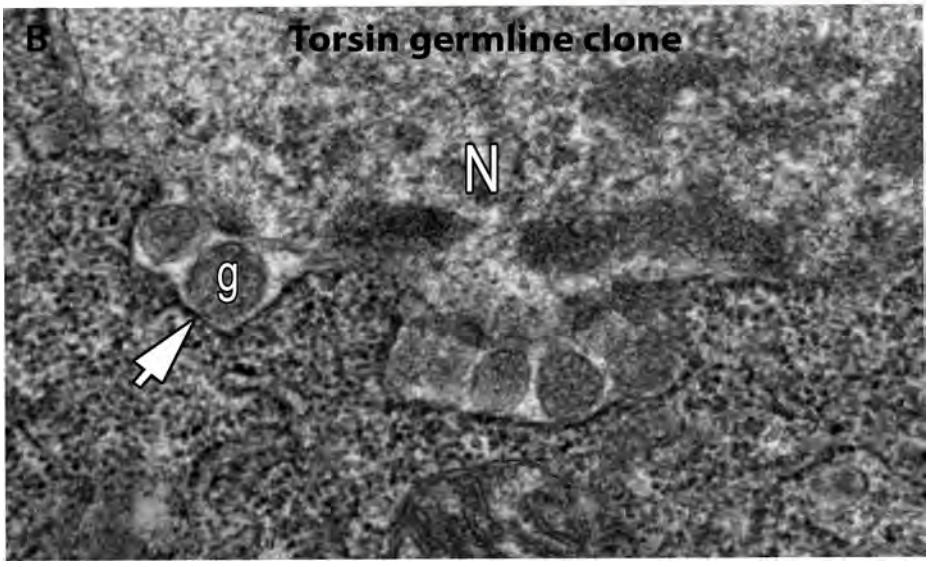

Torsin knockdown causes germline development defects

To examine how knockdown of the budding pathway affects germline development, we examined the gross morphology of the ovary. Ovaries dissected from 3 day-old mated females showed a reduction in size in the Torsin-RNAi (Figure 4.4C-D) and *torsin* germline clone (Figure 4.4B) in comparison to wild-type ovaries (Figure 4.4A).

Next, upon DNA staining of ovaries isolated from 3-day-old wild-type mated females showed ovarioles containing egg chambers of all the stages of oogenesis (Figure 4.4E). However, Torsin-RNAi ovaries had ~60% of ovarioles containing egg chambers arrested at stage 6-8 of development (Figure 4.4F) (n= 25/40 ovarioles in 6 ovaries). Some of the egg chambers appear to have condensed DNA, which is indicative of apoptosis (Figure 4.4F, arrows). Interestingly, a subset Torsin-RNAi ovarioles showed irregular arrangement of egg-chambers (12/40 ovarioles in 6 ovaries). These ovarioles had egg chambers where a mature stage preceded an earlier stage egg (Figure 4.4G) instead of having a linear arrangement of developmental stages (Figure 4.4E). These could likely represent escapers that made it further in development.

These defects were associated with the fecundity of the females. Torsin RNAi females are almost completely sterile and have severe egg laying defects (Figure 4.4H Table).

Figure 4.4- *torsin* knockdown causes germline development defects

(A-D) Ovaries dissected from 3 day-old mated (A) wild-type, (B) *torsin*-germline clone (C) Torsin-RNAi (TRIP) (D) Torsin-RNAi (KK) females viewed under bright-field dissecting microscope.

(E-G) DNA staining (DAPI) and phalloidin (green) of ovarioles from ovaries isolated from 3-day-old (E) wild-type, (F,G) Torsin-RNAi (KK) females. (F) Arrowhead shows an egg chamber with condensed DNA. (G) A more mature egg chamber (Stage 10) (arrow) preceding a less mature stage (Stage 6) (arrowhead).

(H) Table representing number of eggs laid per 10 females per day.

Figure 4.4- *torsin* knockdown causes germline development defects

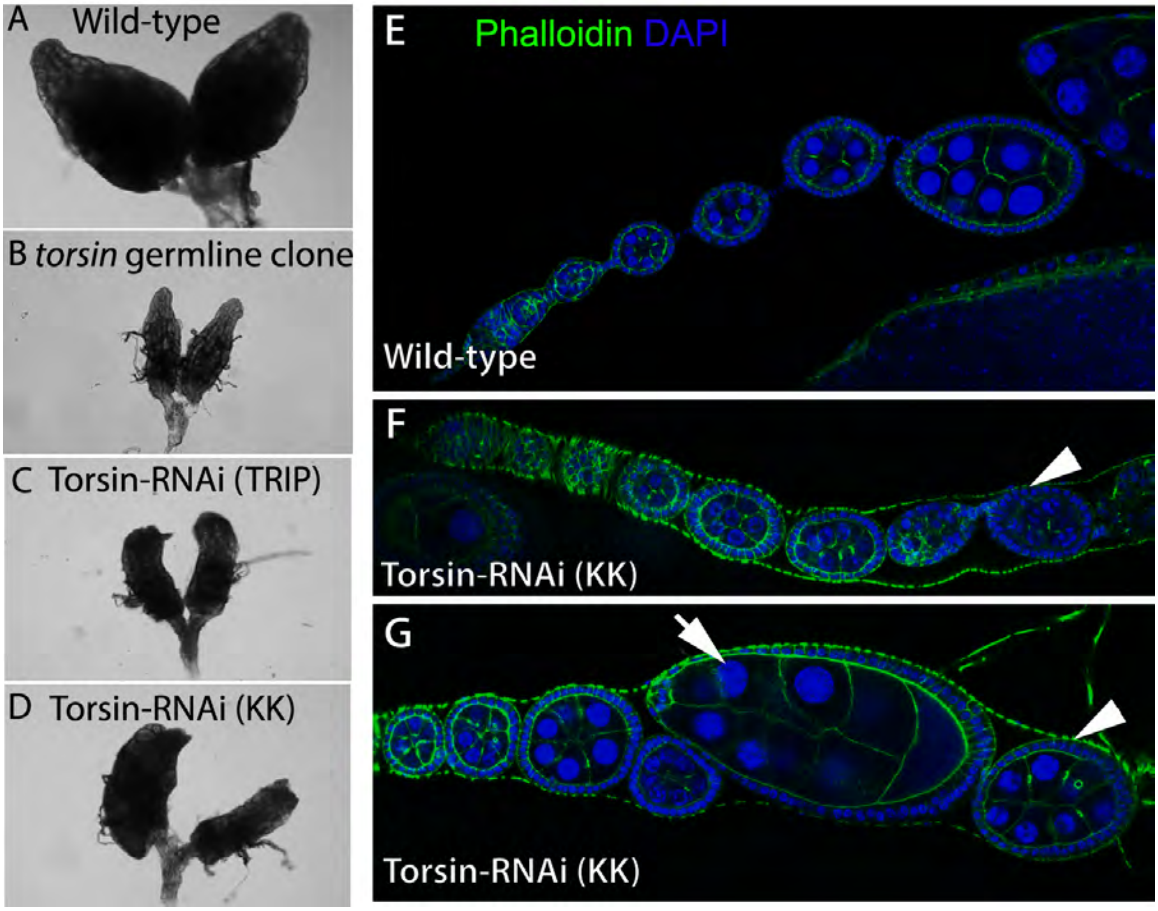

H. Number of eggs/10 3-day-old females/day

	Normal	Fused	None	Short
Driver Control	645	0	0	0
KK RNAi Control	587	0	0	0
Torsin KK-RNAi	8	1	1	3
TRIP RNAi Control	789	0	0	0
Torsin TRIP-RNAi	3	0	1	0

Torsin knockdown causes mislocalization of oskar mRNA

To address the cause of developmental defects we wanted to examine if the levels or localization of specific transcripts is affected in Torsin knockdown. The rare eggs that were laid showed D/V patterning defects. Gurken specifies both A/P and D/V. Downstream of the initial A/P and D/V patterning events are the proper localization of bicoid and oskar. Only when there is proper A/P and D/V patterning of the oocyte, can bicoid accumulate at the anterior and oskar at the posterior. Thus we first examined Gurken localization and observed that Grk was unaffected in Torsin-RNAi (Figure 4.5I) when compared to wild-type controls (Figure 4.5H).

Fluorescence in-situ hybridization (FISH) of *osk* mRNA demonstrated that osk transcript is present in LamC foci (Figure 4.4A). Interestingly, no such localization for *bcd* was observed (data not shown). Furthermore, FISH studies in the Torsin-RNAi demonstrated that *osk* localization to the posterior of the developing oocyte was affected. Instead of localizing as a consolidated tight band at the posterior (Figure 4.4E), *osk* has a punctate distribution throughout the oocyte (Figure 4.4F). Dual in-situ of *bcd* within the same egg chamber where *osk* is mislocalized, *bcd* is unaffected. To corroborate the FISH studies, we used *oskar-MS2-bs* flies. MS2bs is a phage RNA aptamer sequence that can be recognized by the phage MS2 coat protein. This sequence is cloned within the 3'UTR of the transcript and GFP-tagged coat protein is co-exporessed to determine the localization of the transcript. *oskar-MS2-bs* also localized to LamC

foci (Figure 4.5B-C) while MCP-GFP alone showed no localization to LamC foci (Figure 4.5D). To confirm if *oskar* is associated with DFz2C/LamC foci, we performed RNA immunoprecipitation (RIP) and found *oskar* transcript associates with DFz2C (Figure 4.5G). Hence we hypothesize that blocking megaRNA budding pathway may lead to incorrect packaging and transport of this transcript thereby leading to mislocalization of the transcript.

Figure 4.5- *torsin* knockdown causes mislocalization of oskar mRNA

(A) FISH using *oskar* probe (green) and LamC (red)

(B-D) Fluorescence imaging of oskar-MS2-bs X MCP-GFP. High magnification of nurse cell nuclei (B) with MCP-GFP (green) and LamC foci (red). Low magnification of egg chamber (C), arrowhead: *oskar* at the posterior. MCP-GFP only controls (D).

(E-F) Dual FISH, of *oskar* (red) and *bicoid* (green) in wild-type controls (E) and Torsin-RNAi (F).

(G) RIP for *oskar* with DFz2C antibodies

(H-I) Gurken localization (green) colabeled with DAPI (blue) and Phalloidin (red) in controls (H) and Torsin RNAi (I).

Figure 4.5- *torsin* knockdown causes mislocalization of oskar mRNA

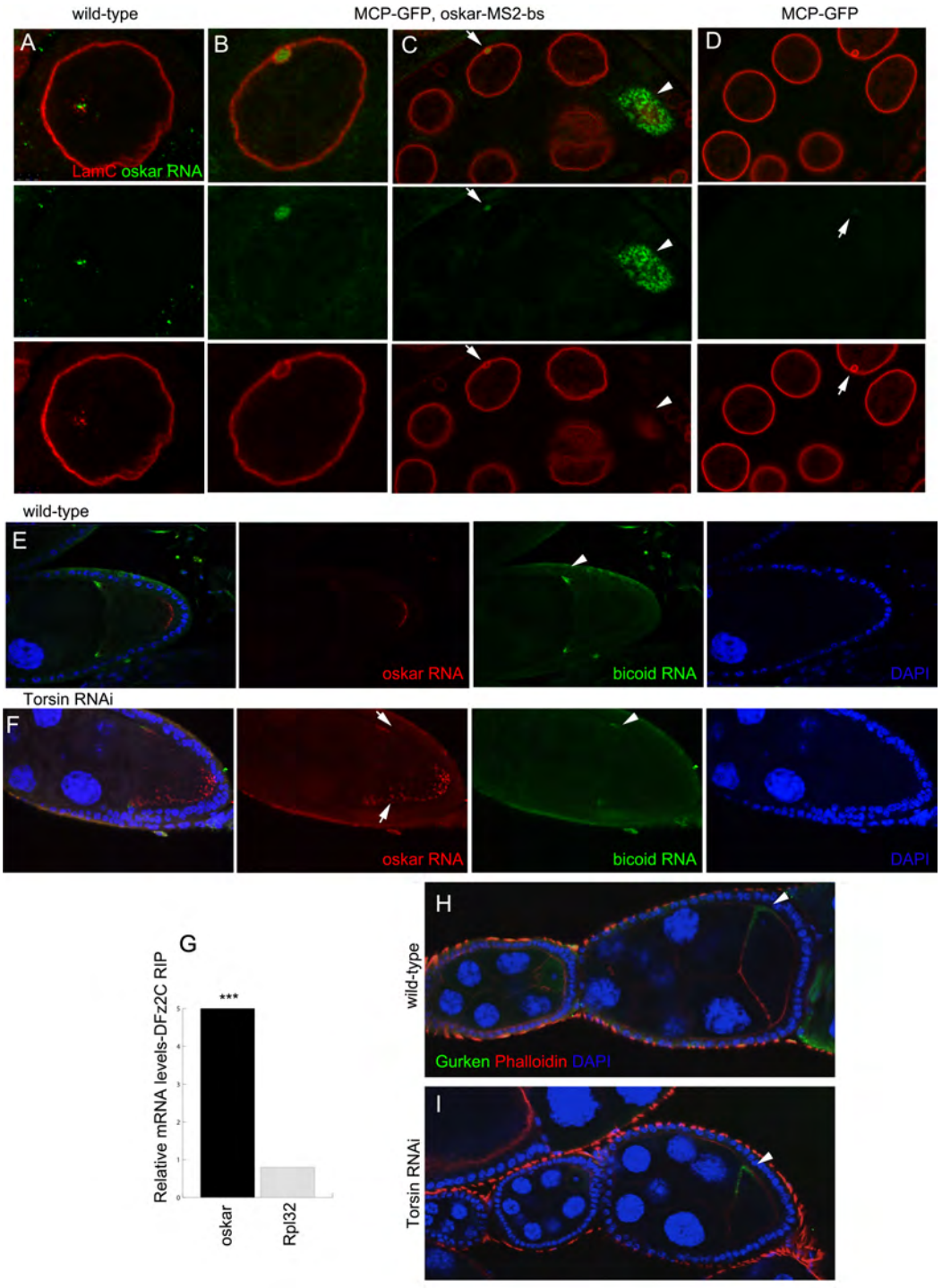

DISCUSSION

Taken together, we find megaRNPs associated with DFz2C/LamC foci in nurse cell nuclei in *Drosophila* ovary. This shows that nuclear envelope budding is a general pathway for large RNP export in other tissue types besides the neuromuscular junction (Jokhi et al., 2013). This pathway could be essential in cell types where rapid RNA synthesis and export takes place. These granules are observed at all stages of oocyte development in wild-type nurse cell nuclei. Knockdown of Torsin leads to an accumulation of these granules in the perinuclear space of the nurse cell nuclei. This is accompanied by an arrest in development of the ovary as indicated from ovary size, ovarioles defects and egg laying defects.

The sole function of nurse cell nuclei is to pump maternal RNA in the developing oocyte and budding could likely be an efficient bulk RNA export pathway. However, considering that only *oskar* mRNA is present in the LamC foci and mislocalized upon Torsin-RNAi, this pathway could be specific. To address this unbiased genome wide analysis need to be performed to determine the repertoire of transcripts that utilize nuclear envelope budding pathway for their export. One approach could involve purifying the RNP granules, either by RNA-IP using DFz2C or PABP-GFP. An alternative approach would be to use nuclear vs cytosolic fractions to determine the loss of cytosolic levels of transcripts upon torsin knockdown. Furthermore, while some *oskar* mRNA can exit the nucleus, what contributes to *oskar* mislocalization in the Torsin RNAi

needs to be determined. To elucidate this, we will examine RNA binding (RBP) and adaptor proteins associated with *oskar* localization and determine if they have a role in megaRNP budding. One possibility is that the absence of adaptors proteins are mistargeting the transcript, other possibility is the absence of adaptors may lead to premature translation of the transcript and oskar protein may contribute to further ectopic accumulation of the transcript (Zimyanin et al., 2007).

The *Drosophila* ovary is a powerful system to study nuclear envelope budding. This tissue is highly amenable for biochemical and high-throughput analysis to purify both the transcripts as well as RBPs associated with megaRNPs. A number of RBPs such as Staufen, Syncrip, SMN, FMR are common between the germline and neurons and thus can provide valuable information about proteins associated with neuronal granules ((Martin and Ephrussi, 2009)). Furthermore, the ovary can also be used to elucidate the next steps in the budding pathway, for e.g. how megaRNPs bud from the perinuclear space to the outer nuclear membrane and released into the cytosol?

In conclusion, megaRNP budding is likely to be a generalized pathway for export of large RNA granules in times of active transcription.

EXPERIMENTAL PROCEDURES

Fly Strains. We used wild type (CantonS; CS), UAS-Torsin-RNAi (TRIP) (Bloomington Drosophila Stock Center-BDSC: 50620), UAS-Torsin-RNAi (ID – 110073; Vienna Drosophila RNAi Center), osk-MS2-bs and MCP-GFP (Zimyanin et al., 2008). For constructing Torsin germline clones: *torsin*^{KO78} (Wakabayashi-Ito et al., 2011), P(hsFLP,neoFRT)19A (BDSC: 31418), P(ovoD1,hsFLP)19A (BDSC: 23880). Flies were reared on standard *Drosophila* medium at 25˚C. RNAi crosses and controls were performed at 29˚C.

Immunocytochemistry. 3-day old mated ovaries were dissected and fixed as in (McKim et al., 2009). We used anti-LamC, 1:30 (LC28.26; Developmental Studies Hybridoma Bank (DSHB)); anti-Grk, 1:50 (1D12; DSHB) anti-DFz2-C(Mathew et al., 2005). Secondary antibodies (Jackson ImmunoResearch and Fisher) were anti-rabbit-DyLight488 (1:200), anti-rabbit- FITC (1:200); anti-mouse-DyLight594 (1:200), anti-rat-Dylight488 (1:200), anti-HRP-Dylight594.

Fluorescence In-situ Hybridization. Procedures for FISH were as in (Zimmerman et al., 2013).

Transmission Electron Microscopy (TEM). TEM was performed as in (Ashley et al., 2005). Ovaries were treated *en bloc* with 1% uranyl acetate for 1 hr prior to dehydration.

Image Acquisition. Confocal images were acquired using a Zeiss LSM700 confocal microscope equipped with a Zeiss 63x Plan-Apochromat 1.4 NA DIC oil immersion objective at a digital zoom of 3X for high magnification images, and 0.7X for low magnification images. Identical settings were used for control and experimental samples processed on the same day. Intact ovaries were imaged using a Ziess Axio a wide field camera on an upright Ziess microscope with a 2.5X objective.

Preface to Chapter V

In this chapter we study the mechanism by which synapse-specific RNPs are targeted to their destination. We identify dNesprin-1, which is a giant transmembrane protein that forms “rail-road tracks” from the nucleus to specific synaptic sites and serve as a path for RNP transport.

My contribution to this Chapter: Figures 5.1A-H,R J-L, 5.2 G-I, 5.4C-G, 5.6K-L, 5.7
Mary Packard contributed 5.2A, 5.3, 5.4A-B F-G, 5.5 A-E, G-J, 5.6A-J
Baojin Ding contributed 5.1Q, 5.2L O
Catalina Ruiz-Canada contributed 5.1I
James Ashley contributed 5.1M-N S-U, 5.2B-C F J-K, 5.5F

The following chapter has been published as:

Packard M*, **Jokhi V***, Ding B, Ruiz-Canada C, Ashley J, Budnik V. *Nucleus to synapse Nesprin1 railroad tracks direct synapse maturation through RNA localization*. **Neuron**. **2015** May 20; 86(4):1015-28 (*Equal contribution)

Chapter V

Nucleus to Synapse Nesprin Railroad Tracks Direct Synapse Maturation Through RNA Localization

INTRODUCTION

A crucial property of synaptic connections is their ability to change, which is thought to be at the core of adaptive processes, such as learning and memory and the refinement of connectivity (Mayford et al., 2012). A key feature of long-term changes in synaptic structure and function is the requirement for new protein synthesis (Mayford et al., 2012). In hippocampal neurons ribonucleoprotein (RNP) granules are transported to the base of dendritic spines, and following plasticity-eliciting stimuli result in RNP translocation to activated spines and induction of protein synthesis (Wang et al., 2010).

An important, yet poorly understood question is “How are RNPs directed to their precise destinations once they exit the nucleus?” Studies in several systems provide evidence for directed trafficking of RNPs by binding to kinesin and dynein motors, thus supporting a role for microtubules in this process (Hirokawa, 2006). However, studies also implicate actin filaments or actin-based motors, such as MyosinV/Didium, in the translocation of RNPs to dendritic spines (Fujii et al., 2005) or the posterior pole of the *Drosophila* oocyte (Krauss et al., 2009). In the oocyte, the precise posterior localization of *oskar* mRNA, required to establish the anterior-posterior axis, requires both the activities of microtubules and actin-based motors. In this process MyosinV/Didium interacts with Kinesin heavy chain (Krauss et al., 2009), suggesting an interplay between the actin and microtubule cytoskeleton. It is proposed that microtubules could mediate long-range movements of RNPs from the nucleus to the periphery, but that precise

localization of RNPs requires short-range interactions between RNPs and the actin-based cytoskeleton (Krauss et al., 2009). However, these long versus short-range interactions are still ill defined.

To determine a potential role of the actin cytoskeleton in the postsynaptic localization of RNPs, we focused on the actin-binding protein MSP300/Nesprin-1 (Nsp1; also known as Syne1), a component of the LInker of Nucleoskeleton and Cytoskeleton (LINC) complex (Simpson and Roberts, 2008; Volk, 1992). The LINC complex links the nuclear cytoskeleton with the actin-based cytoplasmic cytoskeleton. Nsp1 is a giant transmembrane protein of the spectrin superfamily (Noegel and Neumann, 2011; Rajgor and Shanahan, 2013; Zhang et al., 2002b), which is associated with a variety of musculoskeletal disorders, such as X-linked Emery-Dreifuss Muscular Dystrophy (EDMD), movement disorders such as autosomal recessive cerebellar ataxia type 1 (ARCA1), bipolar disorder, and it is a risk gene for schizophrenia and autism (Bione et al., 1994; Cartwright and Karakesisoglou, 2013; Shinozaki and Potash, 2014; Taranum et al., 2012b). The largest isoform of Nsp1 is embedded in the outer nuclear membrane (ONM) via its transmembrane domain. The C-terminal tail, containing a Klarsicht/Anc1/Syne (KASH) domain, faces the nuclear intermembrane space (also referred as to the perinuclear space) between the ONM and the inner nuclear membrane (INM) and interacts with the INM Sad1/Unc84 (SUN) domain-containing proteins, thus connecting ONM and INM proteins. Its giant N-terminal domain faces the cytoplasm and contains multiple spectrin-type repeats as well as two calponin

actin-binding domains. However, many Nsp1 isoforms lack the KASH domain and thus not likely directly linked to the nuclear envelope.

At the mammalian neuromuscular junction (NMJ) Nsp1, is involved in interactions with the acetylcholine receptor (AChR) clustering molecule Muscle-Specific Kinase (MuSK) (Apel et al., 2000). In the central nervous system CPG2, an isoform of Syne1, participates in the trafficking of glutamate receptors (GluRs) (Cottrell et al., 2004). Studies in *Drosophila* and mice show that Nsp1 is required for normal nuclear localization in muscle cells (Volk, 2013; Zhang et al., 2010) and the integrity of muscle cell insertion sites into the cuticle (Volk, 1992). Recently, reports suggest that Nsp1 isoforms lacking the KASH domain are also required for normal *Drosophila* larval locomotion, selective localization of GluR-IIA and synaptic function at the NMJ, independent of its nuclear localization role (Morel et al., 2014a). However, its potential involvement in the localization of synaptic mRNAs has not been investigated.

Here we report that interfering with Nsp1 isoforms at the *Drosophila* NMJ disrupts the postsynaptic localization of mRNAs in muscle, and thus the localization of the proteins encoded by these mRNAs at the postsynaptic region. In addition, mutations in *nsp1* alter synapse development and activity-dependent plasticity. In these mutants mRNAs accumulate in the cytoplasm at the nuclear periphery, suggesting that the defect likely originates from abnormal transport of these mRNAs to synaptic sites and not from the nuclear export of these mRNAs. Strikingly in wild type muscles, Nsp1 protein is organized into long striated

filaments, dubbed “railroad tracks”, which extend all the way from the nucleus to the periphery of the NMJ. Nsp1 railroad tracks are the first postsynaptic elements found to associate specifically with immature synaptic boutons formed during NMJ expansion or upon spaced stimulation. We show that Nsp1 binds to a synaptically localized RNA. In addition, Nsp1 colocalizes and cosediments with F-actin, confirming its relationship with the actin cytoskeleton. Furthermore, its exclusive localization around nascent synaptic boutons is similar to the distribution of the unconventional actin motor, Myo31DF, the *Drosophila* ortholog of human Myo1D. Null mutations in *myo31DF* mimic the phenotypes of the severe hypomorphic $nsp1^{sZ75}$ mutant, and both Nsp1 and Myo31DF are required for each other’s localization. These studies unravel a novel filamentous network connecting the nucleus to nascent synaptic boutons, and this network functions with actin motors for proper localization of postsynaptic RNPs.

RESULTS

Nsp1 is required for normal mRNA localization at the NMJ

To determine a potential role of Nsp1 in the postsynaptic localization of mRNAs, we carried out fluorescent *in situ* hybridization (FISH) with probes to mRNAs previously found enriched at the larval NMJ. *Drosophila* larval NMJs are composed of synaptic boutons organized as beaded strings (Figure 5.1R). These NMJs innervate identified muscles of the body wall in a stereotypic manner, making comparisons across animals and genotypes straightforward. Synaptic boutons contain multiple glutamate release sites, and the entire presynaptic arbor can be selectively labeled with antibodies to HRP, which crossreact with neuronal carbohydrate epitopes (Jan and Jan, 1982). At the postsynaptic muscle region, synaptic boutons are apposed by the postsynaptic membrane containing GluR clusters in register with presynaptic active zones. Surrounding GluR clusters is the subsynaptic reticulum (SSR) a highly folded membrane structure derived from the muscle plasma membrane (Guan et al., 1996). This postsynaptic SSR is strongly labeled by antibodies to Discs-Large (Dlg) a scaffolding protein of the PSD95 family (Figure 5.1R) (Lahey et al., 1994).

In this study, we focused on transcripts encoding the PDZ-scaffolding proteins, Par6 and MAGI (Jokhi et al., 2013b; Speese et al., 2012). As reported, in wild type larvae *par6* and *magi* FISH signals were enriched at the postsynaptic region of the NMJ, outside of the HRP-labeled presynaptic terminal (Figure 5.1A,C). In contrast, in the severe hypomorphic mutant, $nsp1^{sZ75}$, the NMJ FISH

signal was markedly decreased (Figure 5.1B,D,J). This reduction was specific to mutations in *nsp1,* as the defect was completely rescued by a duplication of the *nsp1* locus (Figure 5.1J). Other mRNAs not concentrated at the NMJ, such as *dlg*, were not affected in *nsp1*^{sZ75} mutants (Figure 5.1L).

The *nsp1*^{sZ75} mutation introduces an early stop codon into the 12th exon of the *nsp1* gene, thus predicting the truncation of 80% of the giant full-length protein (~1.5 MDa) and potentially generating truncated protein species of 260-300 kDa (Yu et al., 2006). Nsp1 immunoprecipitation from body wall muscle protein extracts using an antibody that recognizes nearly all Nsp1 isoforms (Volk, 1992) shows that the *nsp1*^{sZ75} mutation eliminates all giant Nsp1 isoforms (above 1 MDa), although lower molecular mass species (below 300 kDa), which may include truncated species, are still observed at lower levels (Figure 5.1I). Thus, in the absence of giant Nsp1 isoforms, transcripts known to localize at the postsynaptic region are severely decreased.

The depletion of *par6* and *magi* mRNAs at the NMJ could be explained by abnormal *nsp1* transcription, RNP packaging/ RNA stability, defective nuclear export, or inappropriate transport of RNPs to the NMJ. To discern between these possibilities we examined the distribution of *par6* and *magi* transcripts within the nucleus and in the cytoplasm around the nucleus. Notably, the reduction of postsynaptic *par6* and *magi* mRNA in *nsp1*^{sZ75} mutants was correlated with a two-fold increase in FISH signal in the cytoplasm at the nuclear periphery (Figure 5.1N,O,M). The increase in signal resulted from both an increase in the number

of bright fluorescent punctae and a more diffuse signal and was completely rescued by a duplication of the *nsp1* locus (Figure 5.1N-P,M). Together with the data showing that levels of *par6* and *magi* RNA are decreased at postsynaptic sites, these observations raise the possibility that in *nsp1*^{sZ75} mutants megaRNPs are exported normally from the nucleus but that their transport to postsynaptic sites might be disrupted. Consistent with this idea, the total levels of *par6* RNA in larval body wall muscles was not decreased in *nsp1*^{sZ75} mutants as determined by real time PCR (Figure 5.1Q), further suggesting that RNA stability is unlikely to be affected in the *nsp1*^{sZ75} mutant. Similarly, the levels and distribution of Torsin at the nuclear envelope were normal (data not shown) and we never observed abnormal megaRNP granules in the *nsp1*^{sZ75} mutant as in the case of *torsin* mutants at the EM level (Jokhi et al., 2013b)(not shown; N: 37 nuclei from 3 animals). Taken together, the most straightforward explanation for the decrease in FISH signal at the postsynaptic region is a defective RNA transport.

A decline in the transport of *par6* and *magi* mRNA from the perinuclear area to the NMJ should be reflected in a decrease in the levels of postsynaptic Par6 and MAGI protein, which was tested using antibodies specific for these proteins (Jokhi et al., 2013b; Ruiz-Canada et al., 2004). As with the FISH signal at the NMJ, we found that mutations in *nsp1*^{sZ75} led to a substantial decrease in the levels of Par6 and MAGI immunoreactivity at the postsynaptic site, which was completely rescued by a duplication of the *nsp1* locus (Figure 5.1E-H,K). Interestingly, an additional *nsp1* mutation (*nsp1*$^{\Delta KASH}$) lacking the C terminal

region, including the nuclear transmembrane domain and the KASH domain, a domain known to link Nsp1 to nuclear envelope proteins, showed no such alteration in Par6 protein localization (Figure 5.1S-U). Thus, interfering with giant *nsp1* isoforms, but not deletion of the transmembrane and KASH domains, prevents normal transport of transcripts that are normally localized at the NMJ, and this defect interferes with normal postsynaptic protein composition.

Figure 5.1- *magi* and *par6* mRNAs are depleted at the NMJ of *nsp1*^{sZ75} mutants

(A-D) Larval NMJs labeled with anti-HRP and FISH to (A,B) a *par6* probe and (C,D) a *magi* probe in (A,C) wild type and (B,D) *nsp1*^{sZ75} mutants.

(E-H) Larval NMJs labeled with anti-HRP and either (E, F) anti-Par6 or (G,H) anti-MAGI in the indicated genotypes.

(I) Immunoprecipitation of Nsp1 in wild type and *nsp1*^{sZ75} mutants.

(J-L) Quantification of postsynaptic signal intensity normalized to wild type control (see Methods) for (J) *par6* and *magi* RNA, (K) Par6 and MAGI protein and (L) DLG RNA and protein, in wild type, *nsp1*^{sZ75}, and *nsp1*^{sZ75} mutants containing 2 copies of a duplication of the *nsp1* locus (rescue).

(M) Ratio of FISH signal (intensity:background) in the region surrounding the nucleus in the above genotypes.

(N-P) Muscle nuclei labeled with Hoechst, and FISH to *par6* in (N) wild type, (O) *nsp1*^{sZ75} mutants, and (P) rescue. (Q) qPCR of *par6* mRNA from wild type and *nsp1*^{sZ75} mutants normalized to e*f1α48D*. Calibration scale(μm): A-H:4; N-P:6. Error bars represent ±SEM (*p<0.05, **p<0.001, ***p<0.0001).

Number of samples (animals:arbors/muscles)= (J) 20:38,18:36,10:20,9:18,10:20,9:18; (K) 8:15,8:16,8:15,8:16,8:15,8:16; (L) 9:18,9:18,9:18,9:18; (M) 7:13,7:14,7:13,6:12,6:12,6:12; (Q) 3.

(R) wild type NMJ labeled with anti-HRP and anti-Dlg, to label pre- and postsynaptic compartments, respectively.

(S,T) NMJs labeled with anti-Par6 and anti-HRP in (S) wild type and (T) *nsp1*$^{\Delta KASH}$ mutants. Calibration scale (μm): (R)12 (left column), 4 (right column); (S,T) 4. Error bars represent ±SEM.

(U) Quantification of postsynaptic Par6 signal intensity in the indicated genotypes.Sample numbers in (U) are (animals:muscles): 4:14,4:23.

Image panels correspond to single confocal slices.

Figure 5.1- *magi* and *par6* mRNAs are depleted at the NMJ of *nsp1*^{sZ75} mutants

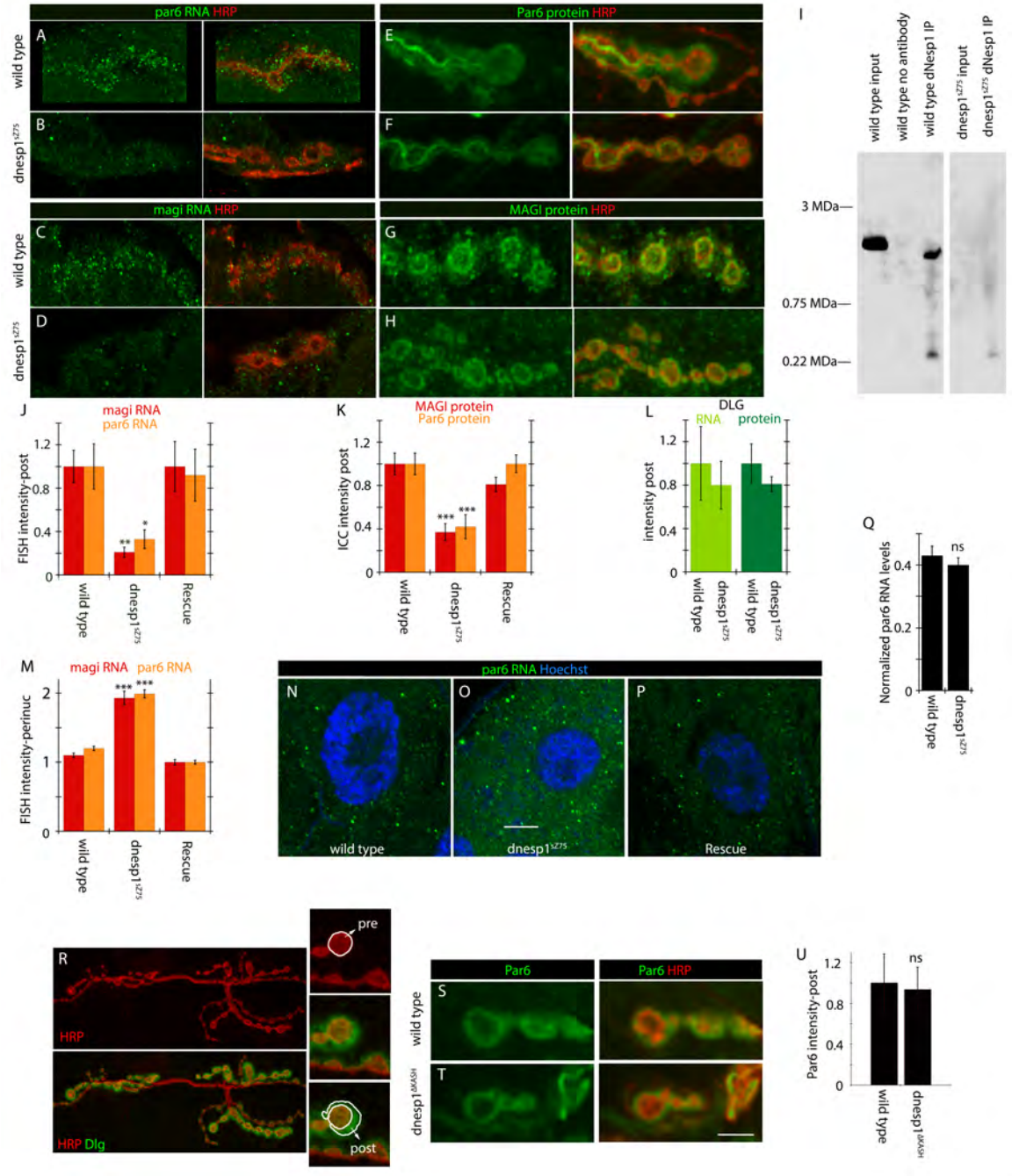

Nsp1 establishes a long-range filamentous network that specifically interacts with nascent boutons at the NMJ

We next determined how Nsp1 could participate in the transport of postsynaptic mRNAs to the NMJ. We first examined the distribution of Nsp1 protein in wild type body wall muscles using *Drosophila* anti-Nsp1 antibodies (Volk, 1992). As previously reported (Elhanany-Tamir et al., 2012a), Nsp1 had a wide distribution in muscle cells, showing strong immunoreactivity at Z-bands within the contractile apparatus (Figure 5.2A) and throughout the muscle cell cortical region. Nsp1 immunoreactivity also outlined the nucleus, but was excluded from the nucleoplasm (Figure 5.2A,B). We also observed long Nsp1 positive filaments that fully extended all the way from the nuclear periphery to distant regions of the muscle cell cortex, including regions neighboring the NMJ (Figure 5.2B,G; arrowheads). Similar filaments were observed in *nsp1*$^{\Delta KASH}$ (Figure 5.2C, arrowheads), suggesting that these filaments do not depend on direct interactions between Nsp1 and the nuclear envelope. These filaments, similar to the filaments observed at Z-bands had a striated appearance (Figure 5.2G; arrowheads), and thus we dubbed them “railroad tracks”.

Although extending towards the NMJ, Nsp1 was largely excluded from the majority of synaptic boutons at the NMJ (Figure 5.2A). However, Nsp1 signal was often observed surrounding a very small number of synaptic boutons (Figure 5.2A; arrows). This NMJ Nsp1 signal was examined in conjunction with pre- and postsynaptic markers (anti-HRP to label the presynaptic compartment and anti-

DLG to label the postsynaptic NMJ region). Strikingly, boutons that were surrounded by Nsp1 immunoreactivity were devoid of Dlg signal and thus correspond to “ghost” boutons (Figure 5.2D,E,I). Previous studies show that during larval development, presynaptic boutons are first formed from an expanding NMJ arbor, and that the recruitment of their postsynaptic proteins occurs after bouton extension (Ataman et al., 2008). Thus, ghost boutons correspond to a transient, immature synaptic bouton developmental stage, which lacks the post-synaptic apparatus. The filamentous postsynaptic localization of Nsp1 at ghost boutons was also demonstrated using STimulated Emission Depletion (STED) microscopy (Figure 5.2F). Quantification of the association of Nsp1 with ghost boutons revealed that 97% of ghost boutons were surrounded by Nsp1. Figure 5.2J shows relative intensities of Nsp1, HRP and Dlg at the peak of HRP intensity (±0.4 μm; bouton border) in mature and ghost boutons, showing that in contrast to mature boutons, ghost boutons are associated with Nsp1 and have minimal Dlg signal (Figure 5.2J,K).

Nsp1 immunoreactivity was specific, as it was virtually eliminated in the *nsp1*^{sZ75} severe hypomorphic mutant (Figure 5.2H). In addition, the localization of Nsp1 to ghost boutons was unaffected in the *nsp1*$^{\Delta KASH}$ mutants (Figure 5.2M,N), suggesting that direct anchoring of Nsp1 to the nuclear envelope is not required for Nsp1 targeting to ghost boutons. This is consistent with the observation that the levels of postsynaptic Par6 were not affected in the *nsp1*$^{\Delta KASH}$ mutants (Figure 5.1S-U). To our knowledge, Nsp1 is the first identified protein that

specifically marks these immature boutons, raising the possibility that Nsp1 is involved in the first stages of synaptic bouton maturation. Further, the lack of postsynaptically localized transcripts in the severe hypomorphic mutant, combined with the accumulation of these transcripts at the periphery of the nucleus, implicates Nsp1 railroad tracks in the transport of mRNAs required for the formation of postsynaptic structures.

To determine if Nsp1 could associate with RNAs, we immunoprecipitated Nsp1 from body wall muscle protein extracts and tested whether *par6* RNA co-precipitated with Nsp1 in wild type and $nsp1^{sZ75}$ mutants. We found that *par6* RNA indeed co-precipitated with Nsp1 in wild type (over 12-fold increase compared to no antibody control), and that the levels of *par6* coprecipitation was substantially reduced in $nsp1^{sZ75}$ mutants (~2-fold increase compared to no antibody control; 5.2L). The association between Nsp1 and *par6* RNA was specific, as the negative control transcripts, *ef1α48D* and *rpL32,* co-precipitated with Nsp1 to a far lesser extent in both wild type and $nsp1^{sZ75}$ mutants (Figure 5.2O).

In wild type larvae, ghost boutons are observed infrequently presumably because they rapidly mature. However, previous studies show that ghost boutons are induced by spaced electrical stimulation paradigms based on motor nerve stimulation, activation of motorneuron-expressed Channelrhodopsin 2 (ChR2), or high K^+-induced depolarization (Ataman et al., 2008). To determine if Nsp1 associates with newly formed ghost boutons, we first used a spaced paradigm of

5 cycles of high K^+-induced depolarization, each separated by 15 min of rest, to induce ghost bouton formation. Then, preparations were fixed and triple-labeled with antibodies to HRP, DLG, and Nsp1. In unstimulated controls, ghost boutons were seldom observed (Figure 5.3A). However, in stimulated preparations many ghost boutons that were surrounded by Nsp1 were formed, (Figure 5.3B; see below for quantification of ghost boutons upon stimulation). These observations support the notion that Nsp1 is one of the earliest localized proteins at postsynaptic sites during synaptic bouton formation.

Figure 5.2- Nsp1 railroad tracks specifically wrap around ghost boutons

(A-I) Body wall muscles and NMJs labeled with anti-Nsp1, anti-HRP and anti-DLG in (A,B,D-G, I) wild type, (C) *nsp1*$^{\Delta KASH}$ and (H) *nsp1*^{sZ75} mutants. Arrowheads point to Nsp1 railroad tracks; z=Z-line; n=nucleus. (D,E) are high magnification views of the regions marked by the boxes in (A,I, respectively) showing the presence of ghost boutons (arrows), which are labeled with anti-Nsp1 and anti-HRP, but not with anti-DLG. (F) STED image of a ghost bouton, showing Nsp1 label wrapping around a ghost bouton.

(J) Quantification of anti-DLG, anti-Nsp1, and anti-HRP signal at the bouton border (see Methods; N=6) normalized to HRP intensity.

(K) Representative relative signal intensity across the midline of a mature and a ghost bouton.

(L) Relative levels of *par6* RNA immunoprecipitated with Nsp1 as measured by real time PCR (N=3 biological replicates).

(M-N) NMJs labeled with anti-Nsp1, anti-HRP, and anti-DLG in (M) wild type and (N) *nsp1*$^{\Delta KASH}$ mutants, showing Nsp1 at ghost boutons (arrows). Calibration scale: 11µm. Images are single confocal slices. (O) Real time PCR of the control transcripts *ef1α48D* and *rpL32* (n=3 biological replicates).

Calibration scale(µm): A-C,G-I:10; D,E:4; F:2. Number of samples in (J) is 6 boutons. Image panels represent single confocal slices. Error bars represent ±SEM (*p<0.05, **p<0.001, ***p<0.0001).

Figure 5.2- Nsp1 railroad tracks specifically wrap around ghost boutons

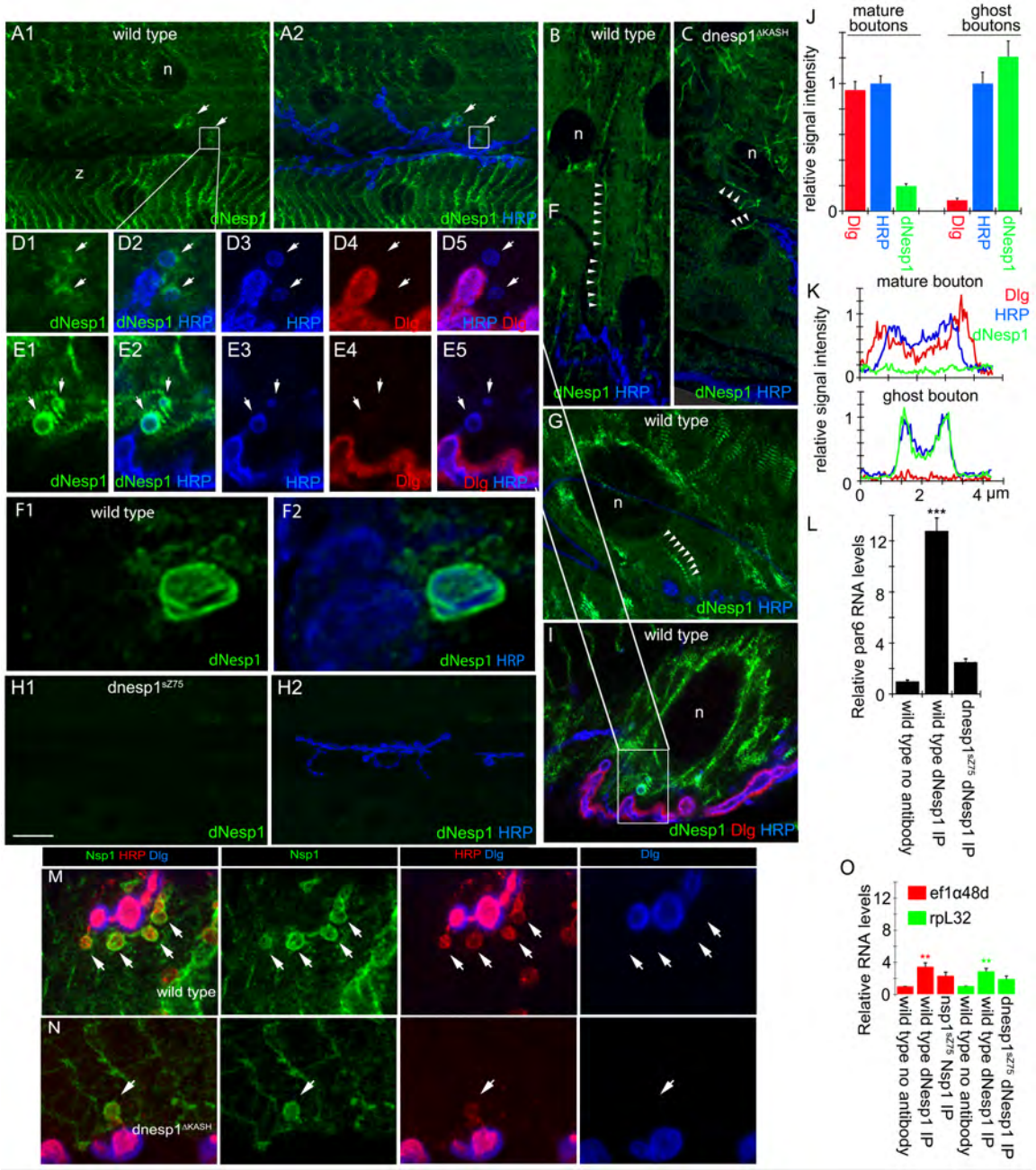

Figure 5.3- Nsp1 is localized to new ghost boutons induced by spaced stimulation (see Figure 5.5 for quantification).

(A,B) Wild type NMJ arbors labeled with anti-Nsp1, anti-HRP and anti-DLG in (A) unstimulated samples (box in A1 is shown at higher magnification in A2), and (B) samples subjected to high K^+ stimulation (boxes in B1 are shown at high magnification in B2 and B3), showing that activity-induced ghost boutons (arrows) are wrapped by Nsp1. Calibration scale (μm): A1,B1:50; A2,B2,B3:20. Image panels represent single confocal slices.

Figure 5.3- Nsp1 is localized to new ghost boutons induced by spaced stimulation

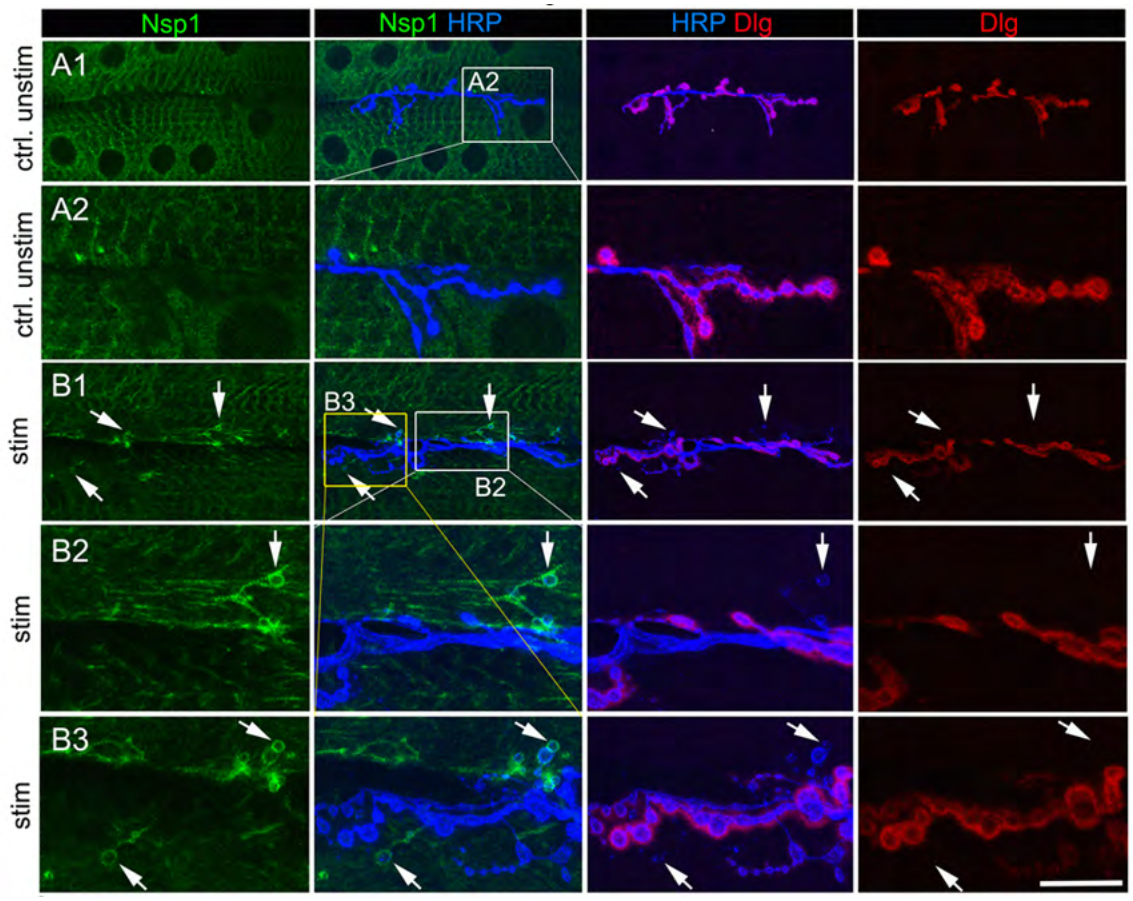

Nsp1 function is required for normal synaptic bouton maturation and activity-dependent plasticity

To determine the role of Nsp1 during synaptic bouton formation, we examined the NMJ in mature 3rd instar larvae in wild type and *nsp1*^{sZ75} mutants. We found that in *nsp1*^{sZ75}, the number of synaptic boutons was markedly reduced (Figure 5.4A,C,F). Furthermore, as in other mutants that prevent synaptic bouton maturation (Ataman et al., 2006a; Korkut et al., 2009), NMJs from *nsp1*^{sZ75} mutants had a significant increase in the number of ghost boutons (Figure 5.4B,D,E (arrows),G). These mutant phenotypes were specific, as they were completely rescued by two copies of a duplication of the *nsp1* locus (Figure 5.4F,G). Interestingly, *nsp1*^{sZ75}/+ heterozygotes also showed an enhancement in the number of ghost boutons, which was on average more pronounced than *nsp1*^{sZ75} homozygotes (Figure 5.4G). However, this difference between the *nsp1*^{sZ75} homozygote and heterozygote was not statistically significant. The defect in the hererozygote was rescued by introducing one copy of the duplication of *nsp1* (Figure 5.4G). Notably, no significant changes were observed in the number of synaptic boutons or ghost boutons in a *nsp1* mutation deleting the C-terminal region, including the transmembrane and KASH domains, *nsp1*$^{\Delta KASH}$ (Figure 5.4F,G). These results support a role for Nsp1 in synaptic maturation and suggest that this role is independent of interactions between Nsp1 and nuclear envelope proteins.

We also determined whether Nsp1 functions in the postsynaptic muscle or presynaptic neuron during NMJ development as Nsp1 is expressed in both tissues (http://flybase.org/reports/FBgn0261836.html). In these experiments we expressed Nsp1-RNAi either in neurons (using the neuronal elav-Gal4 driver) or muscles and quantified the number of synaptic boutons and ghost boutons in the third instar larval stage. Downregulating Nsp1 in neurons elicited a small but significant decrease in the number of synaptic boutons (Figure 5.4F). However, this decrease was not accompanied by an increase in the number of ghost boutons (Figure 5.4G). In contrast, the phenotype of the *nsp1*^{sZ75} mutant was completely recapitulated by downregulating Nsp1 in muscles, with respect to total bouton count (Figure 5.4F) and number of ghost boutons (Figure 5.4G). Thus, Nsp1 appears to function in both neurons and muscles, but its contribution to NMJ expansion is predominantly exerted by its function in muscle. This is consistent with our finding that maturation of ghost boutons requires a retrograde signal from muscle (Korkut et al., 2013).

We next determined if, in addition to a role in synaptic maturation, Nsp1 could be involved in rapid activity-dependent bouton formation. In these experiments, both wild type and *nsp1*^{sZ75} mutants were subjected to the spaced high K^+ stimulation paradigm. Interestingly, both wild type controls and *nsp1*^{sZ75} mutants were capable of generating new ghost boutons in response to spaced stimulation (Figure 5.5 A-D, I). However, the response of *nsp1*^{sZ75} mutants was significantly reduced (Figure 5.5I), providing support for the notion that Nsp1 is

required for bouton formation. We also determined the likely fate of ghost boutons over 8hrs after formation. In these experiments, intact (un-dissected) larvae expressing Channelrhodopsin2 (ChR2) in motor neurons were stimulated with blue light following our spaced protocol (Ataman et al., 2008; Koon et al., 2011). Then, larvae were dissected at 2 and 8 hr after the start of stimulation. Similar to K^+ stimulation, wild type larvae exhibited a highly significant increase in the number of ghost boutons upon light stimulation (Figure 5.5J). At 8 hrs, however, the number of ghost boutons was significantly decreased suggesting that these newly formed boutons either matured or were eliminated (Figure 5.5J). In *nsp1*^{sZ75} mutants, ChR2 activation by light also resulted in an increase in the number of ghost boutons, although significantly smaller than wild type, consistent with the results with K^+ stimulation. Notably, however, these ghost boutons persisted even after 8hrs (Figure 5.5J). Together with the observations that *nsp1*^{sZ75} mutants have significantly fewer mature boutons, and an accumulation of ghost boutons, these results suggest that in *nsp1*^{sZ75} mutants newly formed boutons fail to mature.

Figure 5.4- NMJ expansion and synaptic bouton maturation depend on *nsp1*, but are independent from the KASH domain

(A-E) Larval NMJs labeled with anti-HRP and anti-DLG shown at (A,C) low and (B,D,E) high magnification from (A,B) wild type and (C-E) *nsp1*^{SZ75} mutant. Arrows point to ghost boutons, which are devoid of DLG label.

(F,G) Quantification of (F) synaptic bouton number and (G) ghost bouton number (divided by total bouton number and normalized to wild type controls) in the indicated genotypes.

Calibration scale(μm): A,C:40; B,D,E:12. Error bars represent ±SEM (*p<0.05, **p<0.001, ***p<0.0001).

Number of samples are (animals:arbors; from left to right)

(F) 31:62,28:56,33:65,23:45,28:55,12:24,12:24,12:24,12:24,12:24.

(G) 31:62,28:56,33:65,23:46,29:57,12:24,12:24,12:24,12:24,12:24.

Image panels correspond to (A,C) a maximal intensity Z-stack projection and (B,D,E) single confocal slices.

Figure 5.4- NMJ expansion and synaptic bouton maturation depend on *nsp1*, but are independent from the KASH domain

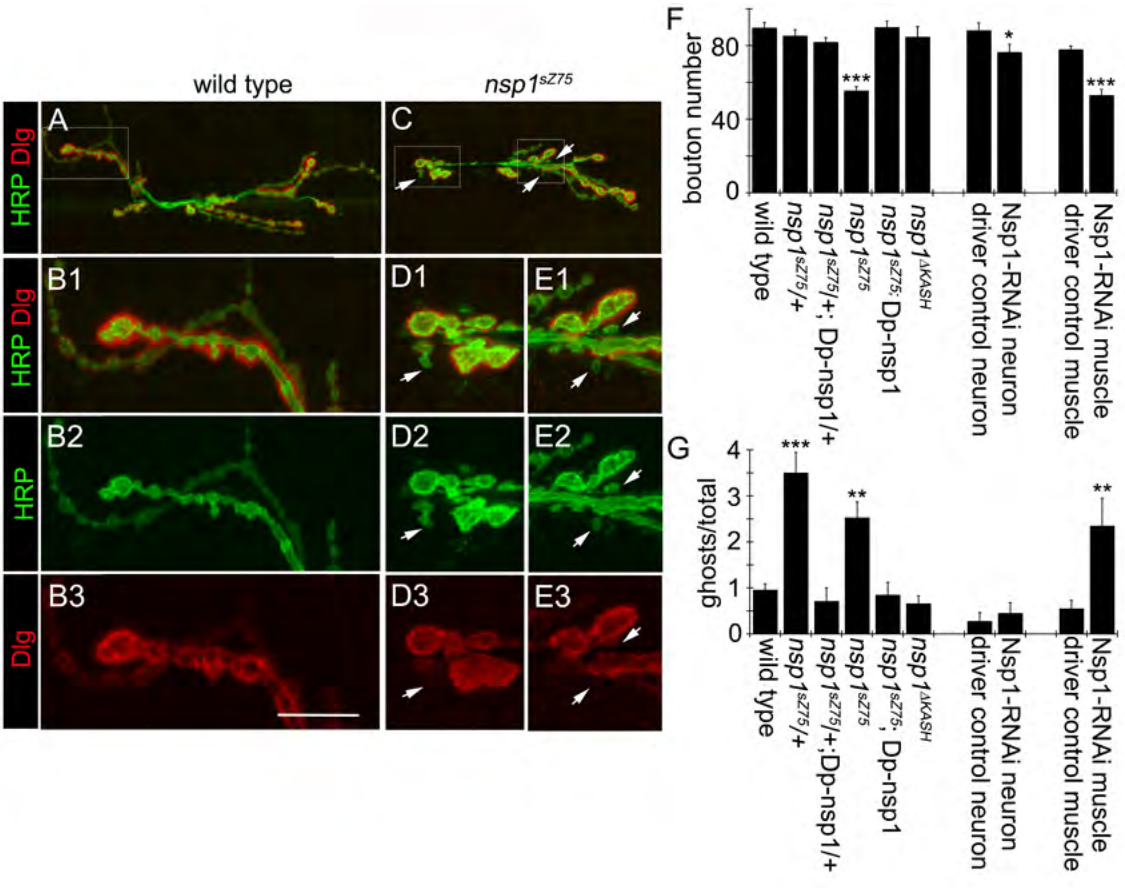

Nsp1 railroad tracks colocalize with F-actin filaments

The above observations suggest a role of Nsp1 railroad tracks in the transport of mRNAs required for postsynaptic development. As both F-actin and microtubules have been implicated in the transport of RNPs, we next determined if Nsp1 railroad tracks were associated with these cytoskeletal components. Labeling preparations with fluorescently conjugated phalloidin revealed that Nsp1 railroad tracks coincided with F-actin microfilaments (Figure 5.5E,G,H). As with Nsp1, F-actin filaments had a striated organization and the striations were staggered with those of Nsp1 with a period of ~0.5 μm (Figure 5.5G,H). The association of Nsp1 and F-actin is consistent with previously published observations suggesting that Nsp1 cosediments with F-actin in both in mammals and *Drosophila* (Volk, 1992; Zhang et al., 2002b), which was confirmed for body wall muscle extracts (data not shown). They are also consistent with the presence of two calponin actin-binding domains in Nsp1. In contrast, no colocalization was observed between Nsp1 railroad tracks and microtubules, which were labeled with an antibody to tyrosinated tubulin (Figure 5.5F).

Figure 5.5- Mutations in *nsp1* alter activity-dependent bouton formation and Nsp1 railroad tracks contain F-actin

(A-D) NMJ arbors labeled with anti-HRP and anti-DLG from (A,C) unstimulated controls and (B,D) body wall muscles subjected to high K^+ spaced stimulation, in (A,B) wild type and (C,D) *nsp1*^{sZ75} mutants. Arrows point to ghost boutons. (E,G,H) Larval body wall muscle labeled with anti-Nsp1, fluorescent phalloidin to mark F-actin, and anti-HRP showing that (E) long Nsp1 railroad tracks (arrow) spanning from the nucleus to the NMJ contain F-actin, and (G,H) that these railroad tracks are composed of staggered F-actin and Nsp1 striations.

(F) Larval body wall muscle labeled with anti-tubulin and Nsp1, showing that Nsp1 and microtubules are non-overlapping. Box in F1 is shown at high magnification in F2.

(I,J) Quantification of ghost bouton number (divided by total bouton number and normalized to wild type controls) from animals stimulated with spaced (I) high K^+ or (J) Chr2 stimulation in the indicated genotypes showing that *nsp1*^{sZ75} mutants have reduced activity-dependent induction of ghost boutons and synaptic bouton maturation.

Calibration scale(μm): A-D (panels 1,2):18; A-D (panel 3):6; E:7, F:10; and G,H:3. Error bars represent ±SEM (*p<0.05, **p<0.001, ***p<0.0001). Number of samples (animals:arbors; left to right)=(I) 31:62,33:65,11:21,11:22;(J) 30:59,33:66,28:56,30:59,19:37,28:56.

Image panels correspond to (A-D) maximal intensity Z-stack projections and (E-F) single confocal slices.

Figure 5.5- Mutations in *nsp1* alter activity-dependent bouton formation and Nsp1 railroad tracks contain F-actin

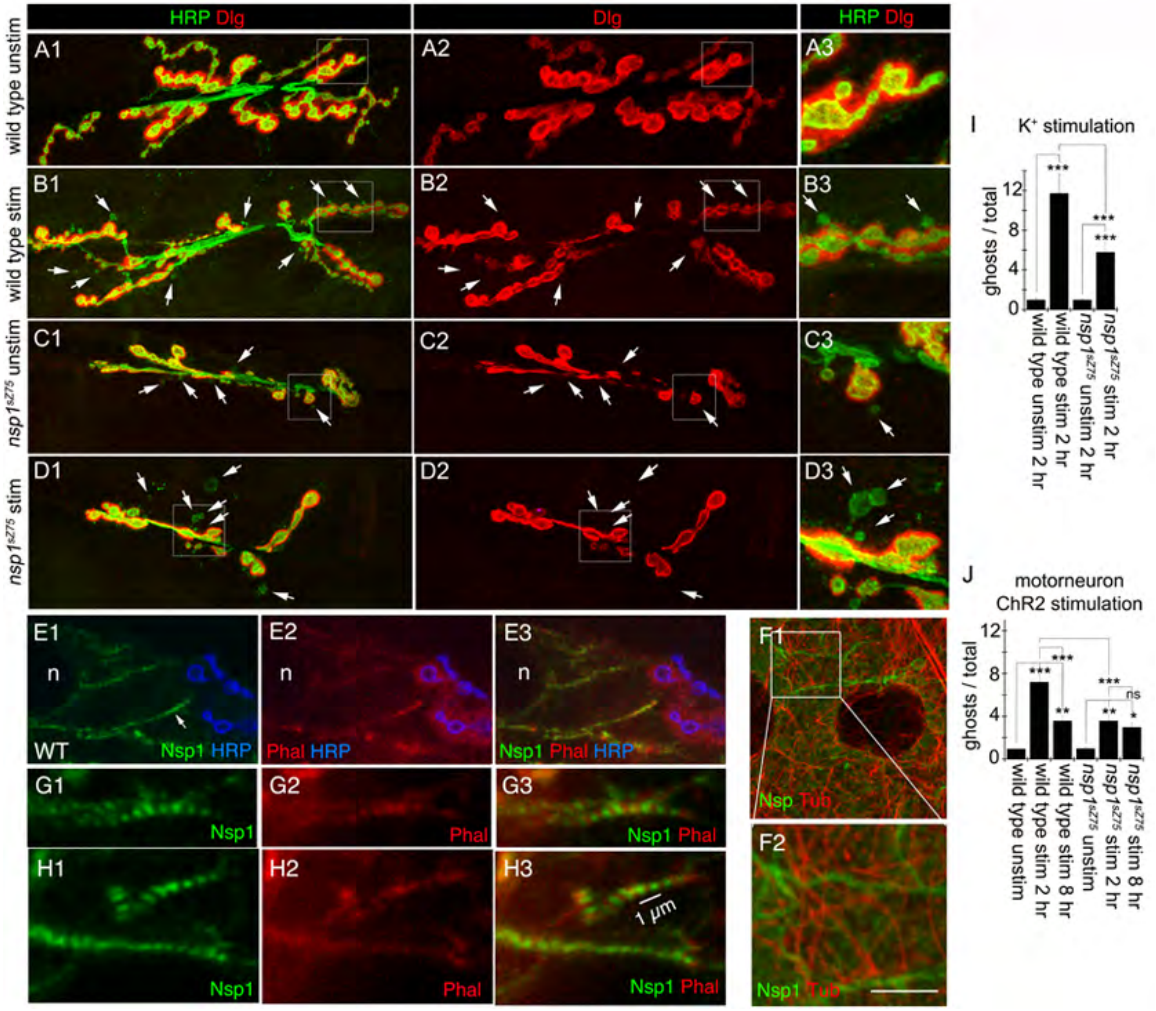

Nsp1 function requires a Myosin 1 actin motor

If Nsp1 railroad tracks serve to transport RNPs, then we predict that actin motors should be associated with Nsp1. We found that a member of the myosin1 family, Myo31DF, which is 53% identical to human Myo1D was highly enriched at ghost boutons, although it was also observed at low levels at the entire NMJ (Figure 5.6A). The immunoreactivity was specific as it was eliminated in the trans-allelic *myo31DF* mutant combination $myo31DF^{K1}/myo31DF^{K2}$ (Figure 5.6B). As expected, ghost boutons labeled by Myo31DF were also labeled by anti-Nsp1 (Figure 5.6C). In the muscle cytoplasm Myo31DF had a low intensity punctate appearance (Figure 5.6C). Unfortunately, optimal preservation of Nsp1 railroad tracks required fixation conditions different from those required to visualize Myo31DF and although some of the Myo31DF puncta colocalized with Nsp1 railroad tracks (insets in Figure 5.6C4), it was not possible to conclusively determine if Myo31DF was always associated with Nsp1 railroad tracks. Figure 5.6G shows the Pearson's colocalization index between Nsp1 and Myo31DF in the cytoplasm, at mature boutons, and at ghost boutons, showing near perfect colocalization at ghost boutons. Nevertheless, *myo31DF* null mutations not only mimicked the decrease in bouton number observed in $nsp1^{sZ75}$ hypomorphic mutants (Figure 5.6H), but also far surpassed $nsp1^{sZ75}$ mutants in ghost bouton accumulation (Figure 5.6I).

To determine the extent of the similarities between $nsp1^{sZ75}$ and *myo31DF* mutant phenotypes, we induced ghost bouton formation using the spaced

stimulation protocol either using high K^+-induced depolarization or motorneuron stimulation via ChR2 in wild type and *myo31DF* mutants. As in *nsp1*^{sZ75} mutants, *myo31DF* mutants showed a significant reduction in activity-dependent formation of ghost boutons (Figure 5.6J). Similarly, whereas in stimulated wild type controls ghost boutons significantly decreased in number 8 hr after initiation of stimulation, in *myo31DF* mutants they remained unchanged at 8 hr (Figure 5.6J). Importantly, unlike wild type controls (Figure 5.6D), in the absence of Myo31DF, Nsp1 failed to surround any of the ghost boutons induced upon stimulation (Figure 5.6E). Thus, Myo31DF is required for the proper extension of Nsp1 railroad tracks to nascent boutons.

The abnormal localization of Nsp1 in *myo31DF* mutants raised the question of whether Nsp1 had a similar role in Myo31DF localization. We found that in *nsp1*^{sZ75} mutants the distribution of Myo31DF was completely altered (Figure 5.6F). Instead of localizing at low levels at the NMJ and being enriched around ghost boutons, Myo31DF formed filaments in the muscle cortical region near the NMJ (Figure 5.6F2) suggesting that Myo31DF and Nsp1 are mutually required for each other's localization. Taken together, the above results suggest that Nsp1 and Myo31DF function together in synaptic bouton formation and maturation. This hypothesis was tested by examining if *nsp1* and *myo31DF* interacted genetically. Neither heterozygous *nsp1*^{sZ75}/+ or *myo31DF*/+ had a significant decrease in the number of boutons, but transheterozytotes *nsp1*^{sZ75}/+, *myo31DF*/+ had a significant decrease (Figure 5.6K). Most strikingly, while

nsp1^{sZ75}/+ heterozygotes had a substantial increase in the number of ghost boutons, this phenotype was completely suppressed in the *nsp1*^{sZ75}/+, *myo31DF*/+ transheterozygote (Figure 5.6L). These observations suggest that *nsp1* and *myo31DF* interact genetically and that *myo31DF* is downstream of *nsp1*.

Since in *myo31DF* mutants ghost boutons are no longer surrounded by Nsp1, we also expected that in these mutants *par6* and *magi* RNA transport to the NMJ should be severely inhibited. We found that indeed, both *par6* and *magi* transcripts were depleted from the NMJ (Figure 5.7A-D,I). In addition, there was a drastic reduction in postsynaptic Par6 and MAGI protein levels at the NMJ (Figure 5.7E-H,J). Thus Nsp1 and Myo31DF are mutually required for specific transcript localization.

Figure 5.6- Myo31DF colocalizes with Nsp1 at ghost boutons in a mutually dependent manner and mutations in *myo31DF* mimic *nsp1^{sZ75}* mutant phenotypes

(A-E, I) NMJs from stimulated (A,C,D) wild type and (B,E,I) *myo31DF$^{K1/K2}$*, labeled with: (A,B) anti-Myo31DF (Myo1), anti-HRP, and anti-DLG, showing (A) enrichment of Myo31DF at ghost boutons and (B) elimination of Myo31DF signal in *myo31DF* mutants; (C) anti-Myo31DF and anti-Nsp1 showing colocalization of both proteins at ghost boutons (insets in C4 show colocalization between Nsp1 and Myo31DF at railroad tracks); (D,E) anti-Nsp1, anti-HRP and anti-DLG showing that while activity induced ghost boutons in (D) wild type are surrounded by Nsp1, (E) *myo31DF* mutants show no Nsp1 signal at these boutons;

(F) anti-Myo31DF and anti-HRP showing that the localization of Myo31DF at the NMJ is disrupted in *nsp1^{sZ75}* mutants.

(G-L) Quantification of (G) Pearson's colocalization coefficient of Myo31DF and Nsp1 signal at different regions, (H,K) total bouton number and (I,J,L) ghost bouton number (divided by total bouton number and normalized to wild type controls). Preparations in (J) were stimulated with high K^+ saline.

Calibration scale(μm): A(1-3):40; B-E(1-3), I:30, A-D(4), I2:12. Error bars represent ±SEM (*p<0.05, **p<0.001, ***p<0.0001). Number of samples (animals:arbors) (G) 6,6,6; (H) 31:62,33:65,27:54,26:51,5:10; (I) 31:62,33:65,27:54,19:37,5:10; (J) 30:59,11:21,13:25,19:37,5:9,5:10; (K,L) 31:62,28:56,27:54,18:37. Image panels represent single confocal slices.

Figure 5.6- Myo31DF colocalizes with Nsp1 at ghost boutons in a mutually dependent manner and mutations in *myo31DF* mimic *nsp1*^{sZ75} mutant phenotypes

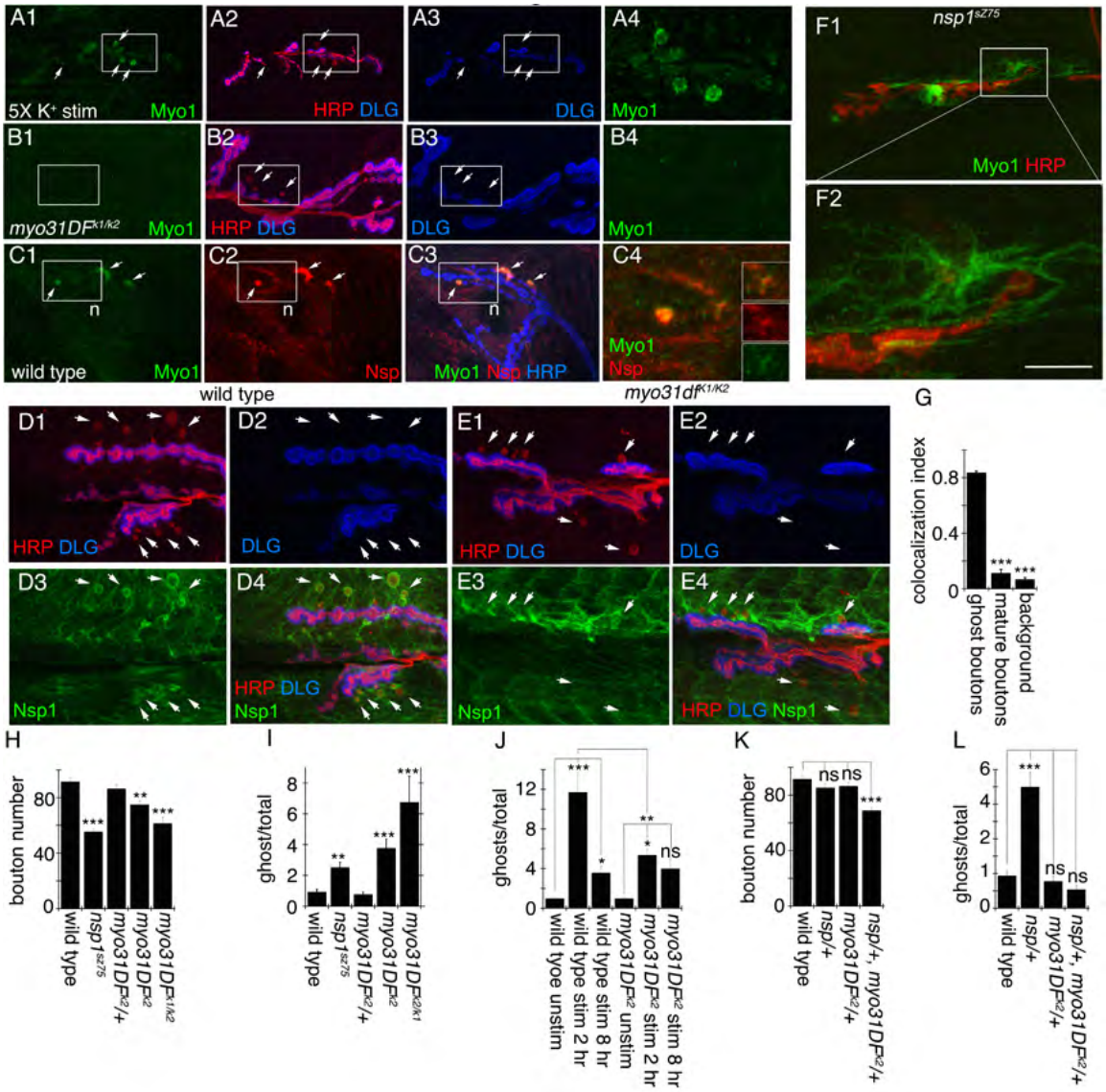

Figure 5.7- Postsynaptic *par-6* and *magi* mRNA and protein are decreased in *myo31DF* mutants

(A-D) Larval NMJs labeled with anti-HRP and FISH to (A,B) *par6* and (C,D) *magi* transcripts in (A,C) wild type and (B,D) *myo31DF*^{K2} mutants.

(E-H) Larval NMJs labeled with anti-HRP and either (E, F) anti-Par6 or (G,H) anti-MAGI in (E,G) wild type and (F,H) *myo31DF*^{K2} mutants.

(I-J) Quantification of postsynaptic Par6 and MAGI (I) RNA and (J) protein signals in the indicated genotypes.

Calibration scale: (A-H) 8μm. Error bars represent ±SEM (*p<0.05, **p<0.001, ***p<0.0001). Sample numbers (animals:arbors) (I) 10:20,11:21,7:25,8:20,10:21,15:25; (J) 6:15,6:28,6:21,6:15,6:22,6:20.

Image panels represent single confocal slices.

Figure 5.7- Postsynaptic *par-6* and *magi* mRNA and protein are decreased in *myo31DF* mutants

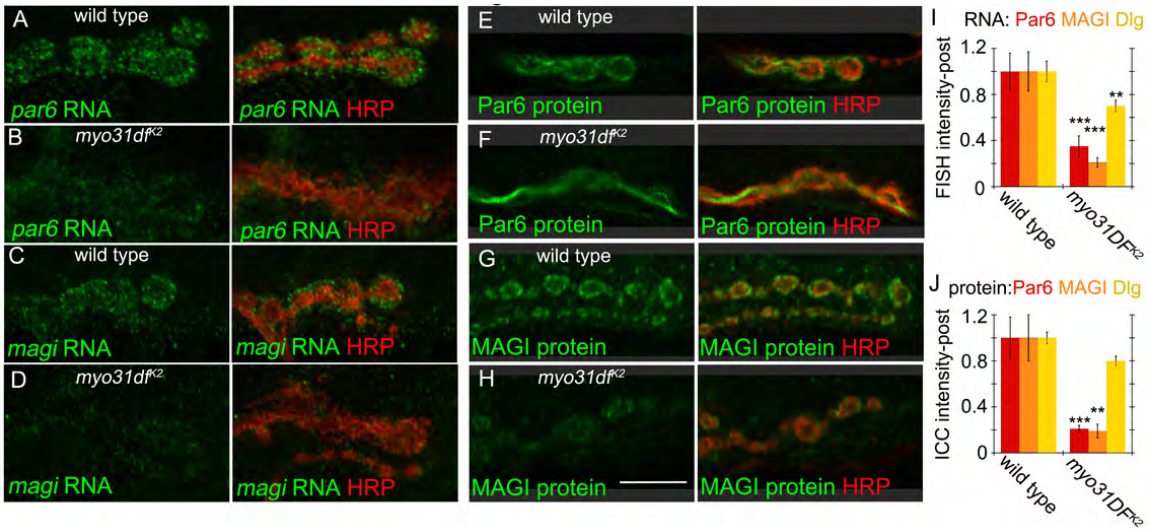

DISCUSSION

mRNA localization and local translation are critical for the formation and plasticity of synaptic connections. However, the exact mechanisms involved in precisely localizing mRNAs are still unclear. Here we provide evidence for a novel mechanism of mRNA delivery at the *Drosophila* larval NMJ, from the muscle nucleus to developing postsynaptic sites. We find that F-actin-associated Nsp1 railroad tracks, which run through the muscle cell cortex, bridge the distance from the nuclear envelope to the NMJ. At the NMJ, these railroad tracks enwrap immature synaptic boutons becoming the first identified proteins localized to boutons, which until this point lack postsynaptic proteins. Thus, Nsp1 railroad tracks provide a pathway of communication between the nucleus and sites of synapse formation. Our results suggest that Nsp1 railroad tracks serve to transport mRNAs required to build the postsynaptic machinery, since severe reduction in Nsp1 results in accumulation of postsynaptically enriched transcripts at the nuclear periphery and their depletion from the NMJ. Consistent with the association of Nsp1 railroad tracks with F-actin suggested by labeling body wall muscles and by the finding that Nsp1 cosediments with Nsp1, we found that a myosin1 motor, Myo31DF, colocalized with Nsp1. Absence of Myo31DF mimicked the synaptic phenotypes of $nsp1^{sZ75}$ mutants. In addition, Myo31DF was required for normal association of Nsp1 with immature boutons and with transport of postsynaptic transcripts. Taken together, we propose that Nsp1 railroad tracks form a pathway for the polarized transport of mRNAs to immature

synapses during development of postsynaptic structures. Further, based on the known properties of the Myosin1 family, we propose that this motor is required to either anchor Nsp1 railroad tracks to the membrane in their pathway to ghost boutons, to locally polymerize actin, or serve as motor to specifically transport RNPs to maturing postsynaptic sites.

Nature of Nsp1 railroad tracks

We show that Nsp1 filaments can go all the way from the nuclear envelope to sites of postsynaptic maturation. Nsp1 is part of the LINC complex linking the nucleoskeleton to the cytoskeleton (Taranum et al., 2012a). However, many Nsp1 isoforms lack the transmembrane and KASH domain. Whether these isoforms are still linked to the nuclear envelope through dimerization with transmembrane and KASH domain-containing isoforms is not known, but there is evidence that Nesprins can associate with each other and form filaments as observed in other proteins of the spectrin family (Mislow et al., 2002). Particularly prominent is the giant cytoplasmically localized N-terminal rod domain of about 300-500 nm which projects into the cytoplasm. The long rod domain contains multiple spectrin repeats similar to other proteins of this family, such as spectrin, α-actinin, dystrophin and utrophin. Of these, α-actinin has been shown to form F-actin based striated filaments with staggered F-actin and α-Actinin striations (Friedrich et al., 2011) at a similar periodicity (0.5μm) to those described here for F-actin and Nsp1. If Nsp1 does behave as an antiparallel dimer, as observed

with α-actinin (Friedrich et al., 2011) and suggested in vitro for Nsp1 (Mislow et al., 2002), the actin-binding CH domains located at each end of the dimer could bind to F-actin, in a repeated manner, forming striations. Similar striated filaments have been observed in the case of actomyosin filaments (containing MyosinII) in several cell types and believed to convey elastic properties to the cells (Friedrich et al., 2011). Indeed, such actomyosin filaments have also been proposed to precede muscle myofibril formation (Sanger et al., 2005). In our studies we were unable to determine if F-actin also formed these arrangements with Myo1, as the fixation conditions to examine both proteins with antibodies and fungal toxins were incompatible. Here we demonstrate that these Nsp1 striated filaments can extend all the way from the nuclear envelope to sites of postsynaptic maturation, and enwrap these sites.

Nsp1 railroad tracks and synapses

Our studies demonstrate a specific association between Nsp1 railroad tracks and ghost boutons that are naturally occurring in wild type NMJs, as well as those induced by patterned electrical stimulation. Ghost boutons are thought to represent a transient state of synaptic bouton maturation, in which postsynaptic proteins have not yet been recruited (Ataman et al., 2008). So far, Nsp1 and Myo31DF are the first proteins found to be localized at the postsynaptic region of ghost boutons. This is consistent with the model that these proteins participate in the earliest events during postsynaptic maturation,

particularly the localization of specific postsynaptic mRNAs. Mutations that disrupt the maturation of ghost boutons result in NMJ arbors with fewer synaptic boutons and an overall accumulation of ghost boutons (Ataman et al., 2006a; Ataman et al., 2008; Jokhi et al., 2013b; Speese et al., 2012). Most of these mutations are associated with alterations in Wnt signaling, which is essential for postsynaptic maturation. Interestingly, mutations in the *C elegans* Nesprin 1, ANC-1, also lead to defects in synapse formation through interaction with Wnt signaling molecules (Tulgren et al., 2014).

In mammals, the first Nesprin 1 isoform (Syne1) was isolated in a yeast two-hybrid screen using the muscle specific kinase protein (MuSK) as bait (Apel et al., 2000). MuSK is a protein required for postsynaptic differentiation. Interestingly, Syne1 was found to be exclusively associated with synaptic muscle nuclei, the subset of nuclei that transcribe synaptic genes needed for postsynaptic assembly (Apel et al., 2000). Subsequent studies at mammalian central glutamatergic synapses revealed that CPG2, an activity-dependent brain-specific isoform of Syne-1 was present at the postsynaptic region of excitatory synapses (Cottrell et al., 2004). Altering CPG2 levels resulted in abnormal dendritic spine size and disrupted constitutive endocytosis of AMPA receptors (Cottrell et al., 2004), which is linked to synaptic plasticity. Notably, mutations in *syne-1* have been linked to autosomal recessive cerebellar ataxia (Gros-Louis et al., 2007), Emery Dreifuss muscular dystrophy (Zhang et al., 2007), autism, and

bipolar disorder (Yu et al., 2013) , suggesting its importance in nervous system function.

At the *Drosophila* NMJ, Nsp1 is also involved in regulating the subunit composition of glutamate receptors (GluRs), synaptic transmission and larval locomotion (Morel et al., 2014a). However, in these studies the authors used a single Nsp1 mutation lacking the KASH domain. Our studies revealed that the KASH domain is not required for the regulation of bouton number or the localization of Par6 protein. Thus, the GluR phenotypes are most likely to represent a different function of Nsp1 in later stages of synaptic bouton maturation.

Role of Myosin I within cells and synapses

Myo31DF is a conserved protein belonging to the Myosin ID family of unconventional myosins. Class 1 myosins are monomeric and can interact with membranes through their C-terminal Tail Homology 1 (TH1) domain containing a Pleckstrin Homology (PH) lipid-binding domain. In addition, they bind to actin through their N-terminal ATPase motor head. Connecting the C- and N-terminal domains is the neck region, which binds to Calmodulin and behaves as a lever arm for force generation and membrane deformation. The monomeric nature of Myo1D makes it unlikely to function as a processive motor for cargo transport. However, MyoI ensembles have been shown to generate directed membrane movements when anchored to actin filaments (McConnell and Tyska, 2007). In

rats, Myo1D is believed to mediate vesicular transport (Huber et al., 2000) and fly Myo31DF interacts with dynamin (Speder et al., 2006). Studies in the fly have also suggested that Myo1D regulates contacts between cells since mutations in *myo31DF* lead to defective left-right asymmetry, a process highly dependent on adherens junctions (Speder et al., 2006). In the mammalian nervous system, Myo1D is found in dendrites and axons during development (Bahler et al., 1994; Benesh et al., 2012). As in the case of Nesprin 1, human Myo1D has also been linked to autism (Stone et al., 2007).

Similar to Nsp1, we found that Myo31DF was enriched at ghost boutons, was required for activity dependent ghost bouton formation and maturation, and was needed for proper localization of *par6* and *magi* mRNA at the postsynaptic region of the NMJ. The remarkable similarity between the phenotypes, as well as the colocalization of the proteins at ghost boutons suggest that Nsp1 and Myo31DF function in the same early process of bouton maturation. Supporting this conclusion is the observation that Nsp1 and Myo31DF were required for each other's localization at ghost boutons and that both genes genetically interact. In *myo31df* mutants, cytoplasmic Nsp1 filaments were still observed, but they no longer associated with ghost boutons. Considering the properties of members of the myosin I family, it is possible that Myo31DF serves to direct and anchor Nsp1 railroad tracks to the postsynaptic membrane apposed to newly formed ghost boutons. Alternatively, or in addition, Myo31DF might be required for F-actin polymerization (Evangelista et al., 2000) and thus the formation of

Nsp1 railroad tracks around newly formed ghost boutons. Interestingly, Myo31DF binds to Calmodulin light chains and Nsp1 contains Calmodulin-binding sites (Rosenberg-Hasson et al., 1996), which might serve as a site for direct interaction.

Nuclear envelope budding and megaRNP transport and localization

We have recently determined that *par6* and *magi* mRNAs exit the nucleus as part of large RNPs which exit the nucleus through a mechanism of budding at the nuclear envelope (Speese et al., 2012). Two lines of evidence suggest that the phenotypes observed in this study are unlikely to result from blocking nuclear envelope budding. First, the $nsp1^{\Delta KASH}$ mutation lacking the C-terminus region required to associate Nsp1 with the nuclear envelope had normal Par6 protein levels at the NMJ and did not display the morphological NMJ defects associated with the severe hypomorphic $nsp1^{sZ75}$ mutant. Second, in $nsp1^{sZ75}$ mutants *par6* and *magi* RNAs were observed in the cytoplasm, suggesting that they are exported from the nucleus. However, they accumulated around the nucleus and were not transported to postsynaptic sites. We propose that in the absence of Nsp1 railroad tracks in the severe hypomorphic $nsp1^{sZ75}$ mutant, megaRNPs fail to be transported in a polarized manner to the postsynaptic region of the NMJ.

RNA localization is a major mechanism for the regulation of translation, as demonstrated by the observation that most cellular mRNAs are localized mRNAs (Lecuyer et al., 2007). The localization of mRNAs at postsynaptic sites allows a

rapid and synapse-specific translation of plasticity related transcripts in response to appropriate patterns of electrical activity, which appear essential for long-term synaptic plasticity (Wang et al., 2010). Studies of RNA localization to synapses and other cellular regions have implicated both microtubules and kinesin motors, as well as F-actin and myosin motors in transporting RNPs to their site of translation (Bramham and Wells, 2007; Hirokawa, 2006; Medioni et al., 2012). It has been suggested that microtubules constitute a long-range transport mechanism for RNP transport to sites close to the membrane while microfilaments may serve as a short-range transporters at the cellular cortex, with the unconventional myosins V and VI and the conventional myosinII serving as motors (Glotzer et al., 1997). Recent studies however have demonstrated that actin can serve as tracts for long-range transport of vesicles (Schuh, 2011). Our studies uncover a novel acto-Nesprin filamentous pathway, Nsp1 railroad tracks, which serve as a long-range pathway for mRNA localization and synapse maturation during development and plasticity.

EXPERIMENTAL PROCEDURES

Fly stocks. The following stocks were used: CS (wild type; Bloomington Drosophila Stock Center; BDSC), Dp(2;1)B19 (duplication of the nsp1 locus; BDSC), nsp1$^{\Delta KASH}$ mutant (BDSC), C380-Gal4 (Budnik et al., 1996), C600-Gal4 (this report) nsp1^{SZ75} mutant (Volk, 1992)., myo31df^{K1} and myo31df^{K2} mutants (Speder et al., 2006), UAS-NLS-GFP (BDSC), and UAS-ChR2 (Schroll et al., 2006) torsin^{KO78} (Jokhi et al., 2013b).

***Immunocytochemistry*.** Late third instar larvae were dissected in Ca^{2+}-free saline (128mM NaCl, 2mM KCl, 4mM $MgCl_2$, 35.5mM sucrose, 5mM HEPES, 1mM EGTA) and fixed in 4% paraformaldehyde in 0.1M phosphate buffer for 10 min. The following antibodies were used: guinea pig anti-Nsp1 (1:2000) (Volk, 1992), rat anti-Myo31DF (1:50) (Petzoldt et al., 2012); mouse anti-DLG (1:500; 4F3 - Developmental Studies Hybridoma Bank), rat anti-Par6 (1:50; fixed in Bouin's fixative) (Ruiz-Canada et al., 2004), rat anti-MAGI (1:1000) (Jokhi et al., 2013b), rabbit anti-DLG$_{PDZ}$ (1:40,000) (Koh et al., 1999), rat anti-tubulin (1:50; Millipore MAB1864), sheep anti-digoxigenin (1:100; Sigma), rabbit anti-FITC (1:700; Invitrogen); mouse anti-Torsin (1:100; D-7,SantaCruz). Secondary antibodies were DyLight-594 or DyLight -649 conjugated goat anti-HRP (1:200; Jackson

ImmunoResearch), DyLight-405, DyLight-488, DyLight-594 or DyLight-649 conjugated anti-rat, anti-mouse, or anti-rabbit (1:200; Thermo Fisher), and FITC conjugated anti-sheep (Jackson ImmunoResearch). Phalloidin conjugated to Rhodamine was used at a concentration of 1:100, and Hoechst 33342 was used at a concentration of 1µg/ml. Preparations were mounted in Vectashield (Vector Labs, Burlingame, CA).

Fluorescent *In situ* hybridization (FISH). NMJ FISH was performed as in (Speese et al., 2012).

Morphometric analysis. For quantification of synaptic bouton and ghost bouton number, preparations were labeled with presynaptic marker, anti-HRP and postsynaptic marker, anti-Dlg. The number of boutons was determined by counting the boutons labeled with anti-HRP. The number of ghost boutons was determined as the number of boutons that lack Dlg staining. For quantification, NMJs labeled were processed simultaneously and imaged at identical settings for control and experimental groups using either a spinning disk confocal or a Zeiss LSM700 confocal microscope. Quantification was carried out using Volocity software as in (Korkut et al., 2009), unless otherwise specified. Samples were masked, such that the quantifying researcher was blind to the genotype, and quantified with the same automated routines, making this quantification unbiased. To control for different bouton volumes, total fluorescence intensity was divided by the respective bouton volume. Quantitation of FISH signal around the nucleus

was carried out using ImageJ software (NIH). Within a single slice, mean fluorescence intensity was quantified within a defined rectangle in the area of the nucleus, and then the same rectangle was used to quantify the mean fluorescence intensity in a region away from the nucleus (close to the cell membrane). Mean intensity ratio was calculated by dividing the mean intensity in the nuclear area by the mean intensity in the cytoplasm. To determine Nsp1 localization at mature and ghost boutons, preparations labeled with anti-HRP, anti-Dlg and anti-Nsp1 were imaged using identical confocal settings. At the midline of each bouton, a single line was drawn through the center of each bouton, and an intensity histogram was generated. Dlg, Nsp1 and HRP intensities were measured within a ± 0.4μm range of the HRP peak intensity at the bouton border and mean signal intensity for each antibody was calculated and normalized to the mean HRP intensity for each bouton. For colocalization studies, regions of interest (cytoplasm, mature boutons or ghost boutons) were selected, and the Pearson's Coefficient was measured with Volocity.

For STED (STimulated Emission Depletion) imaging, samples were imaged using a TCS SP8 STED 3X confocal system using a tunable white light laser for excitation and 592nm and 660nm quenching lasers (for quenching Alexa488 and Alexa568 respectively).

Spaced stimulation. Samples were stimulated as in (Ataman et al., 2008).

Quantitative real-time PCR (qPCR). For comparison of total *par6* RNA, RNA was extracted from 3 sets each of 10 larval body wall muscles from wild type and

nsp1^{sZ75}, and treated with DNase. cDNA was synthesized using random hexamer primers. Real-time PCR was performed in triplicate as described previously (Ding et al., 2013). Par6 RNA levels were calculated by the $2^{-\Delta Ct}$ method, normalized to the reference transcript, *ef1α48D*, and presented as percentage of this reference transcript. For qPCR of *Nsp1* RIP product, a similar approach was used, with *ef1α48D* and *rpL32* as negative controls. Results were normalized to no antibody control and expressed as fold enrichment.

Statistical Analysis. Statistical analysis was done using the Student-t test for pair-wise comparisons or a one-way ANOVA with Tukey post-hoc test for comparison of multiple samples.

Nsp1 immunoprecipitation and RNA immunoprecipitation (RIP). Third instar body wall muscles were dissected and frozen prior to use. Then, they were homogenized at 4˚C in RIP buffer (50mM HEPES-KOH pH7.5, 140mM NaCl, 1mM EDTA, 1% Triton X-100, 0.15% sodium deoxycholate, protease Inhibitors (Complete from Roche) and RNasin 40U/ml (Promega)) using a Kontes tissue grinder. Extracts were centrifuged at 20,000 g for 5 min at 4˚C and the supernatant precleared with protein A/G magnetic beads (Pierce) for 2hr at 4˚C. In parallel, fresh A/G beads were incubated first with 1.3µg of Donkey anti-guinea pig and then, after washing with RIP buffer, with guinea pig anti-Nsp1 (0.5 µl of serum per assay). Precleared extracts were incubated with the above antibody-beads overnight at 4˚C. Beads were then washed 3 times with RIP buffer and once with TE buffer (100mM Tris-Cl pH 8, 10mM EDTA plus RNasin 40U/ml),

resuspended in RIP elution buffer (100mM Tris-Cl pH 8, 10mM EDTA, 1% SDS plus RNasin 40U/ml), and treated with 20µg of proteinase K (Promega) for 1 hr at 42˚C. RNA was extracted with acid phenol/chloroform and precipitated with sodium acetate. Precipitated RNA was resuspended in RNAse-free water and treated with Turbo DNase (Ambion) for 30 min at 37˚C. cDNA was synthesized using the SuperScript III First Strand kit (Invitrogen). To visualize Nsp1 protein, extracts and immunoprecipitates were run in an agarose gel as in (Warren et al., 2003).

F-actin cosedimentation assay. Larval body wall muscles were lysed in 50mM Tris-HCl (pH 7.4), 140mM NaCl, 0.1% Na-Deoxycholate, 1% Triton X-100 and protein inhibitor cocktail (Roche) at 4°C and were cleared by centrifugation at 100,000 g for 30 min. To the lysate 0.4mg/ml of G-actin from rabbit skeletal muscle was added. Actin was allowed to polymerize by the addition of 0.1mM ATP and 0.1mM β-mercaptoethanol, 1mM $MgCl_2$ for 30 min at room temperature and then centrifuged at 100,000 g for 30 min using a TLA100 rotor. The pellets and lysates were run in agarose gels as above.

Chapter VI

General Discussion

GENERAL DISCUSSION

FNI signaling and assembly of megaRNP granules

Secreted Wnts are important modulators of synapse development and plasticity (Speese and Budnik, 2007). At the larval NMJ, Wg released by the presynaptic motor neuron binds to the DFz2 receptor on the postsynaptic muscle and activates the Frizzled nuclear import (FNI) pathway. In this pathway, DFz2 receptors are internalized and trafficked toward the nucleus (Ataman et al., 2006a; Ataman et al., 2008). At the nuclear periphery, an 8 KDa cytoplasmic C-terminal tail of DFz2 (DFz2C) is cleaved and the DFz2C fragment is imported into the nucleus (Mathew et al., 2005). Within the nucleus, DFz2C fragments form prominent foci associated with the nuclear envelope and surrounded by a Lamin C (A-type lamin) framework. These DFz2C granules associate with poly (A)-binding protein 2 (PABP2/PABPN1; a nuclear poly (A) binding protein required for mRNA maturation) and contain poly-A RNA as evidenced by an oligo-dT in-situ hybridization.

Ultrastructural analysis of these foci reveal that the DFz2C foci are composed of electron dense granules that are ~200 nm in size and accumulate in the perinuclear space. Wnt signaling and increased activity induces the assembly of these DFz2C foci-associated with RNPs in the nucleus (Ataman et al., 2008; Speese et al., 2012). We have yet to identify another signaling pathway that triggers their assembly. Furthermore the role of DFz2C once the granules exit the nucleus, remains to be investigated. The C-terminal region of DFz2 has a

PDZ binding motif that is recognized by PDZ domains (Ataman et al., 2006a). Interestingly, many proteins that form the postsynaptic density have PDZ domains. An intriguing possibility is that the PDZ motif can function as a “zip code” to target transcripts back to synaptic sites. A potential experiment to test the nuclear role of DFz2C would be to tag DFz2 after the cleavage site with a photo-convertible fluorescent protein like Dendra (Gurskaya et al., 2006). DFz2C-Dendra, once present in the nucleus can be photo-converted at 405nm from green to red. This would allow one to follow the fate or localization of nuclear DFz2C. However, a challenge in this experiment is to tag this small 8kDa C-terminus of DFz2C with a fluorescent tag like Dendra (26kDa) at a site such that DFz2C remains functional.

Composition of RNP granules and specificity of transcripts

Using a candidate approach we found that transcripts encoding proteins that play a role in the development of the postsynaptic region are enriched in the perinuclear granules. One such mRNA is *par6.* LamC mutants that fail to assemble granules, also demonstrate a failure to recruit Par6 at the postsynaptic region thus suggesting that these transcripts are targeted to the synapse for local translation. Some outstanding questions are: (1) Is there a specific signature in terms of RNA sequence, structure or function in transcripts that exit via this pathway? Recent studies in the lab also indicate that besides synaptic transcripts, some nuclear-encoded mitochondrial transcripts are also present in

these large RNP granules at the *Drosophila* NMJ (Li Y et al., Manuscript in preparation). However the complete repertoire of transcripts is unknown. (2) Is this pathway upregulated under circumstances wherein a bolus of transcripts is required to be delivered rapidly into the cytoplasm? This explanation seems plausible since in the *Drosophila* ovary, the function of the nurse cell nuclei is to pump RNAs in the developing oocyte. In the case of the NMJ, locomotion is main function of the expanding NMJ, and thus mitochondrial and synaptic transcripts are required in abundance. (3) Is each individual granule composed of a single RNA species or multiple species of mRNA? And do they travel as a "care-package" wherein all the transcripts required for the maturation of the synapse are packaged in one granule and delivered to the synapse? Based on our candidate screen, preliminary studies hint that these granules contain single species of mRNA. A possible advantage of having bulk transport of single species of mRNA is that it allows transport of many transcripts simultaneously and could be kinetically or energetically more efficient.

Some of these questions may be addressable by high-throughput analysis to identify the complete set of transcripts and their signature sequences (deep-sequencing and bioinformatic analysis) and RNA binding proteins (mass-spectrometry) present in these granules. Other will require in-situ analysis via multicolor imaging or live imaging of megaRNP specific transcripts to study the kinetics of megaRNP export.

RNP granule assembly at the nuclear envelope

In our model, we demonstrate that RNP granules are assembled within the nucleus. However we know little about how and where in the nucleus these RNPs assemble. At ultrastructural level, we rarely find these granules “naked” in the nucleus i.e., without the nuclear envelope wrapped around it. This suggests that megaRNPs likely assemble at the nuclear envelope. Is there a specific receptor or docking protein that targets the megaRNPs? How is membrane curvature mediated? One hypothesis for a possible mechanism is that an adaptor or receptor protein at INM signals RNA accumulation and specialized INM proteins may mediate membrane curvature. Second, these mRNAs may be translated close to INM and push through the INM as they accumulate. A genome-wide screen in S2 cells to identify molecular players that mediate a role in megaRNP assembly in the earlier stages may help address these questions. Studies from other labs suggest that RNP granules exist in a “hydrogel-like” state (Kato et al., 2012). Thus it is a possibility that specialized “pockets” are formed at the INM, after local dissolution of LamC that would allow the hydrogel-like RNPs to push through the INM.

Why assemble large RNP granules in the nucleus?

We know little about the RNP granules once they get across the INM or the fate of these granules once they enter the cytoplasm. Do these megaRNPs remain intact till they are transported to their destination or are they disassembled in the

cytoplasm? If the granules disperse in the cytoplasm, then why are they assembled in the first place? It is possible that bulk export via budding could have potential advantages in terms of kinetics of export or have a single export signal to transport multiple RNAs contrary to the NPC. However, the fact that we are able to capture these granules at ultrastructural levels in the nucleus suggests that kinetics of budding is not rapid. An alternative possibility is that megaRNPs transcribed and stored in the nucleus in these large granules, awaiting a second signal for nuclear export. In the case of the dystrophin gene (2600kbp), transcription takes 16 hrs; hence it is believed that the dystrophin mRNA is transcribed and stored in the nucleus before it is exported (Tennyson N et al., 1995). Thus, similarly, megaRNPs may serve to store mRNPs, which are subsequently exported into the cytoplasm where they disperse and are transported to synaptic sites.

Perinuclear granules in Literature

Through an extensive literature survey, we have found that perinuclear granules resembling megaRNPs have been identified in many species and also in different cell types. Granules have been observed in yeast (Wente and Blobel, 1993), rat oocytes (Szollosi, 1965), mouse oocytes (Szollosi and Szollosi, 1988), human oocytes (Tesarík J, 1988) and even in plants (Dickinson, 1971). Some of the early studies even suggested that perinuclear granules may be indicative of another mode of nucleocytoplasmic communication (Dickinson, 1971). However,

due to a lack of any light microscopy markers or methods to stimulate or induce the formation of these foci, they remained descriptive observations and their biological role wasn't studied further. Thus large perinuclear granules resembling megaRNPs are likely to be present in different tissue-types and organisms mediating different biological processes.

Nuclear Envelope Budding and Herpes Virus Egress

Our studies at the neuromuscular junction indicate that large RNPs exit the nucleus via budding through the nuclear envelope, a mechanism resembling the egress of Herpes viruses. This is due to the fact that like viral capsids, these RNPs are too large to exit the nucleus via a canonical NPC where the cut-off is ~40nm. Previously, this pathway was thought to be mediated by viral proteins and unique to the viruses (Roller, 2008). We now know that like the virion capsids, the large RNP granules assembled in the nucleus need to phosphorylate with aPKC and locally breakdown the lamina by recruiting the protein kinase aPKC to gain access to the INM. There are however instances where, large RNP complexes like the Balbiani mRNP can disassemble and thread out of the NPC (Zhao J, 2002) and NPC can also dilate 50nm (Solmaz SR, 2013). These mechanisms appear to be distinct from nuclear envelope budding since there is no involvement of nuclear membranes in these processes.

Figure 6.1: Model of FNI pathway and budding of megaRNP granules (Image courtesy: Vivian Budnik)

A model depicting release of Wg by the presynaptic motor neuron. The Wg then binds to DFz2 receptor on the muscle surface. This receptor gets internalized, and targeted towards the nucleus. A C-terminal fragment of the receptor is cleaved and imported in the nucleus. (Inset) In the nucleus DFz2C associates with large assembled RNPs, which exit the nucleus by budding through the nuclear envelope, a process that requires aPKC to locally break-down the LamC network. These mRNA granules are transported back to the synapse where they function in maturation of newly formed synaptic boutons.

Figure 6.1: Model of FNI pathway and budding of megaRNP granules

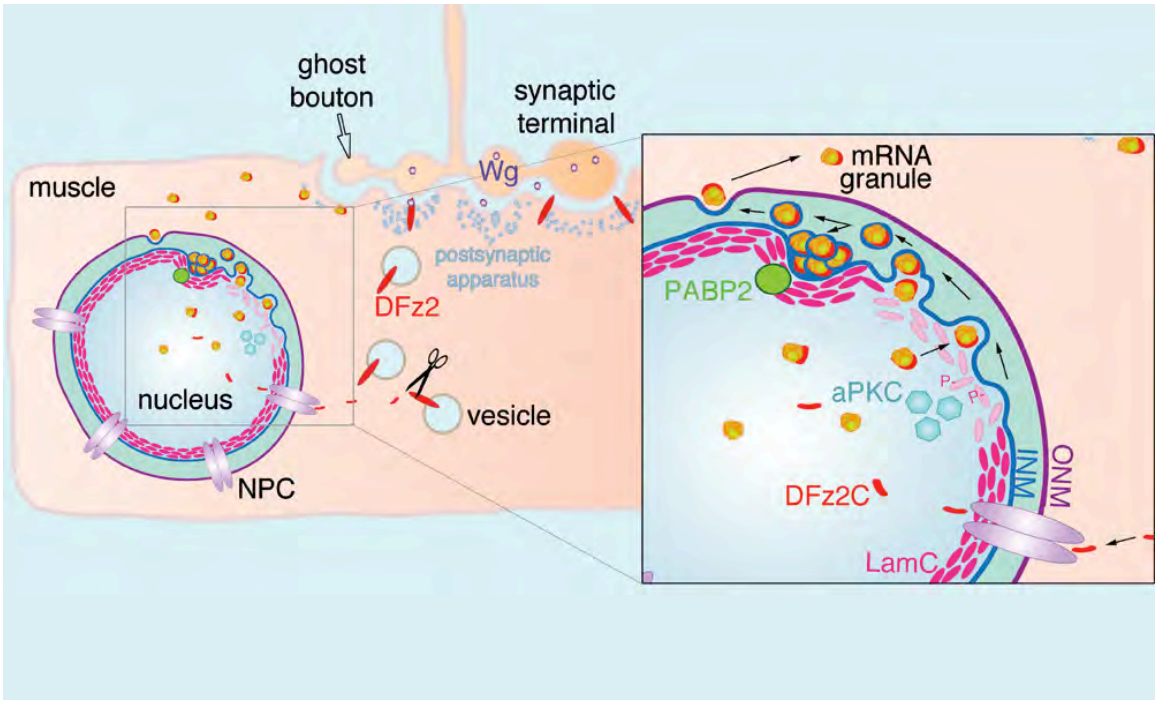

Role of Torsin in Nuclear envelope budding

Once the megaRNPs disassemble the Lamin framework, and have access to the INM, they undergo primary envelopment, followed by scission of INM. The membrane surrounded vesicular RNP then fuses with the ONM to release the RNP.

To understand the molecular players involved in the budding pathway, we started a pilot screen in S2 cells. Since S2 cells have both, a basal level of FNI signaling and megaRNP granules, they should likely thus have the molecular machinery to mediate nuclear budding. Candidates were selected for this screen based on their ability to remodel the membranes, their function in RNA export or the cellular location. Loss of one such protein, Torsin was previously linked to nuclear envelope integrity (Goodchild et al., 2005, Kim et al., 2010) and thus an important candidate in our pilot screen.

Upon knockdown of Torsin in S2 cells, DFz2C associated with megaRNPs displayed altered localization. Instead of forming prominent foci surrounded by a LamC framework, DF2C speckles appeared as small puncta that were juxtaposed to LamC. This was also observed upon the knockdown of Torsin in the larval muscles. Ultrastructural analysis revealed that these granules appeared “stuck” at the INM via a collared neck. Further EM analysis revealed that Torsin accumulates at the neck and thus could likely mediate scission at the INM after the primary envelopment process. Torsin being a AAA-ATPase, and its previously characterized role in NE integrity therefore indicates that it has the

potential to remodel membranes. AAA-ATPases adopt either spiral or ring conformations and use the energy from ATP hydrolysis to disassemble their target complex (Erberger and Berger, 2006). Similar to other ring-conformation AAA-ATPases, like NSF (disassembles SNARE complexes during vesicle recycling) and Vps4 (disassembles the ESCRT-III complex during mutivesicular body biogenesis) (White and Lauring, 2007); Torsin may provide the motive force to mediate the disruption of a yet-unknown scission complex. If Torsin adopts a spiral conformation, it could likely wrap around the INM and itself mediate scission. This can be addressed by studies that entail a detailed understanding of Torsin targets at the INM and its structure.

Consequence of loss of functional Torsin

Our studies show that synapse-specific transcripts packaged in megaRNPs fail to localize to their target synaptic sites where they are normally enriched upon knockdown of Torsin. As a consequence of this, synapses fail to mature. This study could provide an explanation of how a perinuclear protein affects synaptic development. Human patients (as well as mouse models) of dystonia have altered dopamine neurotransmission (Balcioglu et al., 2007; Hewett et al., 2010). It would therefore be interesting to examine if loss of Torsin in these murine models leads to mislocalization or nuclear accumulation of specific transcripts involved in dopamine metabolism. Such a study could further our understanding of the etiology of the disease and provide a link between the

nuclear phenotype observed and dopamine regulation.

Other “stuck” granules

The *C.elegans* Torsin ortholog, *ooc-5* mutants have abnormal nuclear envelope evaginations and deficits in nuclear pore insertion (VanGompel et al., 2015) but do not display RNPs trapped at the INM. Although they did not test with oligo-(dT) in-situ or regressive EDTA for electron microscopy to determine if RNPs are affected. In our studies at the *Drosophila* NMJ, NPCs and nuclear envelope appear to be intact (Figure 3.3) upon knockdown of Torsin.

Little is known about the mechanisms underlying new NPC insertion. During cell division there is a breakdown of the nuclear envelope, which is reassembled post-mitosis and studies reveal that the endoplasmic reticulum plays a role in NPC reassembly (Hetzer and Wente, 2009; Schooley et al., 2012). Recent studies are uncovering mechanisms underlying new NPC insertion in post-mitotic nuclei (Field et al., 2014). In our studies at NMJ or the nurse cells, both represent post-mitotic nuclei, which would require new NPC insertion with increase in cell size. It is likely that, Torsin may also contribute to remodeling the nuclear membrane during new NPC insertion. It will be essential to undertake further studies to understand and distinguish the contribution of the two pathways in RNA export. Furthermore, there is likelihood that vast accumulations of megaRNPs in the nuclear membrane could block sites for NPC insertion.

Another study in yeast found that an accumulation of perinuclear granules (that appear similar to the “stuck” granule phenotype in Torsin mutants), may represent a nuclear compartmentalization site for storage of improperly assembled or malformed nuclear pores (Webster et al., 2014). Recent studies in our lab (in collaboration with Mary Munson’s lab) demonstrate that this subset of perinuclear granules is most likely distinct from megaRNP granules (Ding et al., unpublished results) although at ultrastructural level they may appear morphologically similar. Future studies will involve careful analysis to distinguish RNPs and other perinuclear granule-like accumulations to classify and distinctly characterize the different types of granules seen at the nuclear envelope.

Nuclear Pore vs Budding

While RNA export through the NPC has been extensively studied, we are only beginning to learn more about nuclear envelope budding. Do distinct sets of transcripts utilize this pathway for their export or is there an overlap? Does this pathway function during high energy or demand conditions that require to rapid delivery of large amounts of mRNAs? Do these pathways compensate for each other? While there is selection of mature transcripts at the NPC, how is this selection mediated in the budding pathway? A preliminary study in our lab indicates that blocking canonical NPC-mediated RNP export may lead to an increased export via budding (Ding et al., unpublished results).

Quality control of megaRNP specific transcripts

Export of mRNPs through the NPC requires surveillance for quality checks of mRNPs before they are exported into the cytoplasm (Kohler and Hurt, 2007; Grunwald et al., 2011). This involves RBPs and NUPs in NPC mediated RNP export. What is the mechanism underlying quality checks in the case of budding? Studies indicate that a group of NUPs can function as a permeability barrier independent of the NPC at the cilia to mediate ciliary transport (Kee et al., 2012; Schmidt and Gorlich, 2015). These NUPs allow for selective RNP export in the cilia. This raises questions if individual nuclear NUPs could act as a sieve to select for mature RNAs that are exported by budding to maintain a quality control check of transcripts that exit via budding. In our studies, while we used RNA dyes (Speese et al., 2012), we did not perform live imaging of a megaRNP granules export. As in the study of nuclear export of β-actin mRNA (Grunwald and Singer, 2010), performing high resolution live imaging of a megaRNP-specific transcript, along with co-labeling individual NUPs, can answer some of these questions. These studies would also allow comparisons of the rate of RNP export and efficiency of the budding and NPC pathways.

Figure 6.2- Model demonstrating how nuclear Torsin affects synapse development (Figure courtesy: Vivian Budnik)

(left) megaRNPs that assemble in the nucleus exit the nucleus via nuclear envelope budding. Torsin mediates INM scission and the RNPs are targeted to synaptic sites where they are locally translated leading to synapse maturation. (right) In the absence of torsin (top), or in the presence of mutant torsin (bottom), these RNPs accumulate at the INM, thus fail to reach they synaptic sites where they are normally localized, resulting in an abnormal post-synapse.

Figure 6.2- Model demonstrating how nuclear Torsin affects synapse development

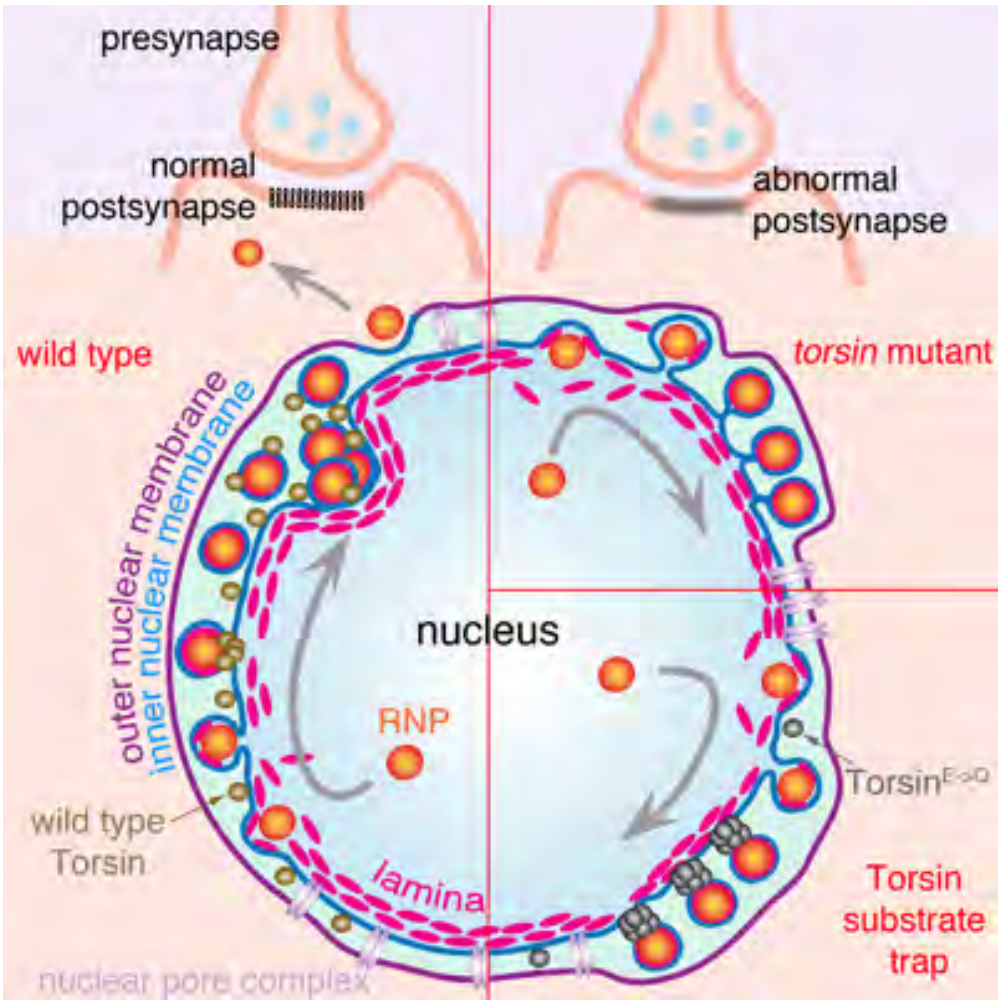

The Drosophila ovary as a model system to study megaRNP budding

We now know that megaRNP budding is a more generalized mechanism for RNP export and nurse cell nuclei of *Drosophila* ovary have megaRNP granules. Disruption of this pathway causes severe defects in germline development and females are rendered sterile. This suggests that besides the NMJ, other tissue types also use this pathway, which may serve as an efficient mechanism for RNA export.

The *Drosophila* ovary is a powerful system to study nuclear envelope budding. A number of RBPs such as Staufen, Syncrip, SMN, FMR are common between the germline and neurons and thus can provide valuable information about proteins associated with neuronal granules (Martin and Ephrussi, 2009). Studies also indicate that the RNPs for localized transcripts are assembled in the nucleus (Besse and Ephrussi, 2008). However, there is very little known about how these RNPs export the nurse cell nuclei. The abundance of megaRNPs in this system along with the ease to perform biochemical analysis means that Drosophila ovaries can provide valuable information to elucidate the next steps in the budding pathway, identify proteins and mRNA that export via budding. The Drosophila ovary could be used as a screening system to identify other molecular players in budding process; like how the RNPs exit the ONM, is there a receptor-like molecule at the INM that triggers RNP accumulation. It is likely that these molecular players are conserved in neuronal tissue and these findings could potentially be relevant to understanding neuronal RNA granules.

Nesprin1 filament localization

The cytoskeleton and associated proteins play critical roles in RNP localization. However, little is known about how RNPs are targeted from the nucleus to “specific” synaptic sites that are undergoing dynamic changes. Nesprin1 is a giant transmembrane protein present at the outer nuclear membrane and belonging to the spectrin superfamily of proteins. We found that Nsp1 forms striated F-actin-based filaments that span all the way from the nucleus to the NMJ. Upon detailed observation, we found that interestingly these tracks wrap specifically around immature boutons that lack post-synaptic specializations. This wrapping was independent of the transmembrane domain of Nsp1 since *nsp1*$^{\Delta KASH}$ mutants also enwrap immature boutons. Thus Nsp1 is the identified first postsynaptic marker for ghost boutons.

Nesprin1 tracks and RNA targeting

We hypothesized that these F-actin-Nsp1 “rail-road tracks” could serve as a pathway for long-distance communication between the nucleus and the NMJ. In the absence of Nsp1, mRNAs that normally localize at postsynaptic sites are missing and instead they now accumulate around the nucleus. Thus suggesting that the railroad tracks serve to direct the RNA to new synaptic sites. As a consequence of this, the NMJs do not expand normally and have fewer synaptic boutons. This indicates that Nsp1 railroad tracks likely serve as a path to target specific RNAs from the nucleus to postsynaptic sites. In the absence of these

tracks, the RNAs fail to localize to the postsynaptic region, resulting in an accumulation of immature boutons lacking postsynaptic proteins. We also found that the Nsp1 railroad track association with immature boutons depended upon an unconventional myosin, Myo1D, which is an actin motor protein.

How do RNAs walk along Nsp1 railroad tracks?

While our studies suggest an important mechanism by which dNsp1 railroad tracks, which serve as a long-range pathway for mRNA localization and synapse maturation, certain questions need further investigation. How is polarity established along Nsp1-Actin tracks? Do these tracks serve as a path for retrograde signaling too, as in the case of microtubules? What are the long-range processive motor proteins that are involved in trafficking along Nsp1-Actin tracks? What signals target Myo1D and Nsp1 to ghost boutons?

Very little is known about the role of actin in long-range RNP transport. An alternative hypothesis could be that Nesprin-actin rail-road tracks mark sites for synaptic maturation and serve to trap or enrich synaptic RNA.

Trafficking of RNAs to synaptic sites is an important step for achieving synaptic plasticity. This is of significant importance since Nsp1 is associated with a variety of musculoskeletal disorders, such as X-linked Emery-Dreifuss Muscular Dystrophy (EDMD), movement disorders such as autosomal recessive cerebellar ataxia type 1 (ARCA1), bipolar disorder, and it is a risk gene for schizophrenia and autism.

Figure 6.3- Model demonstrating how nuclear Nesprin-1 affects synapse maturation and growth

(Left) In wild-type animals, as synapses develop and there is new bouton formation, where the presynaptic motor neuron form new synaptic boutons (red). At this point these immature boutons lack any post-synaptic specialization (purple). Nsp-1 railroad tracks (green) extend from the nucleus all the way to synaptic sites and specifically wrap around these immature boutons. These tracks serve as long-range communication from the nucleus to the synapse and paths for trafficking megaRNPs to specific synaptic sites. These transcripts are locally translated which then lead to mature bouton formation (Left bottom). (Right) In Nsp-1 mutants, due to the absence of these railroad tracks, mega-RNPs accumulate around the nucleus and fail to reach synaptic sites where they are normally localized; leading to an accumulation of ghost boutons and poor synaptic development (right bottom).

Figure 6.3- Model demonstrating how nuclear Nesprin-1 affects synapse maturation and growth

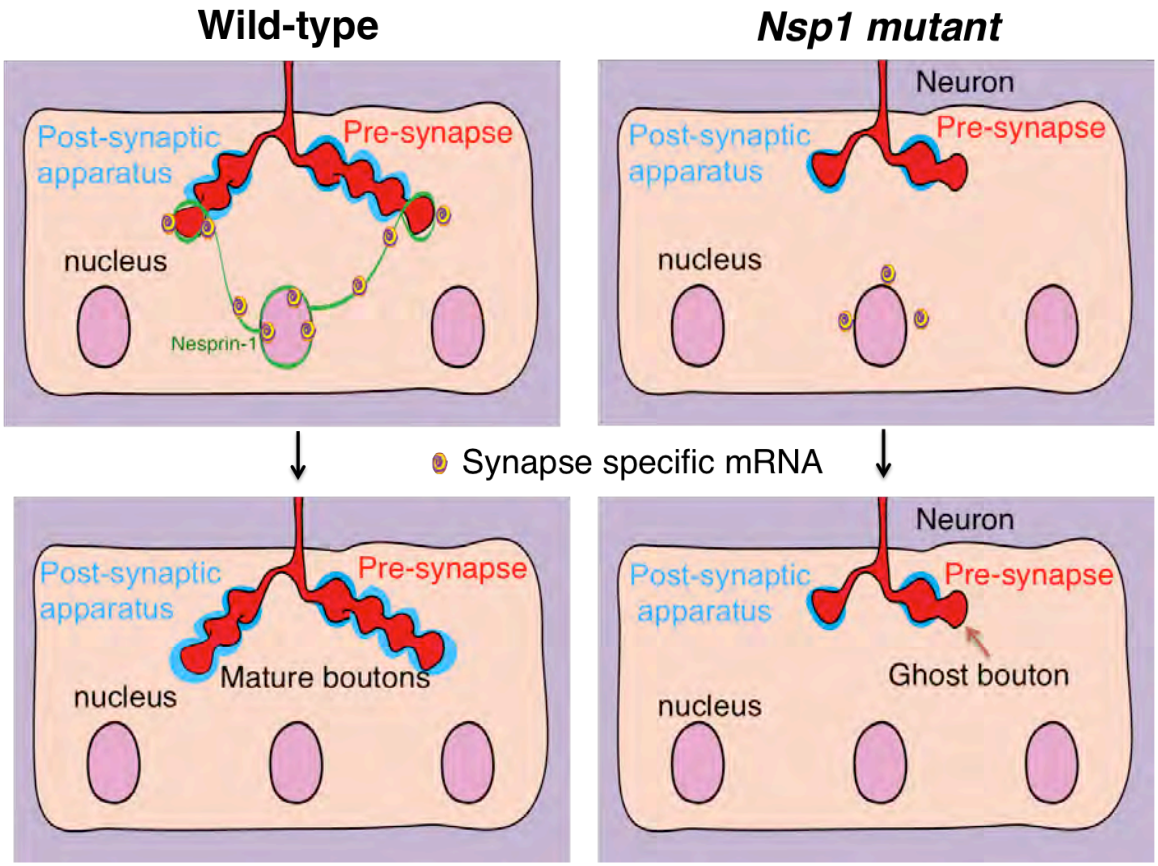

RNP granule export and transport in development and diseases.

LamC is essential for megaRNP assembly. Mutations in LamC have been implicated in muscular dystrophies (Burke and Stewart, 2002). These mutants affect skeletal muscle and studies reveal that skeletal defects appear long before signs of neurodegeneration (Mejat et al., 2009). In addition, Torsin has been implicated in early onset dystonia; a movement disorder characterized by involuntary and sustained muscle contractions (Robottom et al., 2011) and is essential for megaRNP export. Taken together, our studies provide mechanistic insights into how nuclear proteins affect synapse development.

A large number of neurological disorders are linked to RNA binding proteins (e.g. Fragile X syndrome FMR1) (Mazroui et al., 2002), or RNP granule assembly, (e.g. FUS whose mutation underlies Amyotrophic lateral sclerosis) (Bosco et al., 2010). Thus, RNP granule studies could provide a better understanding of molecular mechanisms underlying neurodegeneration and neuropsychiatric disorders.

FINAL CONCLUSION

In summary, the studies detailed in this dissertation have addressed fundamental questions regarding the mechanisms of RNP granule export and transport during synapse development and plasticity. This thesis has focused on the identification of a) a novel RNP export pathway, b) a prominent protein Torsin, implicated in early-onset dystonia involved in export of synaptic transcripts in this pathway of RNP granule egress from the nucleus and c) Nsp1-Actin tracks that serve as a mode of nucleo-synaptic communication to target synaptic RNA. These studies reveal the importance of localized RNAs in synaptic development and plasticity. Further elucidation of these basic cell biological pathways in model organisms like *Drosophila* can facilitate a better understanding of complex processes occurring in the brain as well as provide insights in the processes that go awry in neurological diseases.

REFERENCES

Ainger, K., Avossa, D., Morgan, F., Hill, S.J., Barry, C., Barbarese, E., and Carson, J.H. (1993). Transport and localization of exogenous myelin basic protein mRNA microinjected into oligodendrocytes. J Cell Biol *123*, 431-441.

Apel, E.D., Lewis, R.M., Grady, R.M., and Sanes, J.R. (2000). Syne-1, a dystrophin- and Klarsicht-related protein associated with synaptic nuclei at the neuromuscular junction. J Biol Chem *275*, 31986-31995.

Aris, J.P., and Blobel, G. (1989). Yeast nuclear envelope proteins cross react with an antibody against mammalian pore complex proteins. J Cell Biol *108*, 2059-2067.

Ashley, J., Packard, M., Ataman, B., and Budnik, V. (2005). Fasciclin II signals new synapse formation through amyloid precursor protein and the scaffolding protein dX11/Mint. J Neurosci *25*, 5943-5955.

Ataman, B., Ashley, J., Gorczyca, D., Gorczyca, M., Mathew, D., Wichmann, C., Sigrist, S.J., and Budnik, V. (2006a). Nuclear trafficking of Drosophila Frizzled-2 during synapse development requires the PDZ protein dGRIP. Proceedings of the National Academy of Sciences of the United States of America *103*, 7841-7846.

Ataman, B., Ashley, J., Gorczyca, M., Ramachandran, P., Fouquet, W., Sigrist, S.J., and Budnik, V. (2008). Rapid activity-dependent modifications in synaptic structure and function require bidirectional Wnt signaling. Neuron *57*, 705-718.

Ataman, B., Budnik, V., and Thomas, U. (2006b). Scaffolding Proteins at the Drosophila Neuromuscular Junction. *75*, 181-216.

Bahler, M., Kroschewski, R., Stoffler, H.E., and Behrmann, T. (1994). Rat myr 4 defines a novel subclass of myosin I: identification, distribution, localization, and mapping of calmodulin-binding sites with differential calcium sensitivity. J Cell Biol *126*, 375-389.

Balcioglu, A., Kim, M.O., Sharma, N., Cha, J.H., Breakefield, X.O., and Standaert, D.G. (2007). Dopamine release is impaired in a mouse model of DYT1 dystonia. J Neurochem *102*, 783-788.

Barco, A., Lopez de Armentia, M., and Alarcon, J.M. (2008). Synapse-specific stabilization of plasticity processes: the synaptic tagging and capture hypothesis revisited 10 years later. Neurosci Biobehav Rev *32*, 831-851.

Becalska, A.N., and Gavis, E.R. (2009). Lighting up mRNA localization in Drosophila oogenesis. Development *136*, 2493-2503.

Benesh, A.E., Fleming, J.T., Chiang, C., Carter, B.D., and Tyska, M.J. (2012). Expression and localization of myosin-1d in the developing nervous system. Brain Res *1440:9-22.*, 10.1016/j.brainres.2011.1012.1054. Epub 2012 Jan 1018.

Benoit, B., Nemeth, A., Aulner, N., Kuhn, U., Simonelig, M., Wahle, E., and Bourbon, H.M. (1999). The Drosophila poly(A)-binding protein II is ubiquitous throughout Drosophila development and has the same function in mRNA polyadenylation as its bovine homolog in vitro. Nucleic Acids Res *27*, 3771-3778.

Berg, C.A. (2005). The Drosophila shell game: patterning genes and morphological change. Trends Genet *21*, 346-355.

Berlucchi, G., and Buchtel, H.A. (2009). Neuronal plasticity: historical roots and evolution of meaning. Exp Brain Res *192*, 307-319.

Bernhard, W. (1969). A new staining procedure for electron microscopical cytology. J Ultrastruct Res *27*, 250-265.

Besse, F., and Ephrussi, A. (2008). Translational control of localized mRNAs: restricting protein synthesis in space and time. Nat Rev Mol Cell Biol *9*, 971-980.

Betschinger, J., Mechtler, K., and Knoblich, J.A. (2003). The Par complex directs asymmetric cell division by phosphorylating the cytoskeletal protein Lgl. Nature *422*, 326-330.

Bione, S., Maestrini, E., Rivella, S., Mancini, M., Regis, S., Romeo, G., and Toniolo, D. (1994). Identification of a novel X-linked gene responsible for Emery-Dreifuss muscular dystrophy. Nat Genet *8*, 323-327.

Bischof, J., Maeda, R.K., Hediger, M., Karch, F., and Basler, K. (2007). An optimized transgenesis system for Drosophila using germ-line-specific phiC31 integrases. Proc Natl Acad Sci U S A *104*, 3312-3317.

Bjerke, S.L., and Roller, R.J. (2006). Roles for herpes simplex virus type 1 UL34 and US3 proteins in disrupting the nuclear lamina during herpes simplex virus type 1 egress. Virology *347*, 261-276.

Bliss, T.V., and Lomo, T. (1973). Long-lasting potentiation of synaptic transmission in the dentate area of the anaesthetized rabbit following stimulation of the perforant path. J Physiol *232*, 331-356.

Bosco, D.A., Lemay, N., Ko, H.K., Zhou, H., Burke, C., Kwiatkowski, T.J., Jr., Sapp, P., McKenna-Yasek, D., Brown, R.H., Jr., and Hayward, L.J. (2010). Mutant FUS proteins that cause amyotrophic lateral sclerosis incorporate into stress granules. Hum Mol Genet *19*, 4160-4175.

Bramham, C.R., and Wells, D.G. (2007). Dendritic mRNA: transport, translation and function. Nat Rev Neurosci *8*, 776-789.

Brand, A.H., and Perrimon, N. (1993). Targeted gene expression as a means of altering cell fates and generating dominant phenotypes. Development *118*, 401-415.

Breakefield, X.O., Blood, A.J., Li, Y., Hallett, M., Hanson, P.I., and Standaert, D.G. (2008). The pathophysiological basis of dystonias. Nat Rev Neurosci *9*, 222-234.

Breakefield, X.O., Kamm, C., and Hanson, P.I. (2001). TorsinA: movement at many levels. Neuron *31*, 9-12.

Brown, R.E., and Milner, P.M. (2003). The legacy of Donald O. Hebb: more than the Hebb synapse. Nat Rev Neurosci *4*, 1013-1019.

Budnik, V., Koh, Y.H., Guan, B., Hartmann, B., Hough, C., Woods, D., and Gorczyca, M. (1996). Regulation of synapse structure and function by the Drosophila tumor suppressor gene dlg. Neuron *17*, 627-640.

Budnik, V., and Salinas, P.C. (2011). Wnt signaling during synaptic development and plasticity. Curr Opin Neurobiol *21*, 151-159.

Burke, B., and Stewart, C.L. (2002). Life at the edge: the nuclear envelope and human disease. Nat Rev Mol Cell Biol *3*, 575-585.

Buser, C., Walther, P., Mertens, T., and Michel, D. (2007). Cytomegalovirus primary envelopment occurs at large infoldings of the inner nuclear membrane. J Virol *81*, 3042-3048.

Buszczak, M., Paterno, S., Lighthouse, D., Bachman, J., Planck, J., Owen, S., Skora, A.D., Nystul, T.G., Ohlstein, B., Allen, A.*, et al.* (2007). The carnegie protein trap library: a versatile tool for Drosophila developmental studies. Genetics *175*, 1505-1531.

Buxbaum, A.R., Haimovich, G., and Singer, R.H. (2015). In the right place at the right time: visualizing and understanding mRNA localization. Nat Rev Mol Cell Biol *16*, 95-109.

Cajal, R.y. (1904). The structure and connexions of neurons. Nobel Lecture.

Cao, S., Gelwix, C.C., Caldwell, K.A., and Caldwell, G.A. (2005). Torsin-mediated protection from cellular stress in the dopaminergic neurons of Caenorhabditis elegans. J Neurosci *25*, 3801-3812.

Caricasole, A., Bakker, A., Copani, A., Nicoletti, F., Gaviraghi, G., and Terstappen, G.C. (2005). Two sides of the same coin: Wnt signaling in neurodegeneration and neuro-oncology. Biosci Rep *25*, 309-327.

Cartwright, S., and Karakesisoglou, I. (2013). Nesprins in health and disease. Semin Cell Dev Biol *25*, 00139-00130.

Cerpa, W., Gambrill, A., Inestrosa, N.C., and Barria, A. (2011). Regulation of NMDA-receptor synaptic transmission by Wnt signaling. J Neurosci *31*, 9466-9471.

Chou TB, P.N. (1993). Autosomal P[ovoD1] dominant female-sterile insertions in Drosophila and their use in generating germ-line chimeras. Development *119*, 1359-1369.

Chou TB, P.N. (1996). The autosomal FLP-DFS technique for generating germline mosaics in Drosophila melanogaster. Genetics *144*, 1673-1679.

Ciani, L., Krylova, O., Smalley, M.J., Dale, T.C., and Salinas, P.C. (2004). A divergent canonical WNT-signaling pathway regulates microtubule dynamics: dishevelled signals locally to stabilize microtubules. J Cell Biol *164*, 243-253.

Clevers, H., and Nusse, R. (2012). Wnt/beta-catenin signaling and disease. Cell *149*, 1192-1205.

Cottrell, J.R., Borok, E., Horvath, T.L., and Nedivi, E. (2004). CPG2: a brain- and synapse-specific protein that regulates the endocytosis of glutamate receptors. Neuron *44*, 677-690.

Darlington, R.W., and Moss, L.H., 3rd (1968). Herpesvirus envelopment. J Virol *2*, 48-55.

Davis, L.I., and Blobel, G. (1986). Identification and characterization of a nuclear pore complex protein. Cell *45*, 699-709.

De Ferrari, G.V., and Moon, R.T. (2006). The ups and downs of Wnt signaling in prevalent neurological disorders. Oncogene *25*, 7545-7553.

DeFelipe, J. (2002). Sesquicentenary of the birthday of Santiago Ramón y Cajal, the father of modern neuroscience. Trends Neurosci *25*, 482-485

.

Dickinson, H.G. (1971). Nucleo-Cytoplasmic Interaction following Meiosis in the Young Microspores of Lilium Longiflorum; Events at the Nuclear Envelope. Grana *11*, 2, 117-127.

Dietzl, G., Chen, D., Schnorrer, F., Su, K.C., Barinova, Y., Fellner, M., Gasser, B., Kinsey, K., Oppel, S., Scheiblauer, S.*, et al.* (2007). A genome-wide transgenic RNAi library for conditional gene inactivation in Drosophila. Nature *448*, 151-156.

Ding, B., Wang, W., Selvakumar, T., Xi, H.S., Zhu, H., Chow, C.W., Horton, J.D., Gronostajski, R.M., and Kilpatrick, D.L. (2013). Temporal regulation of nuclear factor one occupancy by calcineurin/NFAT governs a voltage-sensitive developmental switch in late maturing neurons. J Neurosci *33*, 2860-2872. doi: 2810.1523/JNEUROSCI.3533-2812.2013.

Drier, E.A., Tello, M.K., Cowan, M., Wu, P., Blace, N., Sacktor, T.C., and Yin, J.C. (2002). Memory enhancement and formation by atypical PKM activity in Drosophila melanogaster. Nat Neurosci *5*, 316-324.

Dudek, S.M., and Bear, M.F. (1992). Homosynaptic long-term depression in area CA1 of hippocampus and effects of N-methyl-D-aspartate receptor blockade. Proc Natl Acad Sci U S A *89*, 4363-4367.

Elhanany-Tamir, H., Yu, Y.V., Shnayder, M., Jain, A., Welte, M., and Volk, T. (2012a). Organelle positioning in muscles requires cooperation between two KASH proteins and microtubules. J Cell Biol *198*, 833-846. doi: 810.1083/jcb.201204102. Epub 201202012 Aug 201204127.

Elhanany-Tamir, H., Yu, Y.V., Shnayder, M., Jain, A., Welte, M., and Volk, T. (2012b). Organelle positioning in muscles requires cooperation between two KASH proteins and microtubules. J Cell Biol *198*, 833-846.

Erberger, and Berger (2006). Evolutionary relationships and structural mechanisms of AAA+ proteins. Annu Rev Biophys Biomol Struct *35:93-114*.

Evangelista, M., Klebl, B.M., Tong, A.H., Webb, B.A., Leeuw, T., Leberer, E., Whiteway, M., Thomas, D.Y., and Boone, C. (2000). A role for myosin-I in actin assembly through interactions with Vrp1p, Bee1p, and the Arp2/3 complex. J Cell Biol *148*, 353-362.

Field, M.C., Koreny, L., and Rout, M.P. (2014). Enriching the pore: splendid complexity from humble origins. Traffic *15*, 141-156.

Friedrich, B.M., Buxboim, A., Discher, D.E., and Safran, S.A. (2011). Striated acto-myosin fibers can reorganize and register in response to elastic interactions with the matrix. Biophys J *100*, 2706-2715. doi: 2710.1016/j.bpj.2011.2704.2050.

Fujii, R., Okabe, S., Urushido, T., Inoue, K., Yoshimura, A., Tachibana, T., Nishikawa, T., Hicks, G.G., and Takumi, T. (2005). The RNA binding protein TLS is translocated to dendritic spines by mGluR5 activation and regulates spine morphology. Curr Biol *15*, 587-593.

Gagnon, J.A., and Mowry, K.L. (2011). Molecular motors: directing traffic during RNA localization. Crit Rev Biochem Mol Biol *46*, 229-239.

Gay, H. (1956). Nucleocytoplasmic relations in Drosophila. Cold Spring Harb Symp Quant Biol *21*, 257-269.

Gehrig, K., Cornell, R.B., and Ridgway, N.D. (2008). Expansion of the nucleoplasmic reticulum requires the coordinated activity of lamins and CTP:phosphocholine cytidylyltransferase alpha. Mol Biol Cell *19*, 237-247.

Gerber, A.P., Herschlag, D., and Brown, P.O. (2004). Extensive association of functionally and cytotopically related mRNAs with Puf family RNA-binding proteins in yeast. PLoS Biol *2*, E79.

Glotzer, J.B., Saffrich, R., Glotzer, M., and Ephrussi, A. (1997). Cytoplasmic flows localize injected oskar RNA in Drosophila oocytes. Curr Biol *7*, 326-337.

Goodchild, R.E., and Dauer, W.T. (2005). The AAA+ protein torsinA interacts with a conserved domain present in LAP1 and a novel ER protein. J Cell Biol *168*, 855-862.

Goodchild, R.E., Kim, C.E., and Dauer, W.T. (2005). Loss of the dystonia-associated protein torsinA selectively disrupts the neuronal nuclear envelope. Neuron *48*, 923-932.

Goodrich, J.S., Clouse, K.N., and Schupbach, T. (2004). Hrb27C, Sqd and Otu cooperatively regulate gurken RNA localization and mediate nurse cell chromosome dispersion in Drosophila oogenesis. Development *131*, 1949-1958.

Gorczyca, D., Ashley, J., Speese, S., Gherbesi, N., Thomas, U., Gundelfinger, E., Gramates, L.S., and Budnik, V. (2007). Postsynaptic membrane addition depends on the Discs-Large-interacting t-SNARE Gtaxin. J Neurosci *27*, 1033-1044.

Gorczyca, M., Augart, C., and Budnik, V. (1993). Insulin-like receptor and insulin-like peptide are localized at neuromuscular junctions in Drosophila. J Neurosci *13*, 3692-3704.

Grabham, P.W., and Goldberg, D.J. (1997). Nerve growth factor stimulates the accumulation of beta1 integrin at the tips of filopodia in the growth cones of sympathetic neurons. J Neurosci *17*, 5455-5465.

Granata, A., Watson, R., Collinson, L.M., Schiavo, G., and Warner, T.T. (2008). The dystonia-associated protein torsinA modulates synaptic vesicle recycling. The Journal of biological chemistry *283*, 7568-7579.

Granzow, H., Klupp, B.G., Fuchs, W., Veits, J., Osterrieder, N., and Mettenleiter, T.C. (2001). Egress of alphaherpesviruses: comparative ultrastructural study. J Virol *75*, 3675-3684.

Griffith, L.C., and Budnik, V. (2006). Plasticity and Second Messengers During Synapse Development. *75*, 237-265.

Gros-Louis, F., Dupre, N., Dion, P., Fox, M.A., Laurent, S., Verreault, S., Sanes, J.R., Bouchard, J.P., and Rouleau, G.A. (2007). Mutations in SYNE1 lead to a newly discovered form of autosomal recessive cerebellar ataxia. Nat Genet *39*, 80-85. Epub 2006 Dec 2010.

Grunwald, D., and Singer, R.H. (2010). In vivo imaging of labelled endogenous beta-actin mRNA during nucleocytoplasmic transport. Nature *467*, 604-607.

Grunwald, D., Singer, R.H., and Rout, M. (2011). Nuclear export dynamics of RNA-protein complexes. Nature *475*, 333-341.

Guan, B., Hartmann, B., Kho, Y.H., Gorczyca, M., and Budnik, V. (1996). The Drosophila tumor suppressor gene, dlg, is involved in structural plasticity at a glutamatergic synapse. Curr Biol *6*, 695-706.

Gurskaya, N.G., Verkhusha, V.V., Shcheglov, A.S., Staroverov, D.B., Chepurnykh, T.V., Fradkov, A.F., Lukyanov, S., and Lukyanov, K.A. (2006). Engineering of a monomeric green-to-red photoactivatable fluorescent protein induced by blue light. Nature biotechnology *24*, 461-465.

Haas, M., and Jost, E. (1993). Functional analysis of phosphorylation sites in human lamin A controlling lamin disassembly, nuclear transport and assembly. Eur J Cell Biol *62*, 237-247.

Hadek, R., and Swift, H. (1962). Nuclear extrusion and intracisternal inclusions in the rabbit blastocyst. J Cell Biol *13*, 445-451.

Hans, S., Freudenreich, D., Geffarth, M., Kaslin, J., Machate, A., and Brand, M. (2011). Generation of a non-leaky heat shock-inducible Cre line for conditional Cre/lox strategies in zebrafish. Dev Dyn *240*, 108-115.

Hanson, P.I., and Whiteheart, S.W. (2005). AAA+ proteins: have engine, will work. Nat Rev Mol Cell Biol *6*, 519-529.

Hebb, D. (1949). The Organization of Behavior- A neurophysiological Theory.

Herbert, J.M., Augereau, J.M., Gleye, J., and J.P., M. (1990). Chelerythrine is a potent and specific inhibitor of protein kinase C. Biochem Biophys Res Commun *172*, 993-999.

Hetzer, M.W., and Wente, S.R. (2009). Border control at the nucleus: biogenesis and organization of the nuclear membrane and pore complexes. Dev Cell *17*, 606-616.

Hewett, J., Johanson, P., Sharma, N., Standaert, D., and Balcioglu, A. (2010). Function of dopamine transporter is compromised in DYT1 transgenic animal model in vivo. J Neurochem *113*, 228-235.

Hewett, J., Ziefer, P., Bergeron, D., Naismith, T., Boston, H., Slater, D., Wilbur, J., Schuback, D., Kamm, C., Smith, N.*, et al.* (2003). TorsinA in PC12 cells: localization in the endoplasmic reticulum and response to stress. J Neurosci Res *72*, 158-168.

Hirokawa, N. (2006). mRNA transport in dendrites: RNA granules, motors, and tracks. J Neurosci *26*, 7139-7142.

Hochstrasser, M., and Sedat, J.W. (1987). Three-dimensional organization of Drosophila melanogaster interphase nuclei. II. Chromosome spatial organization and gene regulation. J Cell Biol *104*, 1471-1483.

Hodzic, D.M., Yeater, D.B., Bengtsson, L., Otto, H., and Stahl, P.D. (2004). Sun2 is a novel mammalian inner nuclear membrane protein. J Biol Chem *279*, 25805-25812.

Holt, C.E., and Schuman, E.M. (2013). The central dogma decentralized: new perspectives on RNA function and local translation in neurons. Neuron *80*, 648-657.

Huber, L.A., Fialka, I., Paiha, K., Hunziker, W., Sacks, D.B., Bahler, M., Way, M., Gagescu, R., and Gruenberg, J. (2000). Both calmodulin and the unconventional myosin Myr4 regulate membrane trafficking along the recycling pathway of MDCK cells. Traffic *1*, 494-503.

Iyer, L.M., Leipe, D.D., Koonin, E.V., and Aravind, L. (2004). Evolutionary history and higher order classification of AAA+ ATPases. J Struct Biol *146*, 11-31.

Jan, L.Y., and Jan, Y.N. (1976). L-glutamate as an excitatory transmitter at the Drosophila larval neuromuscular junction. J Physiol *262*, 215-236.

Jan, L.Y., and Jan, Y.N. (1982). Antibodies to horseradish peroxidase as specific neuronal markers in Drosophila and in grasshopper embryos. Proc Natl Acad Sci U S A *79*, 2700-2704.

Jia, X.X., Gorczyca, M., and Budnik, V. (1993). Ultrastructure of neuromuscular junctions in Drosophila: comparison of wild type and mutants with increased excitability. J Neurobiol *24*, 1025-1044.

Johnson, D.C., and Baines, J.D. (2011). Herpesviruses remodel host membranes for virus egress. Nat Rev Microbiol *9*, 382-394.

Jokhi, V., Ashley, J., Nunnari, J., Noma, A., Ito, N., Wakabayashi-Ito, N., Moore, M.J., and Budnik, V. (2013a). Torsin mediates primary envelopment of large ribonucleoprotein granules at the nuclear envelope. Cell Rep *3*, 988-995. doi: 910.1016/j.celrep.2013.1003.1015. Epub 2013 Apr 1011.

Jokhi, V., Ashley, J., Nunnari, J., Noma, A., Ito, N., Wakabayashi-Ito, N., Moore, M.J., and Budnik, V. (2013b). Torsin mediates primary envelopment of large ribonucleoprotein granules at the nuclear envelope. Cell Reports.

Kanai, Y., Dohmae, N., and Hirokawa, N. (2004). Kinesin transports RNA: isolation and characterization of an RNA-transporting granule. Neuron *43*, 513-525.

Kandel, E. (2001). The Molecular Biology of Memory Storage: A Dialogue Between Genes and Synapses. Science *294*, 1030-1038.

Kang, H., and Schuman, E.M. (1996). A requirement for local protein synthesis in neurotrophin-induced hippocampal synaptic plasticity. Science *273*, 1402-1406.

Kato, M., Han, T.W., Xie, S., Shi, K., Du, X., Wu, L.C., Mirzaei, H., Goldsmith, E.J., Longgood, J., Pei, J.*, et al.* (2012). Cell-free formation of RNA granules: low complexity sequence domains form dynamic fibers within hydrogels. Cell *149*, 753-767.

Kee, H.L., Dishinger, J.F., Blasius, T.L., Liu, C.J., Margolis, B., and Verhey, K.J. (2012). A size-exclusion permeability barrier and nucleoporins characterize a ciliary pore complex that regulates transport into cilia. Nat Cell Biol *14*, 431-437.

Keene, J.D., and Tenenbaum, S.A. (2002). Eukaryotic mRNPs may represent posttranscriptional operons. Mol Cell *9*, 1161-1167.

Kelso, R.J., Buszczak, M., Quinones, A.T., Castiblanco, C., Mazzalupo, S., and Cooley, L. (2004). Flytrap, a database documenting a GFP protein-trap insertion screen in Drosophila melanogaster. Nucleic Acids Res *32*, D418-420.

Keminer, O., and Peters, R. (1999). Permeability of single nuclear pores. Biophys J *77*, 217-228.

Kennedy, B.K., Barbie, D.A., Classon, M., Dyson, N., and Harlow, E. (2000). Nuclear organization of DNA replication in primary mammalian cells. Genes Dev *14*, 2855-2868.

Keshishian, H., and Chiba, A. (1993). Neuromuscular development in Drosophila: insights from single neurons and single genes. Trends Neurosci *16*, 278-283.

Kiebler, M.A., and Bassell, G.J. (2006). Neuronal RNA granules: movers and makers. Neuron *51*, 685-690.

Kim CE, P.A., Perkins G, Ellisman MH, Dauer WT. (2010). A molecular mechanism underlying the neural-specific defect in torsinA mutant mice. PNAS *107*, 9861-9866.

Kindler, S., Muller, R., Chung, W.J., and Garner, C.C. (1996). Molecular characterization of dendritically localized transcripts encoding MAP2. Brain Res Mol Brain Res *36*, 63-69.

Klann, E., and Dever, T.E. (2004). Biochemical mechanisms for translational regulation in synaptic plasticity. Nat Rev Neurosci *5*, 931-942.

Klupp, B.G., Granzow, H., Fuchs, W., Keil, G.M., Finke, S., and Mettenleiter, T.C. (2007). Vesicle formation from the nuclear membrane is induced by coexpression of two conserved herpesvirus proteins. Proc Natl Acad Sci U S A *104*, 7241-7246.

Knowles, R.B., Sabry, J.H., Martone, M.E., Deerinck, T.J., Ellisman, M.H., Bassell, G.J., and Kosik, K.S. (1996). Translocation of RNA granules in living neurons. J Neurosci *16*, 7812-7820.

Koh, Y.H., Popova, E., Thomas, U., Griffith, L.C., and Budnik, V. (1999). Regulation of DLG localization at synapses by CaMKII-dependent phosphorylation. Cell *98*, 353-363.

Kohler, A., and Hurt, E. (2007). Exporting RNA from the nucleus to the cytoplasm. Nat Rev Mol Cell Biol *8*, 761-773.

Koles, K., Nunnari, J., Korkut, C., Barria, R., Brewer, C., Li, Y., Leszyk, J., Zhang, B., and Budnik, V. (2012). Mechanism of evenness interrupted (Evi)-exosome release at synaptic boutons. J Biol Chem *287*, 16820-16834.

Koon, A.C., Ashley, J., Barria, R., DasGupta, S., Brain, R., Waddell, S., Alkema, M.J., and Budnik, V. (2011). Autoregulatory and paracrine control of synaptic and behavioral plasticity by octopaminergic signaling. Nat Neurosci *14*, 190-199.

Korkut, C., Ataman, B., Ramachandran, P., Ashley, J., Barria, R., Gherbesi, N., and Budnik, V. (2009). Trans-synaptic transmission of vesicular Wnt signals through Evi/Wntless. Cell *139*, 393-404.

Korkut, C., Li, Y., Koles, K., Brewer, C., Ashley, J., Yoshihara, M., and Budnik, V. (2013). Regulation of postsynaptic retrograde signaling by presynaptic exosome release. Neuron *77*, 1039-1039.

Korkut, C.B., V. (2009). WNTs tune up the neuromuscular junction. Nat Rev Neurosci *10*, 627-634.

Krauss, J., Lopez de Quinto, S., Nusslein-Volhard, C., and Ephrussi, A. (2009). Myosin-V regulates oskar mRNA localization in the Drosophila oocyte. Curr Biol *19*, 1058-1063. doi: 1010.1016/j.cub.2009.1004.1062. Epub 2009 May 1028.

Krichevsky, A.M., and Kosik, K.S. (2001). Neuronal RNA granules: a link between RNA localization and stimulation-dependent translation. Neuron *32*, 683-696.

Kuhn, U., Gundel, M., Knoth, A., Kerwitz, Y., Rudel, S., and Wahle, E. (2009). Poly(A) tail length is controlled by the nuclear poly(A)-binding protein regulating the interaction between poly(A) polymerase and the cleavage and polyadenylation specificity factor. J Biol Chem *284*, 22803-22814.

Kustedjo K, B.M., Cravatt BF. (2000). Torsin A and its torsion dystonia-associated mutant forms are lumenal glycoproteins that exhibit distinct subcellular localizations. J Biol Chem *275*, 27933-27939.

Lagace, T.A., and Ridgway, N.D. (2005). The rate-limiting enzyme in phosphatidylcholine synthesis regulates proliferation of the nucleoplasmic reticulum. Mol Biol Cell *16*, 1120-1130.

Lahey, T., Gorczyca, M., Jia, X.X., and Budnik, V. (1994). The Drosophila tumor suppressor gene dlg is required for normal synaptic bouton structure. Neuron *13*, 823-835.

Landgraf, M., and Thor, S. (2006). Development and Structure of Motoneurons. *75*, 33-53.

Lasko, P. (2012). mRNA localization and translational control in Drosophila oogenesis. Cold Spring Harb Perspect Biol *4(10).* a012294. doi: 012210.011101/cshperspect.a012294.

Laudermilch, E., and Schlieker, C. (2016). Torsin ATPases: structural insights and functional perspectives. Curr Opin Cell Biol *40*, 1-7.

Leach, N.R., and Roller, R.J. (2010). Significance of host cell kinases in herpes simplex virus type 1 egress and lamin-associated protein disassembly from the nuclear lamina. Virology *406*, 127-137.

Lecuyer, E., Yoshida, H., Parthasarathy, N., Alm, C., Babak, T., Cerovina, T., Hughes, T.R., Tomancak, P., and Krause, H.M. (2007). Global analysis of mRNA localization reveals a prominent role in organizing cellular architecture and function. Cell *131*, 174-187.

Lee, C.P., and Chen, M.R. (2010). Escape of herpesviruses from the nucleus. Rev Med Virol *20*, 214-230.

Lee, Y.S., and Carthew, R.W. (2003). Making a better RNAi vector for Drosophila: use of intron spacers. Methods *30*, 322-329.

Li, Q., Kim, Y., Namm, J., Kulkarni, A., Rosania, G.R., Ahn, Y.H., and Chang, Y.T. (2006). RNA-selective, live cell imaging probes for studying nuclear structure and function. Chemistry & biology *13*, 615-623.

Lim, E.C., and Seet, R.C. (2010). Use of botulinum toxin in the neurology clinic. Nat Rev Neurol *6*, 624-636.

Lloyd, T.E., and Taylor, J.P. (2010). Flightless flies: Drosophila models of neuromuscular disease. Ann N Y Acad Sci *1184*, e1-20.

Lyford, G.L., Yamagata, K., Kaufmann, W.E., Barnes, C.A., Sanders, L.K., Copeland, N.G., Gilbert, D.J., Jenkins, N.A., Lanahan, A.A., and Worley, P.F. (1995). Arc, a growth factor and activity-regulated gene, encodes a novel cytoskeleton-associated protein that is enriched in neuronal dendrites. Neuron *14*, 433-445.

Lyu, J., Yamamoto, V., and Lu, W. (2008). Cleavage of the Wnt receptor Ryk regulates neuronal differentiation during cortical neurogenesis. Dev Cell *15*, 773-780.

Maric, M., Shao, J., Ryan, R.J., Wong, C.S., Gonzalez-Alegre, P., and Roller, R.J. (2011a). A functional role for TorsinA in herpes simplex virus 1 nuclear egress. J Virol *85*, 9667-9679.

Maric, M., Shao, J., Ryan, R.J., Wong, C.S., Gonzalez-Alegre, P., and Roller, R.J. (2011b). A functional role for torsinA in herpes simplex virus type 1 nuclear egress. J Virol.

Martin, K.C., and Ephrussi, A. (2009). mRNA localization: gene expression in the spatial dimension. Cell *136*, 719-730.

Martin, K.C., and Zukin, R.S. (2006). RNA trafficking and local protein synthesis in dendrites: an overview. J Neurosci *26*, 7131-7134.

Mathew, D., Ataman, B., Chen, J., Zhang, Y., Cumberledge, S., and Budnik, V. (2005). Wingless signaling at synapses is through cleavage and nuclear import of receptor DFrizzled2. Science *310*, 1344-1347.

Mayford, M., Baranes, D., Podsypanina, K., and Kandel, E.R. (1996). The 3'-untranslated region of CaMKII alpha is a cis-acting signal for the localization and translation of mRNA in dendrites. Proc Natl Acad Sci U S A *93*, 13250-13255.

Mayford, M., Siegelbaum, S.A., and Kandel, E.R. (2012). Synapses and memory storage. Cold Spring Harb Perspect Biol *4*.

Mazroui, R., Huot, M.E., Tremblay, S., Filion, C., Labelle, Y., and Khandjian, E.W. (2002). Trapping of messenger RNA by Fragile X Mental Retardation protein into cytoplasmic granules induces translation repression. Hum Mol Genet *11*, 3007-3017.

McConnell, R.E., and Tyska, M.J. (2007). Myosin-1a powers the sliding of apical membrane along microvillar actin bundles. J Cell Biol *177*, 671-681. Epub 2007 May 2014.

McKim, K.S., Joyce, E.F., and Jang, J.K. (2009). Cytological analysis of meiosis in fixed Drosophila ovaries. Methods Mol Biol *558*, 197-216.

Medioni, C., Mowry, K., and Besse, F. (2012). Principles and roles of mRNA localization in animal development. Development *139*, 3263-3276. doi: 3210.1242/dev.078626.

Meignin, C., and Davis, I. (2010). Transmitting the message: intracellular mRNA localization. Curr Opin Cell Biol *22*, 112-119. doi: 110.1016/j.ceb.2009.1011.1011.

Mejat, A., Decostre, V., Li, J., Renou, L., Kesari, A., Hantai, D., Stewart, C.L., Xiao, X., Hoffman, E., Bonne, G.*, et al.* (2009). Lamin A/C-mediated neuromuscular junction defects in Emery-Dreifuss muscular dystrophy. J Cell Biol *184*, 31-44.

Mettenleiter, T.C., Klupp, B.G., and Granzow, H. (2006). Herpesvirus assembly: a tale of two membranes. Curr Opin Microbiol *9*, 423-429.

Mettenleiter, T.C., Klupp, B.G., and Granzow, H. (2009). Herpesvirus assembly: an update. Virus Res *143*, 222-234.

Mettenleiter, T.C., Muller, F., Granzow, H., and Klupp, B.G. (2013a). The way out: what we know and do not know about herpesvirus nuclear egress. Cell Microbiol *15*, 170-178.

Mettenleiter, T.C., Muller, F., Granzow, H., and Klupp, B.G. (2013b). The way out: what we know and do not know about herpesvirus nuclear egress. Cell Microbiol *15*, 170-178. doi: 110.1111/cmi.12044. Epub 12012 Nov 12047.

Miech, C., Pauer, H.U., He, X., and Schwarz, T.L. (2008). Presynaptic local signaling by a canonical wingless pathway regulates development of the Drosophila neuromuscular junction. J Neurosci *28*, 10875-10884.

Milbradt, J., Webel, R., Auerochs, S., Sticht, H., and Marschall, M. (2010). Novel mode of phosphorylation-triggered reorganization of the nuclear lamina during nuclear egress of human cytomegalovirus. J Biol Chem *285*, 13979-13989.

Miller, S., Yasuda, M., Coats, J.K., Jones, Y., Martone, M.E., and Mayford, M. (2002). Disruption of dendritic translation of CaMKIIalpha impairs stabilization of synaptic plasticity and memory consolidation. Neuron *36*, 507-519.

Mislow, J.M., Holaska, J.M., Kim, M.S., Lee, K.K., Segura-Totten, M., Wilson, K.L., and McNally, E.M. (2002). Nesprin-1alpha self-associates and binds directly to emerin and lamin A in vitro. FEBS Lett *525*, 135-140.

Monneron, A., and Bernhard, W. (1969). Fine structural organization of the interphase nucleus in some mammalian cells. J Ultrastruct Res *27*, 266-288.

Moore, M.J. (2005). From birth to death: the complex lives of eukaryotic mRNAs. Science *309*, 1514-1518.

Morel, V., Lepicard, S., A, N.R., Parmentier, M.L., and Schaeffer, L. (2014a). Drosophila Nesprin-1 controls glutamate receptor density at neuromuscular junctions. Cell Mol Life Sci *4*, 4.

Morel, V., Lepicard, S., Rey, A.N., Parmentier, M.L., and Schaeffer, L. (2014b). Drosophila Nesprin-1 controls glutamate receptor density at neuromuscular junctions. Cell Mol Life Sci *71*, 3363-3379.

Morin, X., Daneman, R., Zavortink, M., and Chia, W. (2001). A protein trap strategy to detect GFP-tagged proteins expressed from their endogenous loci in Drosophila. Proc Natl Acad Sci U S A *98*, 15050-15055.

Morris, R.G., Anderson, E., Lynch, G.S., and Baudry, M. (1986). Selective impairment of learning and blockade of long-term potentiation by an N-methyl-D-aspartate receptor antagonist, AP5. Nature *319*, 774-776.

Mosca, T.J., and Schwarz, T.L. (2010). The nuclear import of Frizzled2-C by Importins-beta11 and alpha2 promotes postsynaptic development. Nat Neurosci *13*, 935-943.

Naismith, T.V., Dalal, S., and Hanson, P.I. (2009). Interaction of torsinA with its major binding partners is impaired by the dystonia-associated DeltaGAG deletion. J Biol Chem *284*, 27866-27874.

Naismith, T.V., Heuser, J.E., Breakefield, X.O., and Hanson, P.I. (2004). TorsinA in the nuclear envelope. Proc Natl Acad Sci U S A *101*, 7612-7617.

Neuwald AF, A.L., Spouge JL, Koonin EV. (1999). AAA+: A class of chaperone-like ATPases associated with the assembly, operation, and disassembly of protein complexes. Genome Res *9*, 27-43.

Neuwald, A.F., Aravind, L., Spouge, J.L., and Koonin, E.V. (1999). AAA+: A class of chaperone-like ATPases associated with the assembly, operation, and disassembly of protein complexes. Genome Res *9*, 27-43.

Noegel, A.A., and Neumann, S. (2011). The role of nesprins as multifunctional organizers in the nucleus and the cytoskeleton. Biochem Soc Trans *39*, 1725-1728.

Ostlund, C., Bonne, G., Schwartz, K., and Worman, H.J. (2001). Properties of lamin A mutants found in Emery-Dreifuss muscular dystrophy, cardiomyopathy and Dunnigan-type partial lipodystrophy. J Cell Sci *114*, 4435-4445.

Ozelius, L.J., Hewett, J., Kramer, P., Bressman, S.B., Shalish, C., de Leon, D., Rutter, M., Risch, N., Brin, M.F., Markova, E.D.*, et al.* (1997). Fine localization of

the torsion dystonia gene (DYT1) on human chromosome 9q34: YAC map and linkage disequilibrium. Genome Res *7*, 483-494.

Packard, M., Koo, E.S., Gorczyca, M., Sharpe, J., Cumberledge, S., and Budnik, V. (2002). The Drosophila wnt, wingless, provides an essential signal for pre- and postsynaptic differentiation. Cell *111*, 319-330.

Padan, R., Nainudel-Epszteyn, S., Goitein, R., Fainsod, A., and Gruenbaum, Y. (1990). Isolation and characterization of the Drosophila nuclear envelope otefin cDNA. J Biol Chem *265*, 7808-7813.

Park, R., and Baines, J.D. (2006). Herpes simplex virus type 1 infection induces activation and recruitment of protein kinase C to the nuclear membrane and increased phosphorylation of lamin B. J Virol *80*, 494-504.

Petersen, S.A., Fetter, R.D., Noordermeer, J.N., Goodman, C.S., and DiAntonio, A. (1997). Genetic analysis of glutamate receptors in Drosophila reveals a retrograde signal regulating presynaptic transmitter release. Neuron *19*, 1237-1248.

Petzoldt, A.G., Coutelis, J.B., Geminard, C., Speder, P., Suzanne, M., Cerezo, D., and Noselli, S. (2012). DE-Cadherin regulates unconventional Myosin ID and Myosin IC in Drosophila left-right asymmetry establishment. Development *139*, 1874-1884. doi: 1810.1242/dev.047589. Epub 042012 Apr 047584.

Pinto, B.S., Wilmington, S.R., Hornick, E.E., Wallrath, L.L., and Geyer, P.K. (2008). Tissue-specific defects are caused by loss of the Drosophila MAN1 LEM domain protein. Genetics *180*, 133-145.

Rajgor, D., and Shanahan, C.M. (2013). Nesprins: from the nuclear envelope and beyond. Expert Rev Mol Med *15*, e5.

Ramachandran, P., Barria, R., Ashley, J., and Budnik, V. (2009). A critical step for postsynaptic F-actin organization: regulation of Baz/Par-3 localization by aPKC and PTEN. Dev Neurobiol *69*, 583-602.

Razafsky, D., and Hodzic, D. (2009). Bringing KASH under the SUN: the many faces of nucleo-cytoskeletal connections. J Cell Biol *186*, 461-472.

Reynolds, A.E., Liang, L., and Baines, J.D. (2004). Conformational changes in the nuclear lamina induced by herpes simplex virus type 1 require genes U(L)31 and U(L)34. J Virol *78*, 5564-5575.

Richter, J.D. (2001). Think globally, translate locally: what mitotic spindles and neuronal synapses have in common. Proc Natl Acad Sci U S A *98*, 7069-7071.

Riemer, D., Stuurman, N., Berrios, M., Hunter, C., Fisher, P.A., and Weber, K. (1995). Expression of Drosophila lamin C is developmentally regulated: analogies with vertebrate A-type lamins. J Cell Sci *108 (Pt 10)*, 3189-3198.

Robottom, B.J., Weiner, W.J., and Comella, C.L. (2011). Early-onset primary dystonia. Handb Clin Neurol *100*, 465-479.

Roller, R.J. (2008). Nuclear egress of herpes viruses. Virologica Sinica *23*, 406-415.

Rosenberg-Hasson, Y., Renert-Pasca, M., and Volk, T. (1996). A Drosophila dystrophin-related protein, MSP-300, is required for embryonic muscle morphogenesis. Mech Dev *60*, 83-94.

Ruiz-Canada, C., Ashley, J., Moeckel-Cole, S., Drier, E., Yin, J., and Budnik, V. (2004). New Synaptic Bouton Formation Is Disrupted by Misregulation of Microtubule Stability in aPKC Mutants. Neuron *42*, 567-580.

Ruiz‐Cañada, C., and Budnik, V. (2006). Introduction on The Use of The Drosophila Embryonic/Larval Neuromuscular Junction as A Model System to Study Synapse Development and Function, and A Brief Summary of Pathfinding and Target Recognition. *75*, 1-31.

Ryckman, B.J., and Roller, R.J. (2004). Herpes simplex virus type 1 primary envelopment: UL34 protein modification and the US3-UL34 catalytic relationship. J Virol *78*, 399-412.

Sanger, J.W., Kang, S., Siebrands, C.C., Freeman, N., Du, A., Wang, J., Stout, A.L., and Sanger, J.M. (2005). How to build a myofibril. J Muscle Res Cell Motil *26*, 343-354.

Schmidt, H.B., and Gorlich, D. (2015). Nup98 FG domains from diverse species spontaneously phase-separate into particles with nuclear pore-like permselectivity. Elife *4*.

Schooley, A., Vollmer, B., and Antonin, W. (2012). Building a nuclear envelope at the end of mitosis: coordinating membrane reorganization, nuclear pore complex assembly, and chromatin de-condensation. Chromosoma *121*, 539-554.

Schroll, C., Riemensperger, T., Bucher, D., Ehmer, J., Voller, T., Erbguth, K., Gerber, B., Hendel, T., Nagel, G., Buchner, E.*, et al.* (2006). Light-induced activation of distinct modulatory neurons triggers appetitive or aversive learning in Drosophila larvae. Curr Biol *16*, 1741-1747.

Schuh, M. (2011). An actin-dependent mechanism for long-range vesicle transport. Nat Cell Biol *13*, 1431-1436. doi: 1410.1038/ncb2353.

Schulze, S.R., Curio-Penny, B., Li, Y., Imani, R.A., Rydberg, L., Geyer, P.K., and Wallrath, L.L. (2005). Molecular genetic analysis of the nested Drosophila melanogaster lamin C gene. Genetics *171*, 185-196.

Schulze, S.R., Curio-Penny, B., Speese, S., Dialynas, G., Cryderman, D.E., McDonough, C.W., Nalbant, D., Petersen, M., Budnik, V., Geyer, P.K.*, et al.* (2009). A comparative study of Drosophila and human A-type lamins. PLoS One *4*, e7564.

Shinozaki, G., and Potash, J.B. (2014). New developments in the genetics of bipolar disorder. Curr Psychiatry Rep *16*, 493. doi: 410.1007/s11920-11014-10493-11925.

Shu, X., Lev-Ram, V., Deerinck, T.J., Qi, Y., Ramko, E.B., Davidson, M.W., Jin, Y., Ellisman, M.H., and Tsien, R.Y. (2011). A genetically encoded tag for correlated light and electron microscopy of intact cells, tissues, and organisms. PLoS biology *9*, e1001041.

Siegfried E, P.N. (1994). Drosophila wingless: a paradigm for the function and mechanism of Wnt signaling. Bioessays *4*, 395-404.

Sigrist, S.J., Thiel, P.R., Reiff, D.F., Lachance, P.E., Lasko, P., and Schuster, C.M. (2000). Postsynaptic translation affects the efficacy and morphology of neuromuscular junctions. Nature *405*, 1062-1065.

Simpson, J.G., and Roberts, R.G. (2008). Patterns of evolutionary conservation in the nesprin genes highlight probable functionally important protein domains and isoforms. Biochem Soc Trans *36*, 1359-1367.

Sinnamon, J.R., and Czaplinski, K. (2011). mRNA trafficking and local translation: the Yin and Yang of regulating mRNA localization in neurons. Acta Biochim Biophys Sin (Shanghai) *43*, 663-670.

Solmaz SR, B.G., Melcák I. (2013). Ring cycle for dilating and constricting the nuclear pore. Proc Natl Acad Sci U S A *15*, 5858-5863.

Song, X., and Xie, T. (2003). Wingless signaling regulates the maintenance of ovarian somatic stem cells in Drosophila. Development *130*, 3259-3268.

Speder, P., Adam, G., and Noselli, S. (2006). Type ID unconventional myosin controls left-right asymmetry in Drosophila. Nature *440*, 803-807.

Speese, S.D., Ashley, J., Jokhi, V., Nunnari, J., Barria, R., Li, Y., Ataman, B., Koon, A., Chang, Y.-T., Li, Q.*, et al.* (2012). Nuclear Envelope Budding Enables Large Ribonucleoprotein Particle Export during Synaptic Wnt Signaling. Cell *149*, 832-846.

Speese, S.D., and Budnik, V. (2007). Wnts: up-and-coming at the synapse. Trends Neurosci *30*, 268-275.

St Johnston, D. (2002). The art and design of genetic screens: Drosophila melanogaster. Nat Rev Genet *3*, 176-188.

Starr DA, H.M. (2002). Role of ANC-1 in tethering nuclei to the actin cytoskeleton. Science *298*, 406-409.

Steward, O., and Levy, W.B. (1982). Preferential localization of polyribosomes under the base of dendritic spines in granule cells of the dentate gyrus. J Neurosci *2*, 284-291.

Stone, J.L., Merriman, B., Cantor, R.M., Geschwind, D.H., and Nelson, S.F. (2007). High density SNP association study of a major autism linkage region on chromosome 17. Hum Mol Genet *16*, 704-715. Epub 2007 Mar 2021.

Swanger, S.A., and Bassell, G.J. (2011). Making and breaking synapses through local mRNA regulation. Curr Opin Genet Dev *21*, 414-421.

Szollosi, D. (1965). Extrusion of nucleoli from pronuclei of the rat. J Cell Biol *25*, 545-562.

Szollosi, M.S., and Szollosi, D. (1988). 'Blebbing' of the nuclear envelope of mouse zygotes, early embryos and hybrid cells. J Cell Sci *91 (Pt 2)*, 257-267.

Tam, R., Shopland, L.S., Johnson, C.V., McNeil, J., and Lawrence, J.B. (2002). Applications of RNA FISH for visualizing gene expression and nuclear architecture. In FISH Practical Approach, B.M.S.S.J. Beatty, ed. (New York: Oxford University Press), pp. 93-118.

Tanabe, L.M., Kim, C.E., Alagem, N., and Dauer, W.T. (2009). Primary dystonia: molecules and mechanisms. Nat Rev Neurol *5*, 598-609.

Taranum, S., Sur, I., Muller, R., Lu, W., Rashmi, R.N., Munck, M., Neumann, S., Karakesisoglou, I., and Noegel, A.A. (2012a). Cytoskeletal interactions at the nuclear envelope mediated by nesprins. Int J Cell Biol *2012:736524.*, 10.1155/2012/736524. Epub 732012 Feb 736527.

Taranum, S., Vaylann, E., Meinke, P., Abraham, S., Yang, L., Neumann, S., Karakesisoglou, I., Wehnert, M., and Noegel, A.A. (2012b). LINC complex alterations in DMD and EDMD/CMT fibroblasts. Eur J Cell Biol *91*, 614-628.

Tennyson N, Klamut J, and G, W. (1995). The human dystrophin gene requires 16 hours to be transcribed and is cotranscriptionally spliced. Nature Genetics *9(2):184-90*.

Tesarík J, P.L., Trávník P. (1988). Zona pellucida resistance to sperm penetration before the
completion of human oocyte maturation. J Reprod Fertil *83*, 487-495.

Thomas, M.G., Loschi, M., Desbats, M.A., and Boccaccio, G.L. (2011). RNA granules: the good, the bad and the ugly. Cell Signal *23*, 324-334.

Tiruchinapalli, D.M., Oleynikov, Y., Kelic, S., Shenoy, S.M., Hartley, A., Stanton, P.K., Singer, R.H., and Bassell, G.J. (2003). Activity-dependent trafficking and dynamic localization of zipcode binding protein 1 and beta-actin mRNA in dendrites and spines of hippocampal neurons. J Neurosci *23*, 3251-3261.

Tulgren, E.D., Turgeon, S.M., Opperman, K.J., and Grill, B. (2014). The Nesprin family member ANC-1 regulates synapse formation and axon termination by functioning in a pathway with RPM-1 and beta-Catenin. PLoS Genet *10*, e1004481. doi: 1004410.1001371/journal.pgen.1004481. eCollection 1002014 Jul.

Vander Heyden, A.B., Naismith, T.V., Snapp, E.L., Hodzic, D., and Hanson, P.I. (2009). LULL1 retargets TorsinA to the nuclear envelope revealing an activity that is impaired by the DYT1 dystonia mutation. Mol Biol Cell *20*, 2661-2672.

VanGompel, M.J., Nguyen, K.C., Hall, D.H., Dauer, W.T., and Rose, L.S. (2015). A novel function for the Caenorhabditis elegans torsin OOC-5 in nucleoporin localization and nuclear import. Mol Biol Cell *26*, 1752-1763.

Varela-Nallar L1, A.I., Serrano FG, Parodi J, Inestrosa NC. (2010). Wingless-type family member 5A (Wnt-5a) stimulates synaptic differentiation and function of glutamatergic synapses. Proc Natl Acad Sci U S A *107*, 21164-21169.

Volk, T. (1992). A new member of the spectrin superfamily may participate in the formation of embryonic muscle attachments in Drosophila. Development *116*, 721-730.

Volk, T. (2013). Positioning nuclei within the cytoplasm of striated muscle fiber: cooperation between microtubules and KASH proteins. Nucleus *4*, 18-22. doi: 10.4161/nucl.23086. Epub 22012 Dec 23084.

Wagner, N., Schmitt, J., and Krohne, G. (2004). Two novel LEM-domain proteins are splice products of the annotated Drosophila melanogaster gene CG9424 (Bocksbeutel). Eur J Cell Biol *82*, 605-616.

Wakabayashi-Ito, N., Doherty, O.M., Moriyama, H., Breakefield, X.O., Gusella, J.F., O'Donnell, J.M., and Ito, N. (2011). Dtorsin, the Drosophila ortholog of the early-onset dystonia TOR1A (DYT1), plays a novel role in dopamine metabolism. PLoS ONE *6*, e26183.

Walker, J.E., Saraste, M., Runswick, M.J., and Gay, N.J. (1982). Distantly related sequences in the alpha- and beta-subunits of ATP synthase, myosin, kinases and other ATP-requiring enzymes and a common nucleotide binding fold. Embo J *1*, 945-951.

Wang, D.O., Martin, K.C., and Zukin, R.S. (2010). Spatially restricting gene expression by local translation at synapses. Trends Neurosci *33*, 173-182.

Warren, C.M., Krzesinski, P.R., and Greaser, M.L. (2003). Vertical agarose gel electrophoresis and electroblotting of high-molecular-weight proteins. Electrophoresis *24*, 1695-1702.

Webster, B.M., Colombi, P., Jager, J., and Lusk, C.P. (2014). Surveillance of nuclear pore complex assembly by ESCRT-III/Vps4. Cell *159*, 388-401.

Wente, S.R., and Blobel, G. (1993). A temperature-sensitive NUP116 null mutant forms a nuclear envelope seal over the yeast nuclear pore complex thereby blocking nucleocytoplasmic traffic. J Cell Biol *123*, 275-284.

White, S.R., and Lauring, B. (2007). AAA+ ATPases: achieving diversity of function with conserved machinery. Traffic *8*, 1657-1667.

Wickramasinghe, V.O., and Laskey, R.A. (2015). Control of mammalian gene expression by selective mRNA export. Nat Rev Mol Cell Biol *16*, 431-442.

Wiersma-Meems, R., Van Minnen, J., and Syed, N.I. (2005). Synapse formation and plasticity: the roles of local protein synthesis. Neuroscientist *11*, 228-237.

Wodarz, A., Ramrath, A., Kuchinke, U., and Knust, E. (1999). Bazooka provides an apical cue for Inscuteable localization in Drosophila neuroblasts. Nature *402*, 544-547.

Wu, C.F., Ganetzky, B., Haugland, F.N., and Liu, A.X. (1983). Potassium currents in Drosophila: different components affected by mutations of two genes. Science *220*, 1076-1078.

Yamashita, S., Katsumata, O., and Okada, Y. (2009). Establishment of a standardized post-embedding method for immunoelectron microscopy by applying heat-induced antigen retrieval. J Electron Microsc (Tokyo) *58*, 267-279.

Yoshihara, M., Suzuki, K., and Kidokoro, Y. (2000). Two independent pathways mediated by cAMP and protein kinase A enhance spontaneous transmitter release at Drosophila neuromuscular junctions. J Neurosci *20*, 8315-8322.

Yu, J., Starr, D.A., Wu, X., Parkhurst, S.M., Zhuang, Y., Xu, T., Xu, R., and Han, M. (2006). The KASH domain protein MSP-300 plays an essential role in nuclear anchoring during Drosophila oogenesis. Dev Biol *289*, 336-345. Epub 2005 Dec 2007.

Yu, T.W., Chahrour, M.H., Coulter, M.E., Jiralerspong, S., Okamura-Ikeda, K., Ataman, B., Schmitz-Abe, K., Harmin, D.A., Adli, M., Malik, A.N.*, et al.* (2013). Using whole-exome sequencing to identify inherited causes of autism. Neuron *77*, 259-273. doi: 210.1016/j.neuron.2012.1011.1002.

Zhang, H., Zha, X., Tan, Y., Hornbeck, P.V., Mastrangelo, A.J., Alessi, D.R., Polakiewicz, R.D., and Comb, M.J. (2002a). Phosphoprotein analysis using antibodies broadly reactive against phosphorylated motifs. J Biol Chem *277*, 39379-39387.

Zhang, J., Felder, A., Liu, Y., Guo, L.T., Lange, S., Dalton, N.D., Gu, Y., Peterson, K.L., Mizisin, A.P., Shelton, G.D.*, et al.* (2010). Nesprin 1 is critical for nuclear positioning and anchorage. Hum Mol Genet *19*, 329-341.

Zhang, Q., Bethmann, C., Worth, N.F., Davies, J.D., Wasner, C., Feuer, A., Ragnauth, C.D., Yi, Q., Mellad, J.A., Warren, D.T.*, et al.* (2007). Nesprin-1 and -2 are involved in the pathogenesis of Emery Dreifuss muscular dystrophy and are critical for nuclear envelope integrity. Hum Mol Genet *16*, 2816-2833. Epub 2007 Aug 2829.

Zhang, Q., Ragnauth, C., Greener, M.J., Shanahan, C.M., and Roberts, R.G. (2002b). The nesprins are giant actin-binding proteins, orthologous to Drosophila melanogaster muscle protein MSP-300. Genomics *80*, 473-481.

Zhao, C., Brown, R.S., Chase, A.R., Eisele, M.R., and Schlieker, C. (2013). Regulation of Torsin ATPases by LAP1 and LULL1. Proc Natl Acad Sci U S A *110*, E1545-1554.

Zhao, J., Jin, S.B., Bjorkroth, B., Wieslander, L., and Daneholt, B. (2002). The mRNA export factor Dbp5 is associated with Balbiani ring mRNP from gene to cytoplasm. EMBO J *21*, 1177-1187.

Zhao J, J.S., Björkroth B, Wieslander L, Daneholt B. (2002). The mRNA export factor Dbp5 is associated with Balbiani ring mRNP from gene to cytoplasm. EMBO J *21*, 1177-1187.

Zimmerman, S.G., Peters, N.C., Altaras, A.E., and Berg, C.A. (2013). Optimized RNA ISH, RNA FISH and protein-RNA double labeling (IF/FISH) in Drosophila ovaries. Nat Protoc *8*, 2158-2179.

Zimyanin, V., Lowe, N., and St Johnston, D. (2007). An oskar-dependent positive feedback loop maintains the polarity of the Drosophila oocyte. Curr Biol *17*, 353-359.

Zimyanin, V.L., Belaya, K., Pecreaux, J., Gilchrist, M.J., Clark, A., Davis, I., and St Johnston, D. (2008). In vivo imaging of oskar mRNA transport reveals the mechanism of posterior localization. Cell *134*, 843-853.

Zito, K., Parnas, D., Fetter, R.D., Isacoff, E.Y., and Goodman, C.S. (1999). Watching a synapse grow: noninvasive confocal imaging of synaptic growth in Drosophila. Neuron *22*, 719-729.